APPLICABILITY OF APPROXIMATE METHODS OF ANALYSIS FOR SKEWED STRAIGHT STEEL I-GIRDER BRIDGES

Final Report

FDOT Contract Nos: BEB13 and BED03

Submitted by:

Donald W. White, PhD; Ryan J. Sherman, PhD, PE; and Ajit Kamath

Georgia Institute of Technology

John A. Heath, PE; Brian K. Adams, PE; and Amrithraj Anand, PE

Heath & Lineback Engineers, Inc.

December 2022

DISCLAIMER

The opinions, findings, and conclusions expressed in this publication are those of the authors and are not necessarily those of the State of Florida Department of Transportation.

METRIC CONVERSION CHART

SI* (MODERN METRIC) CONVERSION FACTORS				
APPROXIMATE CONVERSIONS TO SI UNITS				
SYMBOL	**WHEN YOU KNOW**	**MULTIPLY BY**	**TO FIND**	**SYMBOL**
LENGTH				
in	inches	25.4	millimeters	mm
ft	feet	0.305	meters	m
yd	yards	0.914	meters	m
mi	miles	1.61	kilometers	km
AREA				
in^2	square inches	645.2	square millimeters	mm^2
ft^2	square feet	0.093	square meters	m^2
yd^2	square yard	0.836	square meters	m^2
ac	acres	0.405	hectares	ha
mi^2	square miles	2.59	square kilometers	km^2
VOLUME				
fl oz	fluid ounces	29.57	milliliters	mL
gal	gallons	3.785	liters	L
ft^3	cubic feet	0.028	cubic meters	m^3
yd^3	cubic yards	0.765	cubic meters	m^3
NOTE: volumes greater than 1000 L shall be shown in m^3				
MASS				
oz	ounces	28.35	grams	g
lb	pounds	0.454	kilograms	kg
T	short tons (2000 lb)	0.907	megagrams (or "metric ton")	Mg (or "t")
TEMPERATURE (exact degrees)				
°F	Fahrenheit	5(F-32)/9 or (F-32/1.8)	Celsius	°C
ILLUMINATION				
fc	foot-candles	10.76	lux	lx
fl	foot-Lamberts	3.426	candela/m^2	cd/m^2
FORCE and PRESSURE or STRESS				
lbf	poundforce	4.45	newtons	N
lbf/in^2	poundforce per square inch	6.89	kilopascals	kPa
K	Kips	4.45	kilonewtons	kN
APPROXIMATE CONVERSIONS FROM SI UNITS				
SYMBOL	**WHEN YOU KNOW**	**MULTIPLY BY**	**TO FIND**	**SYMBOL**
LENGTH				
mm	millimeters	0.039	inches	in
m	meters	3.28	feet	ft
m	meters	1.09	yards	yd
km	kilometers	0.621	miles	mi
AREA				
mm^2	square millimeters	0.0016	inches	in
m^2	square meters	10.764	square feet	ft^2
m^2	square meters	1.195	square yards	yd^2
ha	hectares	2.47	acres	ac
km^2	square kilometers	0.386	square miles	mi^2
VOLUME				
mL	milliliters	0.034	fluid ounces	fl oz
L	liters	0.264	gallons	gal
m^3	cubic meters	35.314	cubic feet	ft^3
m^3	cubic meters	1.307	cubic yards	yd^3
MASS				
g	grams	0.035	ounces	oz
kg	kilograms	2.202	pounds	lb
Mg (or "t")	megagrams (or "metric ton")	1.103	short tons (2000 lb)	T
TEMPERATURE (exact degrees)				
°C	Celsius	1.8C+32	Fahrenheit	°F
ILLUMINATION				
lx	lux	0.0929	foot-candles	fc
cd/m^2	candela/m^2	0.2919	foot-Lamberts	fl
FORCE and PRESSURE or STRESS				
N	newtons	0.225	poundforce	lbf
kPa	kilopascals	0.145	poundforce per square inch	lbf/in^2
kN	kilonewtons	0.225	Kips	K

TECHNICAL REPORT DOCUMENTATION PAGE

1. Report No.	2. Government Accession No.	3. Recipient's Catalog No.
4. Title and Subtitle Applicability of Approximate Methods of Analysis for Skewed Straight Steel I-Girder Bridges		**5. Report Date** December 2022
		6. Performing Organization Code
7. Author(s) Donald W. White, Ryan J. Sherman, Ajit M. Kamath, John A. Heath, Brian K. Adams, and Amrithraj Anand		**8. Performing Organization Report No.**
9. Performing Organization Name and Address Heath and Lineback Engineers, Inc. 2390 Canton Road, Bldg. 200 Marietta, GA 30066 USA		**10. Work Unit No.**
		11. Contract or Grant No. **FDOT BEB13 and BED03**
12. Sponsoring Agency Name and Address Florida Department of Transportation 605 Suwannee Street, MS 33 Tallahassee, FL 32399-0450 USA		**13. Type of Report and Period Covered** Final Report April 2021 – January 2023.
		14. Sponsoring Agency Code

15. Supplementary Notes

16. Abstract

The skew index, $I_s = w_g \tan \theta / L_s$, is often used to quantify the extent of skew of girder bridges, where w_g is the framing width between the fascia girders, θ is the maximum angle of skew, and L_s is the span length under consideration. The Florida Department of Transportation (FDOT) Structures Design Guidelines currently require a refined method of analysis for straight steel I-girder bridges when the skew index is $0.2 < I_s \le 0.6$; they require a 3D finite element analysis (FEA) when $I_s > 0.6$. FDOT Project BE535 developed three bridge categories based on the bearing line skew angle, bridge skew index, and cross-frame framing arrangement to facilitate the streamlined design application of line-girder analysis (LGA) to parallel skew bridges up to a skew angle of 50° and a skew index of 0.45. Category 1 includes bridges that have $\theta \le 20°$ and cross frames parallel skew; Category 2 includes bridges that have $\theta \le 50°$, $I_s \le 0.3$; and Category 3 includes more extreme skewed bridge geometries that have $0.3 < I_s \le 0.45$. However, the design guidance developed in BE535 was based on 12 bridges that were at the upper limits of the bridge design categories. Hence, the Projects BEB13 and BED03 aim to establish confidence that the LGA design guidance applies to a larger sample size and to consider possible refinements to the recommended LGA-based design guidance proposed in Project BE535, particularly for Categories 1 and 2. Comparative parametric 3D FEA and LGA studies were conducted on 35 bridges emphasizing bridge geometries that fit within Categories 1 and 2. The results confirm that LGA-based procedures developed in Project BE535 apply to the wider range of bridges studied. Subcategories within Category 2 bridges recognizing the type of cross-frame arrangement, contiguous or staggered, are established to provide improved design calculation of girder flange lateral bending stresses and cross-frame and diaphragm forces for designs using LGA.

17. Key Words Skew, Girder bridge design, Structural steel, Line girder analysis, Finite element analysis		**18. Distribution Statement** No restrictions.	
19. Security Classif. (of this report) Unclassified	**20. Security Classif. (of this page)** Unclassified	**21. No. of Pages** 207	**22. Price**

Form DOT F 1700.7 (8-72)　　　Reproduction of completed page authorized

ACKNOWLEDGEMENTS

EXECUTIVE SUMMARY

The skew index, $I_s = w_g \tan \theta / L_s$, is often used to quantify the extent of skew of girder bridges, where w_g is the framing width between the fascia girders, θ is the maximum angle of skew, and L_s is the span length under consideration. FDOT Project BE535 developed bridge categories based on the bearing line skew angle, bridge skew index, and cross-frame framing arrangement to facilitate the streamlined design application of line-girder analysis (LGA) to parallel skew bridges. The study matrix of Project BE535 consisted of 26 bridges, encompassing a wide range of geometric characteristics and variables (e.g., bridge width, span length, skew index, parallel/nonparallel skew, and cross-frame framing arrangement) to establish design guidelines. However, the goal of Project BE535 was to define the limits of LGA; therefore, the geometric characteristics of most bridges in the BE535 bridge matrix were not representative of the typical FDOT bridge inventory (i.e., the project needed to push the bounds to identify the limits of LGA). For Project BEB13, the FDOT steering group provided data that indicated the largest proportion of steel I-girder bridges in Florida have bridge widths of 40-80 ft and span lengths within 130-250 ft. Depending on the skew, such bridges would typically belong to Categories 1 or 2 defined in Project BE535.

Of the 26 bridges studied in Project BE535, only 12 parallel skew bridges qualified for the application of LGA using the recommended guidance. Most of the 12 bridges that qualified for LGA were at the upper limits of the LGA design categories (i.e., most of the bridges were relatively wide and had relatively high skew indices) because the study focused largely on defining the category limits. Hence, the Project BEB13 aims to establish confidence that the LGA design guidance applies to a larger sample size and to consider possible refinements to the recommended LGA-based design guidance proposed in Project BE535, particularly for Categories 1 and 2. Project BED03 supplements BEB13 by focusing on reanalysis of six of the 12 LGA-amenable bridges from BE535, including additional cross-frame fatigue demand calculations based on balloted and approved provisions for the 10th Edition of the AASHTO LRFD Specifications.

The objectives of this research were to (1) confirm that the recommended LGA-based design guidance developed in Project BE535 holds true for a larger sample size of bridges and (2) recommend any needed refinements to the procedures based on the larger sample size. To achieve these objectives, a parametric study was conducted for 35 bridges, with particular emphasis on bridges with geometric characteristics that fit within the boundaries of the Categories 1 and 2 identified by Project BE535. In particular, the studies focused predominantly on four-, five-, and six-girder bridges and contiguous and parallel stagger cross-frame framing arrangements. The selected parametric study bridges were divided into three groups:

- Category 1, corresponding to the Category 1 recommendations in Project BE535: bridges with parallel bearing lines and skew angle $\theta \leq 20°$, having contiguous cross-frame lines that are turned parallel to the skew;
- Category 2C, corresponding to the Category 2 recommendations in Project BE535: bridges with parallel bearing lines, $\theta \leq 50°$, and with a skew index $I_s \leq 0.3$, but specifically having contiguous cross-frame lines that are oriented perpendicular to the girders; and
- Category 2P, also corresponding to the Category 2 recommendations in Project BE535: bridges with $\theta \leq 50°$ and with a skew index $I_s \leq 0.3$, but specifically having a parallel stagger cross-frame framing arrangement (i.e., discontinuous lines of cross frames oriented with a selected work point on each of the cross frames positioned along a line parallel to the bearing lines).

The findings and recommendations from comparative studies performed using three-dimensional finite element analysis (3D FEA) and LGA performed in the current research for routine LGA estimates of girder response quantities may be summarized as follows:

- The LGA estimates were less than 5% and 7% unconservative for the worst-case predictions of girder moments and shears, respectively.
- Girder vertical deflections and layovers were sufficient within the limits of the LGA design categories.
- Additional multiplicative factors of 1.20 for Category 2C bridges and 1.10 for Categories 1 and 2P are recommended for calculation of the fascia girder bearing reactions at the obtuse corners of spans at end abutments. These factors are in addition to the application of the skew correction factor for the span under consideration for the end abutments and the larger of the skew correction factors from the adjacent spans at the pier bearing locations. If the application of the recommended LGA procedures is limited to bridges that do not have any cross frames framing into the bearing locations at interior piers and if the application of the recommended LGA procedures is limited to bridges that satisfy the limits for Categories 1, 2C, and 2P, then no multiplier is required on the exterior girder reactions at the piers of continuous-span bridges.
- Additional multiplicative factors of 1.30 for Category 2C bridges and 1.15 for Category 2P are recommended for calculation of the fatigue live load shear ranges at exterior girder ends at obtuse corners of spans.
- It was found in the initial stages of the project that nine of the 35 bridges exceeded the range of applicability on span lengths, $L_{s,max}$, and the girder longitudinal stiffness factor, K_g, in the AASHTO Article 4.6.2.2 provisions for calculation of live load distribution factors (LLDFs). The range of applicability of the limits was extended on $L_{s,max}$ by 25% and on K_g by 75% to accommodate the nine bridges. Ultimately, it was found that the trends of conservatism or unconservatism associated with the LLDF estimates were similar regardless of satisfaction or violation of the range of applicability of the AASHTO Article 4.6.2.2 procedures within the above-stated limits.
- Rigid cross-section analysis was not needed for single-lane fatigue LLDF evaluations.
- Optional girder live load deflection calculations perform better relative to 3D FEA solutions by applying the AASHTO Article 4.6.2.2 moment LLDFs.

Recommendations were developed for improved design calculation of girder flange lateral bending stresses and cross-frame and diaphragm forces for each design category. Recommendations for flange lateral bending stresses improve upon those from Project BE535. Unfactored flange lateral bending stress estimates due to skew effects (under nominal dead loads plus live load) are provided, along with updated weighted-average load factors for strength and service load combinations. The recommendations in Project BE535 for flange lateral bending stress were more punishing if the offsets or staggers were greater than $4b_f$, where b_f is the larger of the girder flange widths at the location of the offset or stagger.

The current research has refined the recommendations for design using LGA considering the following key observations:

- Flange lateral bending stresses for Category 1 bridges due to skew effects were negligible.
- For Category 2C bridges, the maximum values of flange lateral bending stresses occur at points of discontinuities in the framing arrangement. The largest values are observed in Category 2C bridges near abutments compared to intermediate piers in continuous-span bridges.
- For Category 2P bridges, significantly larger flange lateral bending stresses are observed, particularly in interior girders near the middle of bridge spans. The largest flange lateral bending stresses (equal to the AASHTO limit of $0.6F_y$ in one case) are observed in bridges that have a large skew angle and/or

staggers smaller than $4b_f$, where b_f is the larger of the girder flange widths at the location of the stagger. Intriguingly, the flange lateral bending stresses in the continuous-span bridges studied were comparable near abutments and intermediate piers. However, the flange lateral bending moments were observed to be significantly larger near intermediate piers (as much as 10 times larger in one case) compared to those near abutments. Typically, bottom flanges are sized larger at the piers than at the abutments. This indicates a potential sensitivity of flange lateral bending stress estimates to the size of the flanges utilized; however, this aspect could not be explored further in this research.

Project BE535 provided estimates of cross-frame chord-level connection forces due to skew effects as fractions of the maximum shear and bending moment within the bridge girders. However, it was found that the BE535 approach provides excessively conservative predictions for a large number of the bridges studied in Project BEB13. Hence, coarse upper-bound estimates for cross-frame member forces were developed separately for Categories 1, 2C, and 2P. Additionally, coarse upper-bound estimates were developed for fatigue force ranges using AASHTO LRFD 10th Edition recommendations. Significant reductions were observed in fatigue force ranges. A reduction of about 70% in unfactored fatigue ranges is observed in the study bridges. After incorporating a factor of 0.65 recommended in the AASHTO 10th edition provisions, the net resulting reduction becomes 45%.

The recommended cross-frame force estimates are based on the following key findings:

- The largest cross-frame member forces among the study bridges were observed in the bottom chords of Category 2C continuous-span bridges, especially in bridges that had spans larger than 200 ft. Stiff transverse load path effects are particularly prominent in Category 2C bridges. The maximum forces were observed to occur in the first and/or the second line of contiguous cross frames from the bearing lines spanning the entire bridge width. This region is referred to as the "critical" region, and the remainder of the bridge is referred to as the "non-critical" region for cross-frame design in Category 2C bridges. The magnitude of the cross-frame member forces is significantly smaller in the non-critical region.
- For Category 1 and 2P bridges, cross-frame forces are smaller and simple absolute bounds provide sufficient force estimates.

The synthesized results from the current research improve upon the insights from Project BE535 for various structural attributes influencing the behavior of straight skewed I-girder bridges. Particularly, this research provides evidence of how the framing arrangement influences the behavior of straight skewed I-girder bridges. The research findings allow for refinements and enhancements to the design guidance established in Project BE535 for the application of LGA-based procedures for a wide range of straight skewed I-girder bridges.

TABLE OF CONTENTS

LIST OF FIGURES

xiv

LIST OF TABLES

1. INTRODUCTION

1.1   Background

The Florida Department of Transportation (FDOT) Structures Design Guidelines (FDOT 2022a) currently require a refined method of analysis for straight steel I-girder bridges when the skew index is $0.2 < I_s \leq 0.6$. They require a 3D finite element analysis (FEA) when $I_s > 0.6$. According to FDOT (2021), approximately 250 steel I-girder bridges were constructed in Florida between 2000 and 2014, with over 90 % having a $I_s < 0.3$, defined as

$$I_s = \frac{w_g \tan\theta}{L_s}$$

(1)

where:

w_g = framing width of the bridge, measured between fascia girders
θ = skew angle at a support defined as the difference between the alignment of the support and a line perpendicular to the longitudinal axis of the bridge
L_s = length of the span under consideration.

NCHRP Report 725 (White et al. 2012) indicated that line girder analysis (LGA) is capable of predicting girder noncomposite major-axis bending responses and vertical displacements with a worst-case mean normalized error ≤ 12 % when $I_s \leq 0.3$. Subsequently, $I_s \leq 0.3$ often has been considered a de facto limit for when skew effects are of minor consequence. FDOT (2021) indicates that, based on current design policy, more than one-third of the bridges constructed with $I_s \leq 0.3$ would require a 2D grid or 3D FEA for design when LGA models may have sufficed.

Prior research studies on skewed steel I-girder bridges (e.g., White et al. 2012 and 2015) have emphasized more heavily skewed geometries than the majority of the FDOT steel I-girder bridge inventory. FDOT Project BE535 (White et al. 2020) built on the findings of NCHRP Report 725 and investigated the response of straight skewed bridge geometries having a skew index up to and only slightly larger than 0.3. The primary focus of Project BE535 was to understand the behavior better and to determine when LGA will yield results comparable to those obtained from 3D FEA for these bridge types. The project goal was achieved by a comparative LGA and 3D FEA parametric study of 26 straight skewed steel I-girder bridges. Project BE535 scrutinized procedures for (1) the estimation of major-axis bending stresses, vertical shear forces, and displacements from LGA and various other girder design quantities; and (2) the estimation of girder layover at the bearings using simple expressions based on the skew angle and the girder major-axis bending rotations obtained from LGA. Furthermore, Project BE535 evaluated and provided improvements to existing approaches for the estimation of girder flange lateral bending stresses and cross-frame forces for use in designs using LGA.

Project BE535 developed bridge categories to facilitate the streamlined design application of LGA to parallel skew bridges (Table 1). The categories were based on the bearing line skew angle, bridge skew index, and cross-frame framing arrangement. These attributes have some of the most significant influence on the behavior of straight skewed bridges. To capture the entire design space, BE535 explored a wide range of geometric characteristics and variables (e.g., bridge width, span length, skew index, and cross-frame framing arrangement). The final design guidance was developed on the basis of 26 bridges evaluated in the study; however, only 12 parallel skew bridges from BE535 qualified for the application of LGA using the recommended guidance. Most of the 12 bridges that qualified for LGA were at the upper limits of the LGA design categories (i.e., most of the bridges were relatively wide and had relatively high skew indices)

because the study focused largely on defining the category limits. As a result, many of the bridges had larger cross-frame forces and girder flange lateral bending stresses than might be expected for bridges with more moderate skew that fall within the categories. Further, the representation of the bridge population was limited in some areas of the straight skewed bridge design space; namely, in terms of bridge width, span length, and cross-frame framing arrangement. Therefore, additional investigations are needed to establish confidence that the LGA design guidance applies to a larger sample size and to identify and justify potential improvements to some design estimates.

Table 1. Bridge categories for LGA design from Project BE535.

Category	θ	I_s	CF Framing Arrangement
1	≤ 20	N.A.	Contiguous, parallel to skew
2	≤ 50	≤ 0.3	Contiguous / staggered, perpendicular to girders
3a	≤ 50	$0.3 < I_s \leq 0.4$	Contiguous / staggered, perpendicular to girders
3b	≤ 30	$0.4 < I_s \leq 0.45$	Contiguous / staggered, perpendicular to girders

Two critical findings from Project BE535 that require additional study are related to (1) the influence of cross-frame framing arrangements on the transverse load path, and the corresponding girder flange lateral bending stresses and cross-frame forces generated due to skew effects; and (2) the behavior of more narrow bridges with respect to the AASHTO live load distribution procedures, specifically the importance or lack of importance of rigid cross-section analysis (RCA) calculations. Project BE535 identified one type of cross-frame framing arrangement that was particularly effective at reducing transverse stiffness / load path effects in bridges having higher skew indices (e.g., Category 3 bridges versus Category 2). A staggered framing arrangement with every other intermediate cross frame eliminated from a base contiguous arrangement, consistent with recommendations in AASHTO C6.7.4.2, was found to mitigate the stiff transverse load path sufficiently to permit the application of LGA in a number of the BE535 bridges with larger skew indices, while the same bridges did not qualify for LGA using other comparable contiguous framing arrangements. Another type of a staggered framing arrangement, employed in many straight skewed bridges, is referred to as a "parallel stagger" framing arrangement. In a parallel stagger framing arrangement, a selected work point on each of the cross frames is positioned along a line parallel to the bearing lines. Project BE535 studied two bridges having a parallel stagger framing arrangement that classified as Category 2 bridges and qualified for LGA using the recommended guidance.

Furthermore, Project BE535 included a supplemental comparative study of AASHTO (2020) live load distribution factor (LLDF) calculation procedures versus 3D FEA results. The AASHTO LLDF calculation procedures require an RCA for determining fascia girder LLDFs. This requirement is intended to avoid potential unconservative results for fascia girders. Project BE535 showed that the RCA calculations governed for several bridges with the largest ratio of the span length to the framing width. However, conclusive evidence could not be found because of the limited number of narrow bridges considered in the study.

Additional investigation of the LGA guidance developed in Project BE535, via studies of straight skewed bridges that fit within its proposed LGA design categories, is needed for a more complete understanding of the corresponding skewed bridge behavior. Further, the new studies should consider a broad range of bridges representative of the FDOT skewed steel I-girder bridge inventory, including consideration of framing arrangements commonly adopted for such bridges. Specifically, studies of straight skewed bridges within the LGA design categories are necessary to verify and potentially refine the guidance for estimating cross-frame forces and flange lateral bending stresses.

1.2 Research Objectives

The objectives of FDOT Project BEB13 are to:

1. Confirm that the recommended LGA-based design guidance proposed in BE535 for Categories 1 and 2 holds true for a larger sample size. Specifically, it is desired to consider bridges representative of the current FDOT inventory, including narrow bridges with a minimum of four girders and bridges with both contiguous and parallel stagger cross-frame framing arrangements.

2. Consider possible refinements to the recommended LGA-based design guidance proposed in BE535 for Categories 1 and 2. In particular:
   a) Evaluate if the cross-frame force and girder flange lateral bending stress estimation procedures can be refined to recognize smaller response values for moderately skewed bridges that fit within Categories 1 and 2.
   b) Assess the implications of applying the live load model proposed by NCHRP Report 962 (Reichenbach et al. 2021) for the evaluation of the cross-frame fatigue forces via a refined analysis. Identify and implement refinements to the BE535 procedures, where possible, that provide for estimation of smaller cross-frame fatigue forces from LGA results in bridges with more moderate skew.
   c) Evaluate the efficacy of the several AASHTO LRFD live load distribution calculations (i.e., the AASHTO LRFD empirical equations, the lever rule, and RCA.

3. Simplify the design process and eliminate the need for unnecessarily complex and expensive analysis and design methods.

1.3 Research Approach

The current research addresses the above objectives via six major project tasks:

Task 1 – Literature Review. Project BE535 provided an extensive literature review on the behavior of straight skewed I-girder bridges and various aspects related to its analysis and design. The literature review conducted in Task 1 aims to supplement the review conducted by Project BE535. The findings of Project BE535 are the most relevant to the current project and hence are addressed in Task 1. In addition, findings and observations are summarized from other key relevant research studies.

Task 2 – Parametric Study Bridge Matrix. Project BEB13 emphasizes the study of relatively narrow Category 1 bridges, having contiguous cross frames parallel to the bearing lines, and relatively narrow Category 2 bridges with contiguous and parallel stagger cross-frame framing arrangements. The bridge inventory for BEB13 includes the bridge inventory for Project BE535, and other bridge geometries satisfying the limits of Categories 1 or 2. Supplementing the matrix of variables developed in Project BE535, a thorough data analysis was conducted to identify ranges of several bridge geometric parameters most representative of the FDOT bridge inventory. A matrix of variables was developed, including but not limited to bridge span lengths, bridge articulation (i.e., simple- or continuous-span, and number of continuous spans), framing width, number of girders, girder spacing, skew angle, cross-frame spacing, and framing arrangement (i.e., staggered and contiguous). Subsequently, the bridges were classified into Categories 1, 2, and 3 to facilitate selection of 29 study bridges. The design of the Bridge Matrix in Task 2 emphasized relatively narrow Category 1 bridges, having contiguous cross frames parallel to the bearing lines, and relatively narrow Category 2 bridges with contiguous and parallel stagger cross-frame framing arrangements. Within the 12 bridges that qualified for LGA using the recommended guidance in Project BE535, two bridges were classified as Category 1 shown in Table 1; four bridges were classified as Category 2. In addition, six BE535

bridges belonging to Categories 1 and 2 were reanalyzed by FDOT Project BED03 and included in the current parametric study matrix, bringing the tally of parametric study bridges to 35.

Task 3 – Comparative LGA and 3D FEA Parametric Studies. LGA and 3D FEA parametric studies were conducted on 35 straight skewed steel I-girder bridges selected from Task 2 to determine the extent that LGA adequately calculates girder major-axis bending moments and vertical displacements when compared to 3D FEA results. Modeling techniques and the procedures for comparison and evaluation of LGA and 3D FEA results in Project BE535 were brought forward to Project BEB13. Hence, the detailed parametric studies were preceded by a verification of the modeling techniques and analysis approach from Project BE535. The results of the analyses were evaluated to ascertain the key effects of the different considerations in the matrix of variables developed in Task 2. The comparative parametric studies included noncomposite responses associated with the steel erection and the concrete deck placement, and detailed evaluation of HL93 and fatigue live load effects on the bridges in their final composite condition. A greater emphasis was placed on evaluation of AASHTO LLDF procedures; especially on the potential of expanding the range of applicability of the limits on variables and assessment of RCA.

Task 4 – Recommended Design Guidelines and Details. The results from Task 3 were analyzed to confirm and refine design guidance for the use of LGA developed in Project BE535. Refinements include guidance specific to each bridge category for the estimation of girder flange lateral bending stresses and estimation of force demands for the design of cross frames and diaphragms accounting for skew effects. Included in the Task 4 evaluations were the assessment of the efficacy of a simplified method for the prediction of girder layovers developed by FDOT. The extent of the calculated layover displacements was evaluated at the abutments of the study bridges.

Task 5 – Draft Final Report and Closeout Teleconference. A draft final report was developed, presenting all the executed research tasks and findings.

Task 6 – Final Report. Upon approval of the draft final report, the project team has completed and submitted a final report (this report) to the FDOT research center.

1.4   Organization of This Report

This report is organized into seven main chapters.

Chapter 2 provides a broad review of relevant prior research and guidelines, and aims to supplement the literature review in Project BE535. A summary of the findings and observations from Project BE535 is presented, followed by summaries of findings from relevant research conducted after the conclusion of Project BE535.

Chapter 3 presents the Task 2 data analysis of the bridges screened from the FDOT bridge inventory for the BEB13 project and outlines the development of the suite of 35 bridges for the parametric studies. The suite of 35 bridges includes six bridges that satisfy the requirements of Categories 1 and 2 from Project BE535.

Chapter 4 discusses key LGA and 3D FEA modeling idealizations and identifies key bridge responses that constitute the behavior of skewed I-girder bridges. In addition, considerations related to the load and response calculations for the parametric studies are explained in this chapter. These discussions provide a detailed explanation of the processes and procedures used in Task 3 of the project.

Chapter 5 compiles the measures of differences employed in the comparison of LGA and 3D FEA results and explains the organization of electronic bridge data files that list detailed comparison plots for key bridge responses.

Chapter 6 focuses on detailed comparisons of the LGA and 3D FEA results, considering each of the key bridge responses, that is, the results from the efforts in Tasks 3 and 4.

Chapter 7 summarizes the specific findings and recommendations from this research, emphasizing improvements to the design guidance developed in Project BE535. Contributions of this research to the state-of-the-art of straight skewed I-girder bridge design are highlighted.

2. LITERATURE REVIEW

Project BE535 provided an extensive literature review on the behavior of straight skewed I-girders bridges and various aspects related to its analysis and design. This chapter aims to add to the literature review conducted by Project BE535. The findings of Project BE535 are the most relevant to the current project and hence are addressed in this chapter. The other key recent research relevant to the current project is NCHRP Project 12-113 (Reichenbach et al. 2021). The next two sections review and summarize the findings and observations from these two research studies.

2.1 FDOT Project BE535

Project BE535 aimed to improve the understanding of the behavior of straight steel I-girder bridges having skew indices up to and slightly larger than 0.3 and to evaluate the applicability of LGA in lieu of 3D FEA for these bridges. To achieve this goal, comparative parametric 3D FEA and LGA studies were conducted on a suite of 26 bridges. This section is organized into sub-sections that succinctly explain the key aspects of Project BE535.

2.1.1 Bridge Matrix

The bridges for Project BE535 were configured from a suite of 57 bridges sampled from the FDOT bridge inventory. Key response quantities studied included:

1. Girder positive and negative Strength I (STR I) major-axis bending moments;
2. Girder STR I vertical shear forces;
3. Girder HL-93 live load shear forces, focusing in particular on the live load shear forces at the obtuse corners of the bridge spans;
4. Girder STR I bearing reactions for the exterior girder at 1) obtuse corners at end bents, and 2) piers for continuous-span bridges;
5. Girder total dead load vertical displacements, necessary for cambering of the girders, including consideration of the effects of steel dead load fit (SDLF) detailing of the cross frames;
6. Girder concrete dead load vertical displacements, considering both staged and unstaged deck placement;
7. Girder layovers under the total dead load, which for SDLF detailing of the cross frames are equal to the girder layovers under the concrete dead load;
8. Girder fatigue live load vertical shear forces;
9. Girder fatigue live load flexural stresses;
10. Girder flange lateral bending stresses;
11. Cross-frame and diaphragm forces;
12. Exterior girder LLDFs, considering the conservatism of lever rule and rigid cross-section analysis procedures; and
13. Girder live load deflections.

The suite of 26 bridges represented a gamut of skewed bridges having simple- and continuous-span designs, parallel and nonparallel skew, cross frames parallel to the skew or perpendicular to the girders, contiguous and staggered cross-frame layouts, uniform and nonuniform girder spacing, and girder splay. The 26 bridges were comprised of 20 existing bridges and six bridges that were redesigned using cross-frame arrangements with recommended offsets and staggers as per AASHTO LRFD 9th Edition (AASHTO 2020) and NCHRP 20-07/ Task 355 (White et al. 2015) with the following key considerations:

- Stagger the cross frames within the spans.
- Avoid framing cross frames into bearing locations.
- Frame cross frames or diaphragms along the bearing line at pier supports and offset intermediate cross frames relative to the bearing line.
- For continuous-span bridges, provide diaphragms/cross frames along the bearing lines with no intermediate cross frames framing into the bearing line.

The cross-frame framing arrangements were redesigned to relieve stiff load paths that develop in skewed bridges in the transverse direction, and to maximize the applicability of LGA. Two of the 26 bridges had cross frames arranged parallel to skew. The suite included 21 parallel skew bridges (including two splayed girder bridges) and five nonparallel skew bridges. The skew angles ranged from 10° to 59° and skew indices varied from 0.15 to 0.46. A large proportion of the study bridges in Project BE535 had bridge deck widths larger than 60 ft.

2.1.2 Bridge Categorization

It was found that the accuracy of LGA procedures, with respect to 3D FEA methods, depends on a complex combination of structural attributes. Three of the predominant attributes are:

- The skew index,
- The skew angle of the bearing lines, and
- The framing arrangement of the cross frames and/or diaphragms.

The results demonstrated that routine LGA models, using equal distribution of dead loads to the girders and established AASHTO (2020) LLDFs, provide a fast and sufficient solution for straight steel I-girder bridges with $I_s \leq 0.45$ and $\theta \leq 50°$ within certain qualifications. Three bridge categories were recommended to streamline design using LGA. The three categories are summarized in Table 1 and are reiterated below along with design recommendations.

Category 1 – Parallel skew bridges with $\theta \leq 20°$, and with contiguous intermediate cross-frame lines oriented parallel to the skew. For bridges in this category:

- The girder design demands are calculated directly from the recommended LGA procedures without application of any further adjustment factors.
- The estimated girder flange lateral bending stresses due to skew effects are taken equal to zero.
- The force demands on the intermediate cross-frame lines are relatively large due to their contiguous attribute; however, the force demands on the bearing line cross frames are relatively small.

Category 2 – Parallel skew bridges with $\theta \leq 50°$ and $I_s \leq 0.3$, cross frames oriented perpendicular to the girders. For bridges in this category:

- An additional multiplicative adjustment factor of 1.10 is recommended for calculation of the fascia girder bearing reactions at obtuse corners of the spans at end abutments and at the piers in continuous-span bridges. This is in addition to the application of the AASHTO LRFD skew correction factor for the girder shears to the bearing reactions.
- Estimated non-zero girder flange lateral bending stresses due to skew effects are applied at offsets and staggers in the cross-frame framing arrangements. Different estimates are applied for interior and exterior girders, and the estimated stresses are smaller for AASHTO recommended offsets (i.e., larger than $4b_f$) versus smaller offsets.

7

- The cross-frame force demands are influenced significantly by the cross-frame framing arrangements. The attributes of the framing arrangements include: 1) whether the intermediate cross frames are contiguous or staggered, 2) the magnitude of the offsets provided between adjacent intermediate cross frames, and 3) the magnitude of the offsets provided between intermediate cross frames and bearing lines containing cross frames.

Category 3 – Parallel skew bridges with $\theta \leq 50°$ and $0.30 < I_s \leq 0.40$, or with $\theta \leq 30°$ and $0.40 < I_s \leq 0.45$.

- It was found that the above design requirements could also be applied for the Category 3 bridges. The primary reason for the separate Category 3 was that the LGA results tend to be slightly less accurate for the bridges in this category compared to those for the bridges in Categories 1 and 2.

The research showed that the limits of applicability of LGA for bridges with nonparallel skew (differences in skew between the bearing lines larger than 10°) would need to be more restrictive; however, the scope of the studies was insufficient to identify these limits.

The following sub-sections concisely explain the reasoning behind the design guidance established for the three bridge categories.

2.1.3 Comparison of LGA and 3D FEA Estimates

The comparative studies conducted in the BE535 research showed that routine LGA estimates of girder maximum STR I bending moments tended to be conservative for the bridges studied. The STR I load combination consisted of noncomposite loads, loads applied long-term to the composite structure, and live loads applied as short-term transient loads to the composite structure. Live load was commonly the largest contributor to the STR I bending moments for the bridges studied. The LGA procedures studied used the AASHTO LLDFs in the estimation of bending moments. The LGA estimates for live load bending moments tended to be conservative when compared to 3D FEA estimates. Hence, LGA values for the STR I bending moments tended to be conservative compared to 3D FEA in most cases.

Larger differences between LGA and 3D FEA estimates were observed for STR I shear forces. The comparative studies show that LGA estimates of girder maximum STR I shear forces are less than 10% unconservative for all the bridges studied. The maximum shear forces were typically observed at girder ends at the obtuse corners of spans. The bearing line cross frames aligned along the skew tend to twist the girders to maintain compatibility of displacements, thus developing a torsional moment that tends to increase the load transferred at the obtuse corners and decrease loads at the acute corners. These effects drive additional shear forces at the ends of girders near the obtuse corners. However, it was observed that a cross-frame framing arrangement with adequate staggers reduced the amount of shear at obtuse corners.

BE535 compared LGA and 3D FEA estimates for the total dead load vertical displacement. Many of the bridges considered in the parametric studies had difficulties in satisfying the recommended tolerances because 1) the total dead load displacement estimates do not have the benefit of offsetting conservative live load estimates, which is the case in evaluating the STR I bending moment and shear force quantities; and 2) conservative displacement estimates can be as difficult of a problem as unconservative displacement estimates. Conservative total dead load displacement estimates can result in over-cambering of the girders while unconservative total dead load displacement estimates can result in under-cambering of the girders. However, the bridges that satisfied the I_s and θ limits from any of the three LGA design categories tended to have acceptable LGA predictions of their total dead load displacements.

8

BE535 evaluated the bearing reactions for the STR I load combinations. The STR I reactions from 3D FEA at the bearings on the fascia girders corresponding to obtuse corners at abutments, and all the pier bearings on the fascia girders of continuous-span bridges, were observed to be measurably larger compared to the corresponding LGA reactions. This occurred both at end abutments and at pier bearing lines in continuous-span bridges, since the intermediate bearings correspond to an obtuse corner on one of the spans and an acute corner on the other span on both sides of the bridge cross-section. The study concluded that for bridges within Categories 2 and 3, the STR I bearing reaction on the fascia girder can be predicted accurately-to-conservatively in all cases, where LGA is permitted, by multiplying the corresponding reaction from LGA for the fascia girder at the obtuse corners at end abutments and at the piers in continuous-span bridges by a correction factor of 1.10. This multiplicative factor was in addition to the application of the live load skew correction factor of AASHTO (2020) LRFD Article 4.6.2.2.3c to these reactions. No modifications were required for the girder reactions at other locations. In addition, even after multiplying the fascia girder reactions by the 1.10 factor, the largest reaction may still occur at a location other than the fascia girder bearing. For load combinations other than STR I involving HL-93 loading, and where LGA would be employed, namely SER II and STR V, the ratio of the factored live load to the factored dead load is smaller than for STR I. The need for the 1.10 correction factor was primarily due to the demands from the HL-93 live load. Therefore, it was concluded that the 1.10 multiplicative correction factor may also be applied to the live load portion of the SER II and STR V load combinations as a sufficient approximation. For load combinations other than STR I, it was recommended that the 1.10 correction factor may be applied only to the live load reaction for the fascia girder at the obtuse corners at end abutments and at piers in continuous span bridges, for Category 2 and 3 bridges. The 1.10 multiplicative factor was not required for Category 1 bridges.

2.1.4 Estimation of Flange Lateral Bending Stresses

Recommendations were provided for improved design calculation of girder flange lateral bending stresses. The recommendations for flange lateral bending needed to be more nuanced than the current AASHTO (2020) recommendations because the location and magnitude of maximum girder flange lateral bending stresses are heavily influenced by the type of framing arrangement employed. Article C6.10.1 provides the following rules for a simple upper-bound estimate of the girder flange lateral bending stresses from the skew effects, when LGA is employed:

1. The total unfactored flange lateral bending stress in a girder flange at a cross frame or diaphragm at or near supports, when discontinuous (e.g., staggered) cross frames or diaphragms are used at these locations, may be taken as:
    a. 7.5 ksi for exterior girders.
    b. 10 ksi for interior girders.

    These values are intended as estimates of the flange lateral bending only at discontinuous cross-frame lines in the vicinity of supports. They are not intended as estimates at other locations within the span length. In addition, for all skewed bridges other than those that fall within Category 1, a "discontinuity" or "stagger" in the vicinity of the supports implies that the cross-frame line is not framed directly into the support but rather ends at a certain offset from the bearing line.

2. In regions of the girders where the cross frames or diaphragms are contiguous, flange lateral bending from the skew effects need not be considered (i.e., the flange lateral bending stresses may be taken equal to zero in these regions).

3. The total unfactored flange lateral bending stress in a girder flange at locations within a span other than at or near supports, when cross frames or diaphragms are placed in discontinuous lines (e.g., staggered) throughout the bridge span, may be taken as:
   a. 2.0 ksi for exterior girders.
   b. 10 ksi for interior girders.

The current guidance in the AASHTO (2020) LRFD Article C6.10.1 was refined to consider the influence of cross-frame offsets or staggers greater than or less than $4b_f$, where b_f is the largest flange width within the unbraced lengths on either side of a given cross frame. The recommendations are shown in Table 2. The value $4b_f$ is a current AASHTO (2020) LRFD recommended minimum stagger or offset value. Offsets or staggers smaller than $4b_f$ are allowed but tend to result in larger flange lateral bending stresses.

Table 2. Summary of Project BE535 recommended estimates of the unfactored flange lateral bending stresses, f_t.

Bridge Category	Cross-frame Framing Arrangement	Orientation of Intermediate Cross frames	Girder	Location	f_ℓ (ksi) for O_{min}/b_f < 4	f_ℓ (ksi) for $O_{min}/b_f \geq 4$	f_ℓ (ksi) from AASHTO C6.10
1	Contiguous	Parallel to skew	Exterior and Interior	All	0	0	0
2/3	Contiguous	Perpendicular to girders	Exterior	At or near supports	8	4	7.5
2/3	Contiguous	Perpendicular to girders	Exterior	Throughout the span	0	0	0
2/3	Contiguous	Perpendicular to girders	Interior	At or near supports	10	5	10
2/3	Contiguous	Perpendicular to girders	Interior	Throughout the span	0	0	0
2/3	Staggered	Perpendicular to girders	Exterior	At or near supports	8	4	7.5
2/3	Staggered	Perpendicular to girders	Exterior	Throughout the span	3	2	2
2/3	Staggered	Perpendicular to girders	Interior	At or near supports	10	5	10
2/3	Staggered	Perpendicular to girders	Interior	Throughout the span	15	10	10

Additionally, the current Article C6.10.1 requirement, which states that the estimated nominal flange lateral bending stresses should be proportioned to the dead and live load in the same proportion as the unfactored major-axis dead and live load stresses at the cross section under consideration, was replaced by recommended weighted-average load factors for different load combinations (Table 3). This recognized that the coarseness of the flange lateral bending estimates does not merit an elaborate manual calculation.

Table 3. Project BE535 recommended weighted average load factors for estimation of girder flange lateral bending stresses due to skew effects in straight I-girder bridges.

Load Combination Limit State	Weighted Average Load Factor Applied to Article C6.10.1 Coarse Estimate of f_ℓ
Strength I	1.6
Strength II	1.3
Strength III	1.3
Strength V	1.3
Additional load combination for DC + construction loads, Article 3.4.2.1	1.4
Service I	1.0
Service II	1.2
Fatigue I	1.75
Fatigue II	0.8

2.1.5 Evaluation of Cross-Frame Forces

Comparable coarse upper-bound estimates of bridge cross-frame and diaphragm forces due to skewed geometry effects were recommended to be calculated as percentages of the maximum girder moments and shears obtained from LGA. The estimates are summarized in Table 4. The lowest percentages correspond to common stability bracing strength requirements. Larger percentage estimates are provided as a function of the cross-frame/diaphragm framing arrangements, keyed to the recommended $4b_f$ offset or stagger distance discussed above. The cross-frame components should be designed to resist these forces either in tension or in compression. These values were determined by the evaluation of 3D FEA results for the bridge system effects associated with skew.

The force quantities in Table 4 were defined as follows:

$V_{max.ICF}$ = maximum magnitude of the intermediate cross-frame shear force throughout the bridge span.

$V_{max.BCF}$ = maximum magnitude of the bearing line cross-frame shear force.

$B_{max.cn.ICF}$ = maximum magnitude of the intermediate cross-frame connection horizontal force at the level of the cross-frame bottom chord throughout the bridge span, equal to the maximum magnitude chord force at locations where no cross-frame diagonals frame into the connection plates, and equal to the sum of the maximum magnitude chord force plus the horizontal component of the maximum magnitude diagonal axial force at locations where cross-frame diagonals frame into the connection plates.

$T_{max.cn.ICF}$ = maximum magnitude of the intermediate cross-frame connection horizontal force at the level of the cross-frame top chord throughout the bridge span, equal to the maximum magnitude chord force at locations where no cross-frame diagonals frame into the connection plates, and equal to the sum of the maximum magnitude chord force plus the horizontal component of the maximum magnitude diagonal axial force at locations where cross-frame diagonals frame into the connection plates.

$B_{max.cn.BCF}$ = maximum magnitude of the bearing line cross-frame connection horizontal force at the level of the cross-frame bottom chords, equal to the maximum magnitude chord force at locations where no cross-frame diagonals frame into the connection plates, and equal to the sum of the maximum magnitude chord force plus the horizontal component of the maximum magnitude diagonal axial force at locations where cross-frame diagonals frame into the connection plates.

$T_{max.cn.BCF}$ = maximum magnitude of the bearing line cross-frame connection horizontal force at the level of the cross-frame top chords, equal to the maximum magnitude chord force at locations where no cross-frame diagonals frame into the connection plates, and equal to the sum of the maximum magnitude chord force plus the horizontal component of the maximum magnitude diagonal axial force at locations where cross-frame diagonals frame into the connection plates.

$V_{max.g}$ = maximum magnitude of the girder vertical shear force throughout the bridge span or spans under consideration, due to the force effect under consideration. The shear is determined using LGA with the assumption that the dead loads are equally distributed to all girders. For force effects that include live loads, the LGA analysis is based on the AASHTO LLDF procedures, including the skew correction factor.

$M_{max.g}$ = maximum magnitude of the girder major-axis bending moments (positive or negative) throughout the bridge span or spans under consideration, due to the force effect under consideration. The moment is determined using LGA with the assumption that the dead loads are equally distributed to all girders. For force effects that include live loads, the LGA analysis is based on the AASHTO LLDF procedures (no skew reduction included).

h_{cf} = for the bridge in its composite condition, the distance between the mid-thickness of the bridge deck and the centroid of the cross-frame bottom chord; for the bridge in its noncomposite condition, the distance between the cross-frame chords.

For design of solid-web diaphragms, it was recommended that the diaphragm connections be designed for the shear force plus the sum of the above cross frame bottom and top connection forces applied as a concentric axial force to the diaphragm connections and members, and that h_{cf} should be taken as the distance between the mid-thickness of the bridge slab and the centroid of the solid-web diaphragm. This provided an estimate of the force effects induced in the diaphragm associated with its combined action with the composite bridge deck.

For design evaluation of solid-web diaphragms during construction, it was recommended that the diaphragms be sized for the above shear forces plus the moments at the diaphragm connections equal to the values obtained by applying the top and bottom chord factors in the DC1 & Constr. column of Table 4 directly to the girder moments (the top and bottom chord factors are all the same in this column; a typographical error is corrected in the DC1 & Constr. column of the table from the BE535 project report - the top and bottom chord factors for case 2i are both taken equal to 0.03).

Table 4. Cross-frame shears and chord level connection horizontal forces due to skew effects.

Cross-Frame Case	Load Effect	DC1 & Constr	DC2	DW	HL-93 LL	STR I & SER II	Fatigue LL[*]
1i[a] Shear	$V_{max.ICF}/V_{max.g}$	0.02	0.40	0.03	0.06	0.03	0.06
1i[a] Bottom Chord	$B_{max.cn.ICF}/(M_{max.g}/h_{cf})$	0.02	0.20	0.02	0.06	0.03	0.05
1i[a] Top Chord	$T_{max.cn.ICF}/(M_{max.g}/h_{cf})$	0.02	0.20	0.02	0.05	0.02	0.05
2i[b] Shear	$V_{max.ICF}/V_{max.g}$	0.06	1.20	0.06	0.20	0.09	0.14
2i[b] Bottom Chord	$B_{max.cn.ICF}/(M_{max.g}/h_{cf})$	0.03	0.60	0.04	0.14	0.08	0.12
2i[b] Top Chord	$T_{max.cn.ICF}/(M_{max.g}/h_{cf})$	0.03	0.40	0.02	0.08	0.04	0.08
1b[c] Shear	$V_{max.BCF}/V_{max.g}$	0.02	0.07	0.02	0.02	0.02	0.02
1b[c] Bottom Chord	$B_{max.cn.BCF}/(M_{max.g}/h_{cf})$	0.02	0.04	0.02	0.02	0.02	0.02
1b[c] Top Chord	$T_{max.cn.BCF}/(M_{max.g}/h_{cf})$	0.02	0.10	0.02	0.03	0.02	0.04
2b[d] Shear	$V_{max.BCF}/V_{max.g}$	0.04	0.12	0.06	0.06	0.04	0.06
2b[d] Bottom Chord	$B_{max.cn.BCF}/(M_{max.g}/h_{cf})$	0.02	0.14	0.02	0.08	0.05	0.07
2b[d] Top Chord	$T_{max.cn.BCF}/(M_{max.g}/h_{cf})$	0.02	0.14	0.02	0.03	0.02	0.05

[*] *The fatigue live load calculation pertains to the force range and uses the corresponding maximum range of $V_{max.g}$ and $M_{max.g}$ from LGA.*

a:1i refers to intermediate cross-frames using offsets and staggers greater than or equal to 4bf throughout the span

b:2i refers to contiguous intermediate cross-frames, or intermediate cross-frames with any offsets and staggers less than 4b_f within the span

c: 1b refers to bearing line cross-frames where the offset of intermediate cross-frames relative to the bearing line is greater than or equal to 4b_f

d:2b refers to bearing line cross-frames where the offset of intermediate cross-frames relative to the bearing line is smaller than 4b_f

2.1.6 Evaluation of AASHTO LLDF for Exterior Girders

The NCHRP Project 12-26 report (Zokaie et al. 1991) explained the development of the base empirical equations to calculate LLDFs listed in AASHTO Articles 4.6.2.2.2 and 4.6.2.2.3. However, the NCHRP 12-26 study was conducted for bridges without cross frames or diaphragms. Cross frames and diaphragms typically increase the moments in exterior girders and decrease the moments in interior girders; that is, they further tie the girders together such that the girders and cross frames act as a 3D unit. Hence, RCA is required in the AASHTO (2020) procedures for the determination of fascia girder LLDF, with an intent to avoid potential unconservative LLDF estimates in cases where the bridge girders are "well-connected" by cross frames across the bridge width. Furthermore, for single-lane live load cases, AASHTO (2020) uses the lever rule for calculation of the base moment and shear LLDF on the exterior girders along with also performing the RCA. AASHTO requires that the larger of the lever rule and RCA values should be used in designing for single-lane loadings, such as the fatigue loading case.

The BE535 study found that the LLDF obtained from single lane lever rule is the largest for most of the bridges. However, it was found that the LLDF obtained from RCA is larger than the LLDF obtained from the lever rule and governs for relatively narrow bridges.

2.2   NCHRP Report 962

Steel I-girder bridges are highly indeterminate structural systems often consisting of I-girders, a concrete deck, and cross frames. The behavior of girders in the noncomposite and composite conditions is well understood and methods such as LGA provide reasonable estimates for the design of I-girders in many cases. The behavior of cross frames, however, is not well understood. Cross frames serve a number of critical functions in steel bridges, such as:

- During construction: provide stability bracing, torsional restraint to fascia girders, load path for wind loading, etc.
- During service: provide stability bracing in negative moment regions, distribute live loads between different girders, control differential deflection and girder layovers.
- During re-decking and/or widening: provide stability to partially completed structure

Hence, cross frames serve different functions in the noncomposite and composite conditions and as such, it is challenging to establish simplified design estimates for cross frames. It becomes more challenging in the case of straight skewed I-girder bridges because additional forces are induced in cross frames due to skew. NCHRP Report 962 documents the research performed under NCHRP Project 12-113 aimed at addressing some of the knowledge gaps in analysis and design of cross frames with respect to: 1) fatigue loading criteria, 2) analysis procedures, and 3) stability bracing requirements. The next few sections explain the aspects of NCHRP Project 12-113 that are the most relevant to Project BEB13. Henceforth, in this section, the NCHRP Project 12-113 research team is simply referred to as the research team unless noted otherwise.

2.2.1 Field Studies

The research team performed field experiments on three bridges: a straight three-span continuous bridge, a straight skewed three-span continuous bridge and a curved four-span continuous bridge. Following the field studies, a parametric FEA study of 4104 steel I-girder bridges was conducted. The bridge dataset was generated by varying parameters related to bridge geometry, such as number of spans, number of girders, support skew, radius of curvature, cross-frame framing layout and arrangement, and girder cross sections. The bridge dataset represented a wide range of I-girder bridges in the United States.

Select cross frames and girder bottom flanges near the cross frames were instrumented for the three bridges. Controlled live load tests were performed. Measurements of cross-frame stresses, girder flange stresses, and select girder displacements were recorded during the controlled tests. The field-measured results from the tests were used to validate the detailed FEA models. Additionally, continuous strain histories over a four-week period were recorded and processed into stress range histograms. The measured spectra were used to examine the AASHTO fatigue load model. The current fatigue model was calibrated to address girder response; however, it does not explicitly address cross-frame response to fatigue loading (Modjeski and Masters 2015).

AASHTO (2020) Article 3.6.1.4.3a states, "Where the bridge is analyzed by any refined method, as specified in Article 4.6.3, a single design truck shall be positioned transversely and longitudinally to maximize the stress range at the detail under consideration". To satisfy this requirement, the research team analytically studied the response of bridges by defining lanes in which the fatigue truck can travel longitudinally but are held transversely fixed. Such lanes were assumed to simulate realistic traffic conditions. Different lane passages were considered in transverse increments of 1 ft. The research team classified the lane passages closest to the barriers as overhang loads (i.e., truck passages where one of the transverse wheel lines falls outside the centerline of the exterior girders). All other truck passages were classified as non-overhang loads. Overhang loads were expected to occur less frequently than non-overhang loads during the life of a bridge.

The research team found that the maximum cross-frame forces occur in four regions:

1. Interior cross-frame bay nearest to the end support
2. Interior cross-frame bay closest to the point of maximum positive dead load moment
3. Edge cross-frame bay closest to the point of maximum positive dead load moment
4. Interior cross-frame bay nearest to the intermediate support

In the context of an example two-span continuous bridge, the four regions are shown in Figure 1.
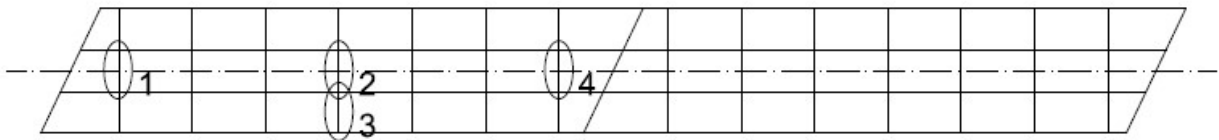
Figure 1. Regions of cross frames having maximum forces in a two-span continuous straight skewed bridge.

It was found that cross frames are sensitive to transverse truck placement. For cross frames in Regions 1 and 2, the longitudinal load influence tends to be localized. In the context of skewed bridges, it was found that the overhang loads represent a large percentage of critical truck passages especially for cross frames in Regions 3 and 4. Furthermore, the maximum forces were observed in the bottom chords at these locations.

Directly relevant to the BEB13 project, NCHRP Project 12-113 quantitatively validates that:

- The fatigue cross-frame force range has a positive correlation with skew index. In other words, the force range increases with increasing skew index.
- Staggering cross frames in the cross-frame layout according to the guidance provided in AASHTO (2020) Article C6.7.4.2 tends to reduce the overall cross-frame force range. This is attributed to the stiffness reduction associated with the discontinuous framing layout.

- A positive correlation is obtained between the number of girders and cross-frame force range. The number of girders is proportional to the bridge width; hence it can be concluded that the cross-frame force range increases with increasing bridge width. The positive correlation with bridge width is also related to the fact that the larger bridge width increases the eccentricity of overhang fatigue load that amplifies the cross-frame force demands.

2.2.2 Cross-Frame Fatigue Design

NCHRP Project 12-113 compares the AASHTO fatigue load model to the measured loading conditions obtained from field testing bridges. This was achieved by calculating the design stress range and comparing the calculated stress range to the stress range obtained after processing data obtained from the instrumentation. It was found that the analytical results significantly exceeded the measured results obtained from the instrumentation. This further points towards the AASHTO fatigue loading being conservative for the design of cross frames. Hence, the research team investigated the fatigue load factors in the context of cross frames and found that an adjustment factor of 0.65 for both the Fatigue I and Fatigue II limit states meets or exceeds the reliability target of unity for each detail category. This gives a load factor of 0.65x1.75=1.14 for Fatigue I limit state and a load factor of 0.65x0.8=0.52 for the Fatigue II limit state.

It should be noted that the adjusted load factors apply to the design of cross frames and associated details only. Fatigue design for girders remains unchanged. Flange lateral bending stresses that develop in girders are closely related to forces developed in cross frames. Traditionally, flange lateral bending stresses are calculated using the assumption of equilibrium between girder flange lateral bending and cross-frame forces. The adjustment of Fatigue I and II load factors in the fatigue design of cross frames leads to the question of "Which load factors are more appropriate to be used in the calculation of flange lateral bending?". The argument of equilibrium noted earlier indicates that the adjusted load factors would be more appropriate. The researchers were questioned regarding this consideration during the presentation of a corresponding 2021 AASHTO Bridge Committee Agenda Item. Their recommendations are that there should be no change from the procedures in the AASHTO 9th Edition Specification for the calculation of all stress quantities for girder design.

Additionally, the research team re-evaluated Fatigue II cross-frame demand-to-capacity ratios for various bridge types (with respect to the high-volume truck traffic in Houston) using reduced load factors. It was observed that load-induced fatigue problems are potential issues in moderately to heavily skewed bridges (i.e., bridges that have skew indices larger than 0.15). Hence, they recommended that design for load-induced fatigue needs to be considered for skewed bridges having skew indices larger than 0.15. In the resulting LRFD Section C6.7.4.1 guidance balloted and approved by the AASHTO Bridge Committee at their July 2021 meeting (AASHTO 2021), the recommendation is that refined analysis is warranted for "… skewed bridges for which $I_s > 0.3$, or curved and skewed bridges for which $I_c > 0.75$ and $I_s > 0.15$" (where I_c is a "connectivity parameter" related to curved I-girder bridge construction). Article C6.7.4.1 also states that "For bridges that do not exceed the limits outlined above, the minimum design requirements specified herein and in Article 6.7.4.2.1 should be applied at a minimum." The balloted and approved Article 6.7.4.1 indicates that diaphragms and cross frames should be designed considering:

- Transfer of lateral wind loads;
- Forces due to overhangs, particularly during concrete placement;
- Provision of stability bracing controlling twist of the noncomposite girder during critical stages of construction (new provisions for stability bracing requirements are provided in Article 6.7.4.2.2);
- Provision of stability bracing in regions of the girders where the bottom flange is subject to compression at the strength limit state, by controlling lateral movement of the bottom flange or

twist of the girder (Article C6.7.4.2.2 subsequently states, "… the stability bracing requirements for cross-frames or diaphragms are not considered to be critical for the design of the composite structure at the strength limit state.);

- Consideration of any flange lateral bending effects; and
- Distribution of vertical dead and live loads applied to the structure.

However, Article C6.7.4.1 also states, "Force demands in intermediate diaphragms or cross-frames, particularly those related to live loads on the completed structure, are generally small in straight I-girder bridges with normal supports or limited skews, as discussed below [referring to discussion including the above quote indicated refined analysis is warranted for straight skewed bridges with $I_s > 0.3$]. As such developing a refined analysis model to obtain diaphragm or cross-frame design forces for these simple bridge geometries is not typically warranted."

Therefore, the most current guidance balloted and approved for the AASHTO LRFD Specifications suggests that the evaluation of cross-frame and diaphragm forces due to skew effects is not warranted for $I_s \leq 0.3$. However, the last two bullet items in the Article 6.7.4.1 list implies the cross-frame and diaphragm forces due to skew effects should be considered.

It is submitted that the research in BE535 and BEB13 focusing on straight skewed I-girder bridges, with I_s up to and slightly larger than 0.3, is directly relevant in clarifying the importance of the force effects due to moderate skew, and when these force effects may be considered to be negligible.

2.2.3 Cross-Frame Stiffness Reduction Factor

Cross frames are commonly modeled as concentric truss elements in 3D FEA software. However, single angle members commonly used in cross frames connect eccentrically to gusset plates. AASHTO (2020) LRFD Article C4.6.3.3.4 recommends a stiffness reduction factor of 0.65 to account for the reduced axial stiffness due to the eccentric connections. The stiffness reduction factor is also called an R-factor. The NCHRP 12-113 research team conducted an R-factor study to assess stiffness reduction factors in the context of composite in-service bridges. A parametric study was conducted where FEA models of composite bridges were built in Abaqus using truss elements with different R-factors. Cross-frame forces obtained were compared to a benchmark solution of the same bridge where the cross frames were modeled using shell elements. The loading applied in the FEA was based on the AASHTO fatigue truck traversing the bridge in the critical lane. The correct R-factor is the one that gives the same cross-frame force as the benchmark shell model. In general, different R-factors were obtained for the top chord, diagonals, and bottom chords. Considerable scatter was observed in the data obtained from the parametric study. However, the research team decided to find a single R-factor from the studies that provides conservative estimates of cross-frame forces for 75% of the bridges. For the remaining 25% of the bridges, estimates obtained from the truss element idealization were found to be within 10% of the benchmark solution. It should also be noted that the R-factor of 0.75 is based on the use of ½ inch thick gusset plates. Using a larger gusset plate will yield a larger R-factor and vice versa. In addition, the R-factor of 0.75 was based on a study of composite bridges. Hence, the research team recommended the use of two separate R-factors: 0.65 for noncomposite construction stages and 0.75 for in-service conditions.

2.2.4 Stability Bracing Force and Stiffness Requirements

A stability study was conducted in NCHRP Project 12-113 to investigate the appropriate stability bracing strength and stiffness requirements for bridge systems via finite element parametric studies on twin I-girder systems. A series of buckling analyses on twin I-girder systems with assumed initial imperfections were performed. The objective was to determine stability bracing force and stiffness requirements for

design of cross frames and diaphragms, focused solely on noncomposite DC loads and any construction loads applied to the fully erected steelwork. The bracing strength study examined the relationship between internal girder moment and brace moment for a variety of bracing configurations, girder cross sections and loading conditions. The research found that using the AISC (2016) requirement of design brace moment equal to 2% of the maximum girder moment significantly underpredicted the required brace moments in certain cases. Hence, the research team recommended a form of torsional brace strength equation employed in the prior AISC (2010) Specification

$$M_{br} = \frac{0.036 M_u L}{n C_b L_b}$$

(2)

to determine brace strength, where:

M_{br} = required strength of a torsional brace

M_u = factored major-axis bending moment for the limit-state load combination specified in Article 3.4.1 or 3.4.2.1, as applicable. (In regions of positive flexure, it is recommended that the maximum factored major-axis bending moment within the region should be employed for M_u. In regions of negative flexure, it is recommended that the factored major-axis bending moment at the interior support under consideration should be employed.)

L = span length

n = number of intermediate braces within the span

C_b = moment gradient factor assuming the beam buckles between the brace points

L_b = unbraced length of the critical segment

Equation 2 differs from the prior AISC equation in that it uses a coefficient of 0.036 whereas the prior AISC (2010) equation used a coefficient of 0.024.

Through parametric studies, it was found that by providing three times the ideal brace stiffness, girder deformation at the brace locations at the critical buckling loads were limited to approximately the initial twist imperfection, θ_o (a total twist rotation of $2\theta_o$). Conversely, the traditional requirement to provide twice the ideal stiffness is better suited to columns. Ideal stiffness is defined as the brace stiffness required for a geometrically perfect (i.e., straight) member to reach the applied load level at incipient buckling of the member and its bracing system, and is given by analytical equations as derived by Yura (2001).

Given these findings, the final recommendation for the required torsional brace stiffness is (AASHTO 2021)

$$(\beta_T)_{req} = \frac{3.6L}{\phi_{sb} n E I_{yeff}} \left(\frac{M_u}{C_b} \right)^2$$

(3)

where the additional variables not defined above are:

E = modulus of elasticity of structural steel, taken as 29,000 ksi

I_{yeff} = effective out-of-plane moment of inertia of the girder, taken as I_y for doubly symmetric girders and taken as $I_{yc} + (t/c) I_{yt}$ for singly symmetric girders

I_y = noncomposite moment of inertia about the vertical centroidal axis of the girder section at the brace point under consideration

18

I_{yc} = moment of inertia of the girder compression flange about the vertical centroidal axis at the brace point under consideration

I_{yt} = moment of inertia of the girder tension flange about the vertical centroidal axis at the brace point under consideration

t = distance from the centroid of the girder section to the centroid of the tension flange at the brace point under consideration, taken as a positive value

c = distance from the centroid of the girder section to the centroid of the compression flange at the brace point under consideration

ϕ_{sb} = resistance factor for stability bracing, defined as 0.80 in AASHTO Article 6.5.4.2

In the final recommendations provided in the balloted and approved 2021 AASHTO Agenda Item (AASHTO 2021), the bracing force requirement from Equation 2 has been changed to an equation that is obtained by multiplying the required brace stiffness, with ϕ_{sb} taken equal to 1.0, by the assumed initial twist imperfection, $\theta_o = L_b/500$:

$$M_{br} = \frac{0.008 L L_b}{nEI_{yeff} h_o} \left(\frac{M_u}{C_b} \right)^2 \tag{4}$$

where:

h_o = distance between the flange centroids of the girder section at the brace point under consideration

This equation is based on an elastic analysis of the girder and its bracing system. For typical unbraced lengths corresponding to the final constructed configuration, this equation can give torsional bracing strength requirements that are significantly smaller than $0.02M_u$. Equations (2) and (4) are also defined in the the AISC (2022) Specification, except that these provisions show Equation 4 with the θ_o term explicitly multiplied by the required brace stiffness term. In addition, the AISC provisions require a minimum torsional brace strength of $0.02M_u$. That is, the torsional brace strength equation in AISC (2022) is:

$$M_{br} = \frac{3.6L}{nEI_{yeff}} \left(\frac{M_u}{C_b} \right)^2 \left(\frac{L_b}{500 h_o} \right) \geq 0.02 M_u \tag{5}$$

The bracing design examples in Reichenbach et al. (2021) are all presented in the context of twin-girders connected by a single bay of cross frames or diaphragms. In cases where cross frames are connected to each side of the girder web, the two cross frames share in providing the required stiffness and strength. However, for brace points where the cross frames or diaphragms are connected only on one side, such as fascia girders, only one cross frame is available at the brace points to provide the torsional bracing requirements. The important point here is that the bracing strength and stiffness requirements tend to be conservative for interior girders that are connected to cross frames on each side at a given brace point.

The above equations for the required torsional bracing strength and stiffness are strictly based on the idealized second-order elastic analysis of a nominally straight girder with an initial twist imperfection of θ_o, restrained only against twist at its brace points, subjected to major-axis bending. The other force and stiffness interactions tied to the response of a skewed bridge structural system are not considered. Other

loading effects such as wind, eccentric loads from overhangs, etc. are not considered. AASHTO (2021) Article C6.7.4.2.2 indicates that the stability bracing forces are to be considered as "an independent load effect" (i.e., it is recommended that they be added with other force effects). This is a gross approximation. In typical cases, the cross-frame stiffness is large enough such that the second-order elastic effects associated with the stability bracing strength equation are small and the predominant force effect on the cross frames is approximated sufficiently as the first-order elastic analysis force effect from the relevant bridge loadings. In hypothetical cases in which the stability bracing stiffness requirements are satisfied without any margin of conservatism, the cross-frame or diaphragm forces potentially can be larger than estimated by adding the stability bracing force requirement from Equation 4 to the first-order analysis forces obtained from an analysis of the bridge system.

3. DEVELOPMENT OF PARAMETRIC STUDY BRIDGE MATRIX

3.1 Target Ranges of Key Geometric Parameters

The BEB13 research targets detailed studies of straight bridges having moderately skewed geometries, specifically bridge geometries that are most representative of FDOT bridge inventory. Two of the key geometric variables considered include the bridge width and span length. Appropriate ranges for these study variables may be ascertained from histograms documenting the characteristics of steel I-girder bridges in FDOT inventory. The histograms were provided by the FDOT steering group.

Figure 2 provides a histogram of bridge deck widths for FDOT steel I-girder bridges. Approximately 44% of the bridges have a moderate deck width in the range of 40 to 60 ft, while another 10% of the bridges have a deck width from 60 to 80 ft. Bridges with overall deck width less than 40 ft would have fewer than four girders or would have a relatively narrow girder spacing. Therefore, the targeted range of bridge deck widths selected for Project BEB13 is 40 to 80 ft, with an emphasis on 40 to 60 ft. Minor deviations from this range may occur to accommodate certain parameters (e.g., Category 3 bridges are typically wider structures and may have a deck width larger than 80 ft in some cases; also, a four-girder bridge with 9 ft girder spacing and 3 ft overhangs would have a deck width of 33 ft).
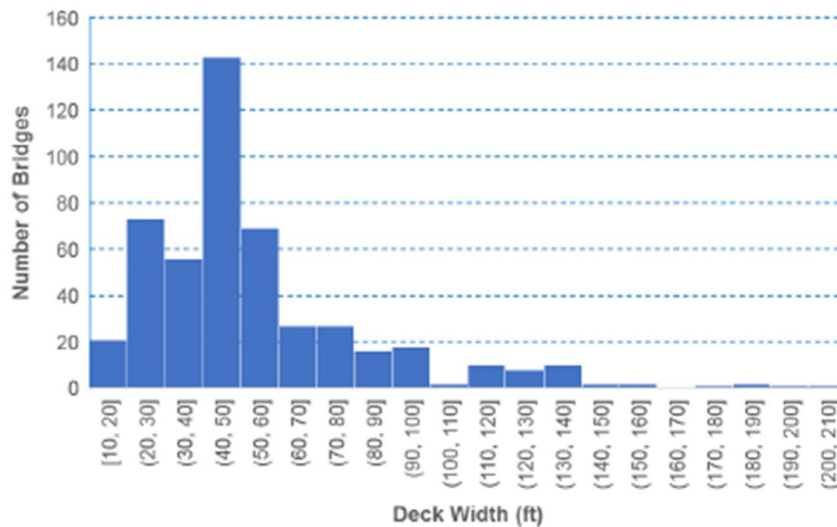
Figure 2. Histogram of bridge deck widths for steel I-girder bridges in Florida (Su et al., 2022).

The framing width, w_g, defined as the width between the fascia girders, is the more fundamental bridge width parameter in this study. For instance, w_g is one of the independent variables in the equation for the skew index. The bounds for framing width may be estimated by assuming a representative deck overhang width of approximately 3.5 ft. Therefore, the target range for the framing width can be taken as approximately 33 to 73 ft.

As noted above, a smaller deck width range of 40 to 60 ft (i.e., a framing width range of 33 ft to 53 ft) is considered to be representative of more moderate bridge geometries. Representative girder spacings adopted in steel I-girder bridge design are 9 ft to 13.5 ft. A four-girder bridge with a girder spacing of 11 ft results in a framing width of 33 ft, while a five-girder bridge using a spacing of 13.5 ft results in a framing width of 54 ft. Therefore, the framing width range of 33 ft to 53 ft (corresponding bridge deck width of

40 to 60 ft) would typically correspond to four to five girders. Hence, a large number of the bridges selected for investigation in Project BEB13 have four or five girder cross sections.

Figure 3 shows a histogram of span lengths for steel I-girder bridges in Florida. Prestressed concrete girder bridges are often more economical for bridge spans up to 125 ft, unless geometric constraints warrant the use of a steel bridge (i.e., curved geometry). The histogram in Figure 3 shows that approximately 72% of the bridges have span lengths in the range of 130 to 250 ft. Further, more than 80% of the Project BE535 bridges that qualified for LGA-based design had span lengths in the range of 130 to 250 ft.
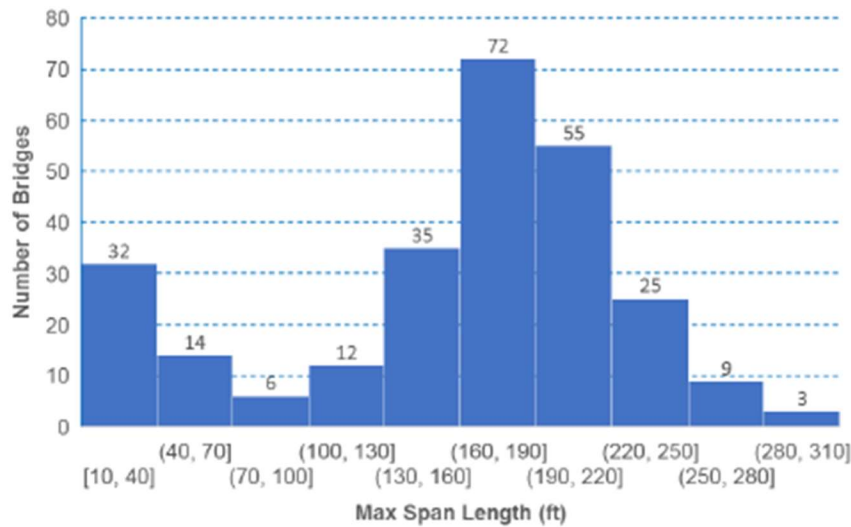
Figure 3. Histogram showing span lengths of steel I-girder bridges in Florida (Su et al., 2022).

Figure 4 shows a histogram of center span lengths of steel I-girder three-span continuous bridges, and Figure 5 shows a histogram of the ratios of end span length to the center span length of steel I-girder three-span continuous bridges. The majority of continuous bridge spans also fall between 130 and 250 ft. In addition, the majority of the three-span continuous bridges have a span ratio between 0.66 and 0.79. Often, three-span continuous bridges are proportioned such that the end spans are equal length and the ratio of the end span to the center span length is approximately 0.78. This ratio makes the maximum positive bending moments in the end and interior spans comparable.
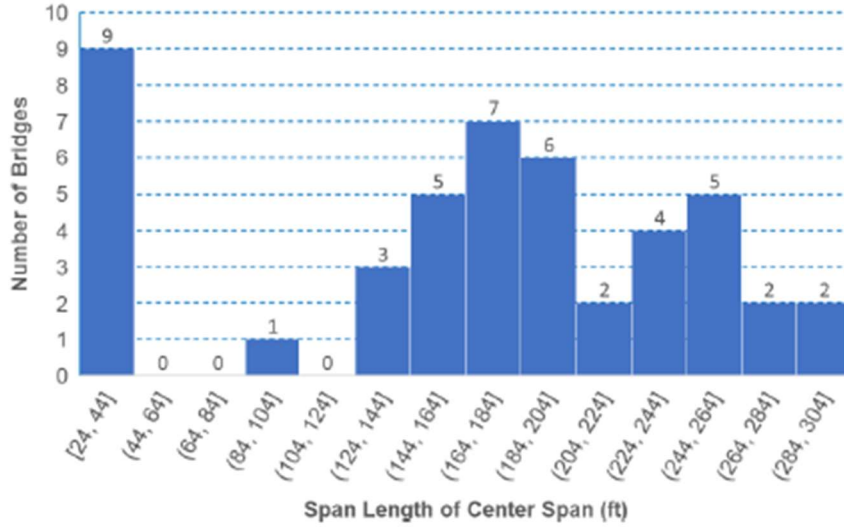
Figure 4. Histogram showing center span lengths of steel I-girder three-span continuous bridges in Florida (Su et al., 2022).
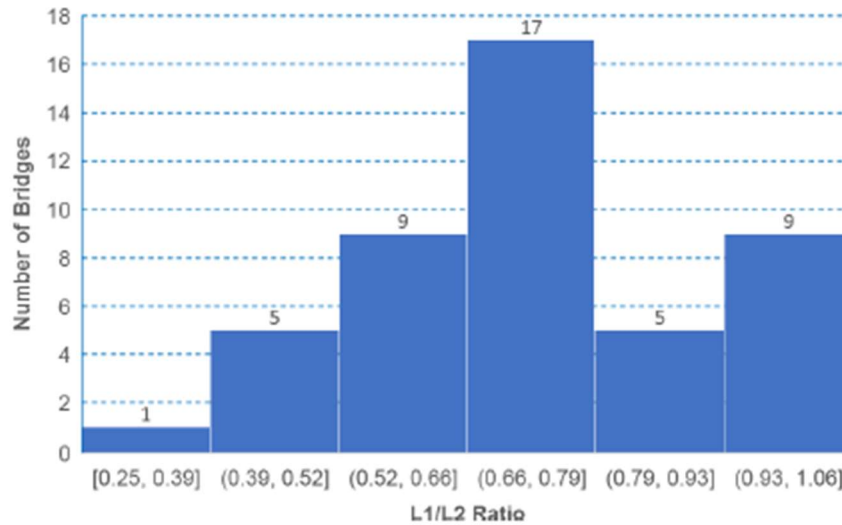
Figure 5. Histogram showing ratios of the end span length to the center span length of steel I-girder three-span continuous bridges in Florida (Su et al., 2022).

3.2   Data Analysis of Bridges Screened by FDOT

The current project (BEB13) targets bridge geometries with more moderate skew effects. The FDOT steering group identified 34 Florida bridges that satisfied this target: 15 two-span continuous bridges and 19 simple-span bridges. Twenty-four of these bridges were screened previously in the BE535 project. These bridges are marked by the prefix "F" and are assigned the number employed in BE535. The *additional* 10 bridges introduced in the BEB13 inventory screening are marked by the prefix "FA" and are numbered sequentially from 1 to 10. These 34 screened bridges are employed as a starting point for the development of a matrix of bridges utilized for the current project parametric studies.

Project BE535 identified the following three essential parameters for characterizing the behavior of straight skewed bridges:

1. Skew index
2. Skew angle
3. Cross-frame framing arrangement

Categories 1, 2, and 3 in Project BE535 were established on the basis of these parameters to identify parallel skew bridges for which the results from LGA are sufficient for design. Each of the BEB13 screened bridges is assigned to one of these categories. In several cases, the parameters of these bridges fall outside of the ranges specified in Table 1. In these cases, the closest category is identified and noted.

Table 5 lists essential data for 14 of the 34 BEB13 screened bridges assigned to Category 1. The skew indices of these bridges vary from 0.02 to 0.10, and the skew angles vary from 5° to 20°. Only Bridges FA4 and F41 have intermediate cross frames aligned parallel to the skew. The other bridges have cross frames perpendicular to the girders. Therefore, strictly speaking, only Bridges FA4 and F41 classify as Category 1. As explained in Section 3.4, the intermediate cross frames of the screened bridges having $\theta \leq 20°$, if not parallel to the bearing lines, are turned parallel to skew when they are considered for the BEB13 Bridge Matrix. Hence, for the purpose of the study, all of these bridges are classified as Category 1. It should also be noted that Bridge FA3 was constructed as a four-girder bridge in 1994 and was widened in 2015 to a seven-girder bridge. The widened bridge is labeled as Bridge FA5 in Table 5.

Table 5. Bridges assigned to Category 1 from the BEB13 screened bridges.

Bridge	I_s*	θ*	w_g (ft)	L_s* (ft)	Bridge Articulation
FA1	0.02	5	34.5	174	Simple
F12	0.03	8	33.8	174	Simple
FA2	0.05	14	33.5	183	Simple
FA3	0.05	20	34.5	263	Simple
FA4[†]	0.06	13	49.1	201	Simple
F16	0.07	19	34.0	172	Simple
F14	0.08	16	54.0	183	Simple
FA5	0.10	20	69.0	263	Simple
F26	0.03	7	48.0	172	2-span cont.
FA6	0.03	7	36.0	172	2-span cont.
F38	0.05	9	44.0	129	2-span cont.
F37	0.06	9	48.0	129	2-span cont.
F41[†]	0.08	18	29.0	115	2-span cont.
F34	0.08	17	40.3	167	2-span cont.

* The skew angles, skew indices, and span lengths are reported for the spans having the largest skew index.
† The intermediate cross frames of this bridge are oriented parallel to skew. All the other bridges in this table actually have cross frames that are perpendicular to the girders.

Table 6 lists 20 of the 34 BEB13 screened bridges that can be classified as Category 2 or 3a bridges. Recall from Section 1.1 that the limit on the skew angle at the bearing lines for Category 2 and 3a bridges is 50°. Bridges F28 and FA7 have skew indices smaller than 0.3, but their bearing lines are skewed at 54°.

Similarly, Bridge FA10 has a skew index of 0.32, but the bearing lines are skewed at 55°. Strictly, Bridges F28 and FA7 would not belong to Category 2, and Bridge FA10 would not belong to Category 3a. These bridges are assigned to the nearest category.

Table 6. Bridges assigned to Categories 2 and 3a from the BEB13 screened bridges.

Bridge	I_s*	θ*	w_g (ft)	L_s* (ft)	Bridge Articulation
F6	0.10	21	48.0	191	Simple
F7	0.10	21	48.0	191	Simple
F19	0.12	24	55.8	198	Simple
F21	0.13	44	33.9	243	Simple
F18	0.14	37	36.0	195	Simple
F17	0.16	44	36.0	218	Simple
F8	0.18	42	33.5	165	Simple
F22	0.18	44	45.1	243	Simple
F11	0.19	42	36.0	172	Simple
F45	0.10	23	30.0	122	2-span cont.
F29	0.11	26	40.3	176	2-span cont.
F46	0.18	40	48.0	217	2-span cont.
F40	0.19	36	52.9	205	2-span cont.
F28$	0.20	54	36.0	251	2-span cont.
FA7$	0.20	54	36.0	251	2-span cont.
F31	0.25	50	51.0	248	2-span cont.
FA8	0.28	40	47.1	144	2-span cont.
F30	0.28	50	58.3	250	2-span cont.
FA9	0.29	44	63.4	207	2-span cont.
FA10¶	0.32	55	37.5	168	2-span cont.

* *The skew angles, skew indices, and span lengths are reported for the spans having the largest skew index.*

$ *This bridge has a skew angle of the bearing lines is larger than 50°, which is outside the ranges of the categories developed by Project BE535. The closest category is Category 2.*

¶ *This bridge has a skew angle at the bearing lines is larger than 50°, which is outside the ranges of the categories developed by Project BE535. The closest category is Category 3a.*

The cross-frame framing arrangement of the 34 BEB13 screened bridges are all contiguous. In addition to contiguous framing arrangements, Project BE535 studied: (1) staggered framing arrangements developed by eliminating every other cross frame from a base contiguous arrangement, herein referred to as a "subway tile stagger" framing arrangement, consistent with recommendations in AASHTO (2020) Article C6.7.4.2; and (2) staggered framing arrangements obtained by arranging cross frames along a line parallel to skew, herein referred to as a "parallel stagger" framing arrangement. Project BE535 demonstrated that the subway tile stagger framing arrangements effectively mitigates transverse load path effects, especially in Category 3 bridges. However, one of the BE535 Category 2 bridges that was close to Category 3 and had a parallel stagger framing arrangement exhibited relatively large flange lateral bending stresses and cross-frame forces. It is anticipated that the behavior

of more moderate Category 2 bridges should not be as sensitive to framing arrangements as Category 3 bridges due to the smaller skew effects. The parallel stagger configuration is common in design practice because it is intuitive to develop. Subway tile stagger arrangements are not as common as parallel stagger framing arrangements. A major focus of the BEB13 project is to study bridge geometries and framing arrangements that are commonplace in bridge practice in the state of Florida. Hence, the BEB13 bridge matrix includes a limited number of the screened bridges modified to employ the parallel stagger framing arrangement.

The 34 BEB13 screened bridges do not include any three-span continuous geometries. Therefore, a number of three-span continuous bridge designs were developed using the NSBA continuous span standard (NSBA 2015) as a starting guide. These designs are described in the following sections. In addition, several simple-span and two-span continuous bridges are designed to cover the selected range of bridge geometries and cross-frame framing arrangements. Category 3 bridges are not studied in this project to facilitate maximum coverage in the range of bridge geometry and cross-frame framing arrangement in Categories 1 and 2.

3.3   Updated Bridge Categorizations for the BEB13 Bridge Matrix

Project BE535 identified and showed that the cross-frame framing arrangement heavily influences the behavior of straight skewed bridges. The matrix of skewed I-girder bridges studied in the current research is subdivided into the following three main groups to draw distinction between different framing arrangements:

- Category 1 bridges, as defined previously in Table 1;
- Category 2 bridges, as defined previously in Table 1, employing a contiguous cross-frame framing arrangement; and
- Category 2 bridges, as defined previously in Table 1, employing a parallel stagger cross-frame framing arrangement.

Names are created for the bridges in each of these groups that describe the category, cross-frame framing arrangement, number of spans, and project bridge number as follows:

1. Category number: 1 or 2.
2. Cross-frame framing arrangement: C for contiguous or P parallel stagger. Note that the Category 1 bridges always have contiguous cross frames.
3. Number of spans: 1 for simple-span bridges, 2 for two-span continuous bridges, and 3 for three-span continuous bridges.
4. Project bridge number: a unique number corresponding to either Project BE535 or BEB13. Bridge numbers up to 26 correspond to bridges carried forward from Project BE535 to Project BEB13 for additional study. In some cases, these have minor modifications of the cross-frame framing arrangement to provide specific improvements. For instance, it was decided based on the evidence cited in Chapter 2 that cross frames should never be connected directly into bearing locations. As such, bridges with this arrangement of the cross frames at the bearing lines were modified to always provide cross frames along the bearing line as well as to offset the first intermediate cross frames from the bearing lines. Bridge numbers 27 and higher correspond to additional bridges studied solely within Project BEB13. For one of the bridges, Bridge 2C2-46, geometry parameters, skew angle, and bridge framing widths, are varied on the same bridge, resulting in versions 46B through 46E.

As an example of the naming convention, Bridge 2C3-47 is a Category 2 bridge with a contiguous cross-frame framing arrangement and a three-span continuous articulation. The bridge is the 47th unique bridge studied at large by the BE535 and BEB13 projects.

The following sections explain the development of the parametric study bridge matrix for the current BEB13 project. The developments are explained for each of the above groupings of bridges, first 1, then 2C, and finally 2P.

3.4   Bridge Matrix Category 1 Bridges

As summarized in Table 1, Category 1 bridges have bearing lines skewed less than or equal to 20° and intermediate cross frames oriented parallel to skew.

The BEB13 matrix of Category 1 bridges consists of 11 bridges from the BEB13 bridge inventory:

- Eight bridges from the BEB13 bridge inventory: five relatively narrow bridges with four or five girders and three relatively wide bridges with six or more girders.
- Bridges 1C1-21 and 1C2-26 from Project BE535.
- An additional two-span continuous bridge, 1C2-50 similar to Bridge 1C2-26 in a number of characteristics but with longer spans that were more representative of welded I-girder bridges.

To maximize the skew effects and characterize the limiting responses as a function of the skew angle, all Category 1 bridges, except BE535 Bridges 1C1-21 and 1C2-26, have bearing lines skewed at 20°, regardless of the skew angle of the corresponding existing bridge. Details of the Category 1 bridges are shown in Table 7. In total, 11 bridges of this type are considered: three simple-span, four two-span continuous, and four three-span continuous. Figures 6 through 16 show the plan sketches for these bridges. Note that the simple-span bridges are listed first, then the two-span continuous bridges, and finally the three-span continuous bridges. This organization is also employed within Categories 2C and 2P.

Bridges 1C1-21 and 1C2-26 from Project BE535 have relatively small skew angles. All the other bridges have θ set to the maximum skew angle for Category 1 (i.e., $\theta = 20°$).

The bridge numbers for the BEB13 study bridges start at 27, continuing from the 26 bridges studied in Project BE535. The key characteristics and framing plan of the Category 1 bridges are shown in Figures 6 to 16. The figure captions list the bridge span lengths, L_s, framing widths between the fascia girders, w_g, skew angles, θ, skew indices, I_s, number of girders, n_g, and the average integer number of cross frames per bay between the girders, n_{CF}. For the continuous-span bridges, the separate span lengths and the average number of cross frames per bay within each span are provided as a list of comma-separated values (e.g., in Figure 10, $L_s = 115, 115$ ft means that each of the two spans are 115 ft, and $n_{CF} = 5, 5$ means that there is an average of five intermediate cross frames within each bay of each span). Table 7 lists the same key characteristics, providing an overall summary of the parametric study bridges. In addition, a column in the table titled "Mod." lists the modifications applied to the existing bridge plans in developing the study bridges. This same format is utilized in the bridge matrix data tables and figures in the subsequent sections.

Additional modifications, beyond those listed in the table, were implemented to develop the bridge geometry for Bridge 1C1-28 (Bridge FA5). Bridge 1C1-28 is a seven-girder simple-span bridge. This bridge was originally built in 1994 as a four-girder bridge. It was widened to a seven-girder bridge in 2015 (i.e., one girder was added at the top of the bridge plan and two more girders at the bottom of the bridge plan). The two girders added at the bottom of the bridge plan have a smaller spacing than the spacing between the

other girders. However, for the purpose of this study, the girder spacing is assumed to be constant and is considered to be the spacing between the four girders of the bridge built in 1994.

Bridges 1C3-31 to 1C3-34 are three-span continuous designs developed using the NSBA continuous-span standard (NSBA 2015) as a starting guide. The NSBA continuous-span standards provide designs of straight non-skewed three-span continuous bridges with a range of span lengths and girder spacings. The standard designs were developed using the 7th Edition of AASHTO LRFD Specifications (AASHTO 2014). The spacing between intermediate cross frames employed in the standard are relatively small compared to typical spacings employed by the BEB13 and BE535 screened bridges. Therefore, these designs were updated using the 9th Edition LRFD Specifications (AASHTO 2020) using a more representative cross-frame spacing of approximately 25 ft.

Bridge 1C2-50 is a two-span continuous bridge similar to Bridge 1C2-26 from Project BE535. Bridge 1C2-26 was a rolled beam bridge with relatively short spans and a narrow girder spacing; as such, the bridge exhibited certain outlier behavior compared to other bridges in Project BE535. Hence, the span lengths of Bridge 1C2-50 were set to twice the span lengths in Bridge 1C2-26. Maintaining the overall framing width equal to the framing width of Bridge 1C-26, the number of girders were reduced to 8 from 10 in Bridge 1C2-26 correspondingly increasing the girder spacing to 9.64 ft from 7.5 ft.

Figures 17 through 19 provide an overview of the overall study design for the Category 1 bridges:

- Figure 17 shows a plot of the framing width vs span length for the simple-span Category 1 bridges from the BE535 and BEB13 bridge matrices. The bold black rectangle shown in the plot depicts the range of targeted bridge geometries established in Section 3.1 (w_g = 33 to 73 ft and L_s = 130 to 250 ft).

- Figure 18 shows a similar plot for the end spans of the continuous-span Category 1 bridges. Both spans of a two-span continuous bridge classify as end spans. The shorter of the two spans has the larger skew index. The end spans of the three-span continuous bridges in this project are equal length and shorter than the interior span; therefore, the end spans of the three-span continuous bridges have a larger skew index than the interior span.

- Figure 19 shows a plot similar to the above for interior spans of the continuous-span Category 1 bridges.

While a few of the Category 1 bridges from the current matrix are outside the lower bound for span lengths, short span lengths lead to higher skew indices. The study of these bridges will provide behavioral insights into the most critical skew effects for Category 1 structures. The distribution is sparse in the region near the upper bound of the span lengths since longer span Category 1 bridges exhibit minor skew effects. The distribution is sparse in the upper-left of the rectangle shown in Figure 17 since the shorter, wider spans are captured by the end- and center-spans of the continuous-span bridges.

Table 7. Geometric characteristics of Category 1 bridges.

Bridge	I_s*	θ*	w_g (ft)	d_e (ft)	L_s* (ft)	n_g	s (ft)	n_{CF}*	Mod. †	Figure
1C1-21	0.15	16	128.1	1.96	241	12	11.6	9		6
1C1-27 (FA1)	0.07	20	34.5	2.75	174	4	11.5	7	a, b	7
1C1-28 (FA5)	0.10	20	69.0	2.75	263	7	11.5	10	b	8
1C2-26	0.15	10	67.5	1.25	79	10	7.50	3		9
1C2-29 (F41)	0.09	20	29.0	1.50	115	4	9.67	5	a, b	10
1C2-30 (F37)	0.14	20	48.0	2.00	129	5	12.0	8	a, b	11
1C2-50	0.16	20	67.5	1.25	158	8	9.64	6	-	12
1C3-31	0.07	20	36.0	1.96	187	4	12.0	7	-	13
1C3-32	0.11	20	48.0	1.96	152	5	12.0	5	-	14
1C3-33	0.17	20	60.0	1.96	129	6	12.0	4	-	15
1C3-34	0.22	20	72.0	1.96	117	7	12.0	4	-	16

* *The skew angles, skew indices, span lengths, and the average number of cross frames per bay are reported for the span having the largest skew index. Additional details are listed in the captions for the bridge plan sketches.*

† *This column shows the modification to the corresponding FDOT bridges used in creating the recommended study bridges for BEB13. These modification are:*

a) The skew angle at the bearing line is modified to 20°.

b) The intermediate cross frames are turned parallel to skew.
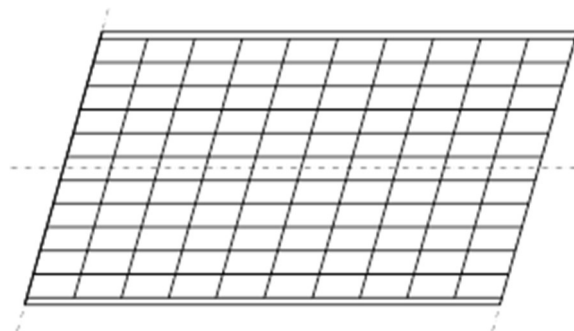
Figure 6. Bridge 1C1-21 (L_s=241 ft; w_g=128.1 ft; θ=16°; I_s=0.15; n_g=12; n_{CF}=9).
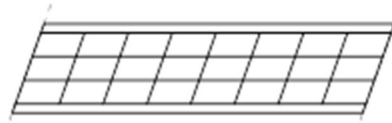
Figure 7. Bridge 1C1-27 (L_s=174 ft; w_g=34.5 ft; θ=20°; I_s=0.07; n_g=4; n_{CF}=7).
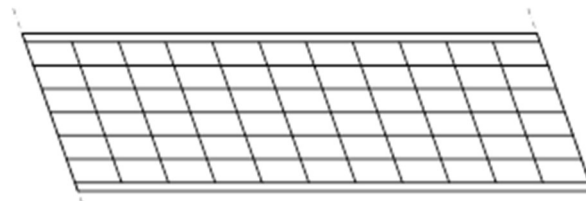
Figure 8. Bridge 1C1-28 (L_s=263 ft; w_g=77.6 ft; θ=20°; I_s=0.10; n_g=7; n_{CF}=10).
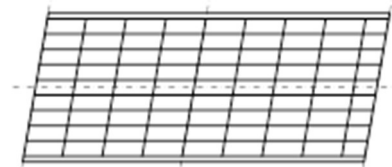
Figure 9. Bridge 1C2-26 (L_s=79 ft, 82 ft; w_g=67.5 ft; θ=10°; I_s=0.15, 0.13; n_g=10; n_{CF}=3, 4).

Figure 10. Bridge 1C2-29 (L_s=115 ft, 115 ft; w_g=29 ft; θ=20°; I_s=0.09, 0.09; n_g=4; n_{CF}=5, 5).
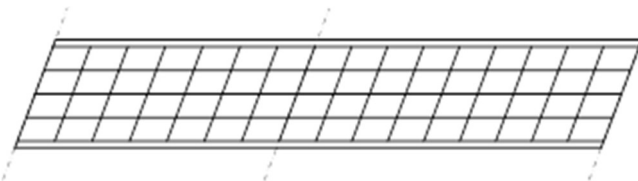
Figure 11. Bridge 1C2-30 (L_s=129 ft, 160 ft; w_g=48 ft; θ=20°; I_s=0.14, 0.11; n_g=5; n_{CF}=6, 8).
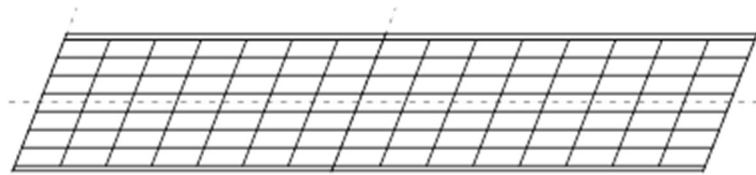
Figure 12. Bridge 1C2-50 (L_s=158 ft, 184 ft; w_g=67.5 ft; θ=20°; I_s=0.16, 0.13; n_g=8; n_{CF}=6, 7).
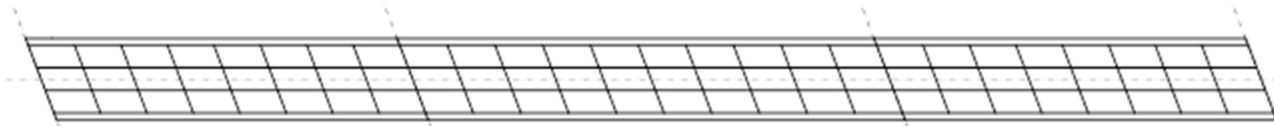
Figure 13. Bridge 1C3-31 (L_s=187 ft, 240 ft, 187 ft; w_g=36 ft; θ=20°; I_s=0.07, 0.06, 0.07; n_g=4; n_{CF}=7, 9, 7).

Figure 14. Bridge 1C3-32 (L_s=152 ft, 195 ft, 152 ft; w_g=48 ft; θ=20°; I_s=0.12, 0.09, 0.12; n_g=5; n_{CF}=5, 7, 5).
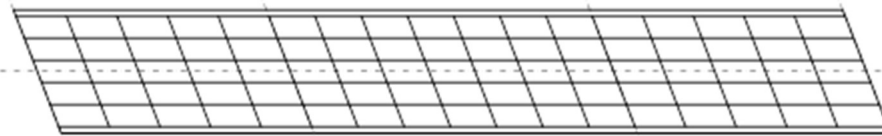
Figure 15. Bridge 1C3-33 (L_s=129 ft, 165 ft, 129 ft; w_g=60 ft; θ=20°; I_s=0.17, 0.13, 0.17; n_g=6; n_{CF}=4, 6, 4).
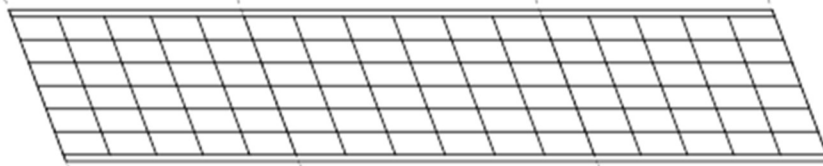
Figure 16. Bridge 1C3-34 (L_s=117 ft, 150 ft, 117 ft; w_g=72 ft; θ=20°; I_s=0.22, 0.18, 0.22; n_g=7; n_{CF}=4, 5, 4).

31
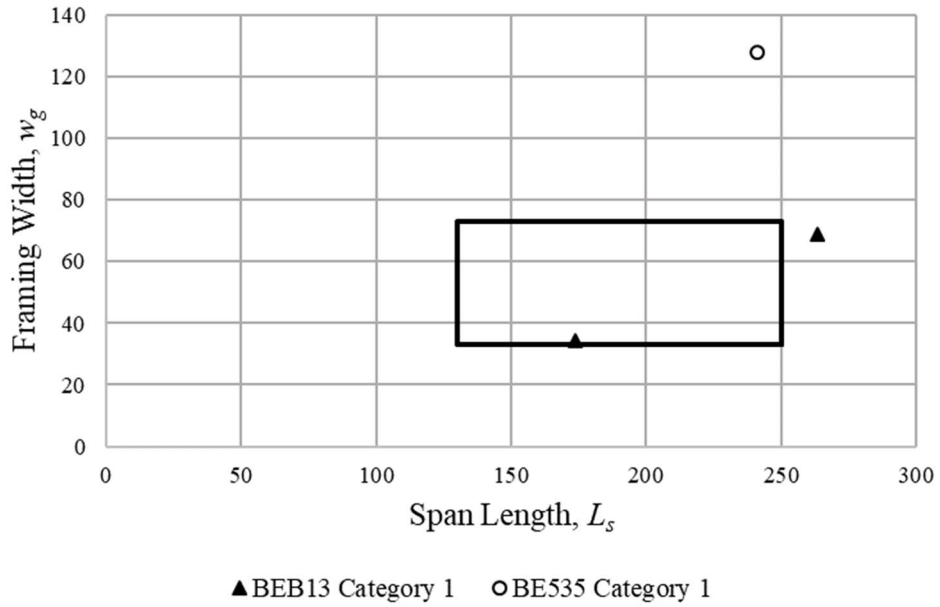
Figure 17. Framing width vs. span length for the Project BEB13 and BE535 simple-span Category 1 bridges.
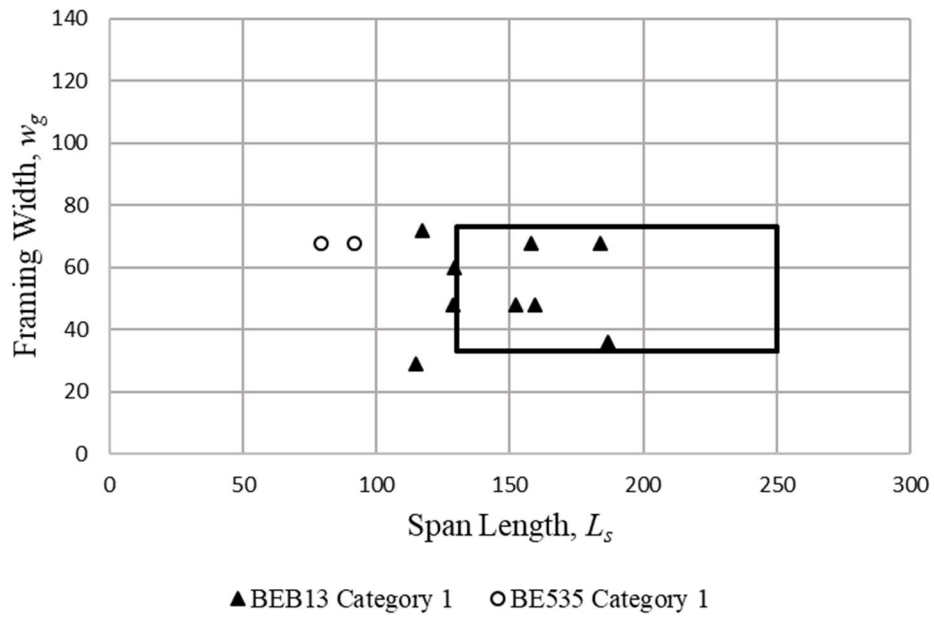
Figure 18. Framing width vs. span length for end spans of continuous-span Project BEB13 and BE535 Category 1 bridges.

32
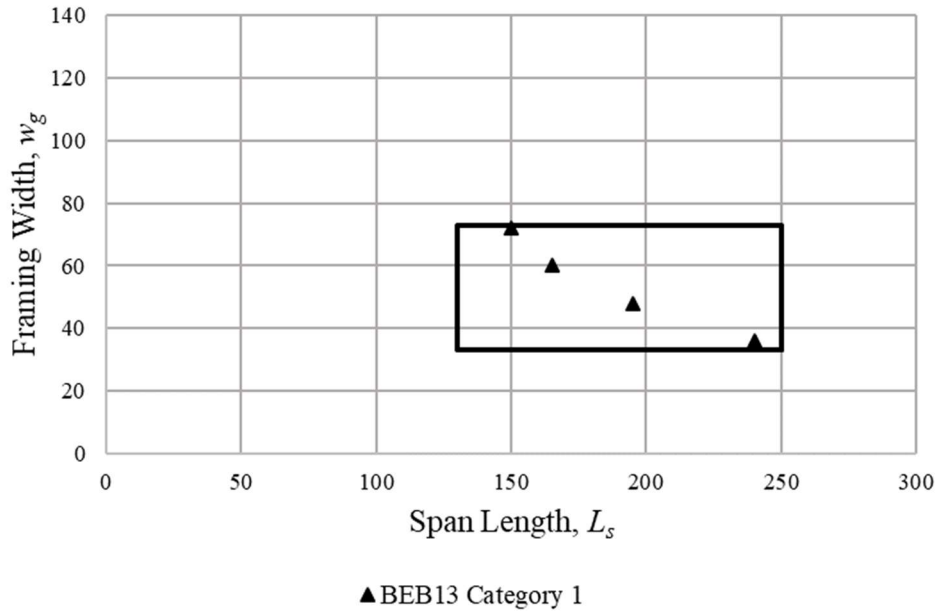
Figure 19. Framing width vs. span length for interior spans of continuous-span Project BEB13 and BE535 Category 1 bridges.

3.5   Category 2C Bridges

Table 8 summarizes the essential geometric characteristics for the Category 2C bridges. This category has a total of 18 bridges: five simple-span, nine two-span continuous, and four three-span continuous. Five of the nine two-span continuous bridges are parametric variations of Bridge 2C2-46. Particularly large cross-frame forces were observed in a preliminary analysis of Bridge 2C2-46. Hence, it was decided to study several parametric variations, Bridge 2C2-46B to 46E to further examine various aspects of behavior resulting in large cross-frame forces. Bridges 2C1-17 and 2C3-11 are from Project BE535. The existing Bridge 2C3-11 studied in Project BE535 omitted cross frames from the bearing lines at the piers and had intermediate cross frames framed directly into the bearings at these locations. The cross-frame pattern is modified for the BEB13 study by employing cross frames along the pier bearing lines and offsetting the first intermediate cross frames from the piers. Bridge 2C1-17 is unmodified from Project BE535 and is included in BEB13 for corroboration with the previous project results and for evaluation of cross-frame fatigue force ranges using the new AASHTO LRFD 10th Edition procedures based on NCHRP Report 962. Figures 20 through 37 show the bridge plan sketches.

The last columns of Table 8 with the headings $O_{min.ext}/b_f$ and $O_{min.int}/b_f$ show the ratio of the minimum offsets to the largest flange widths for the exterior and interior girders adjacent to the bearing lines, respectively. These ratios range from 2.1 to 4.6. In previous work by White et al. (2012) and White et al. (2015) focusing on more highly skewed bridges, some sensitivity has been observed in the cross-frame force and girder flange lateral bending response to these ratios. However, the influence of these ratios on the response is expected to be relatively mild within the above range. The cross-frame forces and girder flange lateral bending stresses is expected to be the smallest, for a given overall bridge geometry, when the offset of the first intermediate cross frame from the bearing lines at the obtuse corners of the spans is made as large as possible (i.e., setting the offsets at these locations equal to a targeted unbraced length for the design of the girders).

Table 8. Geometric characteristics of Category 2C bridges.

Bridge	I_s*	θ*	w_g (ft)	d_e (ft)	L_s* (ft)	n_g	s (ft)	n_{CF}*	$O_{min,ext}/b_f$	$O_{min,int}/b_f$	Mod. [†]	Figure
2C1-17	0.28	42	63.0	2.50	202	7	10.5	10	4.4	2.1	-	20
2C1-35 (F17)	0.16	44	36.0	2.00	218	4	12.0	10	2.7	4.6	c	21
2C1-36 (F22)	0.18	44	45.1	3.04	243	5	11.3	10	4.0	4.0	-	22
2C1-38	0.30	50	48.0	1.96	190	5	12.0	8	4.0	4.0	-	23
2C1-39	0.30	37	60.0	1.96	150	6	12.0	7	4.0	4.0	-	24
2C2-41	0.18	50	38.2	2.46	251	4	12.8	10	4.0	4.0	a, c	25
2C2-43 (FA10)	0.27	50	37.5	3.25	168	4	12.5	9	2.4	2.3	a, c	26
2C2-44 (FA8)	0.28	40	39.0	2.50	144	5	9.75	6	2.1	2.5	-	27
2C2-45	0.28	50	58.3	1.79	250	6	11.7	10	4.0	4.0	d, e	28
2C2-46 (FA9)	0.29	44	63.4	2.31	207	7	10.6	10	4.0	4.0	c	29
2C2-46B	0.26	40	63.4	2.31	207	7	10.6	10	4.0	4.0	c	30
2C2-46C	0.21	35	63.4	2.31	207	7	10.6	8	4.0	4.0	c	31
2C2-46D	0.18	30	63.4	2.31	207	7	10.6	8	4.0	4.0	c	32
2C2-46E	0.15	30	52.8	2.31	207	6	10.6	9	4.0	4.0	c	33
2C3-11	0.26	38	61.0	1.50	185	7	10.6	11	4.0	4.0	c	34
2C3-47	0.28	50	36.0	1.96	152	4	12.0	8	4.0	4.0	-	35
2C3-48	0.29	50	48.0	1.96	199	5	12.0	9	4.0	4.0	-	36
2C3-51	0.29	47	60.0	1.96	222	6	12.0	10	4.0	4.0	-	37

The skew angles, skew indices, span lengths, and the average number of cross frames per bay are reported for the span having the largest skew index. Additional details are listed in the captions for the bridge plan sketches.

† *This column shows the modification to the corresponding FDOT bridges used in creating the recommended study bridges for BEB13. These modifications are:*

a) The skew angle at the bearing line is modified to 50°.

c) The cross-frame arrangement is modified near the bearing lines.

d) The cross-frame framing arrangement is modified to a parallel stagger pattern.

e) Cross frames are added along the intermediate pier.

Figure 20. Bridge 2C1-17 (L_s=202 ft; w_g=63.0 ft; θ=42°; I_s=0.28; n_g=7; n_{CF}=10; $O_{min.ext}/b_f$=4.4; $O_{min.int}/b_f$=2.1).

Figure 21. Bridge 2C1-35 (L_s=218 ft; w_g=36.0 ft; θ=44°; I_s=0.16; n_g=4; n_{CF}=10; $O_{min.ext}/b_f$=2.7; $O_{min.int}/b_f$=4.6).
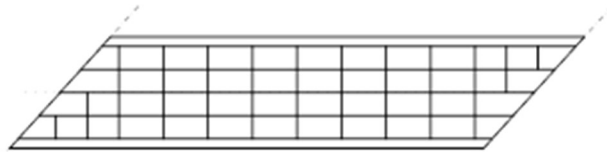
Figure 22. Bridge 2C1-36 (L_s=243 ft; w_g=45.1 ft; θ=44°; I_s=0.18; n_g=5; n_{CF}=10; $O_{min.ext}/b_f$=4.0; $O_{min.int}/b_f$=4.0).
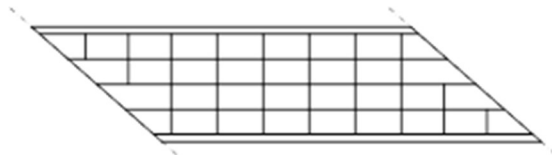
Figure 23. Bridge 2C1-38 (L_s=190 ft; w_g=48.0 ft; θ=50°; I_s=0.30; n_g=5; n_{CF}=8; $O_{min.ext}/b_f$=4.0; $O_{min.int}/b_f$=4.0).
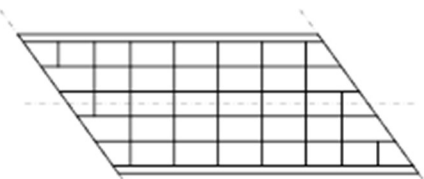
Figure 24. Bridge 2C1-39 (L_s=150 ft; w_g=60.0 ft; θ=37°; I_s=0.30; n_g=6; n_{CF}=7; $O_{min.ext}/b_f$=4.0; $O_{min.int}/b_f$=4.0).
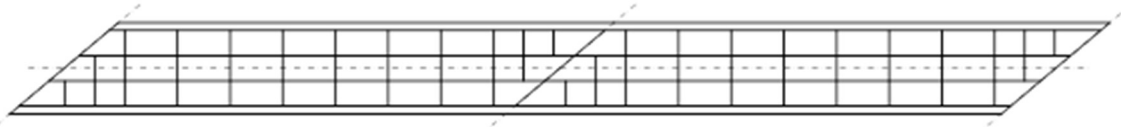
Figure 25. Bridge 2C2-41 (L_s=251 ft, 251 ft; w_g=38.2 ft; θ=50°; I_s=0.18, 0.18; n_g=4; n_{CF}=10, 10; $O_{min.ext}/b_f$=4.0; $O_{min.int}/b_f$=4.0).
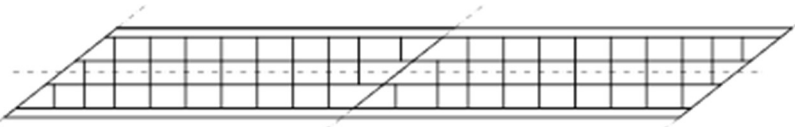
Figure 26. Bridge 2C2-43 (L_s=168 ft, 168 ft; w_g=37.5 ft; θ=50°; I_s=0.27, 0.27; n_g=4; n_{CF}=9, 9; $O_{min.ext}/b_f$=2.4; $O_{min.int}/b_f$=2.3).

Figure 27. Bridge 2C2-44 (L_s=144 ft, 144 ft; w_g=39.0 ft; θ=40°; I_s=0.28, 0.28; n_g=5; n_{CF}=6, 6; $O_{min.ext}/b_f$=2.1; $O_{min.int}/b_f$=2.5).
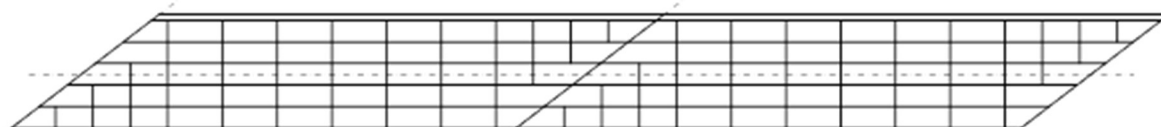
Figure 28. Bridge 2C2-45 (L_s=250 ft, 250 ft; w_g=58.3 ft; θ=50°; I_s=0.28, 0.28; n_g=6; n_{CF}=10, 10; $O_{min.ext}/b_f$=4.0; $O_{min.int}/b_f$=4.0).
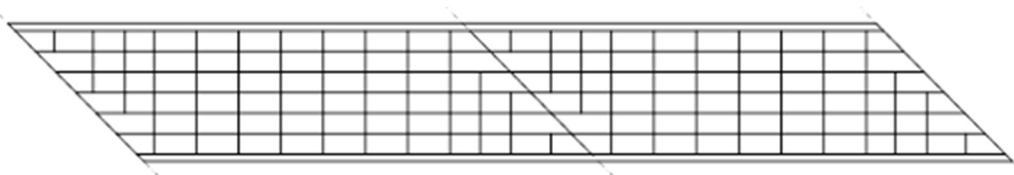
Figure 29. Bridge 2C2-46 (L_s=228 ft, 207 ft; w_g=63.4 ft; θ=44°; I_s=0.27, 0.29; n_g=7; n_{CF}=11, 10; $O_{min.ext}/b_f$=4.0; $O_{min.int}/b_f$=4.0).
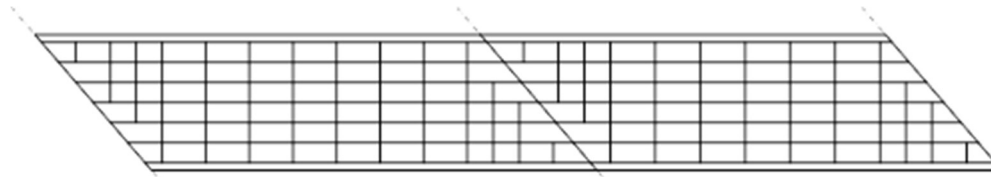
Figure 30. Bridge 2C2-46B (L_s=228 ft, 207 ft; w_g=63.4 ft; θ=40°; I_s=0.23, 0.26; n_g=7; n_{CF}=11, 10; $O_{min.ext}/b_f$=4.0; $O_{min.int}/b_f$ =4.0).
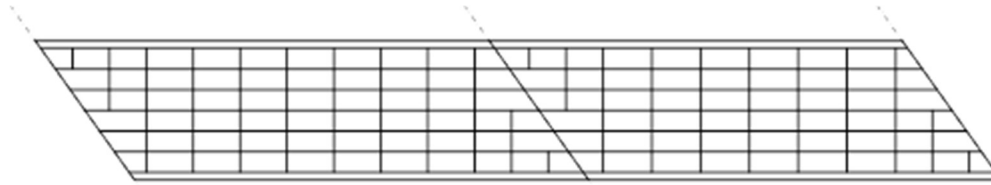
Figure 31. Bridge 2C2-46C (L_s=228 ft, 207 ft; w_g=63.4 ft; θ=35°; I_s=0.20, 0.21; n_g=7; n_{CF}=9, 8; $O_{min.ext}/b_f$=4.0; $O_{min.int}/b_f$ =4.0).

Figure 32. Bridge 2C2-46D (L_s=228 ft, 207 ft; w_g=63.4 ft; θ=30°; I_s=0.16, 0.18; n_g=7; n_{CF}=9, 8; $O_{min.ext}/b_f$ =4.0; $O_{min.int}/b_f$ =4.0).
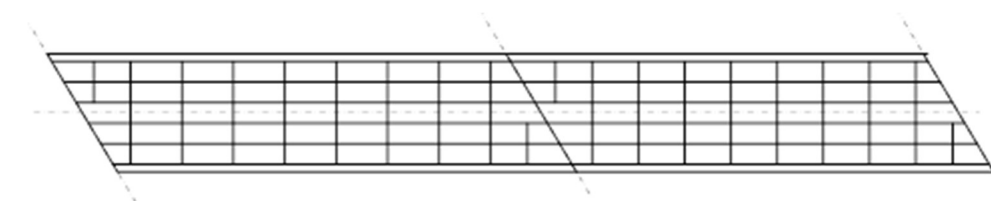
Figure 33. Bridge 2C2-46E (L_s=228 ft, 207 ft; w_g=52.8 ft; θ=30°; I_s=0.13, 0.15; n_g=6; n_{CF}=9, 9; $O_{min.ext}/b_f$ =4.0; $O_{min.int}/b_f$ =4.0).
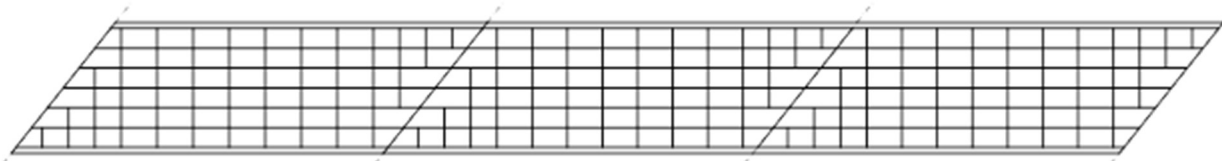
Figure 34. Bridge 2C3-11 (*L$_s$*=188 ft, 186 ft, 185 ft; *w$_g$*=61 ft; θ=38°; *I$_s$*=0.26, 0.26, 0.25; *n$_g$*=7; *n$_{CF}$*=11, 11, 11; *O$_{min.ext}$*/*b$_f$*=4.0; *O$_{min.int}$*/*b$_f$*=4.0).

Figure 35. Bridge 2C3-47 (*L$_s$*=152 ft, 195 ft, 152 ft; *w$_g$*=36 ft; θ=50°; *I$_s$*=0.28, 0.22, 0.28; *n$_g$*=4; *n$_{CF}$*=8, 9, 8; *O$_{min.ext}$*/*b$_f$*=4.0; *O$_{min.int}$*/*b$_f$*=4.0).
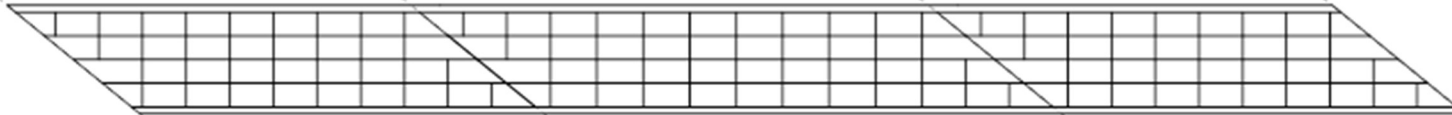
Figure 36. Bridge 2C3-48 (*L$_s$*=199 ft, 255 ft, 199 ft; *w$_g$*=48 ft; θ=50°; *I$_s$*=0.29, 0.22, 0.29; *n$_g$*=5; *n$_{CF}$*=9, 11, 9; *O$_{min.ext}$*/*b$_f$*=4.0; *O$_{min.int}$*/*b$_f$*=4.0).

Figure 37. Bridge 2C3-51 (*L$_s$*=222 ft, 285 ft, 222 ft; *w$_g$*=60 ft; θ=47°; *I$_s$*=0.29, 0.23, 0.29; *n$_g$*=6; *n$_{CF}$*=10, 12, 10; *O$_{min.ext}$*/*b$_f$*=4.0; *O$_{min.int}$*/*b$_f$*=4.0).

Figure 38 shows a plot of the framing width vs span length for the simple-span Category 2C bridges from the BE535 and BEB13 bridge matrices. The bold rectangle shows the bounds established for the representative FDOT bridge geometries in Section 3.1. Figures 39 and 40 show similar plots for the end and center spans of the Category 2C bridges, respectively. The plots indicate a concentration of data points near the targeted lower bound of the bridge widths, especially for the end spans. This reflects the focus on studying moderate bridge geometries in this study.
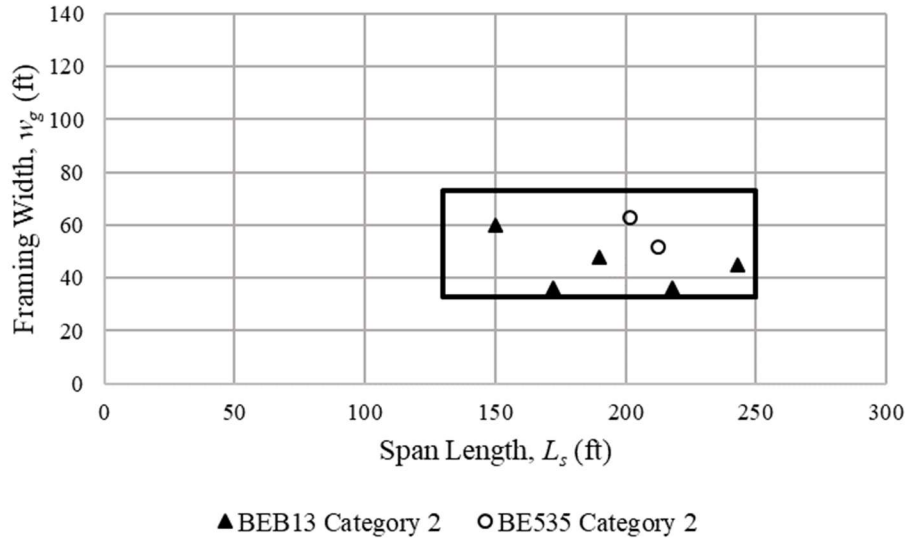
Figure 38. Framing width vs span length for the simple-span Project BEB13 and BE535 Category 2C bridges.
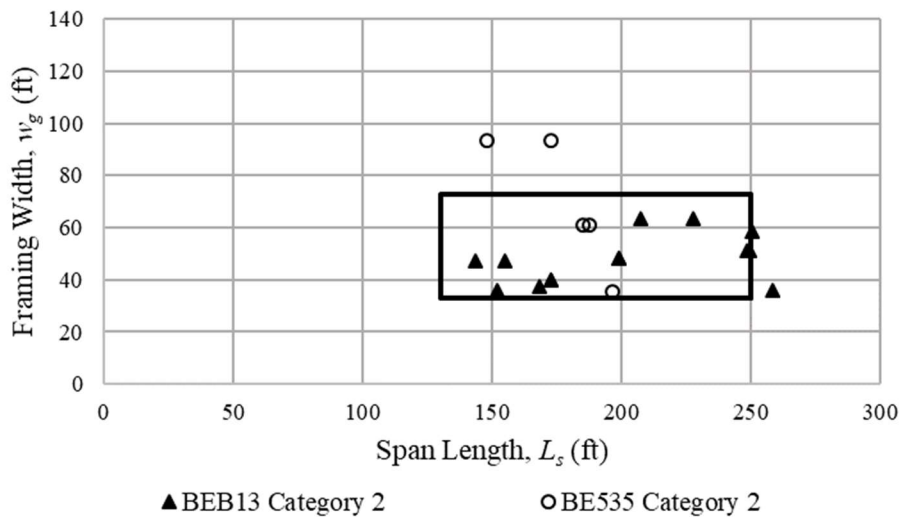
Figure 39. Framing width vs span length for end spans of the continuous-span Project BEB13 and BE535 Category 2C bridges.
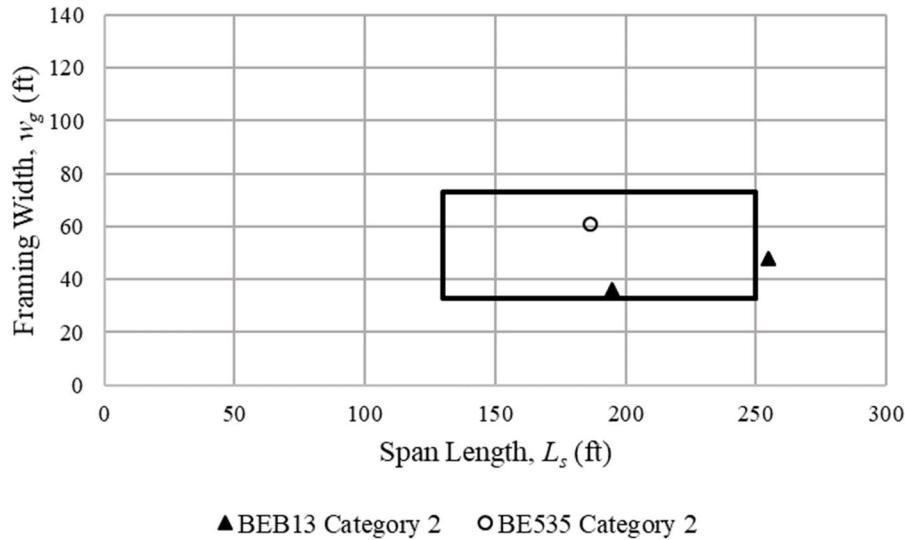
Figure 40. Framing width vs span length for interior spans of the continuous-span Project BEB13 and BE535 Category 2C bridges.

3.6   Category 2P Bridges

Table 9 synthesizes the key geometric characteristics of the Category 2P bridges studied in the BEB13 project. There are six bridges in this category: two single-span, three two-span continuous, and one three-span continuous. Bridges 2P1-18 and 2P2-8 are carried forward from the BE535 project. The parametric variations considered for these bridges are discussed below. Figures 41 through 46 show the plan sketches for these bridges. The original Bridge 8 studied in Project BE535 had cross frames connecting directly into the bearings at the pier. This bridge is modified to provide cross frames along the bearing line and to offset the intermediate cross frames relative to this bearing line.

In addition to the reporting of the offset ratios $O_{min.ext}/b_f$ and $O_{min.int}/b_f$, Table 9 shows the ratio of the stagger distance to the corresponding maximum girder flange widths, Stagger/b_f. For the parallel skew cross-frame layouts, the cross frames are typically spaced within each bay at the targeted unbraced lengths, L_b, along the span for the exterior girder design. This unbraced length, the spacing between the girders, s, and the skew angle, θ, then uniquely establish the stagger distance, which is the minimum distance between the cross frames along the interior girders.

Figure 47 shows a plot of the framing width vs span length for the simple-span Category 2P bridges from the BE535 and BEB13 bridge matrices. The bold rectangle shows the bounds established for the representative FDOT bridge geometries in Section 3.1. Figures 48 and 49 show similar plots for the end and center spans of the Category 2P bridges, respectively. The overall distribution is sparse because of the limited number of Category 2P bridges studied.

Table 9. Geometric characteristics of Category 2P bridges.

Bridge	I_s	θ*	w_g (ft)	L_s* (ft)	d_e (ft)	n_g	s (ft)	n_{CF}*	$O_{min,ext}/b_f$	$O_{min,int}/b_f$	Stagger/b_f	Mod. †	Figure
2P1-18	0.20	40	51.7	212	1.74	6	10.3	10	4.0	4.0	3.2	-	41
2P1-37 (F11)	0.19	42	36.0	172	2.00	4	12.0	7	4.6	4.5	4.5	d	42
2P2-8	0.27	23	93.3	148	2.33	8	13.3	6	9.4	9.4	3.2	c	43
2P2-40	0.12	23	40.0	148	2.33	4	13.3	6	9.4	9.4	3.2	-	44
2P2-42 (F31)	0.24	50	51.0	251	2.46	5	12.8	10	4.6	4.6	4.2	d, e	45
2P3-49	0.29	50	48.0	199	1.96	5	12.0	8	6.4	6.4	5.4	-	46

* *The skew angles, skew indices, span lengths, and the average number of cross frames per bay are reported for the span having the largest skew index. Additional details are listed in the captions for the bridge plan sketches.*

† *This column shows the modification to the corresponding FDOT bridges used in creating the recommended study bridges for BEB13. These modifications are:*

a) The skew angle at the bearing line is modified to 50°.

c) The cross-frame arrangement is modified near the bearing lines.

d) The cross-frame framing arrangement is modified to a parallel stagger pattern.

e) Cross frames are added along the intermediate pier.

Figure 41. Bridge 2P1-18 (L_s=212 ft; w_g=51.7 ft; θ=40°; I_s=0.20; n_g=6; n_{CF}=10; $O_{min.ext}/b_f$=4.0; $O_{min.int}/b_f$=4.0; Stagger/b_f=3.2).

Figure 42. Bridge 2P1-37 (L_s=172 ft; w_g=36.0 ft; θ=42°; I_s=0.17; n_g=4; n_{CF}=7; $O_{min.ext}/b_f$=4.6; $O_{min.int}/b_f$=4.5; Stagger/b_f=4.5).
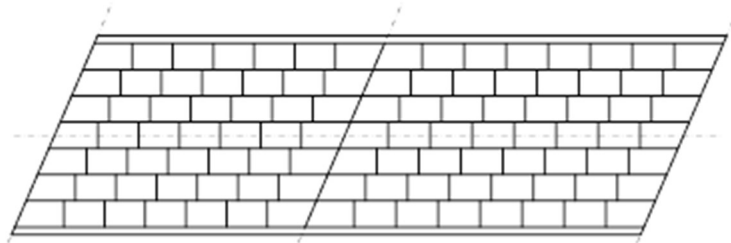
Figure 43. Bridge 2P2-8 (L_s=148 ft, 173 ft; w_g=93.3 ft; θ=23°; I_s=0.27, 0.23; n_g=8; n_{CF}=6, 7; $O_{min.ext}/b_f$ =9.4; $O_{min.int}/b_f$ =9.4; Stagger/b_f =3.2).
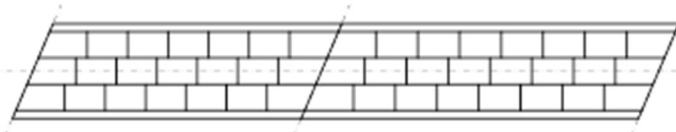
Figure 44. Bridge 2P2-40 (L_s=148 ft, 173 ft; w_g=40 ft; θ=23°; I_s=0.12, 0.10; n_g=4; n_{CF}=6, 7; $O_{min.ext}/b_f$ =9.4; $O_{min.int}/b_f$ =9.4; Stagger/b_f =3.2).
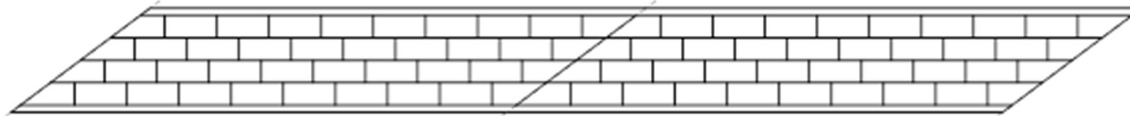
Figure 45. Bridge 2P2-42 (L_s=251 ft, 251 ft; w_g=51 ft; θ=50°; I_s=0.25, 0.25; n_g=5; n_{CF}=10, 10; $O_{min.ext}/b_f$ =4.6; $O_{min.int}/b_f$ =4.6; Stagger/b =4.2).
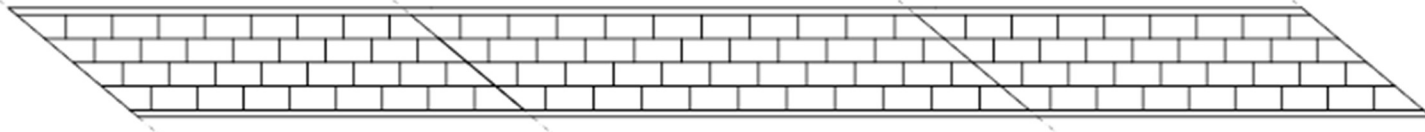
Figure 46. Bridge 2P3-49 (L_s=199 ft, 255 ft, 199 ft; w_g=48 ft; θ=50°; I_s=0.29, 0.22, 0.29; n_g=5; n_{CF}=8, 10, 8; $O_{min.ext}/b_f$ =6.4; $O_{min.int}/b_f$ =6.4; Stagger/b_f =5.4).

.
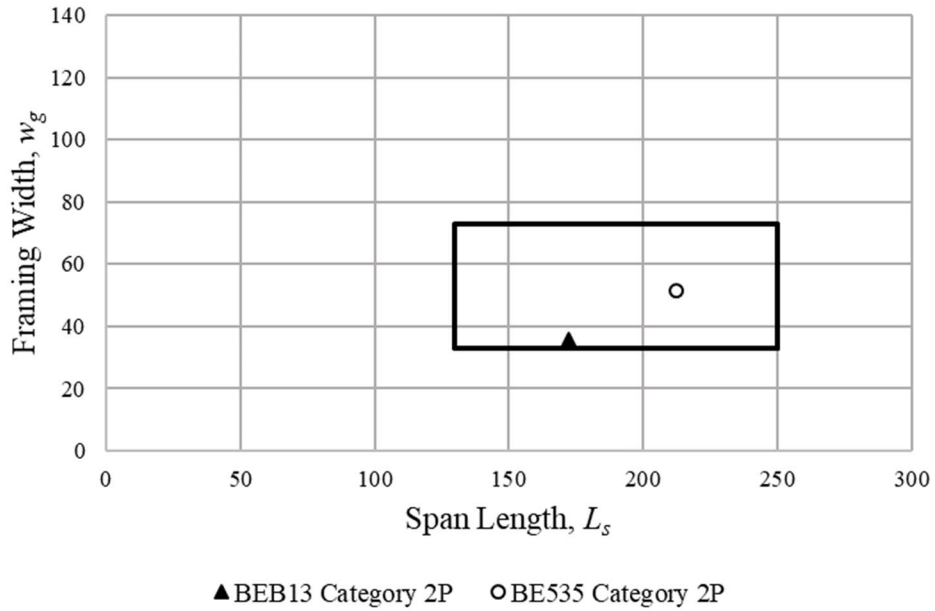
Figure 47. Framing width vs. span length for the simple-span Project BEB13 and BE535 Category 2P bridges.
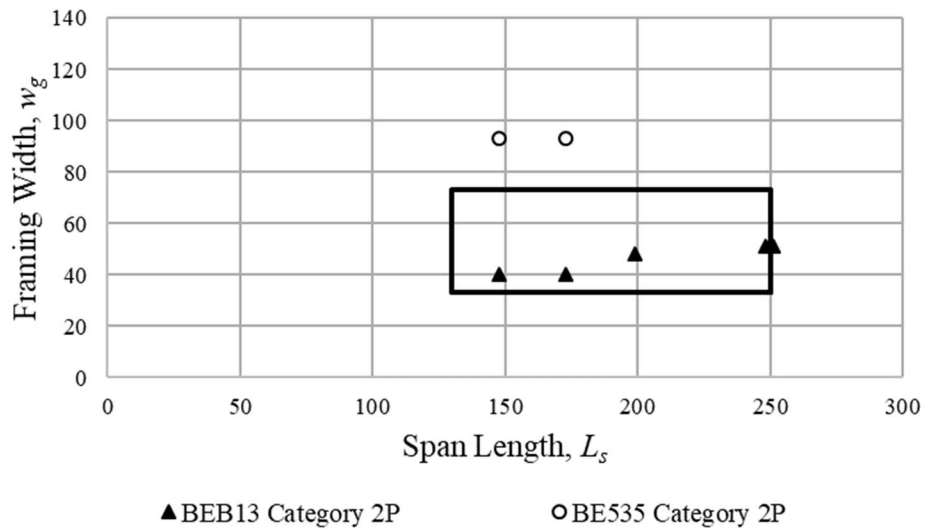
Figure 48. Framing width vs. span length for end spans of the Project BEB13 and BE535 Category 2 bridges.
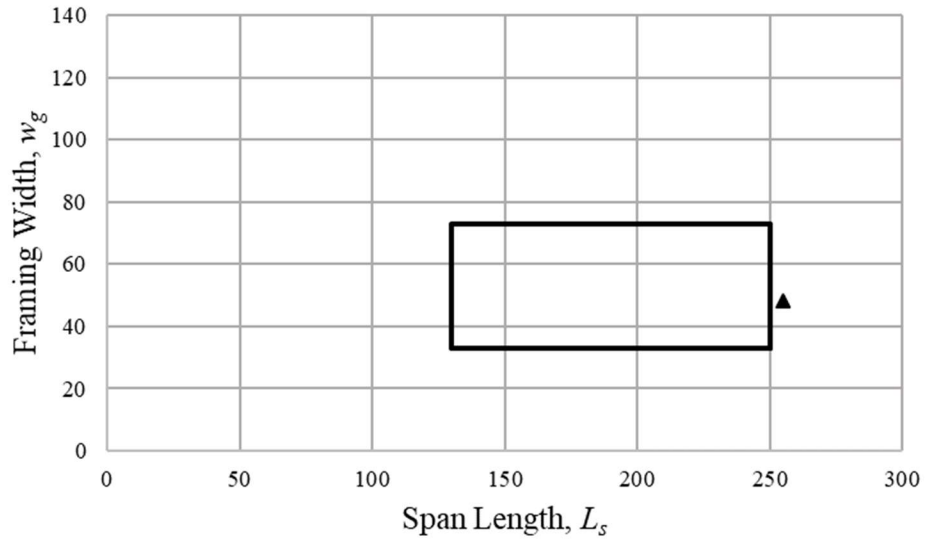
Figure 49. Framing width vs. span length for interior spans of the Project BEB13 and BE535 Category 2 bridges.

4. MODELING CONSIDERATIONS AND CALCULATION OF RESPONSES

In this research, the commercial software CSiBridge Version 24.0.0 (CSi 2022) was used to generate the 3D FEA solutions and the AISC/NSBA LRFD Simon Version 10.4.0.0 software (NSBA 2021) was used for the LGA of the bridges. The design of a parametric study includes numerous considerations related to definition of loads, creation and execution of the analysis models, and collection of responses. It is imperative that the calculation of loads for LGA is consistent with the calculation of loads in 3D FEA. For example, the dead load reactions from the LGA models of the different girders ideally should sum to the total dead load reactions within the 3D FEA model. This chapter summarizes details regarding the modeling idealizations, calculation of loads, and calculation of responses in CSiBridge and LRFD Simon. This is followed by an explanation of the procedures and processes developed for efficient execution of the parametric studies comparing the LGA and 3D FEA results for the 35 bridges identified in Chapter 3.

4.1 3D FEA

The following are key 3D FEA modeling idealizations employed in CSiBridge for this research:

1. Frame and shell elements are used by CSiBridge in the modeling of various components of the bridge.
   a. Girders are modeled using "mixed" frame and shell elements, where the web is modeled by shell elements and the flanges are modeled using frame elements.
   b. Connection plates are modeled using frame elements.
   c. Cross frames are modeled using frame elements with moment releases at the ends.
   d. The deck is modelled using shell elements.
2. To account for the reduced axial stiffness of single angle members in cross frames due to the eccentricity at end connections, a stiffness reduction factor of 0.65 is used, based on the recommendations in AASHTO (2020) LRFD Article C4.6.3.3.4.
3. Cross frames along skewed bearing lines are often connected to the girder connection plates using a bent gusset plate. The bent gusset plate provides additional flexibility to the end bearing-line cross frames that potentially can be beneficial in reducing the skew effects. The bent-plate connection flexibility is not included in the 3D FEA models developed in this research. It is assumed that the connection detail to the girders is such that any additional deformations occurring at the connections are negligible.
4. Live load effects are calculated by CSiBridge using "floating lanes" as explained in Section 4.3.5.
5. Elastomeric bearings are employed in all the bridges studied in this research. A nominal stiffness of 100 kip/ft is used in the lateral and longitudinal directions. It is assumed that the lateral displacements at the elastomeric bearings are smaller than the tolerances necessary to engage with anchor bolts, guides, or other restraining devices; as such, the lateral displacements are restrained only by the lateral stiffness of the elastomeric bearing pads. As discussed by Grubb et al. (2010), rigid modeling of lateral restraint conditions at the bearing locations commonly results in unrealistic large lateral forces that then must be equilibrated within the bridge system model.

4.2 LGA

LGA solutions were conducted for the exterior and interior girders. The following are the specifics of how the LGA was conducted using LRFD Simon:

1. All the dead loads were distributed equally as uniformly distributed loads to each of the girders, with the exception of the steel girder self-weight which was based on the steel cross-sectional area at each position along the girders. Equal distribution to the girders is consistent with the statement "Where bridges meet the conditions herein, permanent loads of and on the deck may be distributed uniformly among the beams and/or stringers" in AASHTO (2020) LRFD Article 4.6.2.2.1. All the bridges evaluated in this study satisfy the conditions specified in this article. The Project BE535 final report (White et al. 2020) discusses the implications of and potential variations from this assumption in detail, and the current parametric studies provide further evaluation of the effectiveness and sufficiency of this assumption.

2. DC1, DC2, and DW loads were calculated for each girder, as discussed in Section 4.3. LRFD Simon accepts the uniformly distributed definition of these loads.

3. The LGA live load calculations were based on positioning the AASHTO HL-93 loads for maximum effect, as specified in AASHTO LRFD Article 3.6.1. This is handled automatically in LRFD Simon based on influence line concepts.

4. Live load distribution to the girders was based on the AASHTO LRFD Article 4.6.2.2 LLDFs in all cases, including bridges where the range of applicability stated in the corresponding tables of this article were not satisfied. LLDFs for bridges that violated the AASHTO range of applicability were manually calculated and input into LRFD Simon. Simon capabilities for calculating distribution factors are utilized in bridges that satisfy the AASHTO range of applicability. The specifics of all the LLDF calculation procedures implemented in addition to the empirical equations as defined in LRFD Simon (NSBA 2021) are:

   a. LRFD Simon Version 10.4.0.0 now includes the AASHTO LRFD RCA calculations. These calculations were not available in prior versions of LRFD Simon. The RCA calculations are implemented precisely as defined in the AASHTO LRFD *Specifications* Article 4.6.2.2.2d; as such, these calculations are not illustrated in this document but are provided in the electronic data files described in Section 4.1.

   b. The application of the AASHTO LRFD skew correction factors parallels the implementation in LRFD Simon. That is, the AASHTO LRFD Article 4.6.2.2.3c skew correction factors for the girder shear forces are applied throughout the lengths of the exterior and first interior girders; however, the AASHTO LRFD Article 4.6.2.2.2e skew correction factors for the girder moments are not applied in any of the cases. The largest of the skew correction factors in the adjacent spans are applied to obtain the LGA estimate of the exterior girder and first interior girder reactions at the obtuse corner of the spans at the end abutments and at the interior pier locations in continuous-span bridges.

For nine study bridges, the range of applicability of the AASHTO Article 4.6.2.2 provisions is violated when any of the bridge span lengths, L_s, exceed 240 ft and/or when the girder longitudinal stiffness parameter, K_g, exceeds 7,000,000 in.[4]. In these instances, Simon provides alternative statical calculations of the LLDFs. It was found that these calculations result in highly-conservative estimates, while the extension of the AASHTO Article 4.6.2.2 provisions to the bridges studied within the current project result in predictions of corresponding 3D FEA solutions that are comparable to the predictions for the other 25 parametric study bridges. Hence, for the nine bridges that violate the AASHTO Article 4.6.2.2 limits, the LLDFs are calculated manually using AASHTO Article 4.6.2.2 and input into LRFD Simon. Appendix A

summarizes the alternative LRFD Simon calculations for bridges that violate the AASHTO Article 4.6.2.2 limits.

4.3   Load Definitions and their Calculations in CSiBridge and LRFD Simon

This section explains the details pertaining to the definition of loads in CSiBridge and LRFD Simon. The emphasis is on maintaining consistency between the 3D FEA and LGA such that the overall results from each of these two analysis types can be compared within a broader context.

The bridge analyses in the parametric studies have been conducted for the following specific load cases:

LC1.   Steel Dead Load (SDL/SDLF), including the influence of steel dead load fit (SDLF) effects;
LC2.   Steel Dead Load (SDL/NLF), neglecting the influence of steel dead load fit (SLDF) effects (i.e., based on No-Load Fit);
LC3.   Concrete Dead Load (CDL), neglecting any influence of prior setup of the concrete during deck placement or due to staged deck placement or phased construction (separate analyses for staged deck placement effects were conducted for a small subset of the bridges studied and the results were discussed in detail in Project BE535);
LC4.   Barrier Rail Load (RL);
LC5.   Future Wearing Surface and Utilities Load (DW);
LC6.   General HL-93 Vehicular Live Load (LL);
LC7.   Girder Fatigue Live Load (Girder Fatigue LL);
LC8.   Cross-Frame Fatigue Live Load (CF Fatigue LL);
LC9.   Live Load with a derived HL-93 loading that consists of 25 % truck load and 100 % of the lane load; and
LC10.   Live Load with a derived HL-93 loading that consists of only the truck load (LL Truck Only).

The bridges were analyzed for each load case using unfactored loads to facilitate the assessment of how the straight skewed bridges respond under the different load types. The responses for a given AASHTO LRFD load combination were obtained by superimposing the results from the appropriate load cases. All of the analyses were material linear elastic and geometrically linear (i.e., first-order linear elastic) analyses, for which superposition is valid.

The first three load cases provide information about the bridge responses in the noncomposite (DC1) condition. For the fourth and fifth load cases (RL and DW), the stiffness of the entire concrete deck is set to the long-term composite loading (modular ratio of $3n$) value. That is, the concrete stiffness is set to 1/3 of its short-term value. Lastly, for the vehicular live load cases, the stiffness of the entire concrete deck is set to its short-term composite loading value. The vehicular live load analyses are conducted to determine the maximum and minimum envelope response values in all of the bridge components being assessed.

Load Case 2 (LC2) is the predominant type of Steel Dead Load analysis performed in current 3D FEA and 2D Grid steel girder bridge design analysis calculations. Conversely, LC1 recognizes the correct analytical influence of the lack-of-fit of cross frames relative to the initial no-load cambered geometry of the girders when the cross frames are detailed for SDLF. For *straight* skewed I-girder bridges with the cross frames detailed in this way, the girders are theoretically plumb under the steel dead load, and the corresponding steel dead load flange lateral bending stresses and cross-frame forces are theoretically zero. This matches with the steel dead load result obtained from LGA. The results from this analysis, when contrasted with LC2, highlight the fact that when the cross frames are detailed for SDLF, refined 3D FEA

and 2D Grid analyses that neglect these effects do not provide the correct analytical steel dead load responses within the structure.

The effect of the SDLF detailing of the cross frames on the bridge responses can be obtained by subtracting the result of LC1 from the result of LC2. These results, while not generated in the parametric study, can be readily generated given the Excel spreadsheets developed. However, it is more informative for bridge engineers to compare and scrutinize the results for SDL/SDLF and SDL/NLF (LC1 and LC2), than to study the effects of SDLF in isolation.

The following sections explain further details of the load calculations for each of the above load cases. Although the given loadings constitute the most basic load cases, setting up these basic load cases involves various approximations that are described below.

4.3.1 Steel Dead Load

Steel dead load is the self-weight of the structural steel contained in the superstructure. This includes the steel girders, the cross frames, and the various miscellaneous steel items, including girder splice plates, girder connection plates at the cross-frame locations, girder transverse stiffeners, gusset plates and spacer plates within the cross frames, bolts, and weld material.

Calculation of the steel dead load of the bridge superstructure in the LRFD Simon LGA models can be summarized as:

- Within each constant-area girder segment (i.e., all the bridge girders are prismatic with stepped changes in the cross section at field and/or shop splices in this research), the nominal steel self-weight of the girders is applied as a uniformly distributed load corresponding to the girder cross-sectional area times the weight density of steel (i.e., 490 pcf). This load is calculated automatically in LRFD Simon.
- The total additional steel self-weight from a miscellaneous steel allowance of 5 % of the total self-weight of the girders, 130 % of any solid-web diaphragms, and 130 % of the cross-frame member self-weights, is calculated and divided by the total length along all of the steel girders. This uniformly distributed load is applied along all the girder lengths.
- The lengths of the cross-frame members and solid web diaphragms are taken as the lengths between work points at the centerline of the girder webs.
- The lengths of the girders are taken as the lengths between the centerlines of the bearings. Girder overhangs beyond the bearing lines are neglected.

The applied loads are handled for the 3D FEA in the same manner as described for the LGA, with the following differences:

- The self-weight of the girders, diaphragms, and cross-frame members is applied directly as a body load for each of these components based on the areas of the components at any given cross section. The 5 % allowance for the steel self-weight of the girders, and the 30 % allowance corresponding to the steel self-weight of the cross frames and solid-web diaphragms, is applied directly to the body load for all of the components. Similar to the calculations of the self-weight for the LGA, the length of all the components is determined using the distances between work points at the centerline of the girder webs. In this study, to streamline the definition of the cross frames, a rectangular cross section is specified for each of the cross-frame members composed of angle or Tee sections. The area of the rectangular section is the same as the area of the physical member. The height of the

rectangular section is taken as two times the distance from the top of the physical member cross section to the centroid of the physical member cross section. This ensures that the cross-frame chords are modeled at the correct physical elevations in CSiBridge. The use of rectangular cross sections for the cross-frame members does not have any impact on the stiffnesses in the bridge model since CSiBridge uses frame elements with end releases to model the chords and diagonals.

- The girder connection plates at diaphragms and cross frames are explicitly modelled in CSiBridge. Without modelling of the connection plates at these locations, the girder webs, represented by shell finite elements, tend to distort excessively due to the eccentricity of the cross-frame chords relative to the girder flanges. In this study, the weight density of the girder connection plates is set to zero to simplify the calculation of consistent self-weights (i.e., same total weight) in CSiBridge and LRFD Simon. The girder connection plate self-weights are assumed to be included within the 30 % miscellaneous steel allowance for the cross frames.

- Two different 3D FEA calculations are considered for the Steel Dead Load:

  (1) Steel Dead Load, Steel Dead Load Fit (SDL/SDLF) and

  (2) Steel Dead Load, No Load Fit (SDL/NLF).

  The steel dead load (self-weight) is the same in both of these analyses. However, for SDL/NLF, the load is applied to the 3D FEA model of the bridge without considering SDLF effects. That is, the 3D bridge model is constructed and these gravity loads are then simply "turned on." Conversely, SDL/SDLF accounts for the actual detailing of the cross frames for SDLF. This is accomplished by using the staged construction feature in CSiBridge to analyze the bridge according to the idealization that the girders are initially supported in a stable manner on the vertical supports and the cross frames are hung from the girders.

Regardless of how the steel self-weight is estimated, it is still a basic *estimate*. The aspect of key importance for the research is that the total of the bearing vertical reactions obtained from the 3D FEA and obtained by summing the reactions from the LGA idealizations for all the girders, should be the same value (within 1 %). This allows for the research to state that the 3D FEA and LGA loadings are indeed "equivalent."

4.3.2 Concrete Dead Load

In this study, concrete dead load is taken as the total weight of the concrete bridge deck, including the weight of stay-in-place metal deck forms (and the concrete within the flutes of these forms), the concrete in the overhangs, and the concrete within the haunches (i.e., bolsters) over the top of the steel girders.

The total weight of the wet concrete is calculated by considering:

- The weight density of concrete (i.e., 150 pcf) times the area of the concrete within the bridge cross section, obtained as the sum of:
  a) The area of the rectangular structural portion of the deck equal to the structural thickness multiplied by the overall width of the deck.
  b) The area of a sacrificial overlay thickness times the overall width of the deck. (In this work, based on guidance from the FDOT Structures Design Guidelines (FDOT 2022a) and from the FDOT steering group for the research, the sacrificial overlay thickness is taken as 0.5 inches for decks with a thickness greater than or equal to 8.5 inches. Furthermore, the sacrificial overlay thickness is taken equal to zero for decks with 8.0-inch thickness or less, and it is taken as the specified depth minus 8.0 inches for decks between 8.0 and 8.5 inches in thickness.)

49

c) The area of the concrete within the girder haunches, taken as the haunch depth minus the thickness of the girder top flange times the flange width for all the girders,

d) A tapered triangular shaped area of the concrete within the two deck overhangs, located below the structural thickness of the deck and varying from zero at the edge of the deck to the haunch depth minus the flange thickness at the tip of the fascia girder top flanges.

- The weight of stay-in-place metal deck forms between the girder flanges, including the weight of the concrete within the flutes of the forms, taken as 20 psf, as specified in the FDOT Structures Design Guidelines (FDOT 2022a).

These loads are divided by the total number of girders, and then applied as equal line loads in the LGA models for the girders in the bridge cross section.

As a simplification, the temporary bridge form loads on the deck overhangs are neglected. This simplification is applied both in the LGA and in the 3D FEA, so that the LGA and 3D FEA results can be compared on a consistent basis. No specific construction loads (e.g., screed rail loads, wheel loads from a screed machine, walkway, and other related loads supported by the bridge during the deck placement, and loads from the construction operations) are considered in this work for either the LGA or for the 3D FEA. In conclusion, the wet concrete loads on the overhangs, as modeled, are taken as a representative set of loads for comparison of the LGA and 3D FEA calculations.

In CSiBridge, the weight of the rectangular structural portion of the bridge deck is considered directly as a body load. All the other contributions to the concrete dead load are determined in a similar fashion to that described for the LGA, then applied as a uniformly distributed area load across the bridge deck.

It should be noted that the above idealization gives a relatively simple approximation of the various torsional effects on the fascia girders from the deck overhangs. In the CSiBridge 3D FEA models, the torsion from the overhang is applied entirely to the corresponding fascia girder. In the physical bridge, the above overhang loads, are applied to the corresponding fascia girder during the deck placement. However, when the overhang forms are removed, the direct torsion on the fascia girder from the overhang support brackets is released and the fascia girder exhibits an elastic rebound due to the release of this torsion. In the remaining structure, the concrete dead load on the overhangs is resisted predominantly by the cantilever action of the deck over the top of the fascia girder. Therefore, the torsional moments on the fascia girders, in their final constructed condition, are overestimated by the selected implementation of the "Wet Concrete Loading" in CSiBridge.

The 3D FEA and LGA solutions can be compared consistently based on the above approximation. The flange lateral bending stresses in the fascia girders are estimated using AASHTO (2020) LRFD Eq. C6.10.3.4.1-1 for the purpose of a consistent comparison with 3D FEA estimates. Further, the total concrete dead load on the bridge is the same in the 3D FEA and LGA solutions.

4.3.3 Barrier Rail Load

Rails that serve as traffic barriers and parapets are placed near the edges of the bridge width and extend throughout the length of the bridge. Barrier rails are erected/installed after the deck hardens; hence, the load is applied to the composite bridge section.

In this study, the various aspects of the calculation of barrier rail loads can be summarized as follows:

- The weight of the barrier rails is applied as a DC2 load, resisted by the long-term section of the girders. Consideration of barrier rail load in the bridge studies is useful to gage the ability of

1D LGA vs 3D FEA to evaluate the bridge response to a long-term composite superimposed dead load that is applied at concentrated positions across the bridge width. In this study, barrier rail loads corresponding to 36-inch single-slope rails were applied in all the bridges. Referring to FDOT (2022a) Structures Design Guidelines Table 2.2-1, the 36-inch single-slope rail weighs 430 plf.

- No other barrier loads, sidewalk loads, etc. that would typically be applied as DC2 loads are considered in this research.

In LGA, the total load from the barrier rails, assumed to be two rails (i.e., one on each side of the bridge deck), is divided by the total number of girders to obtain an equal line load applied to each of the girders in the bridge cross section.

In the 3D FEA model, the barrier rail loads are applied to the concrete deck at the approximate centroid of the 36-inch single-slope rails. This is taken as nine inches from the edges of the deck.

4.3.4 Future Wearing Surface and Utilities Load

Weight of non-integral wearing surface and utilities supported by the bridge constitute the future wearing surface and utilities load.

In this study, various aspects of calculation of future wearing surface and utilities loads can be summarized as:

- A future wearing surface load of 15 psf = (150 pcf) (1.2 inches) is applied to the overall width of the deck. This is divided by the total number of girders in the bridge cross section to obtain an equal nominal DW load applied to each of the bridge girders, using the long-term composite properties of the girders.
- No utility loads are considered in the bridge studies conducted in this research.

In LGA, the total future wearing surface load on the bridge is divided by the total number of girders and the girder lengths to obtain an equal line load applied to each of the girders in the bridge cross section.

In the 3D FEA, the future wearing surface load is the same as specified for the LGA; however, the 15 psf load is applied to the full deck area in the CSiBridge models.

4.3.5 General Vehicular Live Load

Analysis of live load involves determining the most critical locations of the AASHTO design vehicular live load to estimate the maximum critical responses for the various bridge components at all positions. The AASHTO LRFD Specifications require the consideration of n live load lanes (each containing a lane and a truck loading) for a given bridge, where n is the number of 12 ft wide lanes that can be placed between the curb lines on the deck. For calculation of the girder live load demands, these lanes are to be moved or "floated" across the width of the bridge between the curbs disregarding the presence of medians and sidewalks, to obtain the most critical live load response. In this study, which utilizes a geometric linear and elastic analysis, the maximum responses are obtained in the 3D FEA solutions using influence surfaces. For the LGA, the maximum responses are obtained using LLDFs and influence line diagrams.

In the BE535 and BEB13 studies, pedestrian live load and special vehicular live loads (e.g., permit loadings, etc.) are not considered. The HL-93 vehicular live load defined in the AASHTO LRFD Specifications is used to evaluate the sufficiency of LGA for the bridges to be studied. For the overall system analysis of the bridges studied, the tandem loading in the HL-93 load definitions is not expected to produce any significant demands larger than those produced by the HL-93 design truck. For girder

major-axis bending and shear, the tandem loading tends to govern only for relatively short bridges. The local nature of the two 25-kip axles of the tandem, spaced at 4 ft apart, may produce slightly larger girder flange lateral bending or cross-frame forces in some situations; however, the flange lateral bending stresses and the cross-frame forces are also impacted by the overall global major-axis bending and shear actions. Therefore, the HL-93 tandem loading is not considered in the BE535 and BEB13 projects.

Modeling Vehicular Live Load for Calculation of Girder Live Load Demands within CSiBridge

CSiBridge provides very powerful features that greatly facilitate the definition and application of the AASHTO LRFD HL-93 live load model. The HL-93 live load definitions from AASHTO (2020) Article 3.6.1.3.1 are already included in CSiBridge. The application of this model to a bridge is defined in a succinct way by defining a floating lane set. The overall width of the bridge accessible to vehicular live load is taken as the width between the exterior barrier rails in this project. This is specified as the overall width for the floating lane set. Given the standard lane width of 12 ft, the total width of the floating lane set is divided by 12 ft, then rounded down to the closest integer, *n*. This is the number of live load lanes that the width of the bridge can accommodate. CSiBridge then "floats" the *n* lanes across the width of the bridge (i.e., it positions the lanes at various locations across the bridge width) to generate the maximum live load effects. Within each lane, the HL-93 loading rules apply (again, the tandem load is assumed to not govern relative to the HL-93 design truck in this work). The design trucks are positioned such that their wheels are 2.0 ft or more from the lane longitudinal edges. The 10-ft-wide lane loads are positioned against either edge of the 12-ft-wide lanes. For negative moment between the points of contraflexure corresponding to uniform loads on all spans, and for the calculation of pier reactions, 90 % of the effect of two design trucks spaced a minimum of 50 ft between the lead axle of one truck and the rear axle of the other truck, combined with 90 % of the effect of the design lane load is considered. The distance between the 32-kip axles of each truck is taken as 14 ft. The dynamic load allowance factor of 1.33 is included in the "nominal" live load in the definition of the HL-93 vehicle loading.

Within the floating lane set, CSiBridge considers 1, 2, 3, 4, and up to *n* lanes. For the case of one lane positioned within the width of the floating lane set for maximum effect, a multiple presence factor of 1.2 is employed. For two and three lanes, multiple presence factors of 1.0 and 0.85 are employed. For four or more lanes, a multiple presence factor of 0.65 is used (following the AASHTO LRFD requirements). Floating lanes within a lane set are not allowed to cross or overlap each other. CSiBridge calculates the amount that the floating lanes are allowed to move transversely, based on the total width of the lane set and the standard 12-ft lane width.

When positioning the floating lanes at a given station along the bridge length, the following possibilities are considered:

- All lanes adjacent in a single group with no intermediate gaps.
- A single gap between two groups of lanes, each group containing no gaps.

For N floating lanes in a lane set, this leads to N possible groupings. This is shown in Figure 50, taken from the CSi Analysis Reference Manual (CSi 2022) for the case where N = 4. For each case, the one or two groups are moved transversely to find the position that leads to the maximum response.

CSiBridge has lane discretization factors for moving the live loads, which are set to 10 ft in the longitudinal direction. In the transverse lane direction, the discretization is set to a length of (*girder spacing/n*), where *n* is the smallest integer such that the length (*girder spacing/n*) results in a length smaller than 6 ft. That is, CSiBridge varies the positioning of the loads in increments of the discretization lengths in the longitudinal and transverse directions. The discretization points obtained are called lane-load points,

to determine the influence surface ordinates of the lane. The influence surface is constructed through interpolation between the lane-load points, which is further used in determining maximum load effects. In addition, the discretization along the lane is set such that it is never greater than 1/10 of the span length. AASHTO LRFD requires consideration of wheel loads as close as 1 ft from the barrier rail (curb) for design of the overhangs, but only as close as 2 ft for the girder design. However, the focus in this research is on the overall bridge system design. As such, both edges of all the lanes are considered as "interior edges," meaning that wheel loads do not need to be placed closer than 2 ft from the edge of the lane.
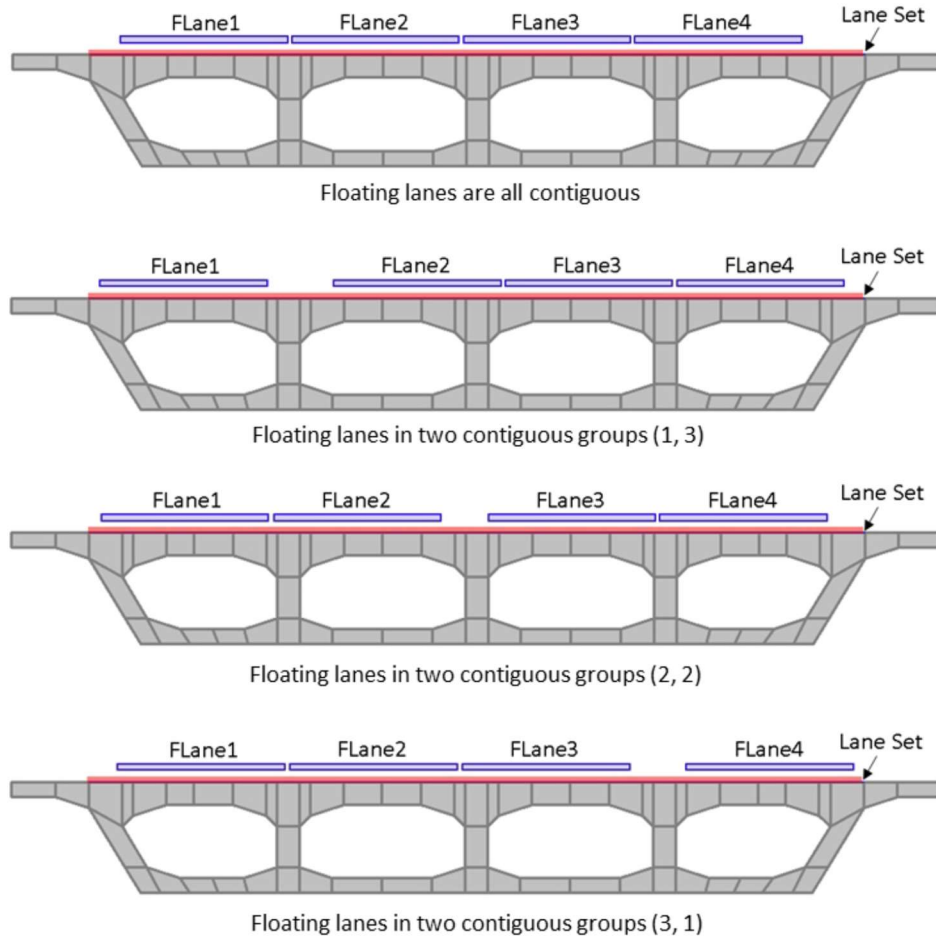
Figure 50. Transverse positioning of four floating lanes showing all possible grouping options, from (CSi 2022).

CSiBridge considers traffic moving in either direction within a given lane in obtaining the maximum live load effects. For the bridges considered in this study, the calculation of the girder live load demands was defined by creating a single floating lane set.

Modeling Vehicular Live Load for Calculation of Girder Live Load Demands in LRFD Simon

In LRFD Simon, live loads are applied to the girders based on AASHTO LRFD LLDFs, as described in Section 3.2. Simon conducts structural analysis to obtain the maximum live load effects, using influence line diagrams to obtain the maximum and minimum envelopes for various response quantities.

4.3.6 General Fatigue Live Load

AASHTO (2020) Article 3.6.1.4.1 defines the vehicle for evaluation of fatigue as follows:

- The fatigue load (unfactored) shall be one design truck, but with a constant spacing of 30 ft between the 32-kip axles.
- A dynamic load allowance of 15 % (1.15) shall be applied to the static effects of the design truck.

Analysis of girder fatigue demands involve positioning the fatigue vehicle in a single lane that spans throughout the bridge length and the roadway width, to obtain the most critical effects. This is achieved in CSiBridge by defining a single lane for fatigue that spans throughout the length and between the rails in the transverse direction. Consideration of cross-frame member fatigue is discussed below. The AASHTO LLDF calculation used in the evaluation of fatigue live load response in LGA follows the LRFD Simon procedures using single-lane LLDFs.

4.3.7 Cross-Frame Fatigue Live Load in 3D FEA

The AASHTO (2021) LRFD 10th Edition Article 6.6.1.2.2 provisions, balloted and approved in June 2021 by the AASHTO Committee on Bridges and Structures, state:

"To determine the range of force in the cross-frame or diaphragm member under consideration, the single fatigue truck shall be positioned as specified in Article 3.6.1.4.3a, but with the truck confined to a single transverse position during each passage of the truck along the bridge."

In addition, the AASHTO (2021) LRFD 10th Edition Article 3.4.5 states:

"The Fatigue I and II live load factors (γ_{LL}) shall be multiplied by an additional factor of 0.65 when evaluating load-induced fatigue in cross-frames and diaphragms."

These changes to the AASHTO LRFD provisions are based on the NCHRP Report 962 (Reichenbach et al. 2021) research findings, which demonstrate substantial conservatism in the calculation of cross-frame fatigue force ranges based on the 9th Edition AASHTO LRFD fatigue live load model (i.e., the model described above in Section 3.3.6). The 9th Edition provisions are still required for all fatigue design other than the fatigue checking of cross frames and diaphragms.

Both the more traditional 9th Edition AASHTO LRFD rules as well as the new 10th Edition rules are implemented in the BEB13 research to evaluate and compare their impact on the cross-frame fatigue force range demands. The new 10th Edition rules are implemented in CSiBridge by:

1. Defining a suite of 10 ft wide lanes to simulate travel paths. The AASHTO fatigue vehicle is centered on the 10 ft width for each of the paths. Therefore, there is no transverse deviation from the centerline of the path when applying the fatigue loading to the bridge for a given path.
2. The outermost travel paths across the bridge width are with the edge of the corresponding lane located at 2 ft from the edge of the barrier rails.
3. Additional travel paths are placed on the bridge that:
    a. Have a wheel line directly over the top of each of the girders,
    b. Are located at the center of each bay between the girders, and
    c. Are centered over each of the girders.
4. For each travel path, it is assumed that the fatigue vehicle can cross the bridge in both of the directions along the path.

The governing cross-frame fatigue force ranges are calculated as the largest range determined from any one of the above travel paths. This typically provides a measurable reduction in the fatigue force range relative to the approach defined in the AASHTO LRFD 9th Edition, in which the fatigue vehicle would be located at all potential longitudinal and transverse positions to create the force range. When multiplied by the additional 0.65 factor cited above, the fatigue force range reductions are even more substantial.

4.3.8 Vehicular Live Load for Deflection Calculations

For optional live load deflection evaluation, the AASHTO (2020) LRFD Article 3.6.1.3.2 states:

If the owner invokes the optional live load deflection criteria specified in Article 2.5.2.6.2, the deflection should be taken as the larger of:

1. That resulting from the design truck alone, or
2. That resulting from 25% of the design truck taken together with the design lane load.

Further, the AASHTO LRFD Specification Article 2.5.2.6.2 states:

1. The vehicular load shall include the dynamic allowance.
2. When investigating the maximum absolute deflection for straight girder systems, all design lanes shall be loaded, and all supporting components should be assumed to deflect equally.
3. For composite design, the stiffness of the design cross section used for the determination of deflection should include the entire width of the roadway and the structurally continuous portion of the railings, sidewalks, and median barriers (it is assumed that none of these are structurally continuous in the calculations for this project).
4. For straight girder systems, the composite bending stiffness may be taken as the stiffness determined as specified above, divided by the number of girders.
5. The live load portion of Load Combination Service I of Table 3.4.1-1 should be used including the dynamic load allowance, IM. Basically, a live load multiplier of 1.0 times 1.33 should be used. In addition, the reference to Table 3.4.1-1 indirectly brings in the consideration of the multiple presence factor, since Article 3.4.1 indicates the use of the multiple presence factor with Table 3.4.1-1.
6. The live load shall be taken from Article 3.6.1.3.2, which brings in the requirement of 25 % of the HL-93 design truck with the lane load, or the HL-93 design truck alone.

Summarizing, all of the above gives the LLDF of $m \times (N_L/N_g)$, applied with 25 % of the HL-93 design truck plus the lane load, or the HL-93 design truck alone, where, where m is the multiple presence factor, N_L is the maximum number of lanes that can be accommodated on the bridge and N_g is the number of girders in the bridge. The LLDF obtained is used in calculating an estimate of the live load deflection.

Grubb et al. (2010) note that the assumption of equal deflections is not applicable for bridges that have a skew angle exceeding 20°. This is because the differential deflections that occur between girders is more important than an average estimate of live load deflection obtained from AASHTO optional live load deflection evaluation. Hence, live loading ranging from one to the maximum number of lanes that can be accommodated on the bridge should be employed in the calculation of live load deflection estimates.

Separate Load Cases 9 (LC9 in Section 4.1), composed of a derived HL-93 vehicle consisting of 25 % truck load and 100 % of the lane load, and LC10, composed of a derived HL-93 vehicle consisting of only the truck load, were considered for the investigation of girder deflections under live load. An impact factor

of 1.33 was applied to the truck load in both these load cases as recommended by the AASHTO (2020) LRFD Specifications.

In order to simulate LC9 and LC10 in CSiBridge, derived HL-93 vehicles pertaining to these load cases were defined from the base vehicle used in the general live load case LC6. LRFD Simon automatically calculates the live load deflection for LC9 and LC10 using the distribution factor $m \times N_L/N_g$ and presents the maximum of the two deflections.

4.4   Consideration of Girder Axial Forces from 3D FEA Models

The elastic 3D behavior of a bridge depends on the relative stiffness of the composite concrete deck and the steel I-girders, which in turn influences the distribution of forces between the concrete deck and the steel girders. When analyzing composite girders using the long-term elastic modulus of concrete for sustained superimposed dead loads and for short term elastic modulus of concrete for vehicular live loads, the portion of slab that acts composite to each steel I-girder is calculated based on the tributary width of the slab for each girder. This assumption has been found to be reasonable and is commonly used in the design of composite bridge girders.

Ideally, in the absence of longitudinally applied axial loads (such as may occur in some cases due to the combination of the bridge skew and specifics of bridge bearing constraints), the axial forces in a composite girder should be zero. In other words, the portion of the slab acting compositely with each girder is such that the axial force on all the girders at a bridge cross section is zero. This action is captured in a 3D FEA of the concrete deck and the steel I-girders.

The relative distribution of loads and thereby, the participation of the deck with each steel I-girder is also influenced by the type and location of the load. The deformed shape of the concrete deck around each steel I-girder provides an insight into the portion of deck that participates with the steel I-girder. For a uniform vertical load spread over the entire area of the bridge, the portion of deck acting with each steel girder is reasonably well approximated by the tributary widths. However, for a load that is effectively a concentrated load applied at a particular position within the bridge cross section, such as the barrier rail load, the 3D FEA can suggest that the portion of deck that participates with the different girders is different than the tributary width.

CSiBridge uses tributary width of the deck composite with each steel I-girder to report the internal forces of the composite girders. As a result, a measurable net axial force is observed on the composite section in some cases, such as the above. It should be noted that the total axial force on the entire bridge cross section is zero (assuming negligible longitudinal constraints and negligible applied axial loading on the bridge cross section, which are considered to be appropriate assumptions within the context of this study). However, due to the assumption of tributary widths of deck acting compositely with each steel I-girder, non-zero axial forces are calculated on the individual composite girders.

Due to the presence of net girder axial forces, the horizontal axis about which the girder bending moments is calculated becomes important. The neutral axis of the composite girders is at different depths for the non-composite, short-term composite, and long-term composite section. The net effect is that the major-axis bending moments and bending stresses are influenced by the presence of the girder axial forces. This effect is more significant for concentrated load cases, such as the barrier rail load.

By default, CSiBridge reports the internal forces at a horizontal axis passing through the mid-web depth of each section. This entails that the bending moment due to the net axial force must be added to the bending moment resultants obtained from CSiBridge to obtain revised bending moments. The bending stress at the

56

flanges can then be calculated using the revised bending moments, and the axial stress due to the axial force can be added to obtain the correct estimates of stress. The stresses at different locations on the girders is calculated directly by the 3D FEA model and can be output directly rather than calculating the resultant moments and then back-calculating the stresses from the resultant moments given the common girder design-analysis cross-section models. A study was conducted to evaluate the effects of axial force on bending moments for girders of Bridge 1 in Project BE535. A maximum error of approximately 1 ksi was found for the barrier rail load case. For practical purposes, a maximum error of 1 ksi, which is 2 % of the material yield strength of 50 ksi, is considered acceptable. Therefore, the effect of the above girder axial forces was ignored in the calculation of the girder major-axis bending moments. However, these axial forces are collected and catalogued in the Excel spreadsheets developed in the study of each bridge.

5. PRESENTATION OF RESULTS

5.1   Organization of Electronic Data Files

In this research, results from LRFD Simon and CSiBridge are processed and compiled in a series of electronic Excel workbooks. Detailed plots and comparison tables from these Excel workbooks have been compiled within a consolidated electronic data file for each of the 35 bridges studied. The presentation of the data from the parametric studies in each of these files is organized such that the results can be readily inspected and understood for the individual bridges studied, as well as for the overall suite of bridges studied. The presentation is predominantly graphical and is organized the same for each bridge. In each individual section of the electronic data files, the most meaningful results are presented for that response quantity or calculation pertinent to the project objectives. Various other data can be examined in the corresponding Excel worksheets.

Each electronic data file corresponds to one of the individual bridges studied. The file begins with a synthesis of results comparisons between the LGA and 3D FEA solutions for the selected bridge. This is followed by various plots and tables providing detailed comparisons of the results. Plots are presented for each of the key girder response quantities discussed below for each of the load cases described in Section 4.3.

The electronic data files focus on the different bridge characteristics, responses, and contexts listed in Table 10. Each of the 35 bridges studied are given a unique name, described at the beginning of Chapter 3, which appears at top of each of the data file page along with the section numbers corresponding to Table 10.

Several of the data file sections have a sub-section number corresponding to attributes (i.e., the girder number in the sub-sections presenting the girder data, the specific cross-frame response in the sub-sections presenting the cross-frame data, etc.).

The results are typically presented for four girders.

- Girder 1, or G1 refers to the fascia girder at the top of the plan view,
- Girder 2, or G2 refers to the interior girder adjacent to this fascia girder,
- Girder 3, or G3 refers to the girder closest to or at the bridge cross-section mid-width, and
- Girder 4, or G4 refers to the fascia girder at the bottom of the plan view.

In a number of bridges where there is symmetry about the mid-length of the overall bridge, the response for Girder 4 is basically a reflection of the response of Girder 1. All of the bridges selected in Chapter 3 have the same cross sections for Girders 1 and 4 throughout their length. In fact, in all the bridges selected in Chapter 3, the cross sections are the same for all the girders, interior and exterior. However, in two-span continuous bridges where the spans are not equal, and in bridges where the cross-frame framing is not completely point symmetric about the mid-length of the entire bridge, there will be some differences between the Girder 1 and Girder 4 responses.

Response quantities 1 to 9 (see Table 10 below) are reported for each girder considered. For the major-axis bending moments, vertical deflections, and vertical shear forces, the responses obtained from 3D FEA and LGA are shown on the same plots. These comparison plots allow for a direct evaluation of the differences between the 3D FEA and LGA predictions. Additionally, bar charts are presented in Section 7b showing values of LGA STR I vertical shear forces for the four girders at abutments and piers.

For the live load vertical displacements, the results presented are based on the maximum values from (1) design truck alone, and (2) 25 % of the design truck taken together with the design lane load, as explained in Section 4.3.8.

Table 10. Organization of electronic bridge response data files.

Section Number	Results or Response Quantity	Context
1	(a) Summary of bridge characteristics (b) Synthesis of comparisons between LGA and 3D FEA solutions	
2	(a) Major-axis bending moments, and (b) fatigue stress ranges for the top and bottom flanges	Four girders
3	Vertical displacements	Four girders
4	Layover displacements	Four girders
5	Twist rotations	Four girders
6	Normalized layovers	Four girders
7	(a) Vertical shear forces (b) Vertical shear forces at abutments and piers	Four girders
8	Top flange lateral bending stresses	Four girders (only for 3D FEA)
9	Bottom flange lateral bending stresses	Four girders (only for 3D FEA)
10	Cross-frame member axial forces	Cross-frame top chords, bottom chords, and diagonal members (only for 3D FEA)
11	Overall cross-frame resultant moments and shears	Overall cross-frame units (only for 3D FEA)
12	Vertical reactions	Each of the individual bridge bearings
13	Bearing lateral displacements	Bridge bearings (only for 3D FEA)
14	Live load distribution factor estimates	Four girders
15	Detailed hand calculations	Various quantities

Regarding the calculation of girder layover displacements, two different values are presented on the same plot in the sub-sections of Section 4 listed in Table 10:

1. Absolute transverse displacement of the top flange and
2. Relative displacement of the top flange with respect to the bottom flange.

The related twist rotations are presented in two different ways in Sections 5 and 6:

1. Twist rotations in radians in Section 5 and
2. Normalized relative layover deflections of the top flange with respect to the bottom flange per foot depth of the web (i.e., the relative displacements from Section 4, divided by 12 inches, in Section 6).

A summary table is provided in the last sub-section of Section 5, providing a comparison of the 3D FEA layovers at the supports to estimates from LGA using procedures recommended by FDOT. The procedure is explained in more detail in Section 7.1.1.

The cross-frame forces are reported as the axial forces in the component cross-frame members, as well as the resultant moments and shear forces on the overall cross frames in the sub-sections of Sections 10 and

11. Cross-frame member axial forces are reported separately for the top chords, the bottom chords, and the diagonal members on separate plots in Section 10 of the electronic data files. In addition, the cross-frame resultant moment and resultant shear forces at a transverse section at the mid-width of each cross frame are reported separately in the subsections of Section 11. For loadings in which the bridge is composite, the resultant moments and shears include the contribution from the bridge deck to the cross-frame internal forces.

The cross-frame results are presented as bar charts showing the forces on a cross-frame-by-cross-frame basis moving along the length of the bridge within each "bay" between the girders. The plots start in Bay 1 between Girders PG1 and PG2 (refer to Figure 51), move toward the top right corner of the plan, then progress downward to the next bay and from left to right again. This is explained in Figure 51 showing a plan view of Bridge 2C3-48, which illustrates the girder numbering PG1 through PG5 as well as the Bays 1 through 4 between the girders.

Figure 52 shows the corresponding plan for Bridge 2P3-49, which is the same as Bridge 2C3-48 but with a parallel stagger cross-frame framing arrangement. The development of this cross-frame arrangement is explained in Section 3.6 of this report.

Figures 53 and 54 show example cross-frame component force results for these two bridges. Specifically, these plots show the top chord forces from 3D FEA, corresponding to the nominal concrete dead load for these bridges. The plots in Figures 53 and 54 are annotated to highlight the cross-frame component member forces corresponding to each of the bays. All cross frames in Bridges 2C2-48 and 2P2-49 are X-shaped truss assemblies. Hence, each bar in Figures 53 and 54 corresponds to the top chord of a cross frame. The finite element model of top chord members in V-shaped cross-frame assemblies consists of two members connected at the node where the diagonals frame into the top chord. Two bars are required to show forces in each top chord in such cross frames. The red dotted boxes annotated with IP-1 and IP-2 indicate the location of cross frames at Intermediate Piers 1 and 2, respectively. In Figure 53, the presentation of forces in the top chords of cross frames in Bay 1 begins with the cross frame at the start abutment. This is followed by top chord forces in nine intermediate cross frames in Span 1. Top chord force in the cross frame along the first intermediate pier is shown next, followed by forces in 11 intermediate cross frames in Span 2. Top chord force in the cross frame along the second intermediate pier is shown next, followed by forces in nine intermediate cross frames in Span 3; and finally, the top chord force in the cross frame along the end abutment. The bar graphs for the other bays are similar.

Figure 54 conveys all the CDL top-chord forces in Bridge 2P3-49. In this case, there are eight intermediate cross frames in the end spans of each bay and 10 intermediate cross frames in the center span. The presentation of top chord forces is similar to Bridge 2C3-48.

Given these plots, various aspects of the cross-frame responses in the different bridges can be readily ascertained. For instance, the development of a transverse load path through the cross frames in the short direction between the obtuse corners of each of these bridges can be observed. In addition, it is easier to compare the overall relative magnitudes of the cross-frame forces. For instance, comparing Figures 53 and 54, one can observe that the maximum cross-frame forces in Bridge 2P3-49 are approximately one-third those in Bridge 2C3-48. Although Bridge 2P3-49 has a larger number of cross frames (i.e., 144) compared to Bridge 2C3-48 (i.e., 110), cross-frame forces in Bridge 2P3-49 are significantly smaller than the corresponding cross-frame forces in Bridge 2C3-48. Potential economies may be gained by recognizing the influence of an alternative cross-frame framing arrangement with ample offsets and staggers.
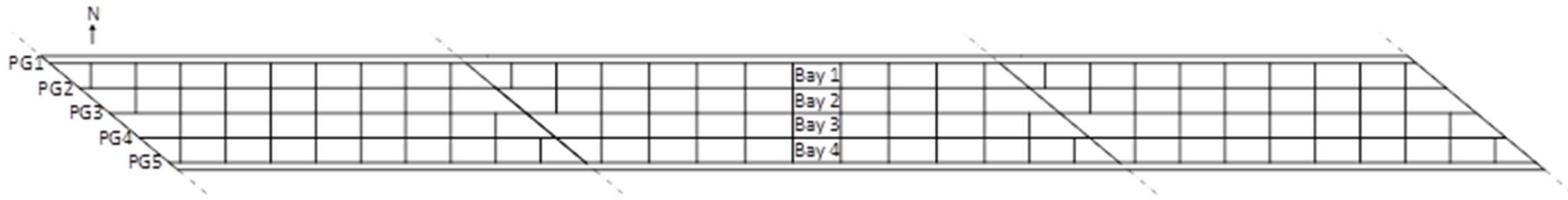
Figure 51. Girder, bay, and cross-frame numbering for Bridge 2C3-48.
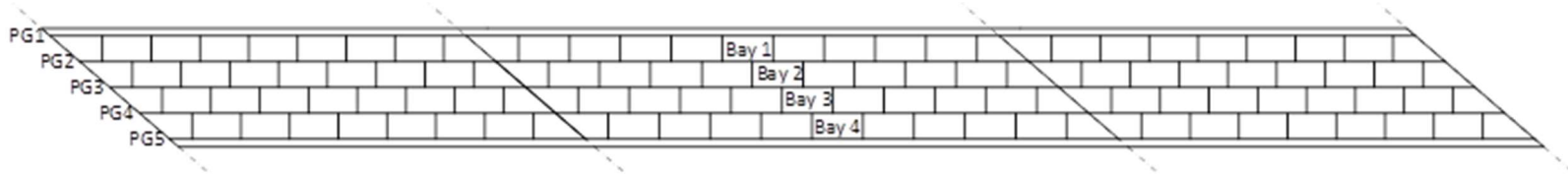
Figure 52. Girder, bay, and cross-frame numbering for Bridge 2P3-49.
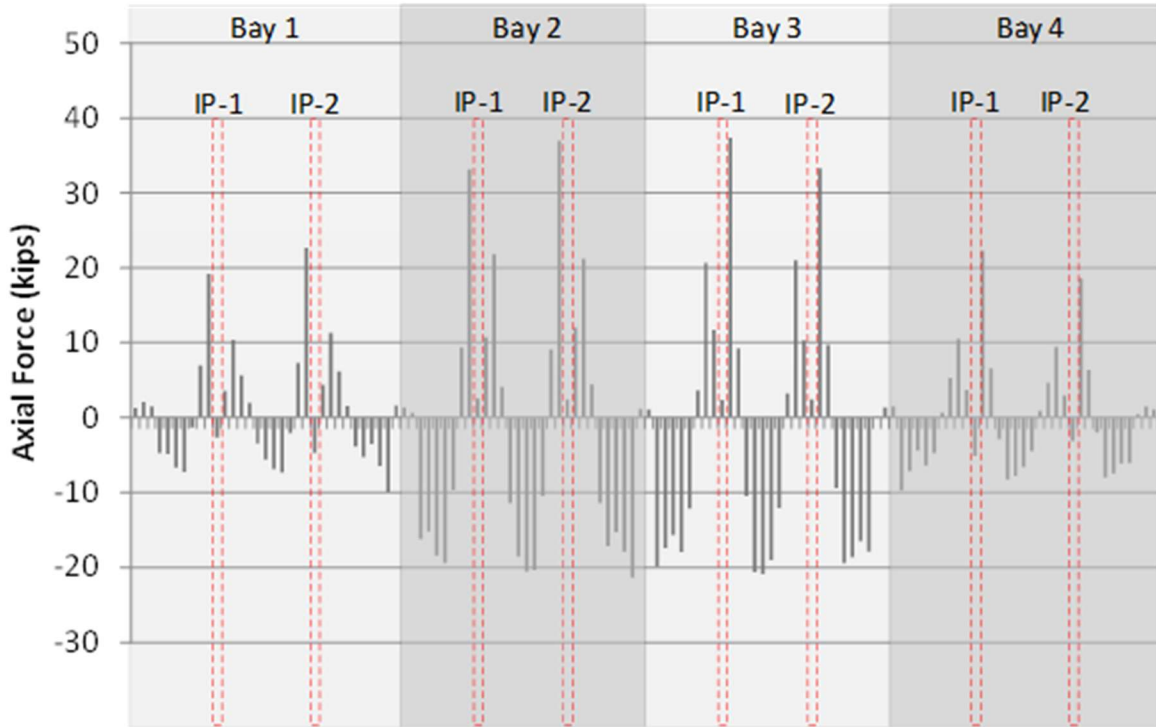
Figure 53. Example cross-frame component force plot (CDL top-chord forces), Bridge 2C3-48.
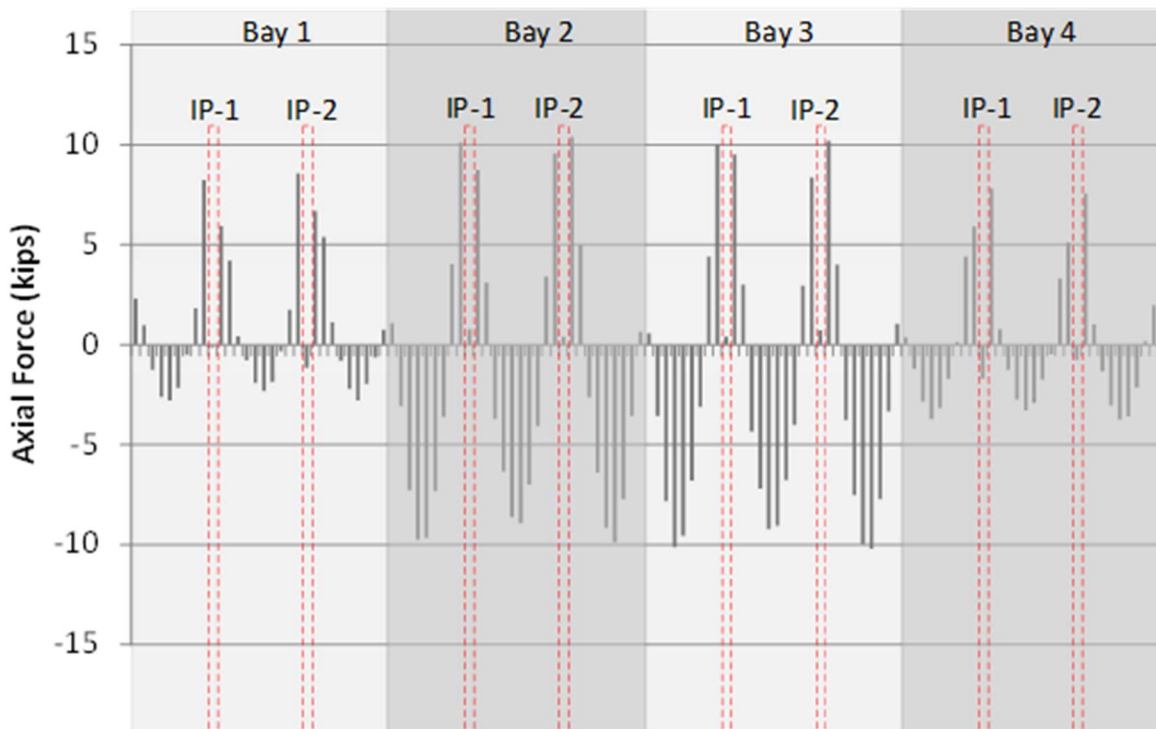
Figure 54. Example cross-frame component force plot (CDL top-chord forces), Bridge 2P3-49.

It is known that theoretically (i.e., based on engineering idealization) the girder flange lateral bending stresses and the cross-frame forces are zero for steel dead load fit under steel dead load. Therefore, these

plots are not included in the electronic data files. To maintain the same page locations for presentation of the different results, the space that would correspond to these plots is blank, making it easier to readily locate and compare the various responses.

Several plots have been added to Section 10 of the electronic data files in Project BEB13 that were not available in Project BE535. These plots are the cross-frame member fatigue force ranges obtained using the new AASHTO (2021) 10th Edition procedures (i.e., the procedures in which the AASHTO fatigue truck is confined to individual longitudinal travel paths for the calculation of force ranges, see Section 3.3.7 of this report). These plots can be compared directly to plots of the cross-frame member force ranges obtained using the AASHTO (2020) 9th Edition procedures, which are provided immediately before the 10th Edition plots. It should be noted that the force ranges in each of these plots are unfactored. For design, the resulting force ranges should be factored by the Fatigue I and Fatigue II factors. In addition, they should be further factored by 0.65 when using the 10th Edition procedures.

In the sub-sections of Section 12 of the electronic data files, as listed in Table 10, vertical reactions are reported at all the bearing locations using bar charts. These bar charts show the reactions for each bearing. For each support line, these quantities are reported for each bearing as one moves from the top to the bottom of the plan view (i.e., from girders PG1 through PGn, where n is the fascia girder number at the bottom of the plan view). For the simple-span bridges, the results are listed starting from the left-most support line and then moving to the right-most support line in the plan view. For multi-span continuous bridges, the vertical reactions are reported at the left-most support line, then the right-most support line, and finally at the intermediate pier supports. For three-span continuous bridges, the bearing reactions at the pier supports are presented starting from the left-most pier and progressing to the right-most pier.

In the sub-sections of Section 13, the 3D FEA lateral displacements perpendicular to the girders at all the bearing locations are presented using bar charts. The order of presentation of this data is the same as that described above for the girder vertical reactions. As mentioned in Section 4.1, a representative elastomeric bearing shear stiffness of 100 kip/ft is assumed at each of the bearing locations in the bridge models. The corresponding bearing lateral forces can be determined by multiplying the lateral displacements (presented in inches) by 100/12.

Significant differences are observed in the live load responses obtained from 3D FEA and LGA. This is readily apparent by comparison of the LLDFs obtained from 3D FEA to the AASHTO LLDFs employed with LGA. In the sub-sections of Section 14, the LLDFs obtained from 3D FEA are compared to the LGA values obtained based on the requirements of Section 4 of the AASHTO LRFD Specifications. LRFD Simon provides live load bending moment envelopes at every tenth point in the spans. If these moment values are divided by the AASHTO LLDF, an envelope of the bending moments corresponding to a LLDF = 1.0 is obtained. The ratio of the 3D FEA live load envelope bending moments at the tenth points to the corresponding bending moments for LLDF = 1.0 obtained from LRFD Simon is presented as the 3D FEA LLDFs. 3D FEA LLDFs are presented for both the positive and negative moment envelopes. The negative moment LLDFs are taken as zero for simple-span bridges. Additionally, 3D FEA LLDF are presented for moments obtained from the fatigue live loading on the bridge.

Section 14 also provides plots of the 3D FEA based LLDFs for the girder moment and for the girder shear ranges obtained from analyses considering the AASHTO fatigue load vehicle. These 3D FEA LLDF are somewhat different from the above values. The fatigue shear range is required in the design of shear connectors. Hence, Section 14 also presents the 3D FEA LLDF for the fatigue shear range. Similar to the ordinary LLDF calculation for moments or shears, the LLDF for the shear range is the ratio of 3D FEA fatigue shear live load shear range at the tenth points to the corresponding shear range for LLDF = 1.0

obtained from LRFD Simon. Three-dimensional effects due to skew tend to amplify the LLDFs at locations where the response quantity is significantly smaller compared to the maximum value of the response quantity. Hence, 3D FEA LLDFs for bending moment, vertical shear force, and shear force range are not shown at datapoints where the ratio of the LGA or 3D FEA response at the given datapoint compared to the maximum value of the LGA or 3D FEA response, respectively for the given girder, is smaller than 30%.

The electronic data files include a separate file for each bridge labeled as Section 15. Section 15 presents the hand calculations of the composite and noncomposite loads, the AASHTO LLDFs including the calculation of the longitudinal stiffness parameter K_g as well as the RCA LLDFs for the fascia girders. For bridges that do not satisfy the range of applicability of AASHTO (2020) Section 4.6.2.2, LLDFs are calculated manually and input into LRFD Simon. These calculations are shown in Section 15.

5.2   Parameters Quantifying the Differences between 3D FEA and 1D LGA Results

For the comparisons presented in the electronic data files, the normalized mean difference and normalized difference of the maximums are used to quantify the differences between the 3D FEA and 1D LGA results.

The normalized mean difference is useful as a broad measure of accuracy, particularly for quantities such as displacement, where both underestimating and overestimating may have negative consequences. The normalized mean difference is defined as follows:

$$\varepsilon_{mean} = \frac{\sum_{i=1}^{n} |LGA - 3DFEA|}{n \times |3DFEA|_{max}}$$
(6)

where

n = number of data points along a given girder throughout the length of the bridge (data sampled at the 10th points) for girder moments, shears, and vertical displacements, or the total number of bearings, for the bridge vertical reactions

The normalized difference of the maximums is a more demanding measure, indicating the worst-case conservative and unconservative differences, normalized by the corresponding maximum 3D FEA response. The normalized difference of the maximums is defined as follows:

$$\varepsilon_{max} = \frac{|LGA|_{max} - |3DFEA|_{max}}{|3DFEA|_{max}}$$
(7)

The normalized difference of the maximums is computed as the difference between the maximum positive LGA and 3D FEA responses, and it is calculated separately as the difference between the maximum negative LGA and 3D FEA responses. The largest of these separate ε_{max} values is then reported as the difference measure for the subject response.

This calculation compares the maximum values without consideration of the specific locations of the responses (i.e., the corresponding girder maximum values in the LGA and in the 3D FEA will generally not be located at the same position along the girder lengths). This quantification of the differences between the LGA and 3D FEA results is judged to be more appropriate than comparing differences point-by-point, or location-by-location, along the girders. For instance, in the maximum positive moment regions of the girders, the maximum LGA moment may be at a slightly different location than the maximum moment

from the 3D FEA. It is submitted that comparing the maximums, occurring at slightly different locations, is more meaningful than comparing the values location-by-location because the girders would be designed for the maximum values in any case in any local region. For negative bending moment, the maximum LGA and 3D FEA moments are typically located at the same positions.

For continuous-span bridges, there can be multiple local maximum girder positive and negative results along the bridge length. In these cases, ε_{max} is calculated using the largest maximums for both the LGA and the 3D FEA responses. In most situations, these maximums occur in the same local region along the bridge. However, in some cases, the local maximums may occur at different positions along the structure.

In Chapter 6, the following additional measures of the differences between the 3D FEA and LGA results are considered. The difference measures presented in the electronic data files provide a more detailed quantification of the results, whereas the difference measures employed in Chapter 6 provide a simpler and more direct quantification of the ability of LGA to capture the more detailed results from 3D FEA.

A large number of the Chapter 6 results are presented directly as the ratio of the corresponding maximum 3D FEA and LGA responses, referred to as the professional factor:

$$\rho_{max} = \frac{\left|3DFEA\right|_{\text{max}}}{\left|LGA\right|_{\text{max}}}$$

(8)

For cases where ρ_{max} is greater than 1.0, the professional factor gives the ratio by which the LGA calculation would need to be scaled to ensure an accurate prediction of the more rigorous result. It is suggested that the ρ_{max} values for the quantities evaluated using this measure should be less than or equal to 1.05. That is, the maximum demand from the 3D FEA should ideally never be more than 5 % larger than the corresponding maximum demand determined from the 1D LGA.

The professional factor is related to ε_{max} by the relation

$$\rho_{max} = \frac{1}{\varepsilon_{max} + 1}$$

(9)

and conversely

$$\varepsilon_{max} = \frac{1}{\rho_{max}} - 1$$

(10)

The calculation of ρ_{max} is handled similarly to the calculation of ε_{max} discussed previously. Separate ρ_{max} results are presented for girder positive and negative bending moments. However, only one ρ_{max} value is determined for girder shears, based on the magnitude of the shear forces throughout the bridge length. In cases where there are multiple local maximum values along the girder lengths, such as continuous-span bridges, ρ_{max} is calculated using the largest maximums for both the LGA and the 3D FEA responses. In most situations, these maximums occur in the same local region along the bridge. However, in some cases, the local maximums may occur at different positions along the structure.

For certain response quantities, namely the maximum girder live load shear forces calculated specifically at the girder ends at the obtuse corners of the spans and the bearing reactions, ρ_{max} is calculated as the ratio of the 3D FEA to the LGA response at the specific named locations. For these cases, the reported value of ρ_{max} is taken as the maximum of these ratios for all of the locations considered.

The following separate normalized measure of the differences is employed to evaluate the girder total dead load vertical displacements in Chapter 5:

$$\varepsilon_{max2} = \frac{\left(\Delta_{LGA}\right)_{\text{max}} - \left(\Delta_{3DFEA}\right)_{\text{max}}}{L_s}$$

(11)

where

$(\Delta_{LGA})_{\text{max}}$ =   girder maximum total dead load vertical deflection from LGA, downward deflections taken as negative

$(\Delta_{3DFEA})_{\text{max}}$ =   girder maximum total dead load vertical deflection from 3DFEA, downward deflections taken as negative

This normalized difference is considered to be a more appropriate measure than ρ_{max} when comparing the LGA total dead load vertical displacement predictions to corresponding 3D FEA values. This is because the ρ_{max} values for the LGA total dead load vertical displacement predictions can be larger than 1.05 and smaller than 0.95 (i.e., $\varepsilon_{max} < -0.05$ or > 0.05). However, depending on the span length, these differences may be acceptable. A limit of 0.0005 on ε_{max2} can be related indirectly to typical tolerances on the roadway smoothness, as discussed below.

The girder total dead load (TDL) displacements are used in setting girder cambers. A significant portion of the camber is removed by the girder vertical deflections during the casting of the deck. Thus, approximations in the TDL displacements can ultimately have some influence on the smoothness of the finished deck as well as other aspects of the bridge construction and the overall constructed geometry of the bridge. Although the smoothness tolerances of the finished deck surface are not directly related to the differences between the LGA and 3D FEA displacements, the smoothness tolerance can be used as an assessment of the differences between LGA and 3D FEA in the prediction of the girder TDL displacements.

Deck smoothness tolerances are provided in Section 400-15.2.5.5 of the FDOT Specifications (FDOT 2022b). This section states the following limit for deviations in the finished deck elevation, measured using a profilograph, longitudinally along the length of the bridge:

"Correct individual bumps or depressions exceeding a cutoff height of 0.3 inch from a chord of 25 feet (see ASTM E1274) on the profilograph trace."

A deviation of 0.3 inch per 25 feet results in a limit of 1/1000. Recognizing that the maximum displacement occurs approximately at the mid-span of the girders, and considering an extension of the deck smoothness limit to vertical deviations along the length of the girders due to approximations from the structural analysis, a similar longitudinal "tolerance" on the deviation between the LGA and 3D FEA vertical displacements can be set as $(L_s/2) / 1000 = L_s / 2000$, where L_s is the span length.

The tolerance of 0.0005 on ε_{max2} can also be related to the positive camber tolerance of 1.5 inches on a welded girder given in Section 3.5.1.3 of (AWS 2020). For a span length of 250 ft, 1.5 in / 250 ft / (12 in/ft) = 0.0005. Therefore, $|\varepsilon_{max2}| < 0.0005$ ensures against deviations between the calculated LGA and 3D FEA deflections being larger than the positive girder camber tolerance for all values of span length for which the recommended LGA procedures can be applied.

In addition, the following normalized difference measure is considered pertaining to the differential displacements across the bridge width, determined by LGA, versus the corresponding values determined using 3D FEA:

$$\varepsilon_{max3} = \max\left\{\begin{array}{c} \dfrac{\left|\left[(\Delta_{LGA})_{\text{max}.G3} - (\Delta_{LGA})_{\text{max}.G1}\right] - \left[(\Delta_{3DFEA})_{\text{max}.G3} - (\Delta_{3DFEA})_{\text{max}.G1}\right]\right|}{w_g}, \\[2ex] \dfrac{\left|\left[(\Delta_{LGA})_{\text{max}.G3} - (\Delta_{LGA})_{\text{max}.G4}\right] - \left[(\Delta_{3DFEA})_{\text{max}.G3} - (\Delta_{3DFEA})_{\text{max}.G4}\right]\right|}{w_g} \end{array}\right\}$$

(12)

where

$[(\Delta_{LGA})_{\text{max}.G3} - (\Delta_{LGA})_{\text{max}.G1}]$ = difference between the maximum girder vertical displacements on the innermost girder G3 and the fascia girder G1 determined by LGA,

$[(\Delta_{3DFEA})_{\text{max}.G3} - (\Delta_{3DFEA})_{\text{max}.G1}]$ = difference between the maximum girder vertical displacements on the innermost girder G3 and the fascia girder G1 determined by 3D FEA,

$[(\Delta_{LGA})_{\text{max}.G3} - (\Delta_{LGA})_{\text{max}.G4}]$ = difference between the maximum girder vertical displacements on the innermost girder G3 and the fascia girder G4 determined by LGA,

$[(\Delta_{3DFEA})_{\text{max}.G3} - (\Delta_{3DFEA})_{\text{max}.G4}]$ = difference between the maximum girder vertical displacements on the innermost girder G3 and the fascia girder G4 determined by 3D FEA, and

w_g = width of the bridge between the fascia girders.

The limit of 0.001 on this measure can be related indirectly to a second deck smoothness tolerance provided in Section 400-15.2.5.5 of the FDOT Specifications (FDOT 2022b):

"Ensure that the surface meets a ¼ inch in 10 feet straightedge check made transversely across the deck."

A transverse deviation of 0.25 inch per 10 feet translates to a limit of 1/480, which rounds to 1/500. Recognizing that cross-slopes are generally built across the deck from the median at the center of the bridge to the two transverse edges of the bridge, and considering an extension of the deck smoothness limit to vertical deviations along the length of the girders due to approximations from the structural analysis, a similar transverse "tolerance" on the deviation between the LGA and 3D FEA vertical displacements can be set as $(w_g/2) / 500 = w_g/1000$, where w_g is the bridge framing width.

It should be noted that $|\varepsilon_{max3}| < 0.001$ is a more relaxed tolerance on the estimate of the maximum differential girder displacements across the bridge width compared to $|\varepsilon_{max2}| < 0.0005$ on the individual girder displacements relative to the span length.

6. COMPARISON OF BRIDGE LGA AND 3D FEA RESPONSES

This chapter presents detailed comparisons of the LGA and 3D FEA girder solutions from the Project BEB13 parametric studies. The structural behavior of a skewed bridge is influenced heavily by a number of factors, such as the bridge articulation (simple- or continuous-span), skew index, bridge width, skew angle, and the cross-frame layout. The behavior of skewed bridges can be explained as being similar to that of an orthotropic plate stiffened by the girders in the longitudinal direction and by cross frames and diaphragms in the transverse direction. Both the girders and the cross frames participate with the bridge deck in delivering loads to the bearing lines.

In continuous-span bridges, the load distribution can be influenced by interaction between the spans, especially in bridges with unequal spans, based on compatibility of deformations of the continuous girders between the adjacent spans. Loads on one span can cause significant internal forces and changes in the displacements and bearing reactions in the other spans. The transverse stiffening from the cross frames and diaphragms influences these interactions. Some cross-frame and/or diaphragm framing arrangements can develop significant continuity effects in the transverse direction at pier locations.

The longitudinal and transverse load paths within the bridge girders are influenced further by the nature of the skew (i.e., parallel or nonparallel). A key characteristic of parallel skew bridges is that all the girders have equal lengths within a span. The span of a bridge with parallel skew has a short and long diagonal direction. A relatively stiff transverse load path tends to form in the short diagonal direction.

Based on the extent of the three-dimensional actions of skewed bridges, such as described above, the exterior, first interior, and the central interior girders are subjected to different internal forces compared to the loads calculated using the assumptions for LGA. Exterior girders directly receive the applied loads from overhangs and the components supported from overhangs. However, they interact with the other girders in the bridge cross section via the interconnection of the girders by the cross frames or diaphragms and the bridge deck, and the continuity of these components across the girders in the transverse direction. Hence, the assumption regarding the distribution of dead loads transversely among the girders can be a potential critical factor influencing the accuracy of LGA.

In this chapter, the results for exterior girders, first interior girders, and the central interior girders are inspected and presented separately to ascertain the influence of the load distribution assumptions, both for the live load and for the dead load, on the LGA accuracy. The professional factor (ρ_{max}), defined by Eq. 22, is employed as the primary summary measure of the differences between the 3D FEA and LGA calculations for the internal force quantities. The ρ_{max} values are useful for indicating the worst-case conservative and unconservative differences between the calculated responses, where values larger than 1.0 indicate unconservative results and values less than 1.0 indicate conservative results. Differences in 3D FEA and LGA responses are tabulated in the individual bridge electronic data files in terms of normalized mean differences (ε_{mean}) and normalized differences of the maximums, ε_{max}, defined in Eqs. 6 and 7. Equations 9 and 10 show the relationships between ε_{max} and ρ_{max}.

The accuracy of the girder displacement predictions is quantified by the measures ε_{max2} and ε_{max3} (Eqs. 11 and 12). As discussed in Section 5.2, these measures provide a more meaningful evaluation of the differences between the LGA and 3D FEA displacements because they are measures normalized by the overall bridge span lengths and framing widths.

The following girder responses pertaining to the design demands are presented in the following sections:

1. The girder positive and negative STR I and SER II major-axis bending moments.
2. The girder STR I and SER II vertical shear forces.
3. The girder HL-93 live load shear forces, focusing in particular on the live load shear forces at the girder ends at the obtuse corners of the spans.
4. The girder STR I bearing reactions at the obtuse corners of simple-spans, and at the fascia girders at the piers in continuous-span bridges.
5. The girder maximum total dead load vertical displacements, including consideration of the effects of steel dead load fit (SDLF) detailing of the cross-frames.
6. The girder fatigue live load vertical shear forces.
7. The girder fatigue live load flexural stress ranges.
8. Interior and exterior girder live load distribution factors (LLDFs).
9. Girder live load deflections.

6.1 STR I and SER II Major-Axis Bending Moments

3D FEA and LGA girder responses are studied for noncomposite dead load, composite dead, and live load cases in the parametric studies. The responses from these basic load cases are combined to obtain the response for the STR I and SER II load combinations. The project electronic data files for each of the 35 bridges studied contains ε_{max} values for all the load cases. The ρ_{max} values are calculated from the ε_{max} values for the above specific design load combinations using Eq. 9. Studying the ρ_{max} or ε_{max} values for the major-axis bending moments for each bridge, it can be seen that 3D FEA solutions and LGA solutions have the largest differences for the rail load and live load cases. The rails are supported on the overhangs of the composite bridge deck, and typically the outer surface of the barrier rails is set flush with the outer edge of the overhang of the bridge deck. Rail loads are idealized as line loads acting at the center of gravity of the barrier rail in the 3D FEA. Distribution of the rail load among the bridge girders is complex, depending on the width of the bridge cross-section, the number of girders, and other attributes. In this research, the rail loads are distributed equally to all the girders in the bridge in the LGA calculations. This assumption introduces differences in the rail load responses obtained from 3D FEA and LGA. The rail load tends to distribute more to the exterior girders than to the interior girders in the 3D FEA; however, the rail loading tends to be relatively small compared to the other load effects.

LLDFs are used to calculate critical live load response envelopes in LGA. The primary AASHTO LRFD LLDFs used in LGA do not account for the action of cross frames in distributing the live load across the width of the bridge. It is intended that this aspect is compensated for when calculating the live load distribution to the fascia girders via the RCA requirement of AASHTO LRFD Article 4.6.2.2.2d. The approximations associated with these LGA tools introduce differences in the bending moments predicted by LGA and 3D FEA. For bridges with parallel skew, the AASHTO LLDF provisions provide some accounting for the tendency of the bridge to transfer significant forces along the short diagonal direction of the bridge spans between the obtuse corners of the spans. This is accomplished via the skew correction factors; however, the skew correction factors do not contain any information pertinent to the size of the bridge cross frames or the ways in which the intermediate cross frames are laid out within the bridge (i.e., cross-frame spacings, contiguous or non-contiguous/staggered cross-frame framing arrangements, etc.).

The steel dead load results with steel dead load fit detailing of the cross frames (i.e., the SDL/SDLF results) from LGA and 3D FEA tend to be in close agreement. Theoretically, SDL/SDLF bending moments should be equal to LGA SDL bending moments. However, the self-weight of the intermediate cross frames is totaled and applied as equal uniformly distributed load to all the girders in the bridge. The specific cross-frame and diaphragm self-weights tributary to each of the girders may be different for each girder, and these self-weights are applied as concentrated loads at their actual locations in the 3D FEA solutions. This introduces small differences between the LGA and 3D FEA girder bending moments. Therefore, the LGA SDL bending moments can be either conservative or unconservative compared to 3D FEA bending moments, but the differences between the LGA and 3D FEA results tends to be small.

The DC1 concrete dead load (CDL) effects tend to be smaller on the exterior girders compared to the interior girders in the bridges studied in this research, since the tributary widths for the exterior girders tend to be smaller than those for the interior girders on these bridges. Therefore, the DC1 (CDL) effect tends to be smaller on the exterior girders relative to that on the interior girders.

The STR I and SER II load combinations consist of noncomposite loads, loads applied long-term to the composite structure, and live loads applied as short-term transient loads to the composite structure. Live load is commonly one of the largest individual contributors to the STR I and SER II bending moments for the bridges studied in this research. The LGA procedures studied use the AASHTO LLDFs in the estimation of bending moments. Any ρ_{max} values greater than unity for STR I or SER II indicate that the LGA solutions are unconservative compared to 3D FEA solutions, and vice versa if ρ_{max} values are smaller than 1.0. The LGA estimates for live load bending moments tend to be conservative when compared to 3D FEA estimates. Hence, LGA values for the STR I and SER II bending moments tend to be conservative compared to 3D FEA in most cases. However, in some situations, the conservatism of the LGA live load calculations does not sufficiently compensate for unconservatism in the dead load calculations; therefore, the ρ_{max} values may be greater than 1.0.

Figures 55 through 57 summarize the ρ_{max} values for the STR I positive bending moments in the 35 bridges evaluated. Figures 58 through 60 summarize the corresponding ρ_{max} values for SER II. Figures 61 to 66 present these results for the negative bending moments. Tables 11 through 15 present all the corresponding numerical ρ_{max} values. The figures all plot ρ_{max} versus the skew index, I_s, given by Eq. 1. The tables list the skew index and the skew angle, θ, along with all the ρ_{max} values. The plots show different symbols for the Category 1, 2C, and 2P bridges. The tables list the bridges in the order of the categories, number of spans, and bridge numbers, as discussed previously in Chapter 3.

Observations regarding the differences between the LGA and 3D FEA results, and the accuracy of the LGA predictions, are as follows:

- The ρ_{max} values for the positive bending moments range from 0.80 to 1.01 for the exterior girders and 0.75 to 1.02 for the interior girders.
- The ρ_{max} values for the negative bending moments range from 0.78 to 0.93 for the exterior girders and 0.74 to 0.97 for the interior girders.
- The ρ_{max} values for the positive bending moments in the Category 1 bridges tend to be slightly larger.
- No consistent trend is identified in the ρ_{max} values in terms of any of the various bridge parameters or attributes. There are numerous attributes that influence the accuracy of LGA for straight skewed bridges. The fact that the highly-simplified LGA procedures are able to produce design results that

fit within a reasonably tight band (i.e., relative minor dispersion in the ρ_{max} values for the responses) is a significant result in itself.

- All of the ρ_{max} values are smaller than the suggested maximum limit of 1.05 for both positive and negative bending moments. The average ρ_{max} values are 0.91 for the STR I positive bending moments and 0.89 for the STR I negative bending moments (the SER II results are comparable). The average STR I ρ_{max} values for positive bending moment in the Category I bridges is 0.91, whereas it is equal to 0.90 for the Category 2C and 0.93 for Category 2P bridges. The average STR I ρ_{max} values tend to be slightly higher for the exterior girders overall (0.90) compared to the interior girders (0.89).

It should be noted that the corresponding STR I and SER II plots look very similar. Also, the values in Table 11 and Table 12 show only a small difference in the ρ_{max} values. This is not an error. The fractions of the factored dead and live loads contributing to the load combinations are different for STR I and SER II. These differences are captured in both the 3D FEA and the LGA solutions. As such, the ρ_{max} values are quite similar for the STR I and SER II results.
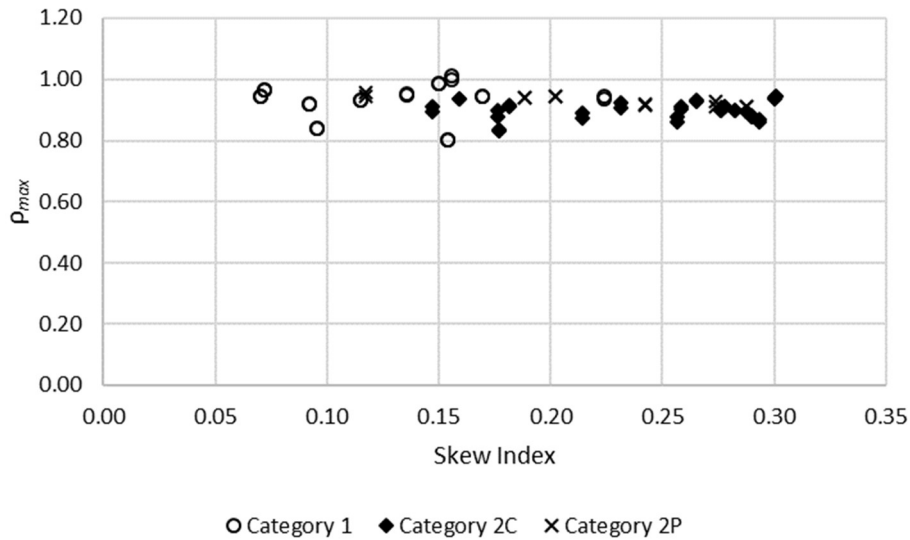
Figure 55. Comparison of ρ_{max} values for STR I positive bending moments for exterior girders.
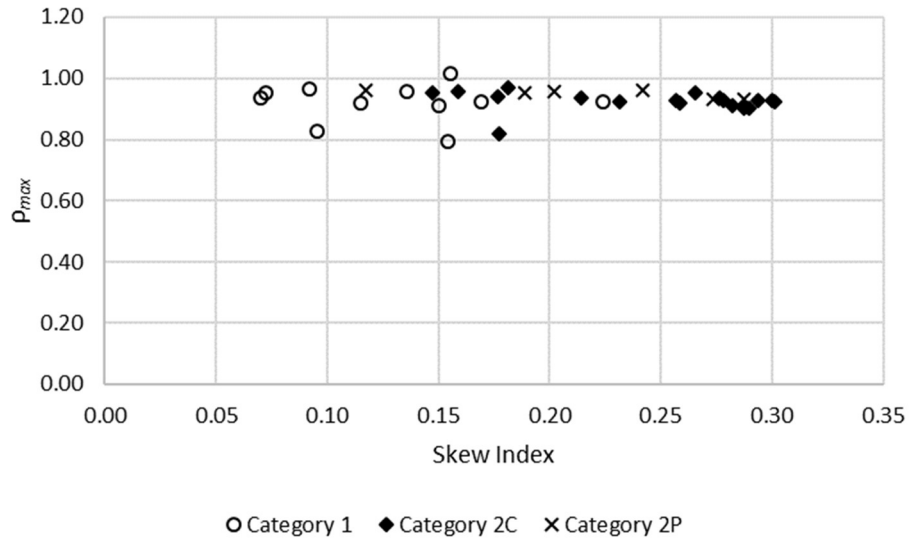
Figure 56. Comparison of ρ_{max} values for STR I positive bending moments for first interior girders.
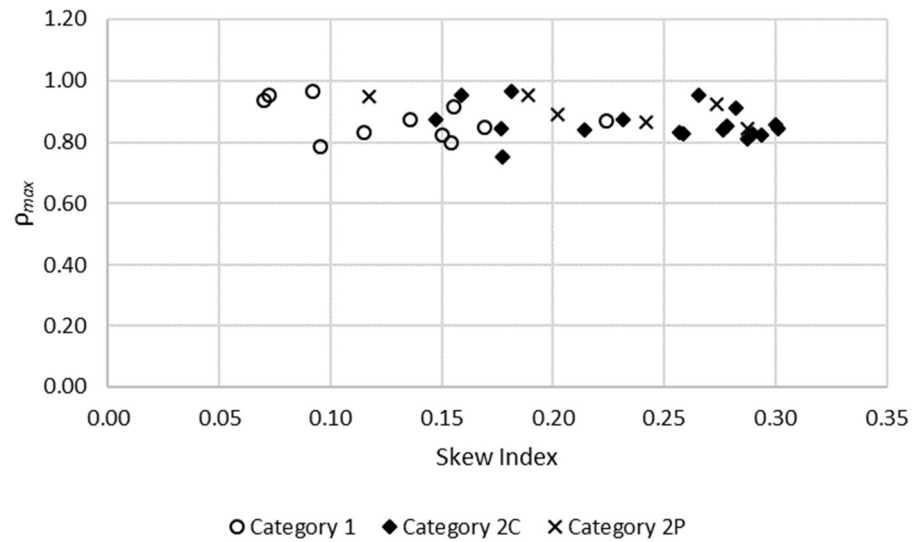
Figure 57. Comparison of ρ_{max} values for STR I positive bending moments for central interior girders.

Table 11. ρ_{max} values for STR I positive bending moments.

Bridge	Skew Index, I_s	Skew Angle, θ (deg.)	ρ_{maxG1}	ρ_{maxG2}	ρ_{maxG3}	ρ_{maxG4}
1C1-21	0.15	16	0.80	0.79	0.80	0.80
1C1-27	0.07	20	0.97	0.95	0.95	0.96
1C1-28	0.10	20	0.84	0.83	0.78	0.84
1C2-26	0.15	10	0.99	0.91	0.82	0.99
1C2-29	0.09	20	0.92	0.97	0.97	0.92
1C2-30	0.14	20	0.95	0.96	0.88	0.95
1C2-50	0.16	20	1.00	1.02	0.92	1.01
1C3-31	0.07	20	0.94	0.94	0.94	0.94
1C3-32	0.11	20	0.93	0.92	0.83	0.93
1C3-33	0.17	20	0.94	0.92	0.85	0.94
1C3-34	0.22	20	0.94	0.92	0.87	0.93
2C1-17	0.28	42	0.90	0.94	0.84	0.90
2C1-35	0.16	44	0.94	0.96	0.95	0.94
2C1-36	0.18	44	0.83	0.82	0.75	0.83
2C1-38	0.30	50	0.95	0.92	0.84	0.94
2C1-39	0.30	37	0.94	0.93	0.86	0.93
2C2-41	0.18	50	0.92	0.97	0.97	0.91
2C2-43	0.27	50	0.93	0.95	0.95	0.93
2C2-44	0.23	40	0.92	0.92	0.88	0.90
2C2-45	0.28	50	0.91	0.93	0.85	0.91
2C2-46	0.29	44	0.86	0.93	0.82	0.87
2C2-46B	0.26	40	0.86	0.93	0.83	0.88
2C2-46C	0.21	35	0.87	0.94	0.84	0.89
2C2-46D	0.18	30	0.88	0.94	0.84	0.90
2C2-46E	0.15	30	0.90	0.95	0.87	0.91
2C3-11	0.26	38	0.91	0.92	0.83	0.90
2C3-47	0.28	50	0.90	0.91	0.91	0.90
2C3-48	0.29	50	0.89	0.90	0.81	0.89
2C3-51	0.29	47	0.88	0.90	0.83	0.88
2P1-18	0.20	40	0.94	0.96	0.89	0.95
2P1-37	0.19	42	0.94	0.95	0.95	0.94
2P2-8	0.27	23	0.91	0.93	0.92	0.93
2P2-40	0.12	23	0.94	0.96	0.95	0.96
2P2-42	0.24	50	0.92	0.96	0.86	0.92
2P3-49	0.29	50	0.91	0.93	0.84	0.91
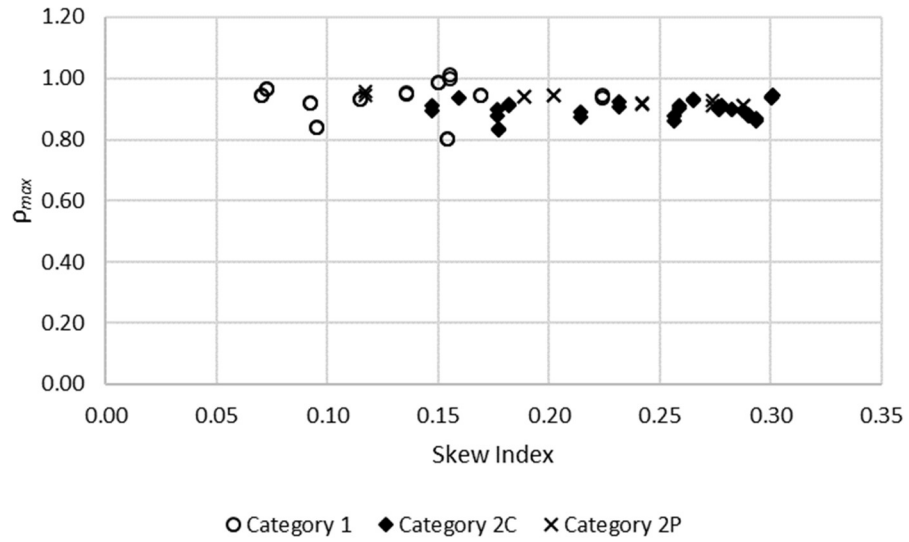
Figure 58. Comparison of ρ*max* values for SER II positive bending moments for exterior girders.
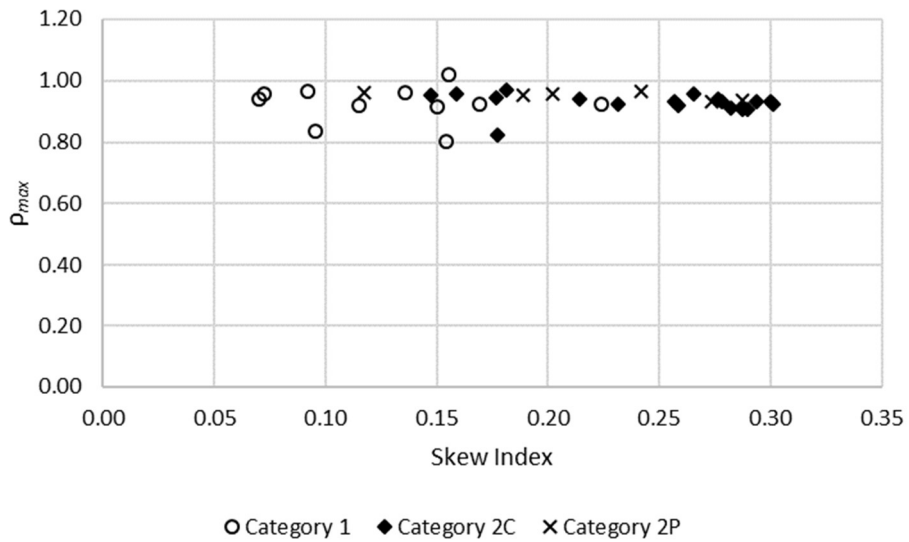
Figure 59. Comparison of ρ*max* values for SER II positive bending moments for first interior girders.
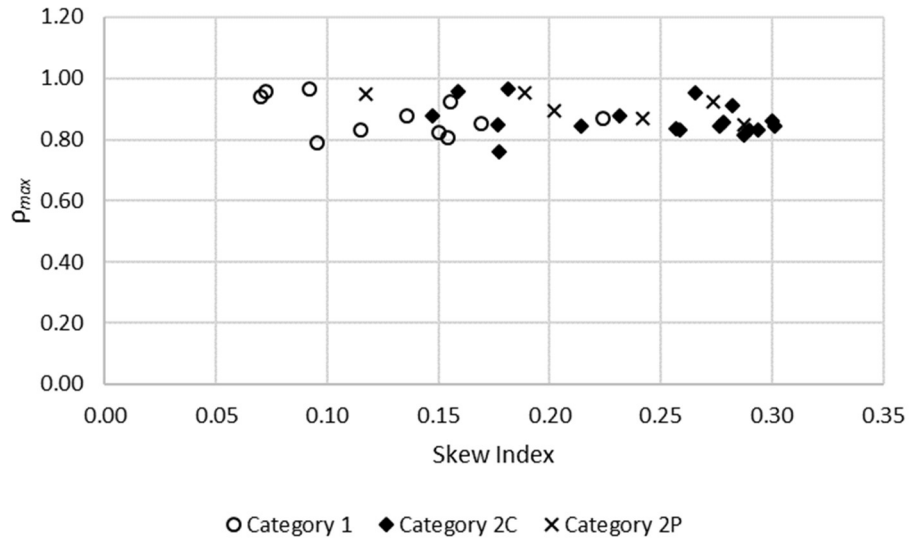
Figure 60. Comparison of ρ*max* values for SER II positive bending moments for central interior girders.

Table 12. ρ_{max} values for SER II positive bending moments.

Bridge	Skew Index, I_s	Skew Angle, θ (deg.)	ρ_{maxG1}	ρ_{maxG2}	ρ_{maxG3}	ρ_{maxG4}
1C1-21	0.15	16	0.81	0.80	0.81	0.81
1C1-27	0.07	20	0.97	0.96	0.96	0.97
1C1-28	0.10	20	0.84	0.84	0.79	0.84
1C2-26	0.15	10	0.99	0.91	0.82	0.99
1C2-29	0.09	20	0.92	0.97	0.97	0.92
1C2-30	0.14	20	0.95	0.96	0.88	0.96
1C2-50	0.16	20	1.00	1.02	0.92	1.01
1C3-31	0.07	20	0.95	0.94	0.94	0.94
1C3-32	0.11	20	0.93	0.92	0.83	0.93
1C3-33	0.17	20	0.95	0.92	0.85	0.95
1C3-34	0.22	20	0.95	0.93	0.87	0.94
2C1-17	0.28	42	0.90	0.94	0.84	0.90
2C1-35	0.16	44	0.94	0.96	0.96	0.94
2C1-36	0.18	44	0.84	0.82	0.76	0.84
2C1-38	0.30	50	0.95	0.92	0.85	0.95
2C1-39	0.30	37	0.94	0.93	0.86	0.94
2C2-41	0.18	50	0.92	0.97	0.97	0.91
2C2-43	0.27	50	0.93	0.96	0.95	0.93
2C2-44	0.23	40	0.93	0.92	0.88	0.91
2C2-45	0.28	50	0.91	0.93	0.86	0.91
2C2-46	0.29	44	0.87	0.93	0.83	0.87
2C2-46B	0.26	40	0.87	0.93	0.84	0.88
2C2-46C	0.21	35	0.88	0.94	0.84	0.90
2C2-46D	0.18	30	0.88	0.94	0.85	0.90
2C2-46E	0.15	30	0.90	0.95	0.88	0.91
2C3-11	0.26	38	0.92	0.92	0.83	0.91
2C3-47	0.28	50	0.90	0.91	0.91	0.90
2C3-48	0.29	50	0.90	0.91	0.82	0.90
2C3-51	0.29	47	0.88	0.91	0.83	0.89
2P1-18	0.20	40	0.95	0.96	0.89	0.95
2P1-37	0.19	42	0.94	0.95	0.95	0.94
2P2-8	0.27	23	0.91	0.93	0.92	0.93
2P2-40	0.12	23	0.95	0.96	0.95	0.96
2P2-42	0.24	50	0.92	0.96	0.87	0.92
2P3-49	0.29	50	0.91	0.94	0.85	0.91
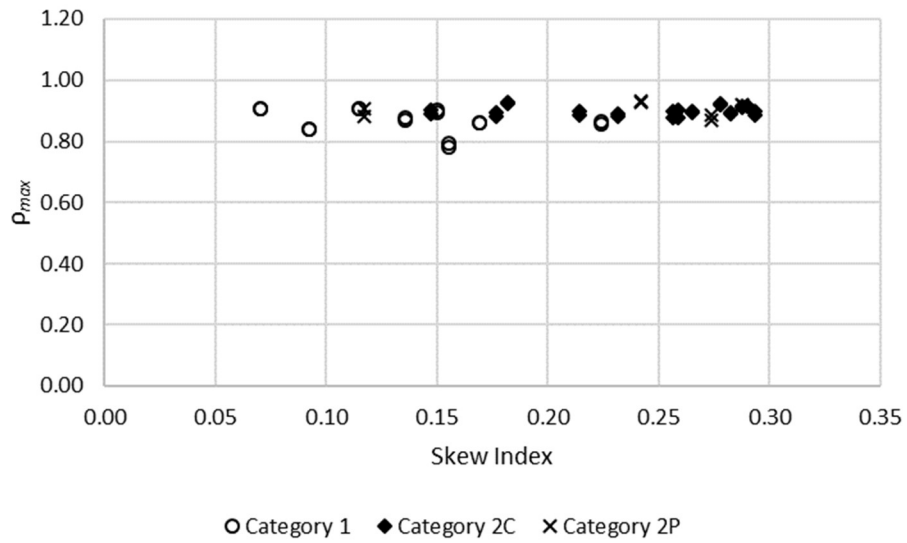
Figure 61. Comparison of ρ*max* values for STR I negative bending moments for exterior girders.

Figure 62. Comparison of ρ*max* values for STR I negative bending moments for first interior girders.

Figure 63. Comparison of ρ*max* values for STR I negative bending moments for central interior girders.

Table 13. ρ_{max} values for STR I negative bending moments.

Bridge	Skew Index, I_s	Skew Angle, θ (deg.)	ρ_{maxG1}	ρ_{maxG2}	ρ_{maxG3}	ρ_{maxG4}
1C1-21	0.15	16	N.A.	N.A.	N.A.	N.A.
1C1-27	0.07	20	N.A.	N.A.	N.A.	N.A.
1C1-28	0.10	20	N.A.	N.A.	N.A.	N.A.
1C2-26	0.15	10	0.90	0.82	0.77	0.89
1C2-29	0.09	20	0.84	0.87	0.87	0.84
1C2-30	0.14	20	0.88	0.88	0.85	0.87
1C2-50	0.16	20	0.79	0.78	0.74	0.78
1C3-31	0.07	20	0.91	0.90	0.90	0.91
1C3-32	0.11	20	0.91	0.89	0.85	0.91
1C3-33	0.17	20	0.86	0.86	0.82	0.86
1C3-34	0.22	20	0.86	0.85	0.83	0.86
2C1-17	0.28	42	N.A.	N.A.	N.A.	N.A.
2C1-35	0.16	44	N.A.	N.A.	N.A.	N.A.
2C1-36	0.18	44	N.A.	N.A.	N.A.	N.A.
2C1-38	0.30	50	N.A.	N.A.	N.A.	N.A.
2C1-39	0.30	37	N.A.	N.A.	N.A.	N.A.
2C2-41	0.18	50	0.93	0.97	0.97	0.92
2C2-43	0.27	50	0.90	0.89	0.89	0.89
2C2-44	0.23	40	0.88	0.89	0.84	0.89
2C2-45	0.28	50	0.92	0.92	0.89	0.92
2C2-46	0.29	44	0.90	0.90	0.88	0.89
2C2-46B	0.26	40	0.90	0.90	0.88	0.88
2C2-46C	0.21	35	0.90	0.91	0.87	0.89
2C2-46D	0.18	30	0.89	0.91	0.87	0.88
2C2-46E	0.15	30	0.90	0.92	0.88	0.89
2C3-11	0.26	38	0.88	0.89	0.83	0.90
2C3-47	0.28	50	0.89	0.90	0.90	0.89
2C3-48	0.29	50	0.92	0.93	0.88	0.91
2C3-51	0.29	47	0.92	0.93	0.89	0.91
2P1-18	0.20	40	N.A.	N.A.	N.A.	N.A.
2P1-37	0.19	42	N.A.	N.A.	N.A.	N.A.
2P2-8	0.27	23	0.89	0.89	0.90	0.87
2P2-40	0.12	23	0.91	0.90	0.91	0.88
2P2-42	0.24	50	0.93	0.94	0.90	0.93
2P3-49	0.29	50	0.92	0.93	0.89	0.92
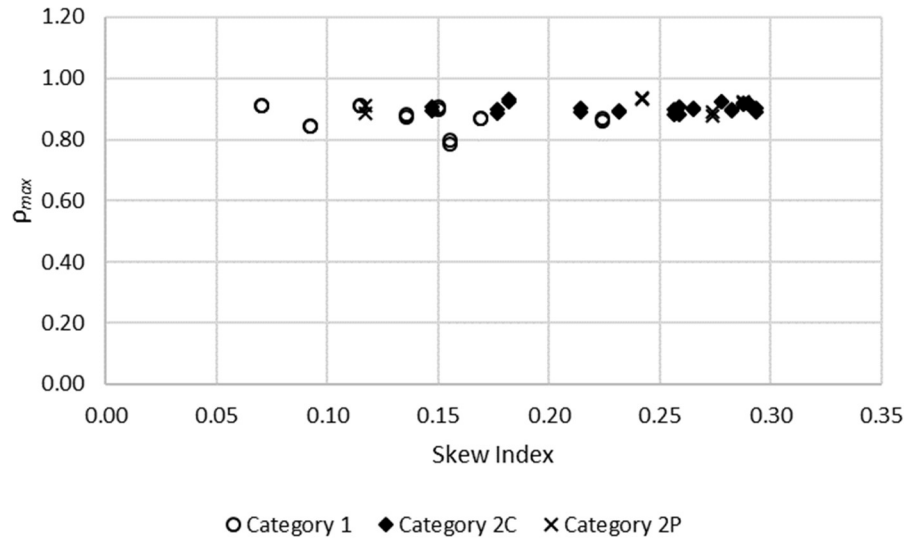
Figure 64. Comparison of ρ*max* values for SER II negative bending moments for exterior girders.
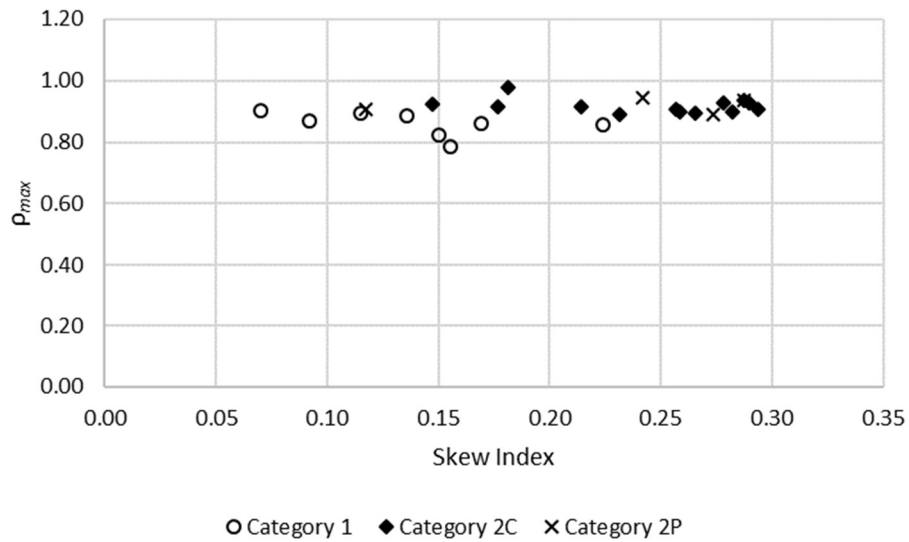
Figure 65. Comparison of ρ*max* values for SER II negative bending moments for first interior girders.
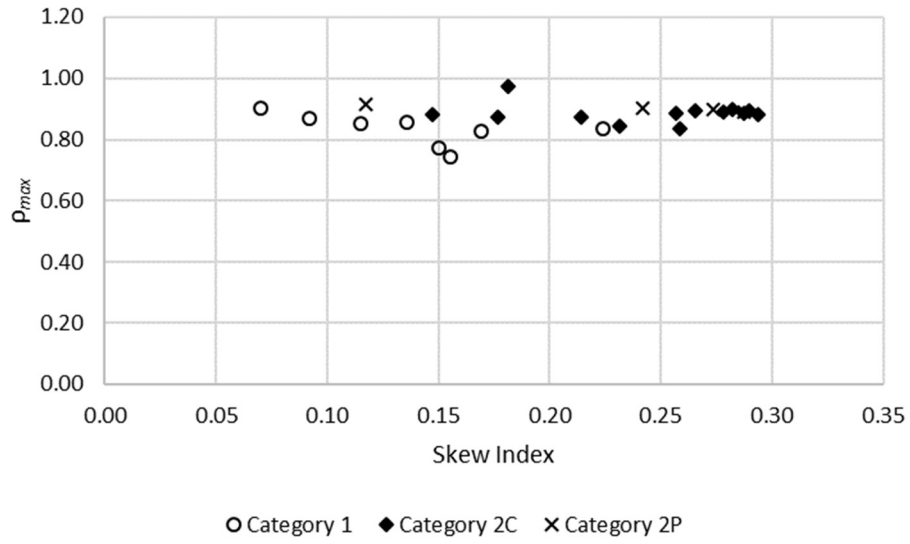
Figure 66. Comparison of ρ*max* values for SER II negative bending moments for central interior girders.

Table 14. ρ_{max} values for SER II negative bending moments.

Bridge	Skew Index, I_s	Skew Angle, θ (deg.)	ρ_{maxG1}	ρ_{maxG2}	ρ_{maxG3}	ρ_{maxG4}
1C1-21	0.15	16	N.A.	N.A.	N.A.	N.A.
1C1-27	0.07	20	N.A.	N.A.	N.A.	N.A.
1C1-28	0.10	20	N.A.	N.A.	N.A.	N.A.
1C2-26	0.15	10	0.91	0.82	0.77	0.90
1C2-29	0.09	20	0.85	0.87	0.87	0.84
1C2-30	0.14	20	0.88	0.88	0.85	0.87
1C2-50	0.16	20	0.80	0.78	0.74	0.79
1C3-31	0.07	20	0.91	0.90	0.90	0.91
1C3-32	0.11	20	0.91	0.89	0.85	0.91
1C3-33	0.17	20	0.87	0.86	0.83	0.87
1C3-34	0.22	20	0.86	0.86	0.83	0.87
2C1-17	0.28	42	N.A.	N.A.	N.A.	N.A.
2C1-35	0.16	44	N.A.	N.A.	N.A.	N.A.
2C1-36	0.18	44	N.A.	N.A.	N.A.	N.A
2C1-38	0.30	50	N.A.	N.A.	N.A.	N.A.
2C1-39	0.30	37	N.A.	N.A.	N.A.	N.A.
2C2-41	0.18	50	0.93	0.98	0.97	0.92
2C2-43	0.27	50	0.90	0.89	0.89	0.90
2C2-44	0.23	40	0.89	0.89	0.84	0.90
2C2-45	0.28	50	0.92	0.93	0.89	0.92
2C2-46	0.29	44	0.90	0.91	0.88	0.89
2C2-46B	0.26	40	0.90	0.91	0.89	0.88
2C2-46C	0.21	35	0.90	0.92	0.87	0.89
2C2-46D	0.18	30	0.90	0.91	0.87	0.89
2C2-46E	0.15	30	0.91	0.92	0.88	0.90
2C3-11	0.26	38	0.88	0.90	0.84	0.91
2C3-47	0.28	50	0.90	0.90	0.90	0.89
2C3-48	0.29	50	0.92	0.94	0.88	0.91
2C3-51	0.29	47	0.92	0.93	0.90	0.92
2P1-18	0.20	40	N.A.	N.A.	N.A.	N.A.
2P1-37	0.19	42	N.A.	N.A.	N.A.	N.A.
2P2-8	0.27	23	0.89	0.89	0.90	0.88
2P2-40	0.12	23	0.91	0.91	0.91	0.89
2P2-42	0.24	50	0.94	0.95	0.90	0.93
2P3-49	0.29	50	0.92	0.93	0.89	0.92

6.2   STR I and SER II Vertical Shear Forces

In a skewed bridge, the intermediate cross frames act to transfer shear forces to the girders at the connecting points. Hence, the shear force diagrams are discontinuous at the locations where the cross frames connect to the girders. The deck, after hardening, also transfers forces due to its stiffness in relationship to the vertical bending displacements in the bridge system. In spans having parallel skew, there is a tendency of the deck, along with the framing of the cross frames, to form a transverse load path between the obtuse corners. Furthermore, the bearing line cross frames aligned along the skew tend to twist the girders to maintain compatibility of displacements, thus developing girder torsional moments that tend to increase the load transferred at the obtuse corners and decrease the load at the acute corners. These effects drive additional shear forces toward the ends of girders near the obtuse corners. Hence, larger ρ_{max} values are observed for STR I shear forces compared to the STR I bending moments. Furthermore, a larger number of discrete changes may be observed in the shear force diagrams when a staggered cross-frame arrangement is used since stagger can increase the number of points along the girders at which cross frames are connected (e.g., parallel stagger arrangements). The discrete changes in shear at these connection points are not modeled in the LGA procedures, adding to the differences observed in 3D FEA and LGA solutions.

Figures 67 through 69 summarize the ρ_{max} values for the STR I vertical shear forces. Figures 71 through 73 summarize the corresponding SER II values. Tables 15 and 16 present the corresponding numerical ρ_{max} values. The format and presentation of the results in the figures and plots is similar to that for the girder bending moments in Section 6.1.

Observations regarding the differences between the LGA and 3D FEA results for STR I and the accuracy of the LGA predictions are as follows (the comparisons for SER II are similar):

- The ρ_{max} values range from 0.91 to 1.07 for the exterior girders and 0.77 to 0.95 for the interior girders.
- The exterior girder ρ_{max} values are largest for the Category 2C bridges and next largest for the Category 2P bridges. It appears that in a few of the Category 2C bridges, the AASHTO skew correction factor on the shear live load distribution slightly underestimates the skew effects on the exterior girder shear forces.
- In the Category 1 bridges, the shear forces tend to be estimated more conservatively for the interior girders, and the ρ_{max} values tend to be slightly smaller than 1.0 for the exterior girders except for Bridge 1C2-26.
- No consistent trend is identified in the ρ_{max} values in terms of any of the various bridge parameters or attributes (e.g., length, skew angle, cross-frame framing arrangement, etc.), suggesting that there are numerous factors that influence the accuracy of LGA for straight skewed bridges, and each influences the results in many different ways.
- The largest ρ_{max} value of 1.07 is slightly larger than the suggested maximum limit of 1.05. However, this occurs for the exterior girders in only one of the 35 bridges studied. It is submitted that the LGA results should be interpreted as acceptable for all the Category 1, 2P, and 2C bridges.
- The average STR I ρ_{max} values are 0.97 for the exterior girders and 0.87 for the interior girders. The average of the ρ_{max} values is 0.95 for the exterior girders in the Category 1 bridges.

It should be noted that the corresponding STR I and SER II plots look very similar. Also, the values in Table 15 and Table 16 show only a small difference in the ρ_{max} values. This is not an error. The fractions of the factored dead and live loads contributing to the load combinations are different for STR I and SER

II. These differences are captured in both the 3D FEA and the LGA solutions. As such, the ρ_{max} values are quite similar for the STR I and SER II results.
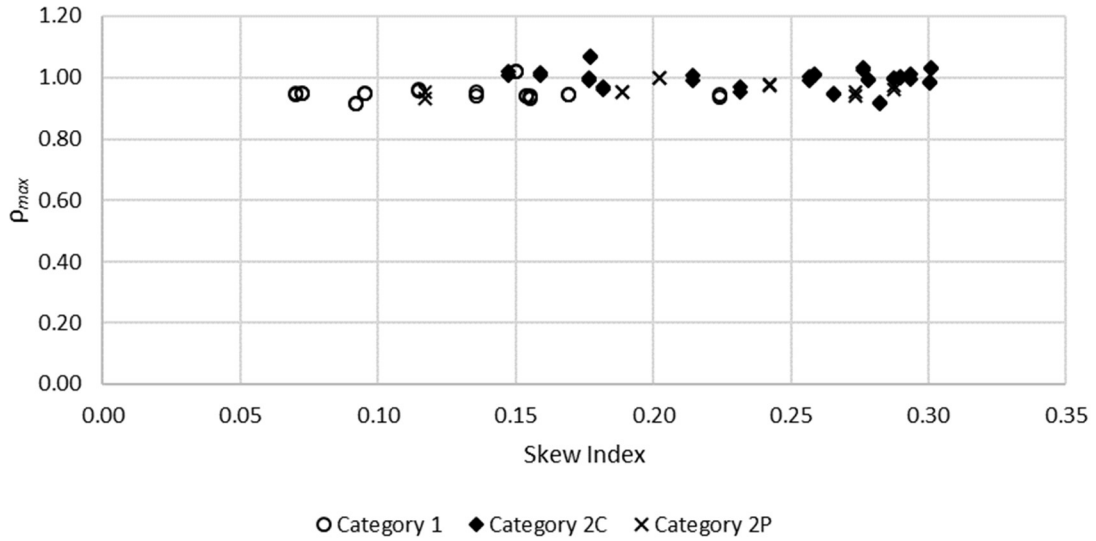
Figure 67. Comparison of ρ_{max} values for STR I vertical shear forces for exterior girders.
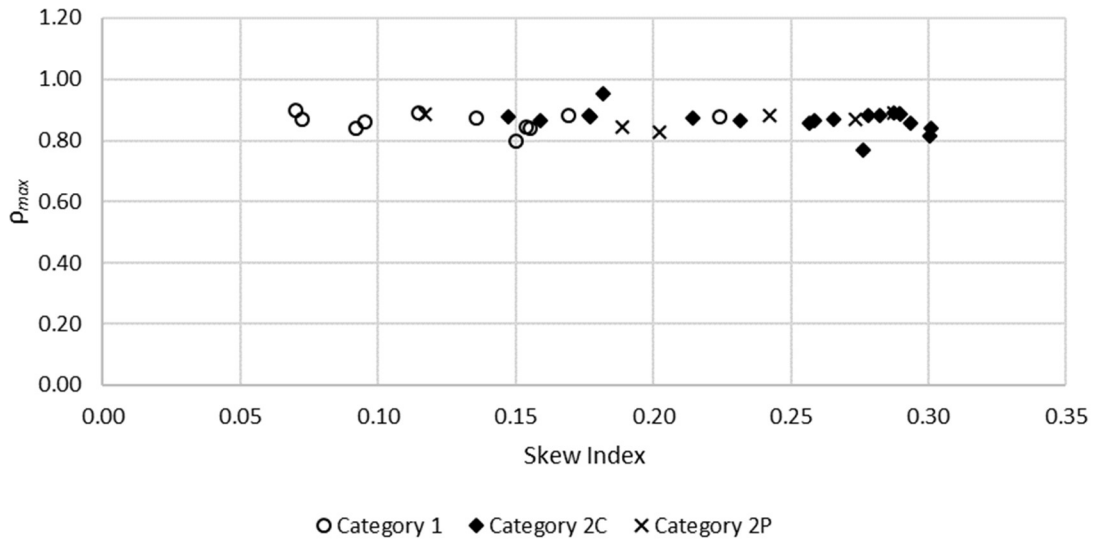
Figure 68. Comparison of ρ_{max} values for STR I vertical shear forces for first interior girders.
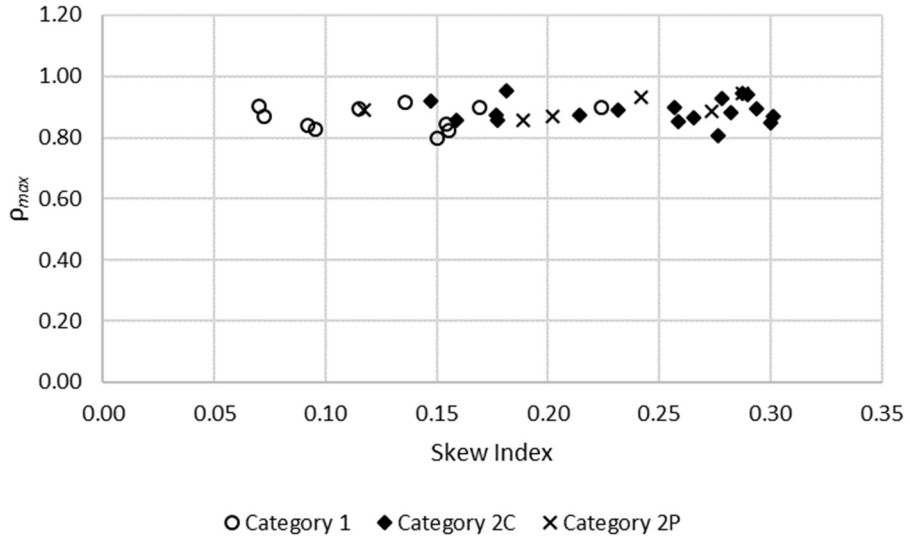
Figure 69. Comparison of ρ*max* values for STR I vertical shear forces for central interior girders.

Table 15. ρ_{max} values for STR I vertical shear forces.

Bridge	Skew Index, I_s	Skew Angle, θ (deg.)	ρ_{maxG1}	ρ_{maxG2}	ρ_{maxG3}	ρ_{maxG4}
1C1-21	0.15	16	0.94	0.85	0.85	0.94
1C1-27	0.07	20	0.95	0.87	0.87	0.95
1C1-28	0.10	20	0.95	0.86	0.83	0.95
1C2-26	0.15	10	1.01	0.80	0.80	1.02
1C2-29	0.09	20	0.91	0.84	0.84	0.91
1C2-30	0.14	20	0.95	0.87	0.91	0.94
1C2-50	0.16	20	0.93	0.84	0.83	0.94
1C3-31	0.07	20	0.95	0.90	0.90	0.94
1C3-32	0.11	20	0.96	0.89	0.90	0.96
1C3-33	0.17	20	0.94	0.88	0.90	0.94
1C3-34	0.22	20	0.93	0.88	0.90	0.94
2C1-17	0.28	42	1.02	0.77	0.81	1.03
2C1-35	0.16	44	1.02	0.86	0.86	1.01
2C1-36	0.18	44	1.07	0.88	0.86	1.07
2C1-38	0.30	50	1.03	0.84	0.87	1.03
2C1-39	0.30	37	0.98	0.82	0.85	0.98
2C2-41	0.18	50	0.97	0.95	0.95	0.96
2C2-43	0.27	50	0.95	0.87	0.86	0.94
2C2-44	0.23	40	0.97	0.87	0.89	0.95
2C2-45	0.28	50	0.99	0.88	0.93	1.00
2C2-46	0.29	44	1.01	0.86	0.89	1.00
2C2-46B	0.26	40	1.01	0.86	0.90	0.99
2C2-46C	0.21	35	1.01	0.87	0.87	0.99
2C2-46D	0.18	30	1.00	0.88	0.87	0.99
2C2-46E	0.15	30	1.02	0.88	0.92	1.01
2C3-11	0.26	38	1.00	0.86	0.85	1.01
2C3-47	0.28	50	0.92	0.88	0.88	0.91
2C3-48	0.29	50	1.00	0.89	0.95	1.00
2C3-51	0.29	47	1.00	0.89	0.94	1.00
2P1-18	0.20	40	1.00	0.83	0.87	1.00
2P1-37	0.19	42	0.95	0.84	0.86	0.95
2P2-8	0.27	23	0.95	0.87	0.88	0.94
2P2-40	0.12	23	0.95	0.88	0.89	0.93
2P2-42	0.24	50	0.98	0.88	0.93	0.97
2P3-49	0.29	50	0.97	0.89	0.95	0.96
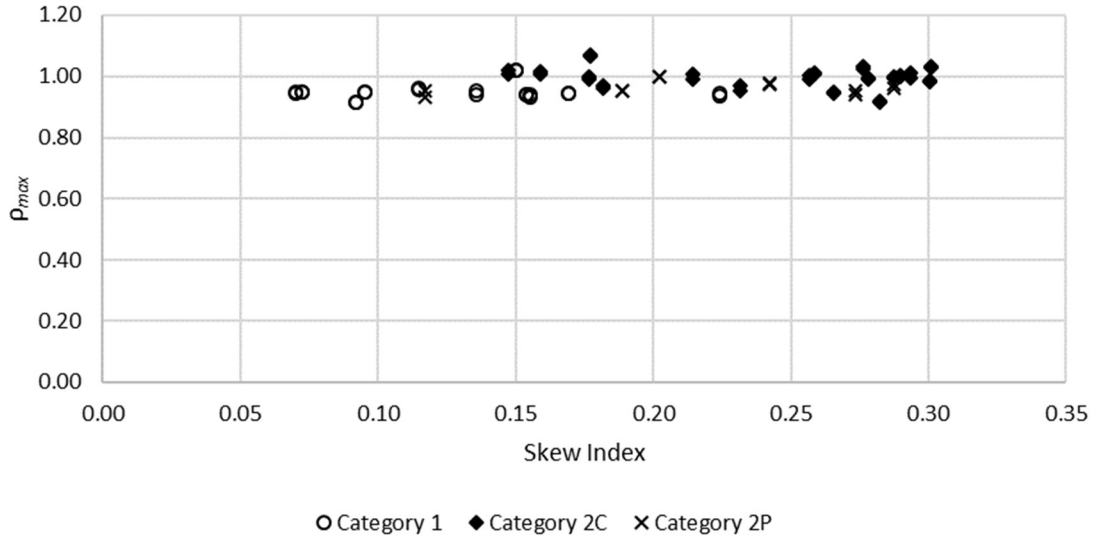
Figure 70. Comparison of ρ*max* values for SER II vertical shear forces for exterior girders.
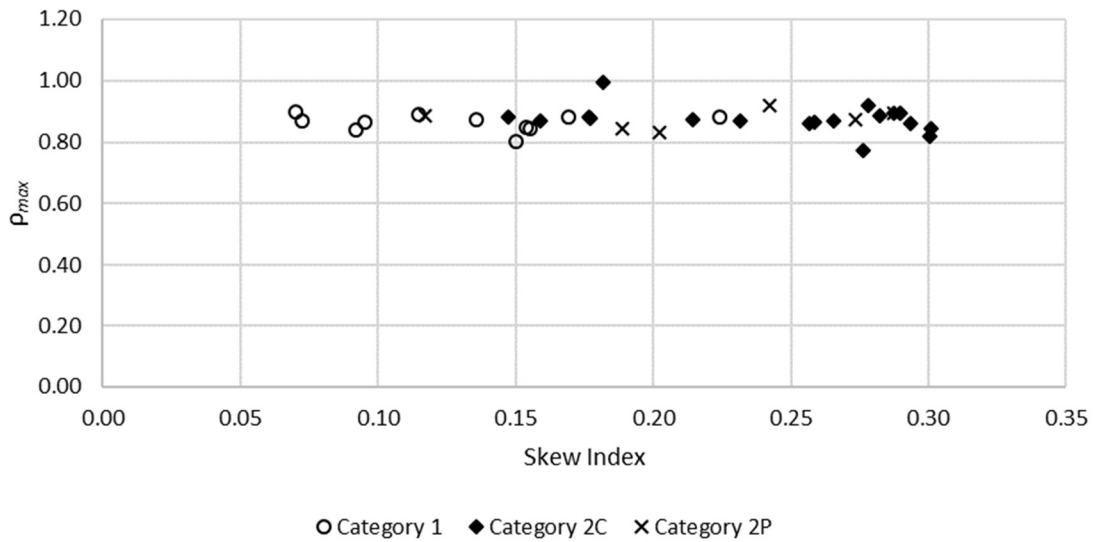
Figure 71. Comparison of ρ*max* values for SER II vertical shear forces for first interior girders.
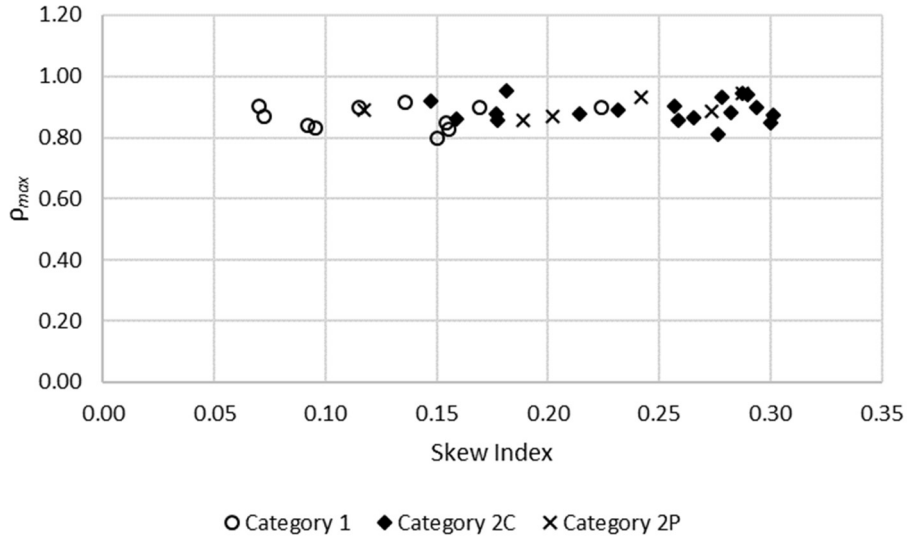
Figure 72. Comparison of ρ_{max} values for SER II vertical shear forces for central interior girders.

Table 16. ρ_{max} values for SER II vertical shear forces.

Bridge	Skew Index, I_s	Skew Angle, θ (deg.)	ρ_{maxG1}	ρ_{maxG2}	ρ_{maxG3}	ρ_{maxG4}
1C1-21	0.15	16	0.94	0.85	0.85	0.94
1C1-27	0.07	20	0.95	0.87	0.87	0.95
1C1-28	0.10	20	0.95	0.87	0.83	0.95
1C2-26	0.15	10	1.02	0.80	0.80	1.02
1C2-29	0.09	20	0.92	0.84	0.84	0.91
1C2-30	0.14	20	0.95	0.87	0.91	0.94
1C2-50	0.16	20	0.93	0.84	0.83	0.94
1C3-31	0.07	20	0.95	0.90	0.90	0.95
1C3-32	0.11	20	0.96	0.89	0.90	0.96
1C3-33	0.17	20	0.94	0.88	0.90	0.94
1C3-34	0.22	20	0.94	0.88	0.90	0.94
2C1-17	0.28	42	1.02	0.77	0.81	1.03
2C1-35	0.16	44	1.02	0.87	0.86	1.01
2C1-36	0.18	44	1.07	0.88	0.86	1.07
2C1-38	0.30	50	1.03	0.84	0.87	1.03
2C1-39	0.30	37	0.98	0.82	0.85	0.98
2C2-41	0.18	50	0.97	0.96	0.95	0.96
2C2-43	0.27	50	0.95	0.87	0.87	0.94
2C2-44	0.23	40	0.97	0.87	0.89	0.95
2C2-45	0.28	50	0.99	0.89	0.93	0.99
2C2-46	0.29	44	1.01	0.86	0.90	0.99
2C2-46B	0.26	40	1.00	0.86	0.90	0.99
2C2-46C	0.21	35	1.01	0.88	0.88	0.99
2C2-46D	0.18	30	1.00	0.88	0.88	0.99
2C2-46E	0.15	30	1.02	0.88	0.92	1.01
2C3-11	0.26	38	1.01	0.87	0.85	1.01
2C3-47	0.28	50	0.92	0.89	0.88	0.91
2C3-48	0.29	50	1.00	0.89	0.95	1.00
2C3-51	0.29	47	1.00	0.89	0.94	1.00
2P1-18	0.20	40	1.00	0.83	0.87	1.00
2P1-37	0.19	42	0.95	0.85	0.86	0.95
2P2-8	0.27	23	0.95	0.87	0.89	0.94
2P2-40	0.12	23	0.95	0.89	0.89	0.93
2P2-42	0.24	50	0.98	0.88	0.93	0.97
2P3-49	0.29	50	0.97	0.89	0.95	0.96

6.3 HL-93 Live Load Shear Forces

Predicting the response of highway bridges to vehicular live load is key to designing for strength and serviceability requirements. 3D FEA solutions calculate maximum and minimum envelopes for response quantities at all locations throughout the structure, algorithmically finding the critical location of the live loads on the bridge deck causing the maximum or minimum response at each location. Hence, the problem of estimating live loads is complex and involves significant computational demands. LLDFs provide a coarse approximation of the transverse distribution of the live loads across the bridge deck. In combination with the use of influence lines to determine the longitudinal positioning of the live loads to cause the largest maximum and minimum effects, LLDFs greatly simplify the live load calculations. Typically, the AASHTO LLDFs are conservative when compared to 3D FEA solutions (AASHTO 2020).

In the parametric studies, the behavior of the 35 study bridges is investigated using the AASHTO HL-93 live load model. As a part of the study, LLDFs using the 3D FEA solutions are calculated and documented in each of the individual bridge electronic data files. Simon provides LGA live load envelopes of bending moments and vertical shears at every tenth point in bridge spans. If these envelope values are divided by the AASHTO LLDF corresponding to the quantity under consideration, an envelope of values corresponding to a LLDF = 1.0 is obtained. The 3D FEA LLDF is defined as the ratio of the 3D FEA live load envelope values at the tenth points to the corresponding LGA values for LLDF = 1.0. These factors are calculated for the live load girder major-axis bending moments and vertical shear forces and are presented in the electronic data files.

The calculated 3D FEA LLDFs can be compared to the distribution factors calculated using the AASHTO LRFD procedures. These comparisons provide insight into the accuracy of LGA with respect to 3D FEA. Such comparisons are presented in Section 6.8.

It is well known that the local effects of skew near the bearing lines and the stiff transverse load path that develops between the obtuse corners in a parallel skew bridge span cause larger shear forces at the ends of girders near the obtuse corners. This section focuses on the accuracy of the AASHTO LRFD prediction of these specific shear forces. It should be noted that the skew correction factor is included in the calculation of the AASHTO LLDFs being considered and in the calculation of the LGA girder shear forces. In a number of cases, the professional factor, ρ_{max}, for the live load shear forces at obtuse corners of bridge spans is observed to be greater than unity. The ρ_{max} values represent multipliers that can be applied to the AASHTO LLDFs to obtain the 3D FEA estimates.

Figure 73 and Table 17 present the ρ_{max} values for the AASHTO LRFD calculation of the fascia girder shear forces at the exterior girder ends at the obtuse corners of the bridge spans. Observations regarding the differences between the LGA and 3D FEA results and the accuracy of the LGA predictions are as follows:

- The ρ_{max} values range from 0.86 to 1.17.
- The ρ_{max} values tend to be smaller, and all < 1.0, for the Category 1 bridges. The average value is 0.90 for the Category 1 bridges.
- The ρ_{max} values tend to be larger for the Category 2P bridges but are all ≤ 1.0. The average value is 0.95 for the Category 2P bridges.
- The ρ_{max} values are largest for the Category 2C bridges, and are > 1.0 for many of the bridges. The average value is 1.03 for the Category 2C bridges.

The largest ρ_{max} value of 1.17 occurs in the three-span continuous bridge 2C3-51, while the largest ρ_{max} value for simple span bridges of 1.13 occurs in 2C1-36. Figure 74 shows the specific live load shear

envelopes corresponding to Bridge 2C1-36; Figure 75 shows the corresponding shear envelope of Bridge 2C3-51 producing the largest ρ_{max} value in Figure 73. The 3D FEA solution for the shear near the obtuse corner in Girder 1 at the start abutment in Bridge 2C1-36 and in the middle span at the right end of Girder 1 in Bridge 2C3-51 has an abrupt increase, just prior to reaching the bearing location, due to the shear transferred by the intermediate cross frame adjacent to the bearing (see Figure 22 and Figure 37 for the bridge plan views of 2C1-36 and 2C3-51, respectively). The LGA does not capture this discrete increase in the shear in the short length at the ends of the girder spans in the two bridges since all but the HL-93 truck loads are represented by uniformly distributed loads in the LGA. Therefore, the LGA estimates of the shear are smaller than the 3D FEA shear in the local regions at the ends of the girder adjacent to the obtuse corners. It may be noted from Figure 75 that discrete "jumps" in shear forces are observed near the obtuse corners in every span. Connected to this behavior is the discrete reduction in shear forces at the acute corners in continuous spans at intermediate piers.

The comparable ρ_{max} values for all the LGA-amenable bridges studied in Project BE535 was less than or equal to 1.0. It appears that the values are larger in many of the BEB13 bridges because of the relatively large number of bridges with contiguous cross-frame arrangements. Even with the offsets of the intermediate cross frames relative to the bearing lines set to $4b_f$, it is apparent that a substantial shear force transfer can occur from the intermediate cross frames, particularly near the obtuse corner of the spans. However, in spite of the underprediction of HL-93 shear forces in several Category 2C bridges, the STR I and SER II estimates are sufficient for the study bridges. Section 6.2 indicates that ρ_{max} values corresponding to STR I or SER II shear are 1.07 and 1.0 respectively for Bridges 2C1-36 and 2C3-51 respectively. This is due to the compensating effects from the dead loads that are assumed to be distributed equally to all girders in a given bridge for the application of LGA. In reality for the study bridges, the exterior girder carries smaller dead loads in the 3D FEA than in the LGA for the steel dead load (self-weight) from the cross frames, the concrete dead load, and the wearing surface and utility loads, which are all assumed to be equally distributed between all the girders in LGA. The DC2 loading from the barrier rails is a different case, where the exterior girders tend to see a larger proportion of that load than obtained assuming equal distribution to all the girders. However, the overall magnitude of the DC2 load is not large enough to make a significant difference for the study bridges.
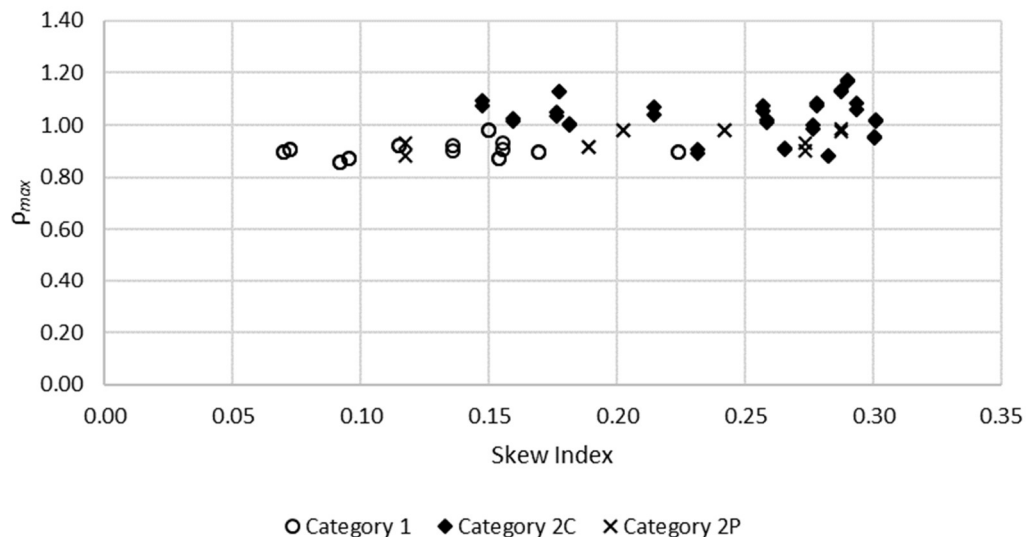
Figure 73. ρ_{max} values for the HL-93 live load shear forces at the exterior girder ends at the obtuse corners of the spans.
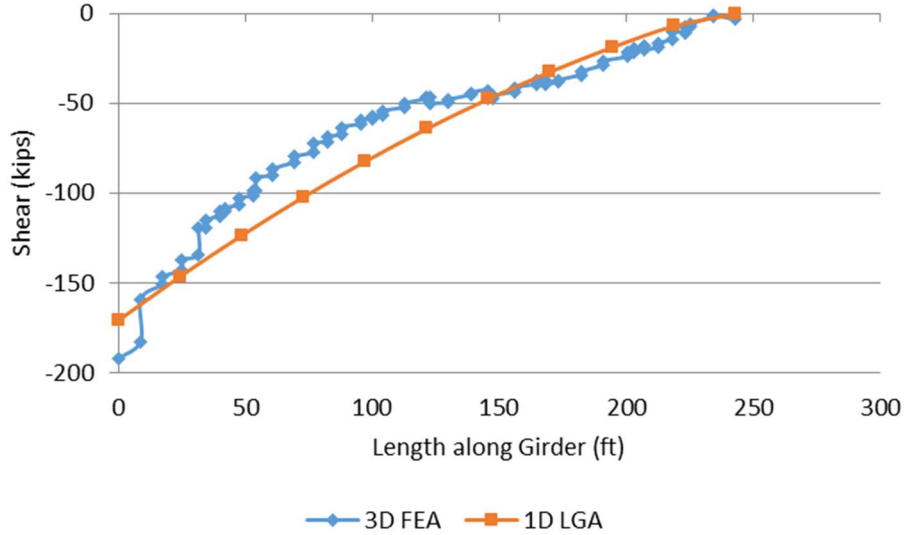
Figure 74. Comparison of maximum negative live load shear forces in the exterior Girder 1 of Bridge 2C1-36 (note that the negative shear sign convention employed in the project electronic data files is opposite from the typical sign convention for beam shear).
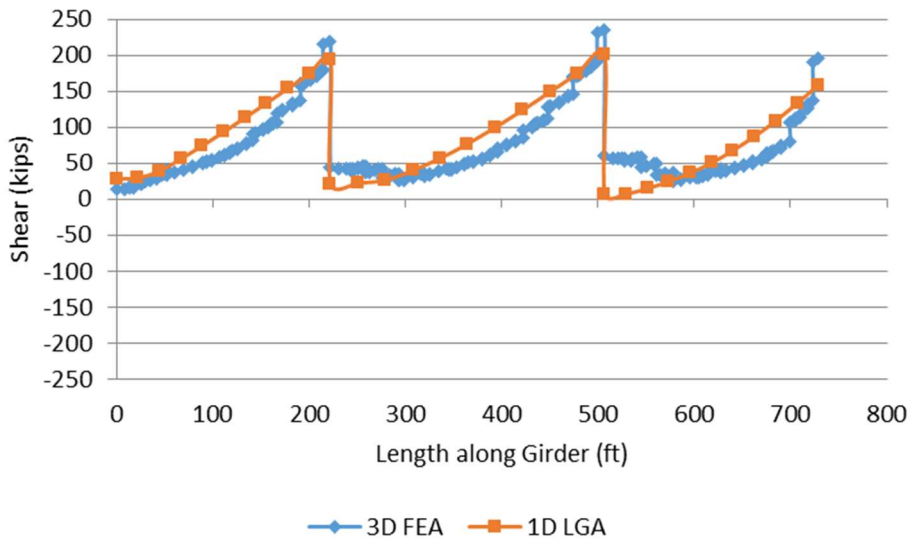
Figure 75. Comparison of maximum negative live load shear forces in the exterior Girder 1 of Bridge 2C3-51 (note that the negative shear sign convention employed in the project electronic data files is opposite from the typical sign convention for beam shear).

Table 17. ρ_{max} values for the HL-93 live load shear forces at the exterior girder ends at the obtuse corners of the spans.

Bridge	Skew Index, I_s	Skew Angle, θ (deg.)	ρ_{maxG1}	ρ_{maxG4}
1C1-21	0.15	16	0.87	0.87
1C1-27	0.07	20	0.91	0.91
1C1-28	0.10	20	0.87	0.87
1C2-26	0.15	10	0.98	0.98
1C2-29	0.09	20	0.86	0.86
1C2-30	0.14	20	0.92	0.90
1C2-50	0.16	20	0.93	0.91
1C3-31	0.07	20	0.90	0.90
1C3-32	0.11	20	0.92	0.92
1C3-33	0.17	20	0.90	0.90
1C3-34	0.22	20	0.90	0.90
2C1-17	0.28	42	0.99	1.00
2C1-35	0.16	44	1.02	1.01
2C1-36	0.18	44	1.13	1.13
2C1-38	0.30	50	1.02	1.02
2C1-39	0.30	37	0.95	0.95
2C2-41	0.18	50	1.01	1.00
2C2-43	0.27	50	0.91	0.91
2C2-44	0.23	40	0.91	0.89
2C2-45	0.28	50	1.07	1.09
2C2-46	0.29	44	1.09	1.06
2C2-46B	0.26	40	1.08	1.05
2C2-46C	0.21	35	1.07	1.04
2C2-46D	0.18	30	1.05	1.03
2C2-46E	0.15	30	1.09	1.07
2C3-11	0.26	38	1.01	1.02
2C3-47	0.28	50	0.88	0.88
2C3-48	0.29	50	1.13	1.13
2C3-51	0.29	47	1.17	1.17
2P1-18	0.20	40	0.98	0.98
2P1-37	0.19	42	0.92	0.92
2P2-8	0.27	23	0.93	0.90
2P2-40	0.12	23	0.93	0.88
2P2-42	0.24	50	0.98	0.98
2P3-49	0.29	50	0.97	0.99

6.4   STR I Bearing Reactions

The bearing reactions include the contributions from the girders through girder shear forces as well as from bearing line cross frames via the cross-frame shear forces. The ρ_{max} values for the STR I bearing reactions for the exterior girders at the obtuse corners at the end abutments are observed to be greater than unity in a significant number of cases (see Figure 76 and Table 18). This occurs even for some of the Category 1 bridges; however, ρ_{max} values larger than 1.0 are particularly prevalent for the Category 2C bridges. One of the ρ_{max} values is as large as 1.20. Nearly all of the ρ_{max} values for Category 2C bridges are greater than 1.0. For Category 2P bridges, 50% of the ρ_{max} values are larger than 1.0, with 1.04 being the maximum. Conversely, ρ_{max} values of the bearing reactions at the piers for the exterior girders of all the continuous-span bridges are smaller than 1.0. Additionally, for the first-interior girder at the obtuse corners at the end abutments, all of the ρ_{max} values are less than 1.0 (data not shown).

It should be noted that the ρ_{max} values shown in Figures 76 and 77, and Table 18, include the application of the girder skew correction factor. In the case of pier bearing reactions, the largest skew correction factor from the adjacent spans is applied. This practice is based on the interpretation and application of the AASHTO LRFD Article 4.6.2.2 rules as implemented in LRFD Simon. These calculations are employed internally in LRFD Simon when its program-defined distribution factors option is employed.

Project BE535 recommended the application of an additional factor of 1.10 be applied to the STR I bearing reactions at both the obtuse corners at end abutments in all cases, as well as to the exterior girder bearing reactions at the piers of continuous-span bridges. The BEB13 results indicate that the factor needs to be increased to 1.20 at the obtuse corners at end abutments, but do not show any need for an additional factor to be applied at the exterior girders at pier locations in any of the continuous-span bridges studied. The BE535 recommendation of a factor of 1.10 at the exterior girders at pier locations in continuous-span bridges was based largely on Bridge 11 in that project, which had intermediate cross frames framing directly into the bearing lines at its piers (resulting in a ρ_{max} for the pier bearing reactions on the exterior girders of 1.11), although one other LGA amenable bridge, Bridge 6 in that project, having contiguous cross-frame lines, had a ρ_{max} for the bearing reactions at its pier of 1.06. However, Bridge 6 is a relatively wide Category 3 bridge. Bridge 2C3-11 has a modified cross-frame framing arrangement employing cross frames directly along the pier bearing lines and offsetting of the intermediate cross frames from its piers. This change in the cross-frame framing arrangement results in a change in the ρ_{max} for the pier exterior girder reactions from 1.11 for Bridge 11 in the BE535 study to 0.91 for Bridge 2C3-11 in Table 18. The maximum value of ρ_{max} for Category 2P bridges is 1.04, which is within the suggested maximum limit of 5%. However, the ρ_{max} values are sensitive to the offsets and staggers in the framing arrangement employed in Category 2P bridges. As such, the sample size of six Category 2P bridges is not large enough to be considered a representative sample of Category 2P bridge that covers the entire range of geometric variables and cross-frame offsets. Hence, a correction factor of 1.10 is recommended for Category 2P bridge to maintain consistency with the BE535 recommendations.

Based on the combined results from BEB13 and BE535, it is recommended that:

- For bridges in Category 2C
    - The exterior girder reactions at the obtuse corners of the spans at end abutments should be multiplied by a factor of 1.20, and
- For Category 1 and 2P bridges
    - The exterior girder reactions at the obtuse corners of the spans at the end abutments should be multiplied by a factor of 1.10.

These factors are in addition to the application of the skew correction factor for the span under consideration for the end abutments, and the larger of the skew correction factors from the adjacent spans at the pier bearing locations. If the application of the recommended LGA procedures is limited to bridges that do not have any cross frames framing into the bearing locations at interior piers, and if the application of the recommended LGA procedures is limited to bridges that satisfy the limits for Categories 1, 2C, and 2P, then no multiplier is required on the exterior girder reactions at the piers of continuous-span bridges. However, if either requirement is violated and the limits of application of the LGA procedures is implemented as define in the BE535 project, then the exterior girder reactions at the interior piers in continuous-span bridges should be multiplied by a factor of 1.10.
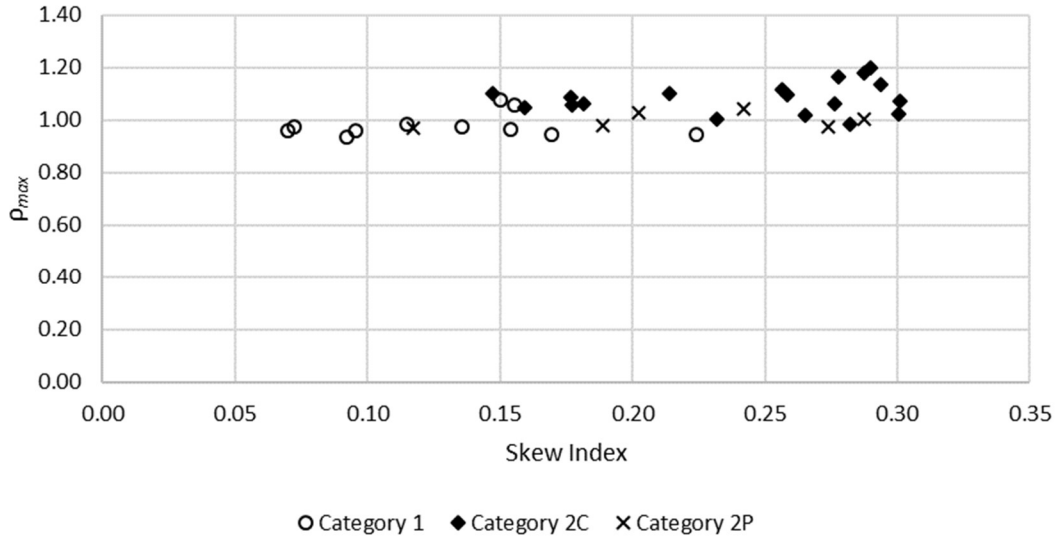
Figure 76. ρ_{max} values for STR I bearing reactions for the exterior girders at the obtuse corners at end abutments
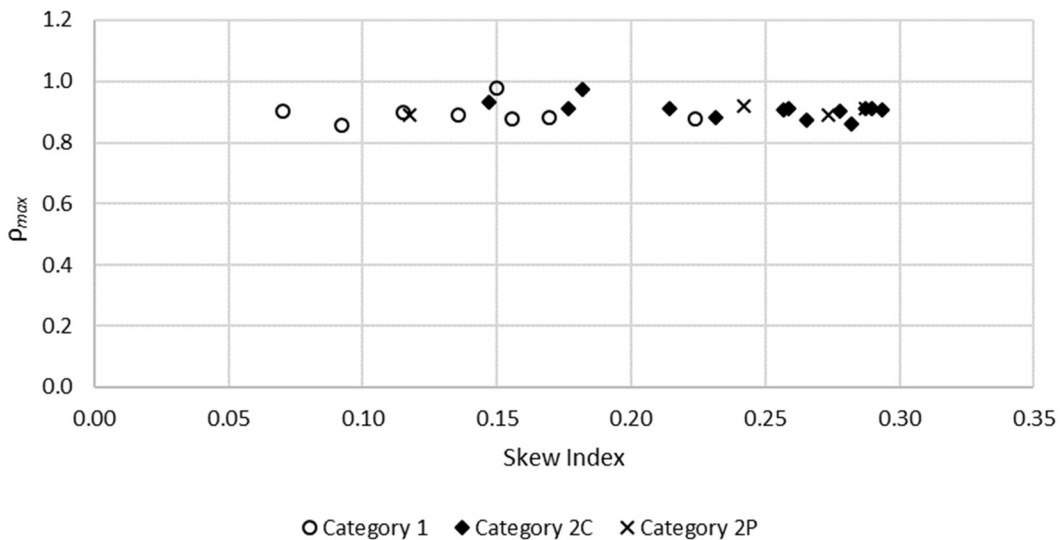
Figure 77. ρ_{max} values for STR I bearing reactions at exterior girders of continuous spans at piers.

Table 18. ρ_{max} values for STR I bearing reactions at obtuse corners at end abutments and at exterior girders of continuous-spans at piers.

Bridge	Skew Index, I_s	Skew Angle, θ (deg.)	$\rho_{max,abut}$	$\rho_{max,pier}$
1C1-21	0.15	16	0.96	N.A.
1C1-27	0.07	20	0.97	N.A.
1C1-28	0.10	20	0.96	N.A.
1C2-26	0.15	10	1.08	0.98
1C2-29	0.09	20	0.94	0.85
1C2-30	0.14	20	0.97	0.89
1C2-50	0.16	20	1.06	0.88
1C3-31	0.07	20	0.96	0.90
1C3-32	0.11	20	0.98	0.90
1C3-33	0.17	20	0.95	0.88
1C3-34	0.22	20	0.94	0.88
2C1-17	0.28	42	1.06	N.A.
2C1-35	0.16	44	1.05	N.A.
2C1-36	0.18	44	1.06	N.A.
2C1-38	0.30	50	1.07	N.A.
2C1-39	0.30	37	1.03	N.A.
2C2-41	0.18	50	1.06	0.97
2C2-43	0.27	50	1.02	0.87
2C2-44	0.23	40	1.00	0.88
2C2-45	0.28	50	1.17	0.90
2C2-46	0.29	44	1.13	0.91
2C2-46B	0.26	40	1.11	0.91
2C2-46C	0.21	35	1.10	0.91
2C2-46D	0.18	30	1.09	0.91
2C2-46E	0.15	30	1.10	0.93
2C3-11	0.26	38	1.10	0.91
2C3-47	0.20	50	0.98	0.86
2C3-48	0.29	50	1.18	0.91
2C3-51	0.29	47	1.20	0.91
2P1-18	0.20	40	1.03	N.A.
2P1-37	0.19	42	0.98	N.A.
2P2-8	0.27	23	0.97	0.89
2P2-40	0.12	23	0.97	0.89
2P2-42	0.24	50	1.04	0.92
2P3-49	0.29	50	1.01	0.91

6.5   Vertical Displacements for TDL/SDLF

In skewed bridges, intermediate cross frames that are perpendicular to the girders will connect to adjacent girders at different longitudinal positions within the span. As a result, the girders do not deflect by the same amount vertically at the opposite sides of a given cross frame. Cross frames employed in the 35 bridges studied in Project BEB13 are primarily V or inverted-V shaped truss-like assemblies. All the cross frames considered in the studies have a top chord. Such cross frames have a high in-plane stiffness. Hence, the cross frames tend to twist the girders such that they essentially have an equal layover at the cross-frame ends due to the differential displacements in the girders. This interaction between the cross frames and girders influences the overall vertical displacement profile of girders in the bridges. After the concrete deck hardens, a similar participation of the deck is observed in maintaining overall compatibility of deformations between the bridge deck, cross frames, and girders. The action of the deck, along with lesser interaction via the cross frames framed parallel to the bearing lines, still influences the girder deflections in the Category 1 bridges.

Additionally, the spans may interact in continuous-span bridges, especially in bridges with unequal spans, due to compatibility of deformations between the continuous girders within adjacent spans. In the recommended LGA calculations considered in this research, the concrete deck loads, barrier rail loads, wearing surface loads, and utilities loads are distributed equally to the girders in the bridge under consideration. However, the complex 3D interaction in skewed bridges do not necessarily match well with the assumption of equal distribution of the dead loads. Hence, significant differences can be observed in the vertical displacements for all the dead load cases, with the exception of the steel dead load (SDLF) load case. Given the steel dead load fit (SDLF) detailing of the cross frames, the girders essentially respond as predicted in by the LGA under the steel dead loads.

Figure 78 shows a representative plot of the LGA and 3D FEA total dead load displacements with steel dead load fit detailing of the cross frames (TDL/SDLF displacements) for Girder 1 in Bridge 2C2-45. The 3D FEA vertical displacements in Span 2 are approximately 1.7 inches larger than the corresponding LGA displacements. These results are influenced by the interaction with adjacent girders in each of the spans, as well as the interaction between the spans in resisting the total dead loads. In this bridge, Girder 4 exhibits the same deflections, but with the deflection pattern reflected about the middle of the overall bridge length such that the maximum Girder 4 displacement from the 3D FEA is in the first span.
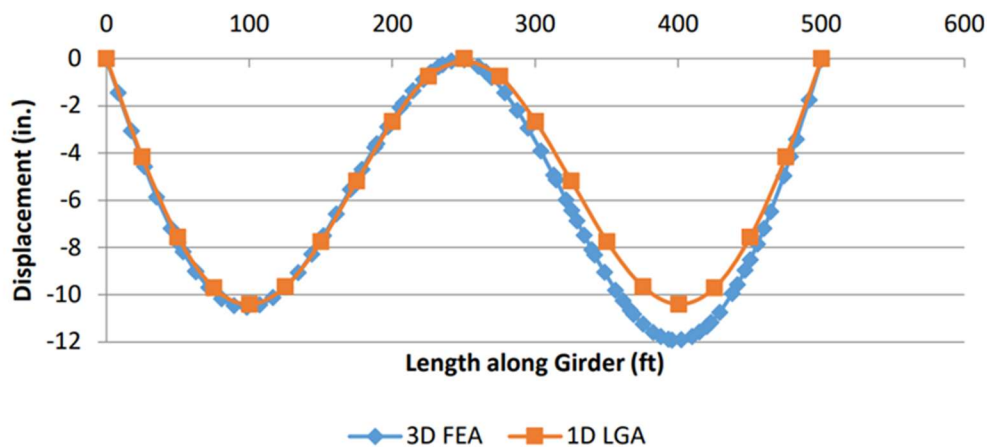
Figure 78. TDL/SDLF vertical displacements for Girder 1 of Bridge 2C2-45.

The LGA vs. 3D FEA difference measures ε_{max2} and ε_{max3} (see Section 5.2) are used for evaluation of the accuracy of the LGA vertical displacement predictions in this research. These difference measures are applied to the maximum TDL/SDLF vertical displacement calculations, as indicated in Eqs. 11 and 12, respectively.

Figures 79 and 80 summarize the ε_{max2} and ε_{max3} values for the 35 bridges studied in BEB13.

Table 19 presents all the specific numerical values. Only one of the bridges, Bridge 1C2-50, violates the suggested limit of 0.005 on ε_{max2} (with a value of 0.0063). The specific LGA prediction of the maximum Girder 1 displacement is −2.2 inches in its Span 1 versus a 3D FEA prediction of −3.9 inches. However, four of the 18 Category 2C bridges and one of the six Category 2P bridges violate the suggested limit of 0.001 on ε_{max3}. The largest ε_{max3} value is 0.0016 for Bridge 2C2-45, the bridge for which the displacements are shown in Figure 78. This difference is based predominantly on the 3D FEA and LGA vertical displacements calculated in Span 2, shown in Figure 78 (and comparable values for Girder 4 in Span 1, which can be viewed in the electronic data file for this bridge), where the LGA underpredicts the displacement by slightly less than 2.0 inches. The LGA and 3D FEA vertical displacement values for the interior Girder 3 essentially match one another (i.e., the differences are less than one-tenth of the differences shown in Figure 78). The LGA versus 3D FEA differential between the maximum Girder 1 and Girder 3 vertical displacements within the spans is approximately 1.1 inches.

It is submitted that although the suggested maximum limits on ε_{max2} and ε_{max3} are violated for a number of the bridges in the parametric study, the differences between the 1D LGA and the 3D FEA calculations is acceptable in all the cases.

Interestingly, the majority of the differences $\Delta_{LGAmax} - \Delta_{3DFEAmax}$ in Table 19 are negative values, indicating that the 3D FEA girder maximum displacements are usually larger than the corresponding LGA displacements for all of the bridge girders, both exterior and interior. In the continuous-span bridges, the larger 3D FEA displacements for Girders 1, 2, and 4 occur mainly due to 3D system effects not captured within the LGA solutions. For example, considering the results shown in Figure 78, the Girder 1 3D FEA TDL/SDLF displacements in the right-hand span of Bridge 2C2-45 are larger than the corresponding displacements in the left-hand span (although the two spans are equal, as shown in Figure 28). In addition, the 3D FEA displacements in the right-hand span are larger than the corresponding LGA displacements in this span while the 3D FEA and LGA displacements in the left-hand span are very similar. When these results are plotted for Girder 4, one finds that the displacements are the same as shown in Figure 78, except that the displacement pattern is reflected about the middle of the overall bridge length (i.e., for Girder 4, the 3D FEA displacements are larger in the left-hand span and they are nearly the same as the LGA displacements in the right-hand span). When the exterior girder displacements are collected and processed to obtain the difference values shown in Table 19, the difference of −1.51 inches is obtained for Girder 1 and the difference of −1.46 inches is obtained for Girder 4. These differences are not the same because of a slight lack of point symmetry of the cross-frame framing about the middle of Bridge 2C2-45. Similar results, although not as large, are obtained due to the 3D system effects captured within the 3D FEA (and not in the LGA solutions) for Girder 2.

The difference result for the middle Girder 3 in Bridge 2C2-45 is a small negative value, −0.36 inches. These results are due to a combination of the following effects: (1) the approximation of the cross-frame weights as a uniformly distributed applied to the girders in the LGA (the application of the corresponding concentrated loads to the girders in the 3D FEA produces slightly larger girder vertical displacements); (2) the simple distribution of the barrier rail loads as equal loads to all the girders in the LGA (which tends

to make the 3D FEA displacements being slightly smaller in the middle Girder 3 compared to the LGA results, while tending to make the 3D FEA displacements slightly larger in Girders 1 and 2 compared to the LGA results, although the barrier rail loads are relatively small compared to the other loads on the bridges); and (3) the simple distribution of the concrete dead loads and the wearing surface and utility loads as equal loads to all the girders in the LGA, which tends to produce the opposite effect to the simple distribution of the barrier rail loads. The net result from all these approximations often results in slightly larger maximum 3D FEA displacements compared to the maximum LGA displacements. These approximations are the prior source of the displacement differences for all the girders in the simple-span bridges. One can observe that in one of the bridges (Bridge 1C1-21) the exterior girder displacement differences, $\Delta_{LGAmax} - \Delta_{3DFEAmax}$, are positive while the interior girder displacement differences are negative.
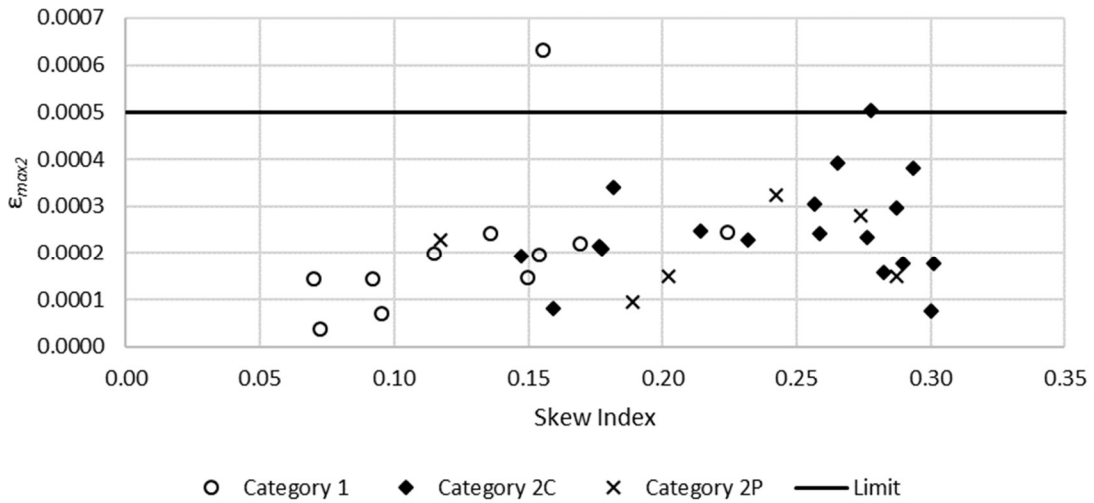
Figure 79. ε_{max2} values for the TDL/SDLF vertical displacements.
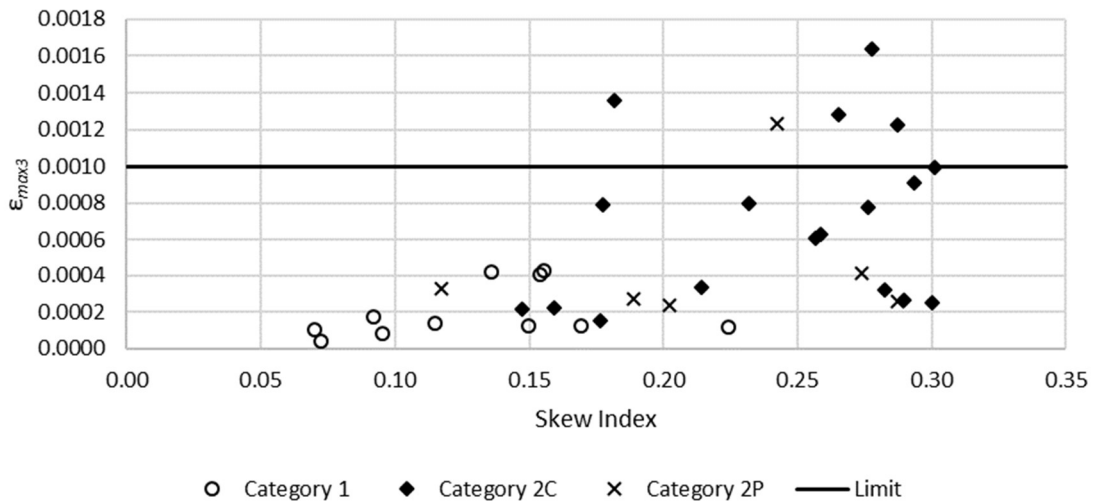
Figure 80. ε_{max3} values for the TDL/SDLF vertical displacements.

99

Table 19. Maximum TDL (SDLF) differences in maximum displacements (inches) between LGA and 3D FEA.

Bridge	Skew Index, I_s	Skew Angle, θ (deg.)	$[\Delta_{LGAmax}-\Delta_{3DFEAmax}]G1$ (in.)	$[\Delta_{LGAmax}-\Delta_{3DFEAmax}]G2$ (in.)	$[\Delta_{LGAmax}-\Delta_{3DFEAmax}]G3$ (in.)	$[\Delta_{LGAmax}-\Delta_{3DFEAmax}]G4$ (in.)	ε_{max2}	ε_{max3}
1C1-21	0.15	16	0.05	-0.22	-0.57	0.05	0.00020	0.0004
1C1-27	0.07	20	-0.08	-0.07	-0.06	-0.07	0.00004	0.0000
1C1-28	0.10	20	-0.15	-0.22	-0.22	-0.15	0.00007	0.0001
1C2-26	0.15	10	-0.14	-0.09	-0.04	-0.14	0.00015	0.0001
1C2-29	0.09	20	-0.15	-0.20	-0.19	-0.13	0.00014	0.0002
1C2-30	0.14	20	-0.14	-0.32	-0.37	-0.13	0.00024	0.0004
1C2-50	0.16	20	-0.85	-1.04	-1.20	-0.86	0.00063	0.0004
1C3-31	0.07	20	-0.28	-0.32	-0.32	-0.28	0.00014	0.0001
1C3-32	0.11	20	-0.28	-0.34	-0.36	-0.28	0.00020	0.0001
1C3-33	0.17	20	-0.26	-0.30	-0.34	-0.25	0.00022	0.0001
1C3-34	0.22	20	-0.24	-0.29	-0.35	-0.24	0.00025	0.0001
2C1-17	0.28	42	-0.56	-0.30	0.02	-0.53	0.00023	0.0008
2C1-35	0.16	44	-0.21	-0.13	-0.11	-0.15	0.00008	0.0002
2C1-36	0.18	44	-0.61	-0.32	-0.18	-0.51	0.00021	0.0008
2C1-38	0.30	50	-0.40	0.01	0.17	-0.35	0.00018	0.0010
2C1-39	0.30	37	-0.14	-0.01	0.04	-0.12	0.00008	0.0003
2C2-41	0.18	50	-1.02	-0.45	-0.40	-0.92	0.00034	0.0014
2C2-43	0.27	50	-0.79	-0.24	-0.22	-0.72	0.00039	0.0013
2C2-44	0.23	40	-0.29	-0.07	-0.02	-0.40	0.00023	0.0008
2C2-45	0.28	50	-1.51	-0.88	-0.36	-1.46	0.00050	0.0016
2C2-46	0.29	44	-0.94	-0.73	-0.25	-0.18	0.00038	0.0009
2C2-46B	0.26	40	-0.76	-0.64	-0.29	-0.17	0.00030	0.0006
2C2-46C	0.21	35	-0.62	-0.58	-0.36	-0.25	0.00025	0.0003
2C2-46D	0.18	30	-0.50	-0.53	-0.40	-0.28	0.00022	0.0002
2C2-46E	0.15	30	-0.46	-0.48	-0.39	-0.26	0.00019	0.0002
2C3-11	0.26	38	-0.29	-0.19	-0.07	-0.53	0.00024	0.0006
2C3-47	0.28	50	-0.29	-0.16	-0.15	-0.26	0.00016	0.0003
2C3-48	0.29	50	-0.71	-0.33	-0.01	-0.69	0.00030	0.0012
2C3-51	0.29	47	-0.47	-0.39	-0.27	-0.44	0.00018	0.0003
2P1-18	0.20	40	-0.38	-0.30	-0.23	-0.34	0.00015	0.0002
2P1-37	0.19	42	-0.19	-0.09	-0.08	-0.14	0.00009	0.0003
2P2-8	0.27	23	-0.05	-0.30	-0.50	-0.03	0.00028	0.0004
2P2-40	0.12	23	-0.28	-0.41	-0.39	-0.24	0.00023	0.0003
2P2-42	0.24	50	-0.97	-0.53	-0.22	-0.89	0.00032	0.0012
2P3-49	0.29	50	-0.35	-0.30	-0.20	-0.31	0.00015	0.0003

6.6   Fatigue Live Load Vertical Shear Force Ranges

Design of bridge girder shear connectors is typically governed by fatigue. AASHTO (2020) Article 6.10.5.3 mandates that the shear buckling resistance in interior panels of transversely stiffened web should be larger than the total shear from the unfactored dead load and factored fatigue load. The corresponding demand quantity is the range of the girder vertical shear force. The recommended LGA procedures utilize the single-lane LLDFs calculated from the AASHTO Article 4.6.2.2.3 provisions. These LLDFs are applied along with the maximum and minimum girder shear envelopes determined from the LGA for calculation of the girder vertical shear force range from the AASHTO Article 3.6.1.4 fatigue truck loading. The corresponding 3D FEA LLDFs can be determined by: (1) taking the difference between the maximum and minimum 3D FEA fatigue shear envelope values at a point of interest; (2) calculating the difference between the maximum and minimum LGA fatigue shear envelope values at this point from LGA using a LLDF of 1.0; and (3) dividing the result from (1) by the result from (2). Generally, the LLDFs determined in this way will be different from the LLDFs calculated using the HL-93 live load model. Therefore, accurate calculation of the LGA HL-93 live load shear forces does not necessarily ensure accurate calculation of the fatigue live load shear force range. In addition, the "true" LLDFs calculated from 3D FEA generally vary along the length of the bridge girders, both for the HL-93 and for the fatigue truck loadings.

In the BEB13 project electronic data files, the 3D FEA "true" LLDFs are calculated for the HL-93 moments and shears as well as for the AASHTO fatigue truck loading moment and fatigue shear ranges. These distribution factors are calculated and presented at each tenth point of the spans and are compared to the AASHTO LRFD moment and shear LLDFs within the electronic data files.

It should be noted that, in the 3D FEA solutions, the back-calculated distribution factors for the maximum shear envelope values, the minimum shear envelope values, and the shear range values are generally all different. The 3D FEA LLDFs for the live load shear range are calculated by dividing the shear range obtained from the 3D FEA solution by the shear range obtained from LGA using a LLDF of 1.0. In the LGA solutions, the LLDFs from AASHTO Article 4.6.2.2.3 are employed (with the exception of the bridges that violate the AASHTO LRFD Article 4.6.2.2.3 limits, discussed subsequently in Section 6.8, in which case the calculations parallel the procedures employed by LRFD Simon).

Figure 81 and Table 20 focus on the more direct evaluation of the LGA accuracy in determining the fatigue shear range in the bridge girders for all the bridges studied. They present the ρ_{max} values for the fatigue live load shear force range corresponding to the fascia girders at the obtuse corners of the spans. Observations regarding the differences between the LGA and 3D FEA results and the accuracy of the LGA predictions are as follows:

- The ρ_{max} values range from 0.81 to 1.30.
- The ρ_{max} values tend to be smaller, and all < 1.0, for the Category 1 bridges. The average value is 0.90 for the Category 1 bridges.
- The ρ_{max} values tend to be > 1.0 for all but one of the Category 2P bridges. The average value is 1.01 for the Category 2P bridges.
- The ρ_{max} values are largest for the Category 2C bridges, and they are > 1.0 for all barring two bridges. The average value is 1.15 for the Category 2C bridges.

Figure 82 and Figure 83 show the specific live load shear envelopes producing the largest ρ_{max} value (1.27) in Figure 81, corresponding to Girder G4 Bridge 2C3-51. The largest ρ_{max} values of 1.26 and 1.27 occur in Girders G1 and G4, respectively, at the obtuse corners at the end of Span 2 and beginning of Span 2, respectively. The 3D FEA solution for the positive shear envelope at this location has an abrupt increase,

immediately after reaching the bearing location at the first intermediate pier, due to the shear transferred by the intermediate cross frame adjacent to the bearing (see Figure 37 for the bridge plan view). The LGA does not capture this discrete increase in the shear near the piers due to 3D skew effects near the obtuse corners of spans. Such effects are exacerbated by the contiguous framing employed in Category 2C bridges. Even with the offsets of the intermediate cross frames relative to the bearing lines set to $4b_f$, it is apparent that a substantial shear force transfer can occur from the intermediate cross frames, particularly near the obtuse corner of the spans. This shear force transfer in the Category 2P bridges is observed to be smaller compared to Category 2C bridges; with most of the LGA solutions within 5 % of the 3D FEA solutions.

Section 6.8 discusses the improvements required in the estimation of LLDFs used in the LGA solutions to obtain estimates of fatigue demands. The shear range estimates are expected to improve with potential improvements in fatigue LLDFs. However, in the interim, it is recommended that:

- For bridges in Category 2C
  - The fatigue live load shear force range at the exterior girders ends at the obtuse corners of spans should be multiplied by a factor of 1.30, and
- For Category 2P bridges
  - The fatigue live load shear force range at the exterior girders ends at the obtuse corners of spans should be multiplied by a factor of 1.15.
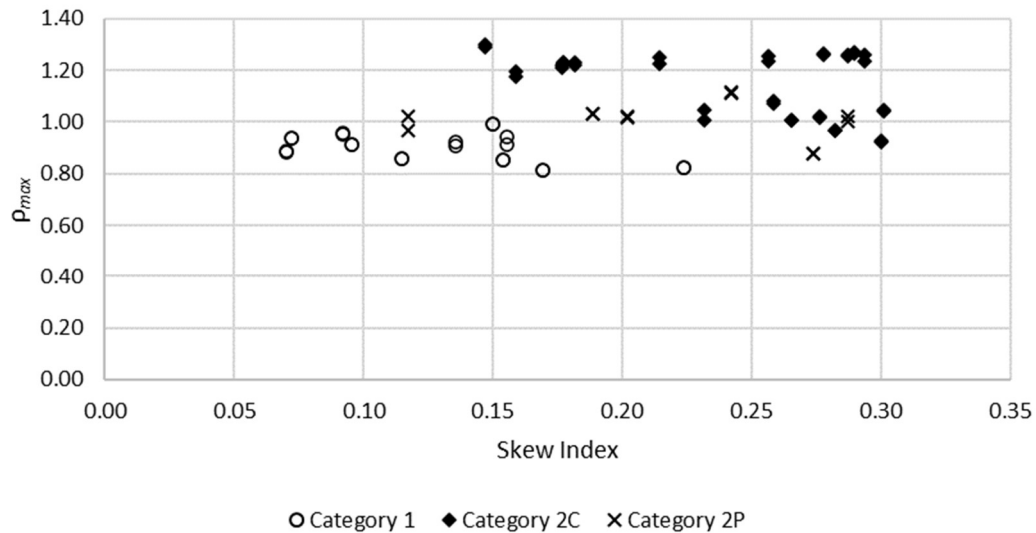
Figure 81. ρ_{max} values for fatigue live load shear force range at the exterior girder ends at the obtuse corners of the spans.
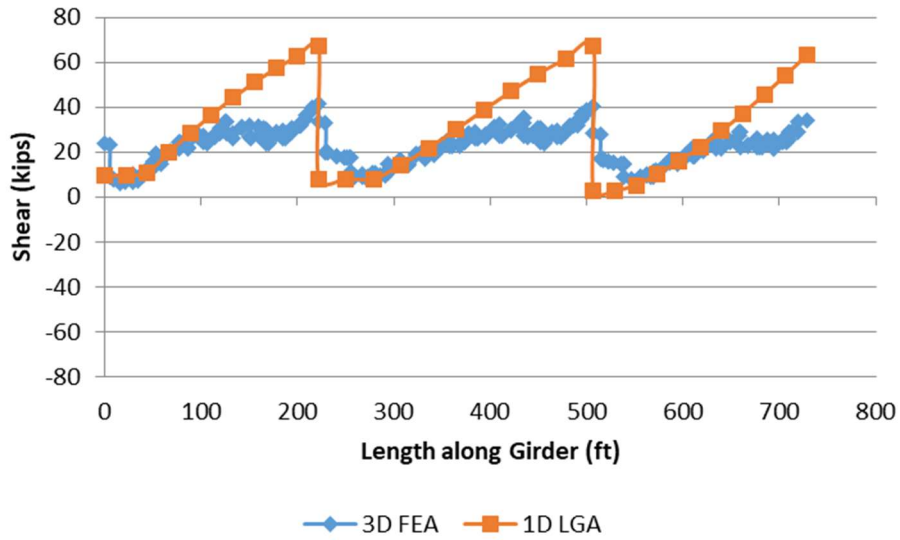
Figure 82. Comparison of maximum positive fatigue live load shear forces in the exterior Girder 4 of Bridge 2C3-51 (note that the negative shear sign convention employed in the project electronic data files is opposite from the typical sign convention for beam shear).
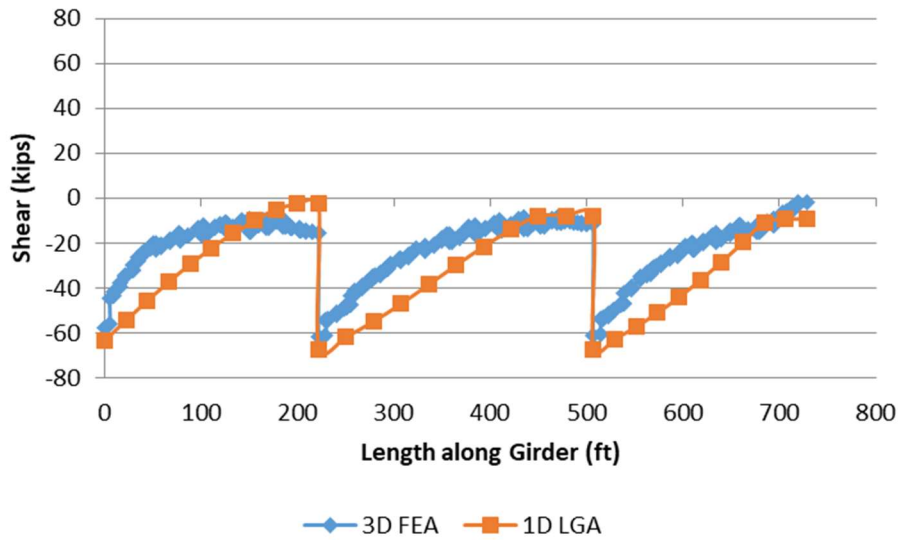
Figure 83. Comparison of maximum negative fatigue live load shear forces in the exterior Girder 4 of Bridge 2C3-51 (note that the negative shear sign convention employed in the project electronic data files is opposite from the typical sign convention for beam shear).

Table 20. ρ_{max} values for fatigue live load shear force range at the girder ends at the obtuse corners of the spans.

Bridge	Skew Index, I_s	Skew Angle, θ (deg.)	ρ_{maxG1}	ρ_{maxG4}
1C1-21	0.15	16	0.85	0.85
1C1-27	0.07	20	0.94	0.94
1C1-28	0.10	20	0.91	0.91
1C2-26	0.15	10	0.99	0.99
1C2-29	0.09	20	0.96	0.95
1C2-30	0.14	20	0.92	0.91
1C2-50	0.16	20	0.94	0.91
1C3-31	0.07	20	0.88	0.89
1C3-32	0.11	20	0.86	0.86
1C3-33	0.17	20	0.81	0.81
1C3-34	0.22	20	0.82	0.82
2C1-17	0.28	42	1.02	1.02
2C1-35	0.16	44	1.20	1.18
2C1-36	0.18	44	1.23	1.23
2C1-38	0.30	50	1.04	1.04
2C1-39	0.30	37	0.93	0.93
2C2-41	0.18	50	1.23	1.22
2C2-43	0.27	50	1.01	1.00
2C2-44	0.23	40	1.05	1.01
2C2-45	0.28	50	1.26	1.26
2C2-46	0.29	44	1.26	1.24
2C2-46B	0.26	40	1.26	1.24
2C2-46C	0.21	35	1.25	1.23
2C2-46D	0.18	30	1.22	1.21
2C2-46E	0.15	30	1.30	1.29
2C3-11	0.26	38	1.07	1.08
2C3-47	0.28	50	0.97	0.97
2C3-48	0.29	50	1.26	1.26
2C3-51	0.29	47	1.26	1.27
2P1-18	0.20	40	1.02	1.02
2P1-37	0.19	42	1.03	1.03
2P2-8	0.27	23	0.88	0.88
2P2-40	0.12	23	1.02	0.97
2P2-42	0.24	50	1.11	1.11
2P3-49	0.29	50	1.00	1.02

6.7   Fatigue Live Load Major-Axis Bending Stress Ranges

Determining the fatigue flexural stress range is critical for the design of the girder flanges at locations of bolted and welded attachments (for example, cross-frame connection plates). The 3D FEA and LGA methods used in the parametric study do not provide the fatigue live load flexural stresses directly. Maximum and minimum envelopes for fatigue live load bending moment can be obtained from both the 3D FEA and the LGA solutions. Flexural stresses are calculated from the bending moment envelopes given the girder composite cross-section properties. Although the girder flexural stresses could be obtained directly from the 3D FEA model, it is considered more reliable to work with the girder moments reported by the 3D FEA software.

For continuous-span bridges, the corresponding LGA estimates are typically larger than the 3D FEA estimates. However, the largest differences typically are observed between the LGA and 3D FEA estimates for simple-span bridges. The LGA procedures employ a line element idealization for the analysis. On the other hand, the 3D FEA procedures involve modeling of the girders, cross frames, diaphragms, bridge deck, bearings, and other structural components at their specific locations in 3D space. For a girder of a simple-span bridge, the LGA idealizations are not capable of capturing girder negative bending moment effects from the live load on the skewed bridge. The negative bending effects are captured by 3D FEA. Section 2a of the electronic data files show comparative plots of fatigue live load bending moment envelopes. Representative plots for the exterior girder of Bridge 2C1-38 are shown in Figures 84 and 85.

Figure 84 indicates that LGA estimates for the maximum envelope of the major-bending moments are quite conservative compared to the 3D FEA estimates. Furthermore, measurable negative moment estimates obtained from 3D FEA are generated in exterior girders near the obtuse corners of simple-span skewed bridges and are reflected in Figure 85. The flexural stress ranges at the bottom flange are calculated using the maximum and minimum envelopes of the bending moments from the above figures. Figure 86 shows the major-axis bending stress range due to fatigue live load calculated for the bottom flange of Girder 1 of Bridge 2C1-38.

Fatigue design of components and details are required if the components or details are subjected to a net tensile stress. The top flange is subjected to compression under the dead load for this simple-span bridge. Hence, it is unlikely that the top flange would be subjected to a net tensile stress. Figure 86 indicates that LGA tends to overpredict the fatigue stress range for the bottom flange of this bridge relative to the 3D FEA solution, which is a typical result. However, due to skew effects at some locations, LGA fatigue stress range estimates are smaller than 3D FEA estimates. The largest LGA underprediction is on the order of 1.5 ksi, which is small enough to not be significant for checking the fatigue design of the bottom flange and the detail at the cross-frame connection plates. These results are representative of the worst-case unconservative predictions of the fatigue flexural stresses upon inspection of the results for the different study bridges in the project electronic data files.
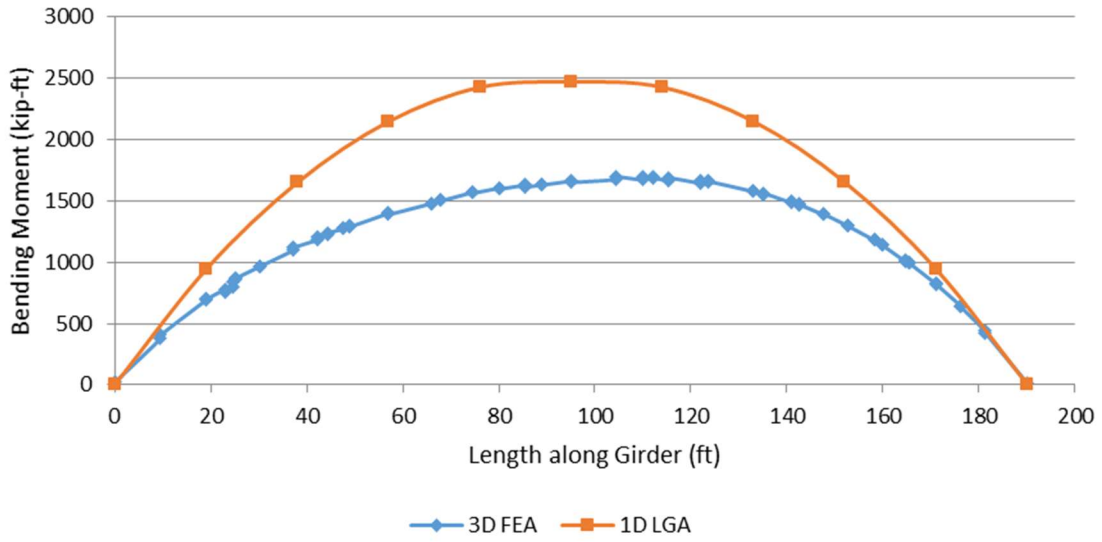
Figure 84. Envelope of maximum major-axis bending moments due to fatigue live loads in Girder 1 of Bridge 2C1-38.
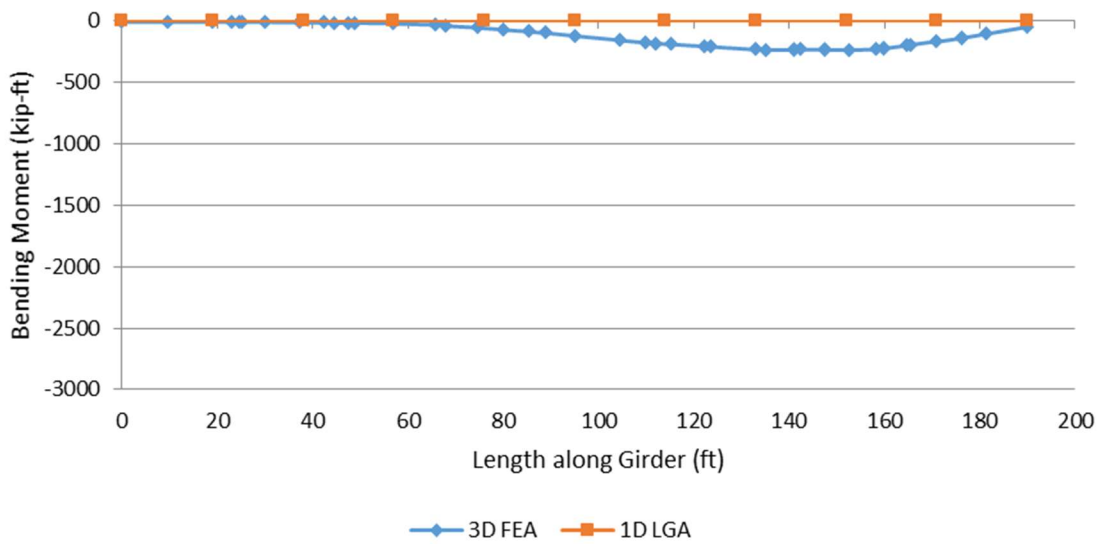
Figure 85. Envelope of minimum major-axis bending moments due to fatigue live loads in Girder 1 of Bridge 2C1-38.
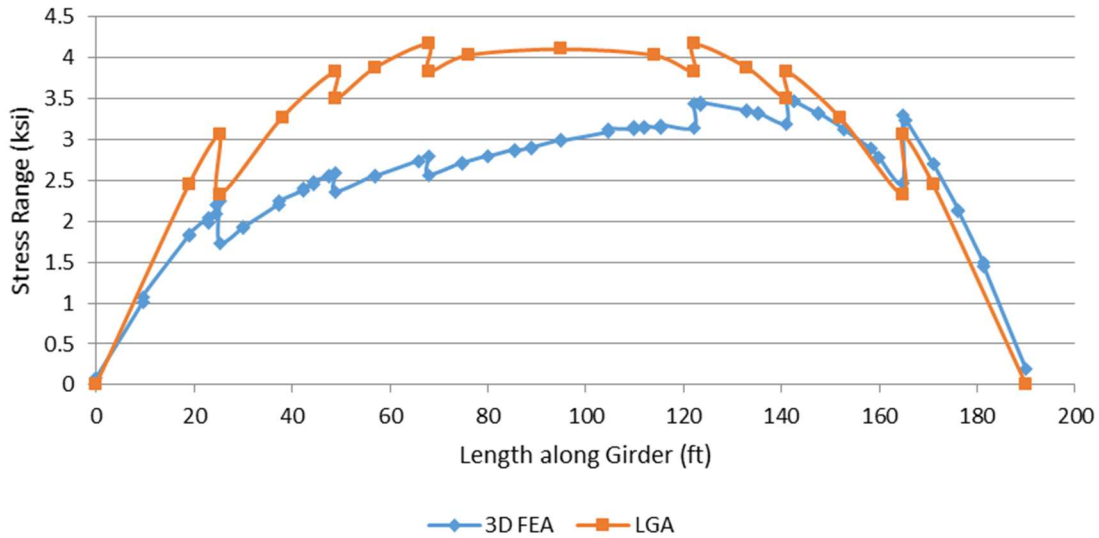
Figure 86. Major-axis bending stress ranges due to fatigue live loads in the bottom flange of Girder 1 of Bridge 2C1-38.

6.8   Live Load Distribution Factors

This section compares the live load distribution factors (LLDFs) obtained using the AASHTO (2020) LRFD Article 4.6.2.2 provisions to the results from 3D FEA for the 35 study bridges in Project BEB13. Insights are developed on ways in which the approximation equations and procedures can be simplified and/or improved.

The AASHTO Specifications recommend the use of refined analysis methods for bridges that fall outside the stated ranges of applicability found in Article 4.6.2.2. Two particular limits are often violated in practice, such as by many of the NSBA continuous-span standard bridges (NSBA 2015), and are violated by nine of the 35 parametric study bridges considered in this research:

- Maximum span length, $L_{s,max}$, less than or equal to 240 ft
- Girder longitudinal stiffness parameter, K_g, less than or equal to 7 x 10^6 in.[4]

Table 21 lists the values of $L_{s,max}$ and K_g for the study bridges. Cells of the table corresponding to bridges that violate the above limits are shaded grey. Nine of the study bridges exceed the range of applicability of the AASHTO provisions as specified in AASHTO (2020) Article 4.6.2.2: two in Category 1, five in Category 2C, and two in Category 2P.

107

Table 21. Longitudinal stiffness parameter (K_g) and maximum span length values of project bridges for determining if AASHTO LLDF equation bounds are satisfied.

Bridge	K_g (x10^6 in^4)	$L_{s,max}$ (ft)
1C1-21*	8.8	241
1C1-27	3.8	174
1C1-28	12.7	263
1C2-26	0.4	92
1C2-29	0.6	115
1C2-30	1.8	160
1C2-50	1.9	184
1C3-31	4.4	240
1C3-32	2.9	195
1C3-33	2.2	165
1C3-34	1.7	150
2C1-17	4.3	202
2C1-35	6.1	218
2C1-36	7.0	243
2C1-38	4.6	190
2C1-39	2.4	150
2C2-41	5.3	251
2C2-43	2.8	168
2C2-44	1.8	155
2C2-45	5.7	250
2C2-46	4.1	228
2C2-46B	4.1	228
2C2-46C	4.1	228
2C2-46D	4.1	228
2C2-46E	4.1	228
2C3-11	2.5	188
2C3-47	2.9	195
2C3-48	5.3	255
2C3-51	6.3	285
2P1-18	4.7	212
2P1-37	3.4	172
2P2-8	2.2	172
2P2-40	2.2	172
2P2-42	5.3	251
2P3-49	5.3	255

Cells corresponding to bridges that violate the AASHTO LRFD limits on K_g and/or $L_{s\,max}$ are shaded grey.

The above limits were established largely based on the range of bridges considered within the NCHRP 12-26 research (Zokaie et al.1991). Nevertheless, it is likely that the trends captured by the Article 4.6.2.2 empirical equations developed by Zokaie et al. may apply sufficiently for designs that exceed the above limits. In addition, a number of the required Article 4.6.2.2 calculations (e.g., lever rule and RCA for exterior girders) are independent of the bridge span length and the girder longitudinal stiffness parameter. As discussed in Section 4.2 and in Appendix A, LRFD Simon implements alternative LLDF calculations for bridges that violate the Article 4.6.2.2 limits. The current research has identified that the switch to the alternative LRFD Simon calculations results in an abrupt and substantial increase in conservatism. Therefore, it was decided to investigate the applicability of the AASHTO Article 4.6.2.2 procedures for the nine parametric study bridges that violate its limits.

In this research, the LLDFs are calculated using AASHTO Article 4.6.2.2 procedures by extending the range of applicability of the limits on $L_{s,max}$ and K_g. Extending the range of applicability by 25% on $L_{s,max}$ and 75% on the K_g is sufficient to address the nine bridges that violate the range of applicability. K_g is applied in the moment distribution and skew correction factor, and the influence of its variation on the overall distribution factors is minor. Hence, it is anticipated that the procedures will be sufficient also for the larger extension of the range of applicability of K_g.

To gain a detailed understanding of the approximate LLDF results, it is useful to outline the equations and procedures that are applied for the calculation of multiple- and single-lane LLDFs for exterior and interior girders. These equations and procedures are summarized for the different cases in the following subsection. Since all the study bridges accommodate more than a single traffic lane, it should be noted that the direct application of the single-lane LLDFs applies only for fatigue evaluations. The approximate AASHTO LLDF calculations are discussed first. The specifics of the AASHTO lever rule, empirical, and RCA calculations are defined clearly in the AASHTO (2020) LRFD Article 4.6.2.2 and are not repeated here. The discussion of the approximate calculations is followed by a summary of several attributes of the rigorous 3D FEA LLDF calculations performed. The discussions of the various procedures are followed by comparisons of the approximate LLDF calculations to the rigorous 3D FEA values.

6.8.1 Live Load Distribution Factor Calculation Procedures

AASHTO Multiple-Lane Exterior-Girder Moment LLDF

For the multiple-lane exterior-girder moment LLDF, the larger value from the following calculations is employed according to the AASHTO LRFD Specifications:

1) The specified AASHTO empirical equation calculated for the interior girders (discussed in the following), multiplied by the parameter *e*.
2) Rigid cross-section analysis (RCA).
3) The single-lane lever rule as defined in AASHTO Article C4.6.2.2.1.

The single-lane lever rule applies here, for the exterior girders, because it typically gives a larger value than the other two calculations, and if the LLDF for a single lane is larger than the LLDF for multiple lanes, the single lane value should be employed also for the multiple-lane cases. Stated another way, when designing for STR I, SER II, or other load combinations involving vehicular live load, the exterior girders need to be able to handle either a single lane or multiple lanes (assuming the bridge roadway is wide enough to accommodate two lanes, which is the case for all the study bridges).

AASHTO Multiple-Lane Interior-Girder Moment LLDF

For the multiple-lane moment interior-girder moment LLDF, the calculation according to the AASHTO LRFD Specifications is simply:

1) The specified AASHTO empirical equation for multiple lanes.

AASHTO Single-Lane Exterior-Girder Moment LLDF

For the single-lane exterior-girder moment LLDF, the following calculations are employed according to the AASHTO LRFD Specifications:

1) The single-lane lever rule (as defined in AASHTO Article C4.6.2.2.1) on the exterior girder.
2) RCA with only a single lane.

AASHTO Single-Lane Interior-Girder Moment LLDFs

For the single-lane interior-girder moment LLDFs, the calculation according to the AASHTO LRFD Specifications is simply:

1) The specified AASHTO empirical equation for a single lane.

It should be noted that AASHTO Article 4.6.2.2.2e defines a reduction factor that can be applied to its calculated moment LLDFs to account for the effects of skew. This factor often is not applied in practice. It is not applied in the Simon programmed LLDF procedures and it is not employed in this research. Given that the values of K_g can be on the larger end of the intended range of application of the empirical equations, leading to smaller values of this correction factor, the reduction factor for skew is mainly an additional complication that offers minimal benefit.

AASHTO Shear LLDFs, Multiple- and Single-Lane on Exterior and Interior girders

For the shear LLDFs, the AASHTO LRFD procedures also follow the above outline for the moment LLDFs. The only differences in the calculations are that:

1) AASHTO specifies different empirical equations for shear compared to its LLDF equations for moment, and
2) The AASHTO Article 4.6.2.2 procedures apply a skew correction factor to LLDFs for the exterior girder and the first interior girder on each side of the bridge cross section.

The skew correction factor accounts for the increase in the end shear forces at or near obtuse corners in the exterior and first interior girders due to the transverse load path that develops in the short diagonal direction between the obtuse corners of the spans in skewed bridges and associated skew. The skew correction factor on the shear LLDFs is applied to all the results listed in the above outlines. That is, it is applied to the empirical equation, the single-lane lever rule (as defined by AASHTO Article C4.6.2.2.1), and the RCA calculations specified by AASHTO Article 4.6.2.2.2d. It should be noted that application of the skew correction factor to both the exterior girder and the first interior girder is important for the accuracy of the calculations.

AASHTO Multiple Presence

It should be noted that whenever any LLDF calculations are applied and "a sketch is required to determine the load distribution" as stated in AASHTO (2020) Article 3.6.1.1.2, a multiple presence factor is applied to the results of the calculations (i.e., 1.2 for a single lane, 1.0 for two lanes, 0.85 for three lanes,

and 0.65 for four or more lanes). Multiple presence factors are not applied to the empirical equation results because the empirical equations inherently account for the multiple presence factor. However, when calculating the single-lane LLDF for the interior girders from the empirical equations for fatigue evaluation, the empirical equation result is divided by the multiple presence factor of 1.2 to adjust for the fact that the multiple presence is included in the empirical equations.

3D FEA LLDFs

As stated in Section 5.1, 3D FEA LLDFs for bending moment, vertical shear force and shear force range are obtained at datapoints where the ratio of the LGA or 3D FEA response at the given datapoint compared to the maximum value of the LGA or 3D FEA response respectively for the given girder is larger than 30%. Within these limits, the largest LLDF value for a response quantity along a given girder is chosen as the governing 3D FEA LLDF.

Typically, the largest 3D FEA LLDF value for moment does not occur at the location of maximum positive or negative bending moment, due to skew effects. Skew effects tend to increase the bending moments in regions of girders in the vicinity of obtuse corners of spans. Larger moment gradients in these regions combined with relatively low values of bending moments tend to amplify the differences between 3D FEA and LGA responses, resulting in larger 3D FEA LLDFs. Especially, at points of very low moments near girder ends, minor differences in 3D FEA results relative to the base LGA calculation with a LLDF of 1.0 may lead to "artificial" spikes in 3D FEA moment LLDFs. Hence, to avoid recording such artificial spikes, 3D FEA moment LLDFs are not calculated where the corresponding moment is smaller than 30 % of the maximum envelope value. Alternatively, for shear, the largest 3D FEA LLDF value occurs at the obtuse corners for exterior girders and near the obtuse corners for interior girders. However, the maximum shear force value may not occur at these locations. Especially for continuous span bridges girders traverse through an obtuse corner, individually at each pier support and at one of the end abutments. The maximum LLDF does not occur at the location where the shear force values are the maximum. Similar to moment LLDFs, 3D FEA shear LLDFs are not calculated where the corresponding shear is smaller than 30 % of the maximum envelope value. Although the governing 3D FEA LLDF values do not always occur at locations of the maximum value of the given response quantity, these locations may correspond to a splice location or a location where the cross section of an I-girder is stepped. Hence, it is essential to evaluate the AASHTO LLDF estimates versus the corresponding 3D FEA values throughout the girder spans wherever the moment or the shear response is of significance.

6.8.2   Comparison of Approximate and Rigorous LLDFs

This subsection provides a comparison of the approximate AASHTO LRFD Article 4.6.2.2 LLDF calculations to the rigorous LLDFs determined from 3D FEA.

The following figures compare the results of all the parts of the above calculations, arranged in the order that the calculations are outlined in Section 6.8.1, to the corresponding LLDFs obtained from the 3D FEA solution for all the 35 parametric study bridges. The ordinate of all the figures is labeled as $1/\rho_{max}$ (i.e., the ordinate of all the plots is the LGA LLDF divided by the corresponding 3D FEA LLDF). Values of $1/\rho_{max}$ greater than 1.0 are conservative, while values less than 1.0 are unconservative.

Note that $1/\rho_{max}$ is used in all the presentations for the LLDFs so that all the ratios are with respect to the 3D FEA "gold standard" result within the denominator of the ratio. This simplifies the comparison of the different results for the LLDFs. In Sections 6.1 through 6.7 and 6.9 of this report, the ratio ρ_{max} is more appropriate. This is because it is more appropriate in these other sections to consider what result does the "gold standard" give relative to the approximate (LGA) calculation.

The figures comparing the approximate to the 3D FEA LLDFs are arranged as follows:

- The multiple-lane LLDF calculations are compared first to the 3D FEA LLDFs obtained using the AASHTO HL-93 live load model (in Figure 87 to Figure 90). This is followed by a comparison of the single-lane LLDF calculations to the 3D FEA solutions of LLDFs for the fatigue moment and shear using the AASHTO fatigue vehicle (in Figures 91 to 94).
- Results are considered first for the exterior girders and then for the first interior girders. The results for the first interior girder are the most critical and least conservative of the interior girders due to the skew effects; hence, the results for these girders are studied rather than the results for the central interior girders.

It should be emphasized that the skew correction is always applied with the AASHTO empirical equations for shear, and RCA. As noted previously, no skew correction is applied for the moment LLDF calculations throughout this work or in LRFD Simon. The detailed case-by-case and calculation-by-calculation observations that can be gleaned from these figures are quite intricate. The following discussion focuses first on the big picture from all these results.

The underlying philosophy of AASHTO LLDF calculation is based on deriving empirical LLDF equations for multiple-lane loading for interior girders and then applying a correction factor to obtain empirical LLDFs for exterior girders (Zokaie et al. 1991). However, for single-lane loading, the lever rule or simple beam distribution as referred to in the traditional AASHTO specifications (e.g., AASHTO, 2002), was recommended for the calculation of LLDFs for exterior girders for moment and shear combined with the application of the skew correction factor for skewed bridges. The lever rule is independent of the empirical equations, and as such does not take the overall bridge geometry into consideration. Hence, it can be stated that an ideological disconnect exists in the methods for estimation of LLDFs for interior and exterior girders. Therefore, it is essential to evaluate the empirical equations and the lever rule to gain appropriate insights into LLDF calculations. The following sections provide such an evaluation. The evaluation also considers the results from the RCA calculations.

The following discussions explain the behavior of the LLDF calculations observed from each of Figures 87 to 94.

Multiple-Lane Exterior-Girder Moment LLDFs

For the multiple-lane exterior-girder moment LLDFs shown in Figure 87, the governing result from the three applicable calculations (single-lane lever rule, empirical equation, and RCA) is unconservative ($1/\rho_{max}$ < 1.0) for 14 of the study bridges. However, the $1/\rho_{max}$ values for the governing LLDFs range from 0.948 to 0.996 and the average value is 0.981 in these 14 cases. Therefore, it can be argued that these LLDFs are still quite accurate. Values of $1/\rho_{max} > 0.94$ here, and in the discussions below, are suggested as being close enough to 1.0 such that the results are sufficient. Three of the bridges have governing LLDFs that are larger than 1.20, but the governing LLDFs in all the other bridges have a $1/\rho_{max}$ smaller than 1.10.

The single-lane lever rule estimates are unconservative for 20 out of the 35 study bridges, although the corresponding $1/\rho_{max}$ is larger than 0.95 for 18 of the bridges and larger than 0.94 for the other two bridges. These values are close enough to 1.0 such that the lever rule can be judged to provide a sufficient approximation of the 3D LLDFs for the study bridges without the consideration of the empirical LLDF or the RCA estimate.
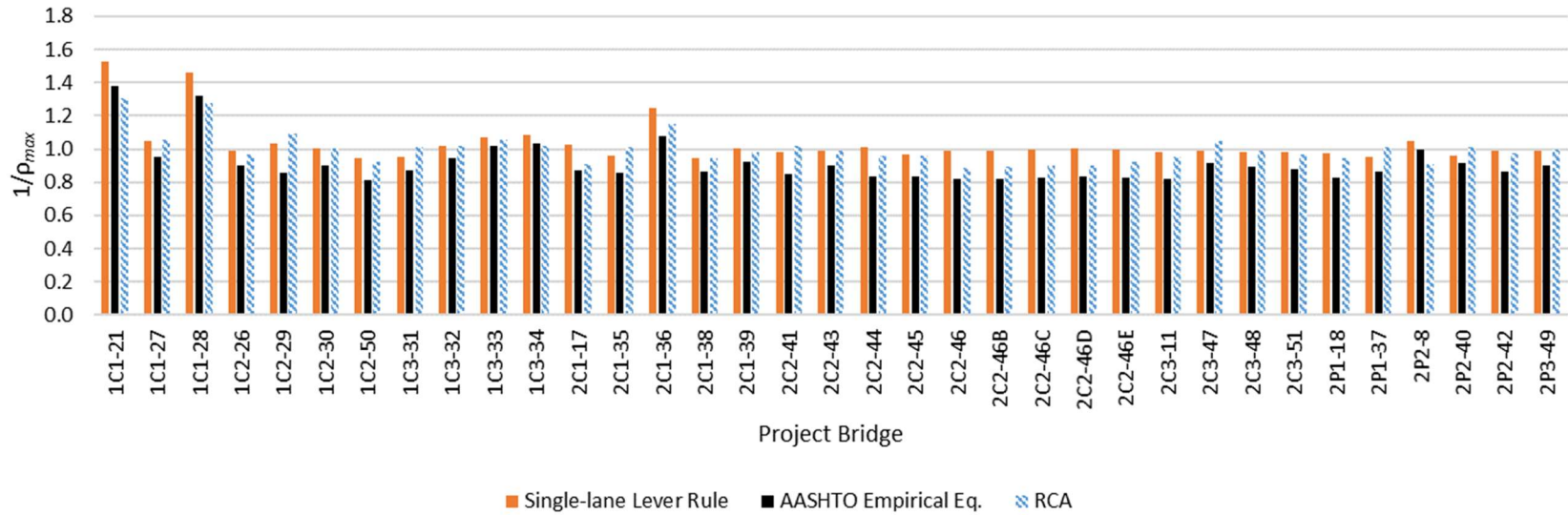
Figure 87. Ratios of the LGA moment LLDFs to the 3D FEA-based HL-93 moment LLDF (multiple lanes) for the exterior girders.
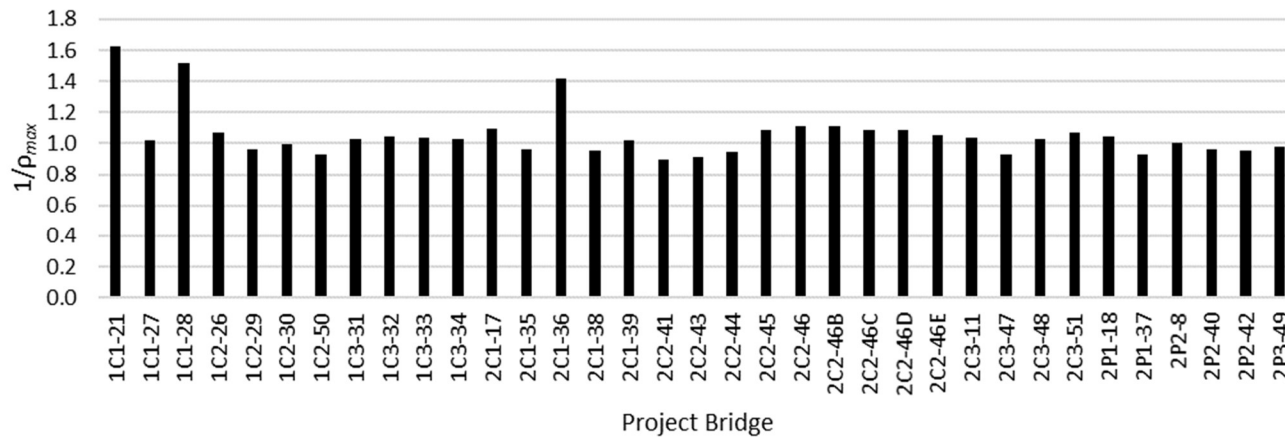
Figure 88. Ratios of the LGA moment LLDFs to the 3D FEA-based HL-93 moment LLDF (multiple lanes) for the first interior girders.
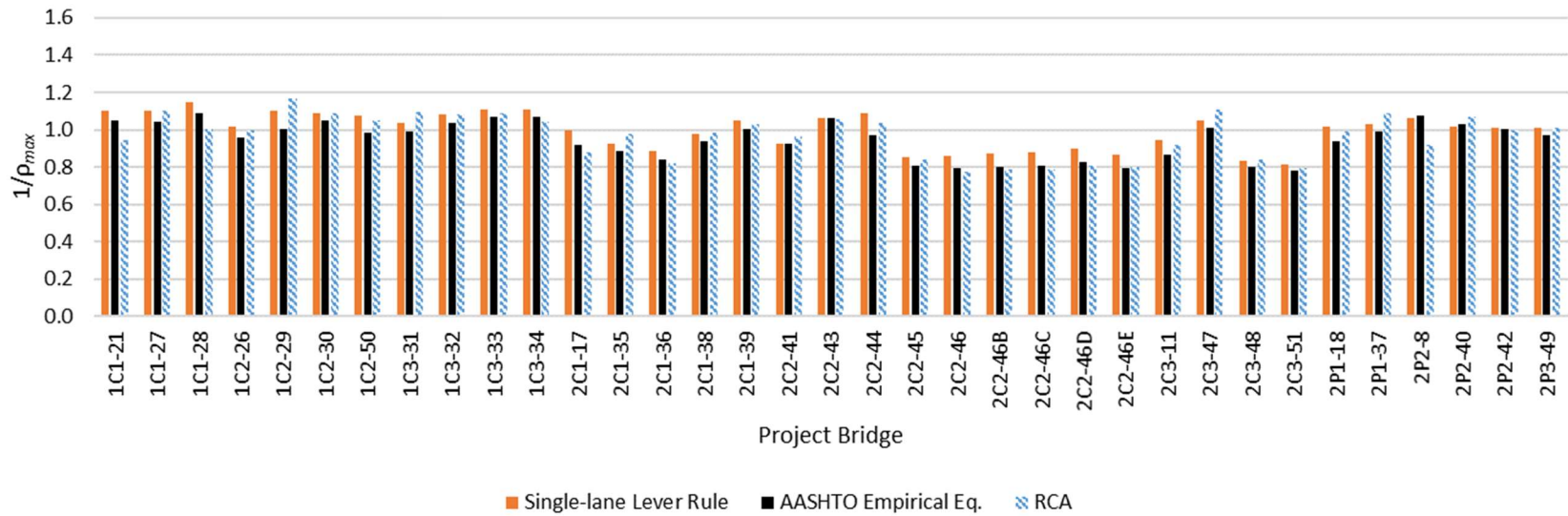
Figure 89. Ratios of the LGA shear LLDFs to the 3D FEA-based HL-93 shear LLDF (multiple lanes) for the exterior girders.
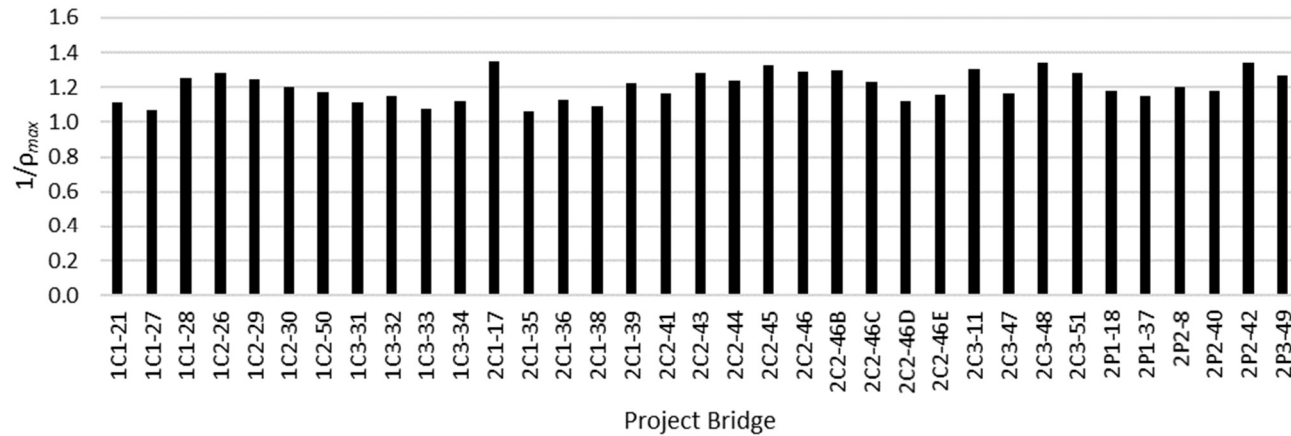
Figure 90. Ratios of the LGA shear LLDFs to the 3D FEA-based HL-93 shear LLDF (multiple lanes) for the first interior girders.

Figure 91. Ratios of the LGA moment LLDFs (single lane) to the 3D FEA-based AASHTO fatigue moment LLDF for the exterior girders.
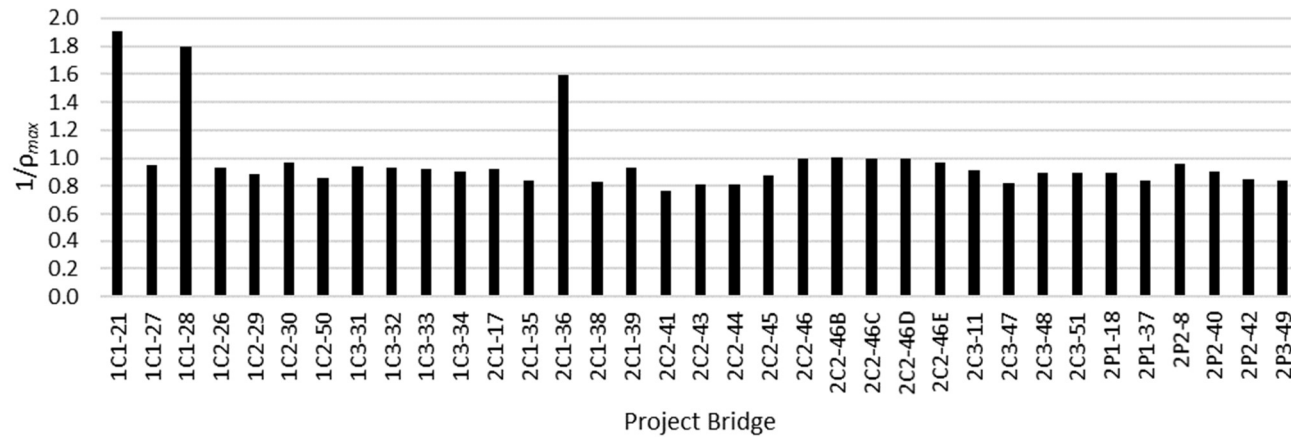
Figure 92. Ratios of the LGA moment LLDFs (single lane) to the 3D FEA-based AASHTO fatigue moment LLDF for the first interior girders.
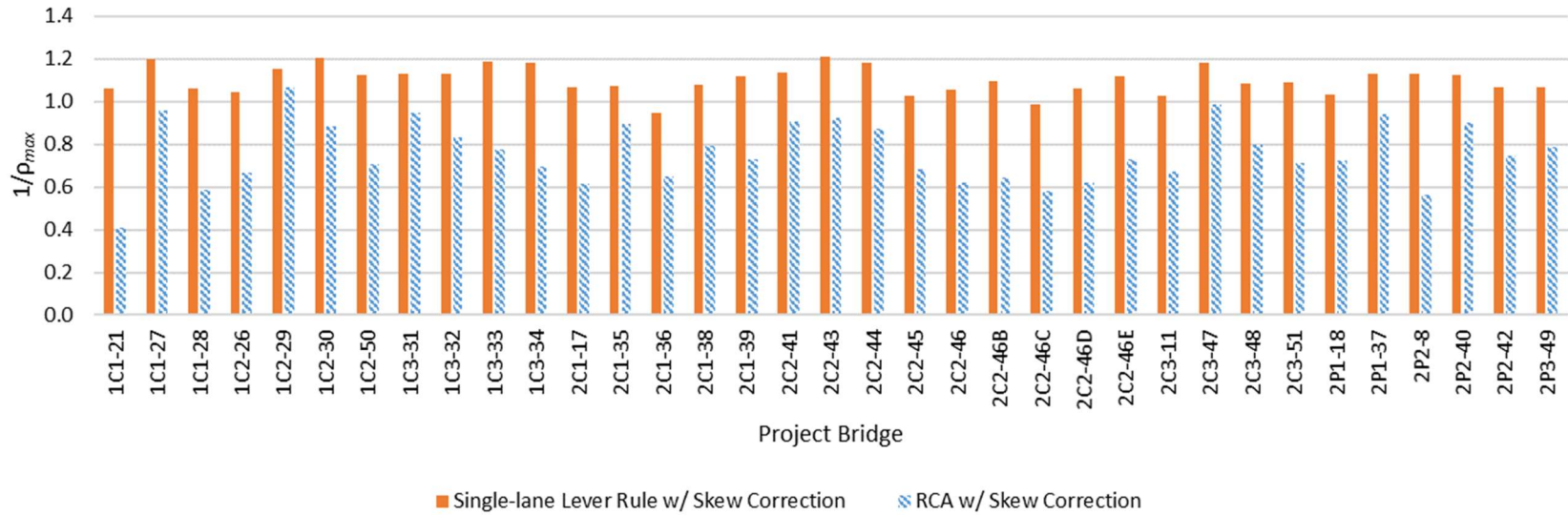
Figure 93. Ratios of the LGA shear LLDFs (single lane) to the 3D FEA-based AASHTO fatigue shear LLDF for the exterior girders.
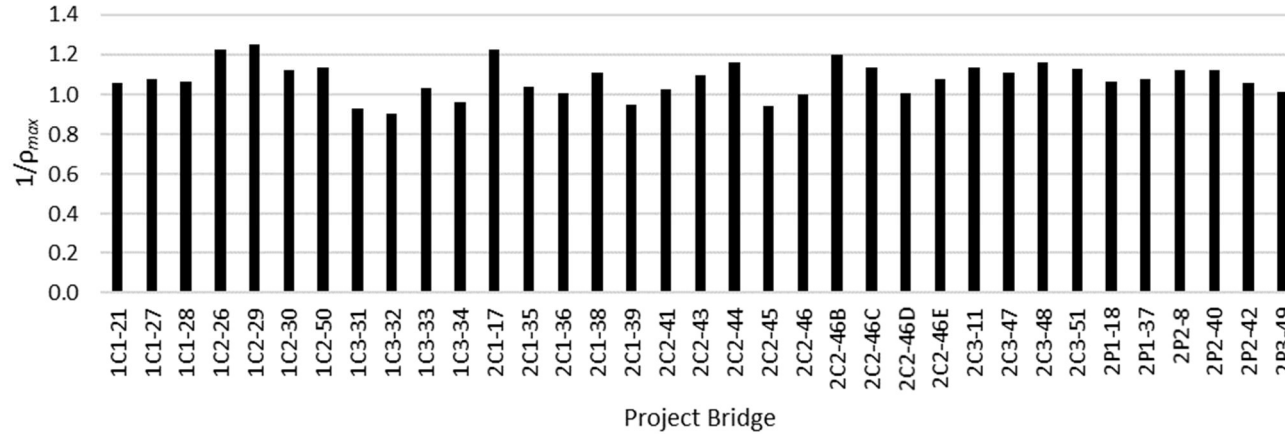
Figure 94. Ratios of the LGA shear LLDFs (single lane) to the 3D FEA-based AASHTO fatigue shear LLDF for the first interior girders.

It is noteworthy that the empirical equation estimates have $1/\rho_{max} < 0.94$ for all but eight of the study bridges, with a minimum value of 0.813. The large number of bridges with $1/\rho_{max} < 0.94$ is due to increases in the rigorous 3D FEA LLDF values at locations of smaller girder bending moments due to skew effects. The empirical equations never govern the overall LLDF result.

The RCA estimates range from 0.886 to 1.309. Table 22 lists the 12 bridges where the RCA calculation governs relative to the other estimates in Figure 87. Notably, many of these bridges have relatively large $L_{s,max}/w_g$ ratios. However, the improvement in the governing LLDF predictions from RCA is minor at best. The maximum increase in $1/\rho_{max}$ relative to the larger value of the other estimates is 0.060.

As discussed in the Project BE535 Final Report, narrow bridges (i.e., bridges with large $L_{s,max}/w_g$) are the most prone to having large exterior girder LLDFs. The primary argument for the application of the RCA calculations is to cover the bases for these types of bridges, since the empirical LLDFs were derived without considering the effect of diaphragms or cross frames within the structural system (HDR 1993). As can be observed from the above discussion, the impact of these additional calculations is rather small for the bridges considered in this research.

Table 22. Span length vs. width ratios for bridges where RCA provides the governing LLDF.

Bridge	$L_{s,max}/w_g$
1C1-27	5.03
1C2-29	3.95
1C3-31	6.67
1C3-32	4.06
2C1-35	6.05
2C1-38	3.96
2C2-41	6.56
2C3-47	5.42
2C3-48	5.31
2P1-37	4.78
2P2-40	4.31
2P3-49	5.31

<u>Multiple-Lane Interior-Girder Moment LLDFs</u>

Figure 88 shows that the multiple-lane interior-girder moment LLDFs have $1/\rho_{max} < 1.0$ for 13 of the study bridges. Five of these bridges have $1/\rho_{max} < 0.94$. The unconservatism occurs across all three bridge categories. The smallest $1/\rho_{max}$ of 0.897 is observed in the first interior girder of Bridge 2C2-41. The particularly low $1/\rho_{max}$ for Bridge 41 is likely related to the fact that this bridge has the second largest $L_{s,max}/w_g$ of all the bridges in the BEB13 study ($L_{s,max}/w_g = 6.56$). The 3D FEA moment live load distribution to the exterior and interior girders in the vicinity of obtuse corners of spans tends to be larger in long narrow bridges. The unconservatism of the LLDF estimates across the three bridge categories is indicative of the fact that the AASHTO multiple-lane empirical equation for the moment LLDF of interior girders does not include any consideration of skew effects.

Multiple-Lane Exterior-Girder Shear LLDFs

For the multiple-lane exterior-girder shear LLDFs shown in Figure 89, the governing result from the three applicable calculations (single-lane lever rule, empirical equation, and RCA) is significantly unconservative ($1/\rho_{max} < 0.94$) for nine of the study bridges. These bridges are all Category 2C. The smallest $1/\rho_{max}$ is 0.811 for Bridge 2C3-51. The governing $1/\rho_{max}$ values are distinctly smaller for the Category 2C bridges compared to Categories 1 and 2P. The smallest $1/\rho_{max}$ for the Category 1 and 2P bridges is only 1.017 and 1.008, respectively, and the $1/\rho_{max}$ for the Category 1 and 2P bridges also has a small standard deviation of only 0.039 and 0.037.

From the above results, it is clear that the shear correction factor of AASHTO Article 4.6.2.2,3c, which is applied to all three of the above estimates, tends to underpredict the skew correction needed for the multiple-lane exterior-girder shear LLDFs in the Category 2C bridges. On average, the contiguous cross-frame lines appear to result in a larger distribution of the live load shear to the exterior girders at the obtuse corners of the spans in the Category 2C bridges. Apparently, the large transverse stiffness contributed by the contiguous cross-frame lines tends to results in a much larger distribution of live load along the short diagonal between the obtuse corners of the spans in the Category 2C bridges.

Ultimately, this is not a problem for the STR I and SER II predictions discussed in Sections 6.1 and 6.2. This is due to compensating effects from the dead loads that are assumed to be distributed equally to all the girders for LGA. The exterior girder carries smaller dead loads in the 3D FEA than in the LGA for the steel dead load of the cross frames, the concrete dead load, and the wearing surface and utility loads, which are all assumed to be equally distributed between all the girders in LGA (i.e., these LGA estimates are conservative relative to the 3D FEA results for these load cases). The DC2 loading from the barrier rails is a different case, where the exterior girders tend to see a larger proportion of that load than obtained assuming equal distribution in LGA. However, the overall magnitude of the DC2 load is not large enough to make a difference for the BEB13 study bridges.

The single-lane lever rule governs relative to the empirical equation estimate for all but two of the bridges in Figure 89. However, the maximum increase in the $1/\rho_{max}$ values from the single-lane lever rule is only 0.119 and the average is 0.049 for all of the study bridges, and the change in $1/\rho_{max}$ is only −0.012 and −0.013 for the bridges where the empirical equation gives a larger value.

The empirical equation provides an accurate estimate of the multiple-lane exterior-girder shear LLDF for the Category 1 bridges (average $1/\rho_{max}$ = 1.031 with a standard deviation of 0.039) and for the Category 2P bridges (average $1/\rho_{max}$ = 1.002 with a standard deviation of 0.044). However, the empirical equation clearly underestimates the LLDF for the Category 2C bridges as discussed above, due to the insufficient skew correction for shear.

Interestingly, the RCA calculation governs the multiple-lane exterior-girder shear LLDF estimates for the same 12 bridges listed in Table 12, for which the above corresponding moment LLDFs were governed by RCA. However, the largest increase in the $1/\rho_{max}$ for the governing LLDF from the RCA calculations is only 0.064 and the average increase for these 12 bridges is only 0.032. Bridge 2C2-41, which has the second largest span-to-width ratio of all the bridges studied in Project BEB13 ($L_{s,max}/w_g$ = 6.56), has a $1/\rho_{max}$ of 0.96 from RCA. Again, the improvement in the governing LLDF predictions from RCA is minor at best.

Multiple-Lane Interior-Girder Shear LLDFs

Figure 90 shows that the empirical multiple-lane interior-girder shear LLDFs are conservative for all the study bridges. The average $1/\rho_{max}$ is 1.205, with maximum and minimum values of 1.347 and 1.061 and a standard deviation of 0.084. There is no obvious trend in the results other than their overall conservatism.

Single-Lane Exterior-Girder Fatigue Moment LLDFs

Figure 91 shows that the governing single-lane exterior-girder fatigue moment LLDFs are conservative for all the study bridges. The average $1/\rho_{max}$ is 1.201, with maximum and minimum values of 1.461 and 1.024 and a standard deviation of 0.091.

It should be noted that, unlike in the multi-lane loading cases, RCA does not come close to governing for any of the bridges in the parametric study. The single-lane lever rule calculation governs for all the bridges. This should be expected since it is relatively obvious that the single-lane loading on the rigid cross-section idealization of the bridges would tend to produce significantly smaller distribution of load to the exterior girder compared to the single-lane lever rule idealization. The RCA LLDF $1/\rho_{max}$ values are all smaller than 1.0, except for Bridge 1C2-29 where the value is 1.022.

Single-Lane Interior-Girder Fatigue Moment LLDFs

For the single-lane interior-girder moment LLDFs shown in Figure 92, 23 of the 35 study bridges have $1/\rho_{max}$ values < 0.94 and all but four of the study bridges have $1/\rho_{max}$ < 1.0. There is no dominant trend in the results; however, the smallest $1/\rho_{max}$ values occur for a number of the Category 2C bridges, suggesting some influence of the contiguous cross-frame arrangements in these bridges on the distribution of the live loads. Bridge 2C2-41 has a $1/\rho_{max}$ of 0.768. The unconservatism of the AASHTO empirical equation for the single-lane interior girder moment LLDF across the three bridge categories is indicative of the lack of consideration of skew effects in its development. The corresponding 3D FEA moment LLDFs are relatively large at locations of smaller girder live load bending moment due to the skew effects.

Single-Lane Exterior-Girder Fatigue Shear LLDFs

Figure 93 shows that the governing single-lane exterior-girder fatigue shear LLDFs are conservative for all but two of the study bridges. The average $1/\rho_{max}$ is 1.103, with maximum and minimum values of 1.211 and 0.948 and a standard deviation of 0.062. The unconservative approximations have $1/\rho_{max}$ close enough to 1.0 such that the calculations may be considered to be sufficient.

Similar to the corresponding single-lane exterior-girder fatigue moment LLDFs, RCA does not come close to governing for any of the bridges in the parametric study. The single-lane lever rule calculation governs for all the bridges. This should be expected since it is relatively obvious that the single-lane loading on the rigid cross-section idealization of the bridges would tend to produce significantly smaller distribution of load to the exterior girder compared to the single-lane lever rule idealization. The RCA LLDF $1/\rho_{max}$ values are all smaller than 1.0, except for Bridge 1C2-29 where the value is 1.067.

Single-Lane Interior-Girder Fatigue Shear LLDFs

Figure 94 shows that the empirical single-lane interior-girder fatigue shear LLDFs have a $1/\rho_{max}$ larger than 0.94 for all but two of the 35 study bridges. The minimum $1/\rho_{max}$ values are 0.929 for Bridge 1C3-31 and 0.900 for 1C3-32. There is no obvious trend in the results. It is apparent that the small $1/\rho_{max}$ values for these bridges is due to minor skew effects on the LLDFs at the first interior girders.

In summary, the following essential observations can be gleaned from the above detailed evaluation of the AASHTO LLDF calculations:

1) For the multiple-lane exterior-girder moment and shear LLDFs, the improvement in the LLDF predictions from RCA is minor at best for the bridges considered in this research (Figures 87 and 89). It is apparent that none of the study bridges has a large enough $L_{s.max}/w_g$ such that the RCA calculations have any significant effect.

2) For the multiple-lane exterior-girder moment and shear LLDFs, the lever rule gives better predictions on average than the empirical equations (Figures 87 and 89).

3) For the multiple-lane interior-girder moment LLDFs, the AASHTO procedures (solely the application of the empirical equations) provide reasonable results for many cases; however, in general, they can be improved by providing some compensation for skew effects exhibited in the corresponding 3D FEA LLDFs at locations of smaller moment (Figure 88).

4) For the multiple-lane exterior-girder shear LLDFs, the skew correction factor is not sufficient for many of the Category 2C bridges (Figure 89).

5) For the multiple-lane interior-girder shear LLDFs, the empirical equations give estimates that are sufficient for all the study bridges (Figure 90).

6) For the single-lane exterior girder fatigue moment and shear LLDFs, it is very unlikely that the RCA calculations would ever govern. Clearly, the RCA calculations do not capture the essential attributes of the response for single-lane loadings, and need not be applied for these cases (Figures 91 and 93).

7) For single-lane loadings, the exterior girder moment and shear LLDF estimates obtained from the lever rule are sufficient (Figures 91 and 93), albeit conservative in some cases. These results are in spite of the fact that the lever rule does not have any attributes that directly account for the live load distribution from the interior of the bridge cross section.

8) For single-lane interior-girder fatigue moment LLDFs, the AASHTO estimates are relatively low compared to the rigorous 3D FEA values (Figure 92). It appears that these LLDF estimates could be improved by providing some accounting for the skew effects exhibited in the 3D FEA LLDFs at locations of smaller girder moments.

9) For single-lane interior girder fatigue shear LLDFs, the AASHTO estimates (empirical equations only) are sufficient for most cases but are marginal in a few cases due to overall skew effects.

Need or Lack of Need for the RCA Calculations for More General Cases

As noted previously, the implementation of the RCA in the AASHTO Article 4.6.2.2 provisions is intended to cover the bases due to the lack of the AASHTO empirical LLDF equations considering the influence of diaphragms and cross frames within the bridge system (HDR 1993). This issue tends to be most critical for bridges that have large spans and small bridge widths. The RCA calculation was observed to govern for a number of the narrow and/or large span study bridges for the case of multiple-lane loading for moment and shear (Figure 87 and Figure 89). However, in both of these cases, the RCA solutions had only a minor influence on the overall LLDF results.

Although the above results are insightful, it is surmised that the range of bridge geometries studied in this research are insufficient to conclude that RCA calculations could be removed entirely from the AASHTO Article 4.6.2.2 procedures. Potentially, a study targeted towards long-span and narrow bridges can provide further insights to expand the observations on RCA from this study. In addition, the ratio of the overhang width to the girder spacing can affect the results of the RCA predictions versus the other estimates.

A broader study to determine further situation where the RCA provisions might be eliminated in general should include a more comprehensive look at the ratio of the overhang width to the girder spacing than exhibited by the bridges considered in the current research.

HDR (1993) provides the primary documentation of the need for RCA to cover the lack of attention to the effects of cross frames and diaphragms in steel I-girder bridges. In this paper, the results from moment LLDF estimates were compared to corresponding 3D FEA values for two four-girder bridges having smaller $L_{s,max}/w_g$ values than the extremes considered in Project BEB13. One of the bridges had an $L_{s,max}/w_g$ of 4.74 and the other had an $L_{s,max}/w_g = 5.2$. The particular geometry attributes for these bridges were as follows:

- Bridge 1: Spans of 185, 180 and 172 ft, s = 11.5 ft, d_e = 2.25 ft., and w_g = 34.5 ft
- Bridge 2: Spans of 157, 243 and 208 ft, s = 13.5 ft, d_e = 3.17 ft, and w_g = 40.5 ft

The reported maximum moment LLDFs for the exterior girders of these bridges from the FEA solutions were 1.92 and 2.26, respectively.

One attribute of the solutions illustrated by Figure 87, Figure 89, Figure 91 and Figure 93 is that the AASHTO single-lane LLDF solution for the exterior girders tends to govern relative to the AASHTO multiple-lane empirical equation for the exterior-girder moment LLDF, and tends to provide an accurate-to-conservative solution for the LLDF in most cases without the need for the RCA. Therefore, it is of interest to compare the AASHTO Article C4.6.2.2.1 single-lane lever rule calculation for the exterior girder moment LLDF to the FEA values reported for the two bridges in the HDR article. These calculations are as follows:

For Bridge 1, LLDF = $1 + d_e/s – 5'/s$ = $1 + 2.25'/11.5' – 5'/11.5'$ = 0.761. The multiple presence factor for the single-lane case is 1.2. Therefore, 0.761(1.2) = 0.913. The FEA solutions presented in the HDR article are in terms of the wheel loads rather than the axle loads. As such, the comparable LLDF from the AASHTO single-lane lever rule for the exterior girders is 0.913(2) = 1.83. The resulting $1/\rho_{max}$ for this estimate is 1.83/1.92 = 0.95.

For Bridge 2, LLDF = $1 + d_e/s – 5'/s$ = $1 + 3.17'/13.5' – 5'/13.5'$ = 0.864. The multiple presence factor for the single-lane case is 1.2. Therefore, 0.864(1.2) = 1.037. Finally, the FEA solutions presented in the HDR article are in terms of the wheel loads rather than the axle loads. As such, the comparable LLDF from the AASHTO single-lane lever rule for the exterior girders is 1.037(2) = 2.07. The resulting $1/\rho_{max}$ for this estimate is 2.07/2.26 = 0.92. Therefore, taking the HDR (1993) results as they are presented, it can be surmised that the AASHTO procedures are sufficiently accurate for Bridge 1 but provide marginal accuracy for Bridge 2.

6.9 Live Load Deflections

For optional live load deflection evaluation, AASHTO (2020) LRFD Article 3.6.1.3.2 states:

"If the owner invokes the optional live load deflection criteria specified in Article 2.5.6.2, the deflection should be taken as the larger of:

1. *That resulting from the design truck alone, or*
2. *That resulting from 25% of the design truck taken together with the design lane load"*

Further, AASHTO (2020) LRFD Article 2.5.2.6.2 states:

1. "… the vehicular load shall include the dynamic allowance."
2. "When investigating the maximum absolute deflection for straight girder systems, all design lanes should be loaded, and all supporting components should be assumed to deflect equally."
3. "For composite design, the stiffness of the design cross-section used for the determination of deflection should include the entire width of the roadway and the structurally continuous portion of the railings, sidewalks and median barriers." (It is assumed that none of these components are structurally continuous in this research.)
4. "For straight girder systems, the composite bending stiffness may be taken as the stiffness determined as specified above, divided by the number of girders."
5. "The live load portion of Load Combination Service I of Table 3.4.1-1 should be used including the dynamic load allowance, IM." Basically, a live load multiplier of 1.0 times 1.33 should be used. In addition, the reference to Table 3.4.1-1 indirectly brings in the consideration of the multiple presence factor, since Article 3.4.1 requires the use of the multiple presence factor along with the factors in Table 3.4.1-1.
6. "The live load shall be taken from Article 3.6.1.3.2." This brings in the above requirement of 25 % of the HL-93 truck with the lane load, or the HL-93 truck alone.

In summary, all of the above, combined strictly with the assumption of equal stiffnesses of the bridge girders, results in an effective LLDF of:

$$DF_{\Delta(LGA)} = m\left(\frac{N_L}{N_g}\right)$$

(13)

applied with 25 % of the HL-93 truck plus the lane load, or the HL-93 truck alone, since these loads are specified to be applied in all of the lanes on the bridge,

where

m = the multiple presence factor,

N = the maximum number of lanes that can be accommodated on the bridge, and

N_g = the number of girders in the bridge.

Therefore, the base LGA live load displacements calculated in this work are obtained as the larger of the displacements from the application of 25 % of the HL-93 truck plus the lane load, and the HL-93 truck alone, using the above LLDF.

It can be argued that for curved and/or skewed bridges, the above idealizations may not be appropriate (Grubb et al. 2010). This is because of the differential displacements that occur across the width of the bridge structure under the live load. Given these differential displacements, the deflections associated with conditions where fewer than all the lanes are loaded on the bridge may be appropriate to consider.

Project BE535 recommended that the live load deflections could be estimated more accurately in straight skewed I-girder bridges by simply applying the moment live load reduction factors to the LGA girder displacements.

In the 3D FEA solutions conducted in this research, the live load displacements envelopes are obtained by positioning the above live loads in one, two, three, up through the total number of lanes accommodated by the bridge.

Figure 95 to Figure 97 plot the ρ_{max} values obtained using the AASHTO (2020) recommendations for estimation of the girder live load deflections for the exterior, first interior, and central interior girders of the study bridges versus the skew index. Each of the figures also reports the corresponding statistics for the ρ_{max} values. Figure 98 to Figure 100 show the corresponding ρ_{max} values and their statistics based on the live load distribution factor recommendation from Project BE535. Table 23 and Table 24 list the data from the evaluations.

Examining Figure 95 to Figure 97, it is evident that the LLDF based on AASHTO (2020) tends to underestimate the displacements significantly, particularly the displacements of the exterior girders. The Project BE535 recommended application of the moment LLDFs provides accurate-to-conservative estimates for all bridges, except for Category 1 Bridges 21 and 26 (Figure 98 to Figure 100). Bridge 21 is a very wide bridge consisting of 12 girders, whereas Bridge 26 is a rolled beam bridge with short spans and a narrow girder spacing. As such, the geometries associated with Bridges 21 and 26 may be considered to be outliers compared to the average bridge geometry described in Section 3.1. The largest ρ_{max} value in the remaining 33 bridges is close to 1.0 (1.02) for all the girder cases in Figures 101 to 103. This indicates that the live load displacements are not underestimated significantly for any of the study bridges. The level of conservatism is observed to be maximum for the central interior girders and the least for exterior girders. In addition, the overall spread (i.e., the difference) between the largest and smallest ρ_{max} values is the smallest when using the recommendation from Project BE535. The mean and the maximum ρ_{max} values for the Project BEB13 study bridges are very similar to the corresponding mean and maximum values in Project BE535.

Figure 95. ρ_{max} values for live load vertical displacements for exterior girders using the live load distribution factor based on the AASHTO (2020) Section 2 and 3 provisions.

123

Figure 96. ρ_{max} values for live load vertical displacements for first interior girders using the live load distribution factor based on the AASHTO (2020) Section 2 and 3 provisions.

Figure 97. ρ_{max} values for live load vertical displacements for central interior girders using the live load distribution factor based on the AASHTO (2020) Section 2 and 3 provisions.
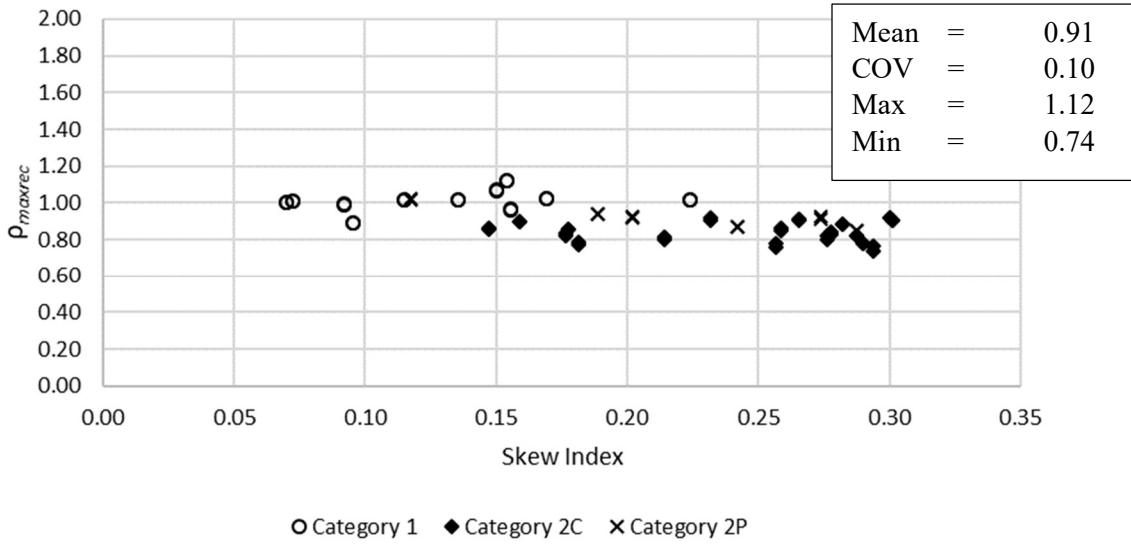
Figure 98. ρ*max* values for live load vertical displacements for exterior girders, using the application of the bending moment LLDF as recommended by Project BE535.

Figure 99. ρ*max* values for live load vertical displacements for first interior girders, using the application of the bending moment LLDF as recommended by Project BE535.

Figure 100. ρ_{max} values for live load vertical displacements for central interior girders, using the application of the bending moment LLDF as recommended by Project BE535.

Table 23. Comparison of maximum live load displacements obtained from 3D FEA and LGA for exterior girders.

Bridge	Skew Index, I_s	Skew Angle, θ (deg.)	ρ_{maxG1} AASHTO	ρ_{maxG4} AASHTO	ρ_{maxG1} BE535	ρ_{maxG4} BE535
1C1-21	0.15	16	1.67	1.67	1.12	1.12
1C1-27	0.07	20	1.54	1.54	1.01	1.01
1C1-28	0.10	20	1.54	1.54	0.89	0.89
1C2-26	0.15	10	1.98	1.97	1.07	1.07
1C2-29	0.09	20	1.61	1.61	1.00	0.99
1C2-30	0.14	20	1.76	1.75	1.02	1.01
1C2-50	0.16	20	1.74	1.74	0.97	0.96
1C3-31	0.07	20	1.49	1.49	1.00	1.00
1C3-32	0.11	20	1.76	1.76	1.02	1.02
1C3-33	0.17	20	1.69	1.69	1.02	1.02
1C3-34	0.22	20	1.64	1.64	1.02	1.02
2C1-17	0.28	42	1.58	1.61	0.80	0.82
2C1-35	0.16	44	1.34	1.34	0.90	0.90
2C1-36	0.18	44	1.63	1.63	0.86	0.86
2C1-38	0.30	50	1.56	1.56	0.90	0.90
2C1-39	0.30	37	1.52	1.52	0.92	0.92
2C2-41	0.18	50	1.33	1.32	0.77	0.79
2C2-43	0.27	50	1.47	1.47	0.91	0.91
2C2-44	0.23	40	1.58	1.61	0.90	0.92
2C2-45	0.28	50	1.33	1.36	0.83	0.85
2C2-46	0.29	44	1.48	1.42	0.77	0.74
2C2-46B	0.26	40	1.51	1.46	0.78	0.76
2C2-46C	0.21	35	1.56	1.54	0.81	0.80
2C2-46D	0.18	30	1.60	1.59	0.83	0.82
2C2-46E	0.15	30	1.78	1.76	0.86	0.85
2C3-11	0.26	38	1.44	1.46	0.85	0.86
2C3-47	0.28	50	1.31	1.31	0.88	0.88
2C3-48	0.29	50	1.42	1.42	0.82	0.82
2C3-51	0.29	47	1.29	1.29	0.78	0.78
2P1-18	0.20	40	1.74	1.76	0.92	0.93
2P1-37	0.19	42	1.40	1.40	0.94	0.94
2P2-8	0.27	23	1.37	1.34	0.92	0.91
2P2-40	0.12	23	1.62	1.61	1.02	1.01
2P2-42	0.24	50	1.61	1.61	0.87	0.87
2P3-49	0.29	50	1.47	1.47	0.85	0.85

Table 24. Comparison of maximum live load displacements obtained from 3D FEA and LGA for interior girders.

Bridge	Skew Index, I_s	Skew Angle, θ (deg.)	ρ_{maxG2} AASHTO	ρ_{maxG3} AASHTO	ρ_{maxG2} BE535	ρ_{maxG3} BE535
1C1-21	0.15	16	1.59	1.58	1.16	1.16
1C1-27	0.07	20	1.22	1.22	0.95	0.95
1C1-28	0.10	20	1.31	1.11	0.90	0.76
1C2-26	0.15	10	1.75	1.52	0.94	0.82
1C2-29	0.09	20	1.36	1.36	1.01	1.00
1C2-30	0.14	20	1.54	1.26	0.98	0.81
1C2-50	0.16	20	1.63	1.30	0.95	0.76
1C3-31	0.07	20	1.21	1.21	0.93	0.93
1C3-32	0.11	20	1.51	1.22	0.93	0.75
1C3-33	0.17	20	1.45	1.26	0.91	0.79
1C3-34	0.22	20	1.50	1.37	0.97	0.88
2C1-17	0.28	42	1.37	1.10	0.86	0.69
2C1-35	0.16	44	1.15	1.15	0.90	0.91
2C1-36	0.18	44	1.36	1.07	0.91	0.72
2C1-38	0.30	50	1.36	1.11	0.85	0.69
2C1-39	0.30	37	1.35	1.17	0.88	0.76
2C2-41	0.18	50	1.17	1.17	0.84	0.76
2C2-43	0.27	50	1.20	1.20	0.92	0.92
2C2-44	0.23	40	1.29	1.16	0.94	0.84
2C2-45	0.28	50	1.18	1.06	0.82	0.74
2C2-46	0.29	44	1.30	1.07	0.83	0.69
2C2-46B	0.26	40	1.32	1.08	0.85	0.69
2C2-46C	0.21	35	1.36	1.09	0.87	0.70
2C2-46D	0.18	30	1.39	1.09	0.89	0.70
2C2-46E	0.15	30	1.53	1.22	0.92	0.73
2C3-11	0.26	38	1.29	1.09	0.85	0.72
2C3-47	0.28	50	1.18	1.18	0.89	0.89
2C3-48	0.29	50	1.26	1.06	0.80	0.67
2C3-51	0.29	47	1.15	1.07	0.77	0.71
2P1-18	0.20	40	1.54	1.27	0.92	0.76
2P1-37	0.19	42	1.20	1.20	0.92	0.92
2P2-8	0.27	23	1.21	1.22	0.89	0.89
2P2-40	0.12	23	1.35	1.34	0.97	0.96
2P2-42	0.24	50	1.38	1.11	0.89	0.72
2P3-49	0.29	50	1.33	1.12	0.84	0.71

.

7. ESTIMATION OF 3D RESPONSES

This chapter presents detailed evaluations for response quantities that LGA is not capable of providing, namely girder layovers, flange lateral bending stresses, and cross-frame forces for the 3D FEA girder solutions from the BEB13 project parametric studies. Recommendations are provided to calculate estimates of layovers, cross-frame forces, and flange lateral bending stresses. Separate estimates for cross-frame forces and flange lateral bending stresses are provided for Category 1, 2C, and 2P bridges.

7.1   Girder Layover under the Concrete Dead Load

Section 2.1 explains the mechanics behind the behavior of straight skewed I-girder resulting in twist rotations in the girders due to compatibility considerations between girders and cross frames. Layovers at girder ends are typically monitored to preempt excessive deformations during erection and deck casting. Such a process involves comparison of measured with the layovers under the load on the bridge. Section 7.1.1 describes a procedure used by FDOT to estimate layovers using vertical displacement values obtained from LGA. Section 7.2.2 evaluates the accuracy of the layover estimates with values obtained from 3D FEA.

7.1.1   Estimation of Girder Layovers

FDOT (2018) recommends estimation of the maximum girder layovers at simply-supported girder bearing lines based on the girder vertical deflections from LGA and a fundamental application of compatibility of deformations. The girder layover is defined as the lateral displacement of its top flange relative to its bottom flange, as shown in Figure 101.
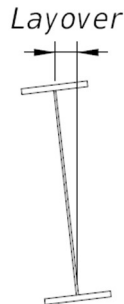
Figure 101. Definition of girder layover.

The steps of the FDOT procedure are as follows:

1. For bridges employing steel dead load fit (SDLF) detailing of the cross frames, the layover under the full steel dead load is taken equal to zero. This recognizes that SDLF detailing results in the girder webs being approximately plumb under the full steel dead load.

2. The girder layover at the completion of the deck placement is of primary interest. This layover is calculated by first estimating the girder major-axis bending rotation, α, due to the concrete dead load (CDL) associated with the bridge deck self-weight. If this rotation is provided directly by the LGA software, then it is recommended to use the provided value. Alternatively, given the associated CDL vertical displacement at the girder 1/10th point within the span, $\delta_{0.1Ls}$, the girder major-axis bending rotation may be estimated as

$$\alpha = \frac{\delta_{0.1L_s}}{0.1L_s}$$

(14)

in radians, where L_s is the span length. This estimate assumes that α is sufficiently small such that $\alpha \cong \tan(\alpha) \cong \sin(\alpha)$, which is the case for any practical bridge girder end rotations. This estimate is employed with the 1/10-point deflections obtained from LRFD Simon in this research.

Another potential set of estimates is

$$\alpha = \frac{3.2\delta_{max}}{L_s}$$

(15)

for simple spans and

$$\alpha = \frac{4.2\delta_{max}}{L_s}$$

(16)

for continuous spans, where δ_{max} is the maximum CDL girder deflection within the span. Equation 15 assumes a simply-supported prismatic girder loaded by a constant uniformly distributed load. This estimate is not recommended unless the prismatic simply-supported condition is approximately satisfied. Similarly, Equation 16 is an estimate of the rotation at the simply-supported end of a continuous-span bridge composed of prismatic girders. The value from this equation is 16 % larger than the rotation at the simply-supported end of a prismatic three-span continuous girder with three equally-loaded equal-length spans. The value from Equation 14 is recommended as a reasonably accurate estimate for all cases.

3. Given the girder major-axis bending rotation, α, and the assumption that the cross-frame deformations are small enough such that the cross frames may be modeled as rigid diaphragms within their own plane, compatibility of deformations between the girders and the cross frames requires that the girders must twist by an angle

$$\phi = \alpha \tan(\theta)$$

(17)

in radians, where θ is the skew angle of the bearing line, equal to zero when the bearing line is perpendicular to the longitudinal axis of the girders.

4. Given the girder twist angle under the CDL, the corresponding layover at the top flange of the girder may be estimated as

$$Layover = D\phi$$

(18)

where D is the girder web depth. Similar to the above calculation of α using Equation 14, this calculation assumes that ϕ is a small enough angle such that $\phi \cong \tan(\phi) \cong \sin(\phi)$.

7.1.2 Accuracy of Girder Layover Estimates

At skewed bearing lines, the cross frames connect to the girders along the skew angle. The girders cannot displace vertically but can rotate at the bearings. The cross frames typically have a high in-plane stiffness compared to the torsional stiffness of the girders. To maintain compatibility with the girder

major-axis bending rotations, the skewed bearing line cross frames twist the girders. In parallel skew bridges, the girders twist in opposite directions at the two ends of the bridge. In this research, the twist at the bridge ends is reported as a twist rotation of the girders in radians. Additionally, the layover is reported as the layover displacement of the top flange relative to the bottom flange.

Girder layovers, calculated by the FDOT recommended procedure described in Section 7.1.1, are considered to be effectively an LGA response estimate, since the corresponding equations are based on fundamental compatibility of displacements (given the assumption that the cross-frame in-plane deformations are negligible).

Figure 102 summarizes the results from 3D FEA, and from the LGA-based calculations using Eqs 28, 31, and 32, for the girder CDL layovers at the left-hand end abutments of the parametric study bridges. Figure 102a shows the results in terms of the girder twist rotations in radians, and Figure 102b shows the results in terms of the layover displacements (i.e., the relative lateral displacement between the girder top and bottom flanges). Table 25 lists all the associated numerical values.

The bridges are listed in Figure 102 and Table 25 in the order of the Category 1 bridges first, followed by the Category 2C and 2P bridges. The Category 1 bridges have skew angles less than or equal to 20° whereas many of the Category 2C and 2P bridges have a 50° skew angle. As such, the twist rotations and layovers are markedly smaller for the Category 1 bridges.

From Figure 102, one can observe that all the girder layovers are predicted with good accuracy. The largest magnitude of the difference in the layover displacement between the LGA estimate and the 3D FEA calculation is -0.16 inches, corresponding to Bridge 2C2-45. This bridge has a skew index of 0.28 and a skew angle of $\theta = 50°$ at its supports (all the bridge plans are presented in Section 3).

The results show that the FDOT recommended procedure, which suggests that the girder layover is proportional to the tangent of the skew angle, gives an accurate estimate of the 3D FEA layovers. This accuracy is achieved although the displacements employed in predicting the layover have trouble satisfying the recommended tolerances on ε_{max2} and ε_{max3} for some of the bridges studied, as discussed in Section 6.5.
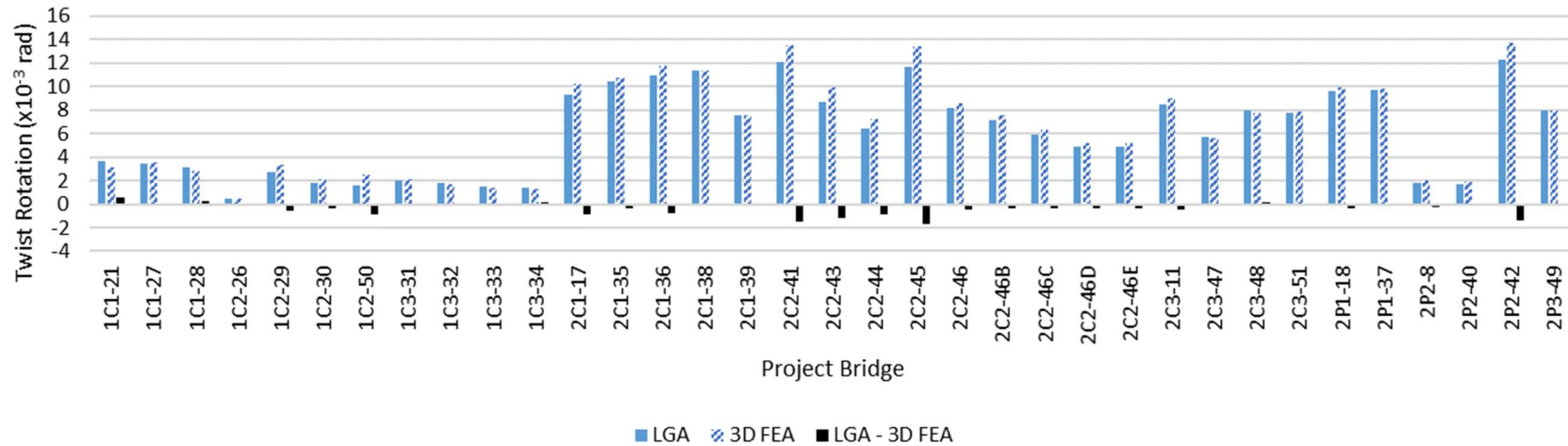
(a) Results presented as girder end twist rotations
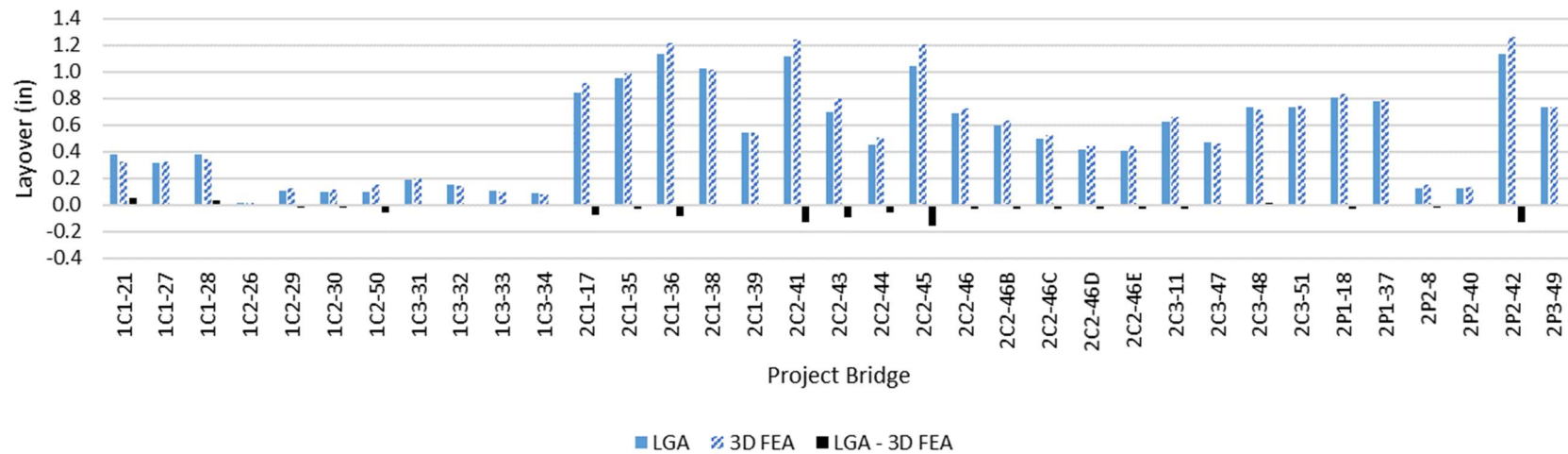
(b) Results presented as layover displacements (i.e, relative lateral displacement between the girder top and bottom flanges)

Figure 102. LGA and 3D FEA CDL layovers at the bearings having the maximum differences in layover at the abutment located on the left end of the plan view of the bridges, and the maximum differences in the girder layovers.

Table 25. LGA and 3D FEA CDL twists and layovers at the bearings having the maximum differences in layover at the abutment located on the left end of the plan view of the bridges, and the maximum differences in the girder layovers.

Bridge	Skew Index, I_s	Skew Angle, θ (deg.)	Web Depth (in.)	Girder	LGA twist ($\times 10^{-3}$ rad)	3D FEA twist ($\times 10^{-3}$ rad)	LGA – 3D FEA twist ($\times 10^{-3}$ rad)	LGA layover (in.)	3D FEA layover (in.)	LGA –3D FEA layover (in.)
1C1-21	0.15	16	102.0	3	3.7	3.2	0.54	0.38	0.32	0.05
1C1-27	0.07	20	90.0	4	3.5	3.6	-0.11	0.31	0.32	-0.01
1C1-28	0.10	20	120.0	1	3.1	2.9	0.27	0.38	0.34	0.03
1C2-26	0.15	10	34.0	4	0.4	0.5	-0.08	0.01	0.02	0.00
1C2-29	0.09	20	38.0	4	2.7	3.3	-0.57	0.10	0.13	-0.02
1C2-30	0.14	20	54.0	3	1.8	2.1	-0.34	0.10	0.11	-0.02
1C2-50	0.16	20	60.0	3	1.6	2.5	-0.89	0.10	0.15	-0.05
1C3-31	0.07	20	96.0	1	2.0	2.1	-0.09	0.19	0.20	-0.01
1C3-32	0.11	20	82.0	4	1.8	1.7	0.08	0.15	0.14	0.01
1C3-33	0.17	20	72.0	4	1.5	1.4	0.11	0.11	0.10	0.01
1C3-34	0.22	20	64.0	4	1.4	1.3	0.16	0.09	0.08	0.01
2C1-17	0.28	42	90.0	1	9.4	10.2	-0.85	0.84	0.92	-0.08
2C1-35	0.16	44	92.0	1	10.4	10.7	-0.31	0.96	0.99	-0.03
2C1-36	0.18	44	103.9	4	10.9	11.7	-0.82	1.14	1.22	-0.08
2C1-38	0.30	50	90.0	3	11.4	11.3	0.01	1.02	1.02	0.00
2C1-39	0.30	37	72.0	1	7.6	7.5	0.04	0.55	0.54	0.00
2C2-41	0.18	50	92.0	4	12.1	13.6	-1.46	1.11	1.23	-0.12
2C2-43	0.27	50	81.0	4	8.7	9.9	-1.22	0.70	0.80	-0.10
2C2-44	0.23	40	70.0	1	6.4	7.3	-0.83	0.45	0.51	-0.06
2C2-45	0.28	50	90.0	4	11.6	13.4	-1.74	1.05	1.20	-0.16
2C2-46	0.29	44	84.0	3	8.2	8.6	-0.41	0.69	0.72	-0.03
2C2-46B	0.26	40	84.0	3	7.1	7.5	-0.39	0.60	0.63	-0.03
2C2-46C	0.21	35	84.0	3	6.0	6.3	-0.34	0.50	0.53	-0.03
2C2-46D	0.18	30	84.0	3	4.9	5.2	-0.32	0.41	0.44	-0.03
2C2-46E	0.15	30	84.0	3	4.9	5.2	-0.36	0.41	0.44	-0.03
2C3-11	0.26	38	74.0	1	8.5	9.0	-0.47	0.63	0.66	-0.03
2C3-47	0.28	50	82.0	3	5.7	5.6	0.09	0.47	0.46	0.01
2C3-48	0.29	50	93.0	3	7.9	7.7	0.19	0.74	0.72	0.02
2C3-51	0.29	47	95.0	3	7.8	7.9	-0.10	0.74	0.75	-0.01
2P1-18	0.20	40	84.3	3	9.6	10.0	-0.37	0.81	0.84	-0.03
2P1-37	0.19	42	80.0	3	9.8	9.9	-0.12	0.78	0.79	-0.01
2P2-8	0.27	23	72.0	3	1.8	2.1	-0.28	0.13	0.15	-0.02
2P2-40	0.12	23	72.0	3	1.7	1.9	-0.20	0.12	0.14	-0.01
2P2-42	0.24	50	92.0	4	12.3	13.7	-1.39	1.13	1.26	-0.13
2P3-49	0.29	50	93.0	4	7.9	7.9	0.01	0.74	0.74	0.00

7.2   Girder Flange Lateral Bending Stresses

7.2.1   Prior Recommendations

In straight skewed bridges, intermediate cross frames that are framed perpendicular to the girders will connect to the girders at different longitudinal positions within the span, resulting in twisting of the girders to maintain compatibility of the girder and cross-frame displacements and rotations. The girder twist produces cross-frame forces and girder flange lateral bending stresses.

Even in Category 1 bridges, where the cross frames are framed parallel to the bearing lines, the girders and the bridge system still exhibit significant twisting action. This is partly due to the compatibility of deformations of the girders with the cross frames at the end abutments, causing girder end twists to be induced by the major-axis bending rotations at the girder ends (as discussed in Section 7.1). Speaking more broadly, the entire bridge structure may be idealized similar to an orthotropic plate composed of the concrete bridge deck with large longitudinal stiffeners (i.e., the bridge girders) and also with substantive transverse stiffeners (i.e., the bridge cross frames and/or solid-web diaphragms). This conceptual orthotropic plate generally exhibits bending and shear deformations and actions longitudinally and transversely, as well as twisting deformations and actions.

AASHTO (2020) LRFD Article 6.7.4.2 recommends generous offsets between the intermediate cross frames and the bearing lines, and/or generous staggers between the cross frames within the span, to soften the transverse load path in skewed I-girder bridges. In most situations, generous offsets and staggers tend to increase the girder flange lateral bending stresses while reducing the magnitude of the cross-frame forces due to the softening of the transverse load path. The cross-frame staggers interrupt and reduce the stiffness of the transverse load path by forcing load transfer via girder flange lateral bending.

Contiguous cross-frame lines can be effective at reducing the magnitude of girder flange lateral bending stresses within the bridge span at the expense of having larger cross-frame forces. However, significant girder flange lateral bending stresses are still encountered at the locations where the cross frames are offset from the girder bearing lines.

For Category 1 bridges, with $\theta \leq 20°$, the orientation of the cross frames in contiguous lines parallel to the supports tends to alleviate the development of large cross-frame forces while also resulting in minimal girder flange lateral bending.

In steel I-girder bridges where the cross frames are detailed for steel dead load fit (SDLF), the girder flange lateral bending stresses and the cross-frame forces are theoretically zero under the steel dead load. However, significant flange lateral bending stresses can be induced by other dead loads and by live load effects. The girder top flanges need to be checked considering flange lateral bending when the girders are in their noncomposite condition during construction; however, AASHTO LRFD does not require any further consideration of flange lateral bending in the top flanges once the bridge is in its final composite condition. This is because the composite bridge deck effectively prevents any significant additional bending of the top flange.

Significant girder flange lateral bending stresses may be caused by wind or by torsion from eccentric concrete deck overhang loads acting on cantilever forming brackets placed along fascia girders during construction. In addition, significant girder flange lateral bending can be caused by the above interactions between the cross frames and the girders in resisting the dead and live load effects (i.e., significant girder flange lateral bending can be induced by the skewed geometry effects on the response to gravity loads).

134

AASHTO (2020) Article C6.10.1 provides the following rules for a simple upper-bound estimate of the girder flange lateral bending stresses from the skew effects, when LGA is employed. These rules are reviewed in Section 2.1.4.

The 3D FEA girder flange lateral bending stresses determined in the Project BE535 and BEB13 research studies are reasonably consistent with the above coarse recommendations. Project BE535 recommended a number of refinements on the above guidance based on its parametric studies as discussed in Section 2.1.4. However, only two Category 1 bridges were considered in that project. In addition, as discussed in Section 3, the number of bridges with parallel skew and contiguous or parallel stagger arrangements was relatively small at the end of that project. Furthermore, the Category 2 (and 3) study bridges that were determined to be amenable for design by LGA in Project BE535 tended to be close to the limits of the categories. Many of the bridges were relatively wide. Therefore, it was decided to study a suite of bridges in BEB13 that fell more within the boundaries of Categories 1 and 2 listed in Table 1, and which mostly had 4, 5, or 6 girders, representative of the majority of skewed I-girder bridges in the FDOT inventory.

In short, the Project BE535 refinements on the AASHTO LRFD commentary guidance involved two main thrusts:

1. Project BE535 aimed to provide coarse estimates of smaller flange lateral bending stresses for situations in which the ratio of the minimum offsets or staggers were greater than $4b_f$, where b_f is the larger of the girder flange widths at the location of the offset or stagger.
2. The project recommended that weighted average load factors for estimation of the factored flange lateral bending stresses. The argument was that it is not appropriate to require the designer to perform many tedious calculations implying high precision with these coarse estimates.

Table 26 lists weighted average load factors for the STR I load combination as well as other load combinations based on the review and refinement of the BE535 recommendations discussed below.

Table 26. Weighted average load factors recommended for estimation of girder flange lateral bending stresses due to skew effects in straight I-girder bridges.

Load Combination Limit State	Weighted Average Load Factor Applied to the Estimated Unfactored f_ℓ for DC+DW+LL
STR I	1.6
SER II	1.2
STR V	1.3
SER I	1.0

The weighted average load factors on STR I and SER II assume that the ratio of the live loads to the total DC ($DC1 + DC2$) loads (i.e., LL/DC ratio) of the critical flange lateral bending stresses is ≤ 2.0. The DC loads include the concrete $DC1$ load and the rail $DC2$ load. The steel dead load flange lateral bending stresses are essentially zero based on steel dead load fit detailing of the cross frames. Based on the magnitudes of loads in the bridges studied, 2.0 is a reasonable upper bound value. The flange lateral bending from DW is typically small; therefore, DW is lumped in with the DC loads in the derivation of the weighted average load factors.

For STR I, the load combination may be written as

$$1.25DC + 1.75LL = LF_{STRI}(DC + LL)$$ (19a)

or

$$1.25 + 1.75\frac{LL}{DC} = LF_{STRI}\left(1 + \frac{LL}{DC}\right)$$ (19b)

Substituting $LL/DC = 2.0$, the equation can be solved to obtain $LF_{STR\,I} = 1.6$ to two significant digits where:

DC = magnitude of DC loads
LL = magnitude of live loads produced by the AASHTO HL-93 live load model, including the AASHTO dynamic load allowance
$LF_{STR\,I}$ = weighted average load factor for STR I load combination

Performing a similar calculation for the SER II load combination, we have

$$1.0 + 1.3\frac{LL}{DC} = LF_{SERII}\left(1 + \frac{LL}{DC}\right)$$ (20)

Substituting $LL/DC = 2.0$, $LF_{SER\,II} = 1.2$ to two significant digits.

For the STR V load combination, the predominant gravity loads are again DC and LL and the simplified gravity load combination is

$$1.25DC + 1.35LL = LF_{STRV}(DC + LL)$$ (21)

Solving in a similar manner and substituting $LL/DC = 2.0$ again, we obtain the weighted average load factor for the STR V load combination, $LF_{STRV} = 1.3$ to two significant digits.

Given the direct 3D FEA calculations of the factored STR I flange lateral bending stresses documented in the current research, the unfactored total flange lateral bending stress due to the gravity loads and due to the bridge skew, $DC1 + DC2 + DW + LL$, is estimated by dividing the STR I results by 1.6.

The STR II load combination pertains to a special design or permit vehicle. Although this load combination can be an important design or rating consideration for some bridges, Table 26 does not provide a recommendation for the STR II weighted average load factor. The estimate of the factor is relatively elaborate for this load combination and may be determined as follows. Hence, an estimate of the ratio of the live load flange lateral bending stresses due to special design or permit vehicles, LL^*, to the ordinary HL-93 LL stresses (LL^*/LL) is required in order to determine an appropriate weighted average load factor. Following the same process as in the load combinations above, the equation is

$$1.25DC + 1.35LL^* = LF_{STRII}\left(DC + LL^*\right)$$ (22a)

or

$$1.25DC + 1.35LL\left(\frac{LL^*}{LL}\right) = LF_{STRII}\left(DC + LL\left(\frac{LL^*}{LL}\right)\right)$$ (22b)

or

$$1.25 + 1.35\left(\frac{LL}{DC}\right)\left(\frac{LL^*}{LL}\right) = LF_{STRII}\left(1.0 + \left(\frac{LL}{DC}\right)\left(\frac{LL^*}{LL}\right)\right)$$

$$\text{(22c)}$$

Substituting $LL/DC = 2.0$, the equation can be solved to obtain the weighted average load factor for the STR II load combination, $LF_{STR\ II}$:

$$LF_{STRII} = \left(\frac{1.25 + 2.7\left(\frac{LL^*}{LL}\right)}{1.0 + 2.0\left(\frac{LL^*}{LL}\right)}\right)$$

$$\text{(23)}$$

If (LL^*/LL) is 1.0, $LF_{STRII} = 1.3$ to two significant digits. If (LL^*/LL) is 2.0, $LL_{STRII} = 1.3$ again to two significant digits. Therefore, the appropriate value for LF_{STRII} may be taken as 1.3.

It should be noted that the weighted average load factors in Table 26 are based on the unfactored flange lateral bending stress due to $DC + DW + LL$. However, Eq. 22a is based on the live load due to the special design or permit vehicle, LL^*. Therefore, the factor that must be applied to the estimated flange lateral bending stress for $DC+DW+LL$ is

$$LF_{STRII} = 1.3\left(\frac{DC + DW + LL^*}{DC + DW + LL}\right)$$

$$\text{(24)}$$

That is, one must estimate the ratio of the unfactored loads ($DC + DW + LL^*$) / ($DC + DW + LL$) if it is desired to determine an estimated flange lateral bending stress for the STR II load combination.

The STR III and STR IV load combinations do not contain live loads. Hence, using an estimated unfactored total flange lateral bending stress due to $DC1+DC2+DW+LL$ for estimating flange lateral bending stresses for these load combinations, which do not contain live load, is considered too contrived. Handling of these load combinations is left to the judgement of the engineer.

Additionally, LRFD Article 3.4.2 provides a special load combination for checking of constructability. A bounded estimate of the flange lateral bending stresses due to the concrete dead load, CDL, is provided to facilitate calculation of flange lateral bending stress estimates for these load combinations. Article 3.4.2 recommends a load factor on the CDL of 1.4. Project BEB13 did not study flange lateral bending stresses due to construction loads. The estimation of flange lateral bending due to construction loads is left to the judgement of the engineer.

Lastly, the Fatigue I and II loadings require a flange lateral bending stress range estimate. Estimates for the unfactored flange lateral bending stress range due to the standard AASHTO fatigue truck loading are provided. These values would be multiplied by the Fatigue I or II factors as appropriate.

Several BEB13 study bridges have offsets or staggers smaller than $4b_f$, as described in Chapter 3. However, based on the results discussed in the following sections, as well as additional unpublished studies, it has been determined that the minimum offsets and staggers generally needed to be larger than $4b_f$ to achieve substantial benefits in terms of lateral bending stress reductions. Based on these more detailed studies of a broader range of bridges and cross-frame framing arrangements, it was decided to modify the BE535 recommendations to provide a simpler table of flange lateral bending stress estimates, providing recommendations similar to those of AASHTO (2020) Article C6.10.1 but with additional refinements. A recommended new table of estimates is provided after the presentation of results in the following section.

It should be emphasized that the flange lateral bending stress estimates provided subsequently are values associated with the unfactored gravity loads $DC1 + DC2 + DW + LL$ in combination with the skew effects. Other loads, such as the construction load mentioned above, and the direct flange lateral bending on the fascia girders due to gravity loads supported by overhang brackets attached to the exterior girders, must be calculated separately and added to these base gravity load effects.

7.2.2 Synthesis of New Results

7.2.2.1 Category 1 Bridges

Table 27 lists the maximum STR I flange lateral bending stresses calculated by 3D FEA for the exterior and interior girders of the 11 Category 1 bridges studied in Project BEB13. It can be observed that the largest stress is 3.2 ksi on Girder G1 in Bridge 1C2-30. Since this is an exterior girder, a portion of the flange lateral bending stress is due to the eccentric bracket loads associated with the concrete deck placement (the wet concrete loading was retained, without considering the removal of forms, as a simplification of the calculations in CSiBridge).

Table 28 lists the maximum fatigue stress range and Table 29 lists the maximum flange lateral bending stress under the wet concrete dead load (CDL) for the exterior and interior girders of Category 1 bridges. It is submitted that the flange lateral bending stresses due to skew are small enough to be neglected without any significant consequence, as recommended in the AASHTO (2020) Article C6.10.1.

Table 27. Maximum STR I flange lateral bending stresses for exterior, first interior, and central interior girders, Category 1 bridges.

Bridge	Skew Index, I_s	Skew Angle, θ (deg.)	$f_{\ell,maxG1}$ (ksi)	$f_{\ell,maxG2}$ (ksi)	$f_{\ell,maxG3}$ (ksi)	$f_{\ell,maxG4}$ (ksi)
1C1-21	0.15	16	1.0	0.7	0.5	1.0
1C1-27	0.07	20	1.6	1.0	0.5	1.5
1C1-28	0.10	20	1.9	1.0	0.8	1.9
1C2-26	0.15	10	2.2	1.1	0.6	2.1
1C2-29	0.09	20	2.3	1.6	1.6	2.2
1C2-30	0.14	20	1.9	1.2	1.1	1.9
1C2-50	0.16	20	2.4	2.1	1.7	1.9
1C3-31	0.07	20	2.5	1.6	1.6	2.4
1C3-32	0.11	20	3.2	1.1	1.0	3.1
1C3-33	0.17	20	2.3	0.9	0.8	2.2
1C3-34	0.22	20	2.2	0.9	0.9	2.2

Table 28. Maximum unfactored fatigue flange lateral bending stress range values for exterior, first interior, and central interior girders, Category 1 bridges.

Bridge	Skew Index, I_s	Skew Angle, θ (deg.)	$f_{\ell,maxG1}$ (ksi)	$f_{\ell,maxG2}$ (ksi)	$f_{\ell,maxG3}$ (ksi)	$f_{\ell,maxG4}$ (ksi)
1C1-21	0.15	16	0.2	0.2	0.1	0.2
1C1-27	0.07	20	0.4	0.4	0.2	0.4
1C1-28	0.10	20	0.3	0.3	0.2	0.3
1C2-26	0.15	10	0.3	0.3	0.2	0.3
1C2-29	0.09	20	0.6	0.6	0.6	0.6
1C2-30	0.14	20	0.4	0.4	0.4	0.5
1C2-50	0.16	20	0.6	0.5	0.3	0.5
1C3-31	0.07	20	0.4	0.4	0.4	0.4
1C3-32	0.11	20	0.3	0.3	0.3	0.3
1C3-33	0.17	20	0.3	0.2	0.2	0.3
1C3-34	0.22	20	0.3	0.2	0.1	0.3

Table 29. Maximum unfactored concrete dead load flange lateral bending stress values for exterior, first interior, and central interior girders, Category 1 bridges.

Bridge	Skew Index, I_s	Skew Angle, θ (deg.)	$f_{\ell,maxG1}$ (ksi)	$f_{\ell,maxG2}$ (ksi)	$f_{\ell,maxG3}$ (ksi)	$f_{\ell,maxG4}$ (ksi)
1C1-21	0.15	16	0.2	0.1	0.1	0.2
1C1-27	0.07	20	0.7	0.1	0.0	0.6
1C1-28	0.10	20	0.4	0.1	0.1	0.4
1C2-26	0.15	10	0.9	0.1	0.1	0.9
1C2-29	0.09	20	0.8	0.2	0.2	0.7
1C2-30	0.14	20	1.0	0.1	0.1	0.9
1C2-50	0.16	20	0.5	0.2	0.3	0.6
1C3-31	0.07	20	1.4	0.2	0.2	1.3
1C3-32	0.11	20	2.0	0.1	0.1	1.9
1C3-33	0.17	20	1.5	0.1	0.1	1.4
1C3-34	0.22	20	1.3	0.1	0.2	1.2

7.2.2.2 Category 2C Bridges

Table 30 summarizes the maximum STR I flange lateral bending stresses calculated by 3D FEA for the exterior and interior girders of the 18 Category 2C bridges studied in Project BEB13. One can observe that the maximum stresses are significantly larger in these bridges, with maximum exterior girder values of 18.2 ksi in Girder 1 of Bridge 2C2-43 and maximum interior girder values of 15.0 ksi in this same bridge.

Figure 103 shows the variation in the bottom flange lateral bending stress in the exterior Girder 1 of Bridge 2C2-43. Dashed lines are drawn at 30 % and 70 % of each span. Dark solid lines indicate the ends of the spans. The regions within a length somewhat less than that between the dashed lines and solid lines may be considered as "at or near the supports," while the remainder of the spans may be considered as

"within the span." It should be emphasized that the 30 % and 70 % boundaries are not to be considered as the limits for "at or near the supports" or "within the spans." Specific recommendations for these limits are discussed subsequently in Section 7.2.2.4.

There is a local spike in the stress at the location where the first intermediate cross frame connects to the girder near the left-hand end of Girder 1 (Figure 26 provides a sketch of the framing plan for this bridge). This location is adjacent to the obtuse corner of the span at the left end abutment, and the offset from the bearing at this location is only 2.4b_f. Figure 103 is representative of the general variation of the flange lateral bending stresses along the exterior girders in I-girder bridges with contiguous cross-frame layouts:

1. There is a local spike in the flange lateral bending stress at the first intermediate cross frame offset from the bearing lines. This spike is largest at the girder end corresponding to the obtuse corner of the span. If the offset is increased as much as possible (e.g., offsetting the first intermediate cross-frame line by a maximum target girder unbraced length, L_b, from the bearing line) this spike in the flange lateral bending stress is significantly reduced. As the offset becomes relatively small, the flange lateral bending stress tends to become relatively large.
2. Moving along the length of the girder from the first intermediate cross-frame location, the flange lateral bending stresses vary between the cross-frame locations akin to the variation in the bending stresses in a fixed-end beam subjected to transverse load. These relatively small stress variations are due to the eccentric bracket loads on the exterior girders, causing twisting of the girders and inducing flange lateral bending due to this twisting action. These stresses are superimposed on top of the overall flange lateral bending stresses due to skew. The flange lateral bending stresses due to skew are relatively small in the region "within the span."
3. There is another typically smaller local spike in the flange lateral bending stress where the girder is continuous across the pier bearing line. This local spike is at 168 ft along Girder 1 in Figure 103.

Figure 104 shows the variation of the STR I bottom flange lateral bending stress in the central interior girder. Again, the flange lateral bending stresses are relatively small "within the span." However, a local spike in flange lateral bending occurs at several cross-frame locations near the girder ends, both near the end abutments and near the interior pier bearing locations. Depending on the many different attributes of the girder designs and the cross-frame framing arrangements, the local spikes in the stresses near the bearing locations may be smaller than or larger than the magnitude of the local spikes near the bearings in the exterior girders.

It can be observed from Figure 104 that the flange lateral bending stresses at the abutments for the exterior and central interior girder of Bridge 2C2-43 are larger than the flange lateral bending stresses at intermediate pier. This trend is consistent across all continuous span Category 2C bridges. Table 31 lists the maximum flange lateral bending stresses near abutments and piers for exterior, first interior and central interior girders for the continuous span Category 2C bridges that exhibit the largest flange lateral bending stresses, identified from Table 30. However, it should be noted that the flange lateral bending stresses are dependent on the flange sizes at the abutments and piers. Figure 105 shows the variation of the STR I bottom flange lateral bending moments in the central interior girder of Bridge 2C2-43. The flange lateral bending moments at the pier are nearly 2x the flange lateral bending moments at the abutments. However, the elastic section modulus for the bottom flange in lateral bending at the pier is nearly 4x that at the abutments, resulting in smaller flange lateral bending stresses at the pier than at the abutment at the left-hand end of the plot.

It is important to note that in some bridges, the ratio of the elastic section moduli of the flanges at the piers and the abutments is even larger than in this example.

Table 30. Maximum STR I flange lateral bending stress values for exterior, first interior, and central interior girders, Category 2C bridges.

Bridge	Skew Index, I_s	Skew Angle, θ (deg.)	$f_{\ell,maxG1}$ (ksi)	$f_{\ell,maxG2}$ (ksi)	$f_{\ell,maxG3}$ (ksi)	$f_{\ell,maxG4}$ (ksi)
2C1-17	0.28	42	10.2	2.3	3.0	10.2
2C1-35	0.16	44	7.2	4.1	4.0	6.9
2C1-36	0.18	44	11.4	6.6	9.2	11.5
2C1-38	0.30	50	9.3	6.2	6.9	9.3
2C1-39	0.30	37	4.7	5.3	7.1	4.6
2C2-41	0.18	50	15.9	14.8	13.8	13.7
2C2-43	0.27	50	18.2	14.4	15.0	17.9
2C2-44	0.23	40	8.2	2.1	11.5	5.3
2C2-45	0.28	50	13.0	6.5	11.1	12.9
2C2-46	0.29	44	6.3	3.4	6.7	4.3
2C2-46B	0.26	40	5.9	3.2	6.5	4.1
2C2-46C	0.21	35	5.7	3.1	5.9	3.9
2C2-46D	0.18	30	5.2	2.9	5.7	3.6
2C2-46E	0.15	30	6.1	2.0	4.1	4.1
2C3-11	0.26	38	10.1	4.6	2.8	9.9
2C3-47	0.28	50	12.0	13.0	13.1	12.2
2C3-48	0.29	50	15.0	8.0	6.0	15.3
2C3-51	0.29	47	12.8	6.7	6.9	13.0
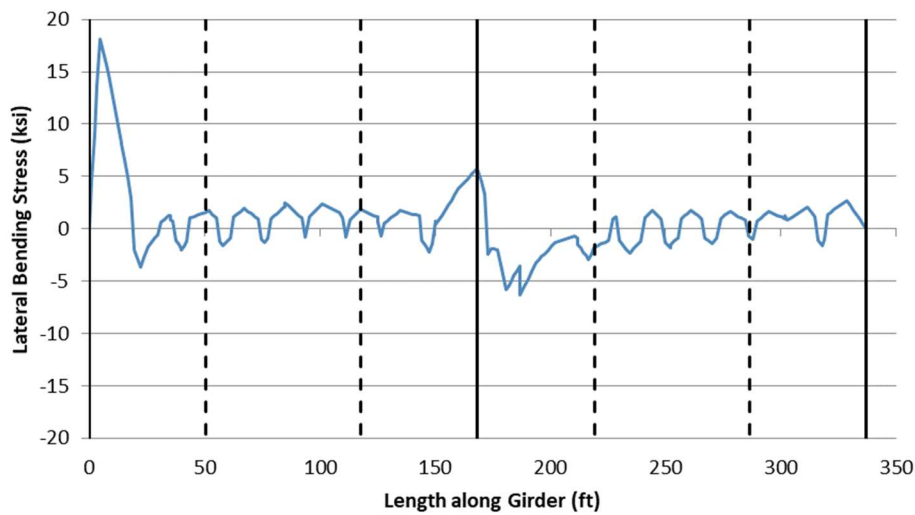
Figure 103. STR I bottom flange lateral bending stress in the exterior Girder 1 of Bridge 2C2-43.
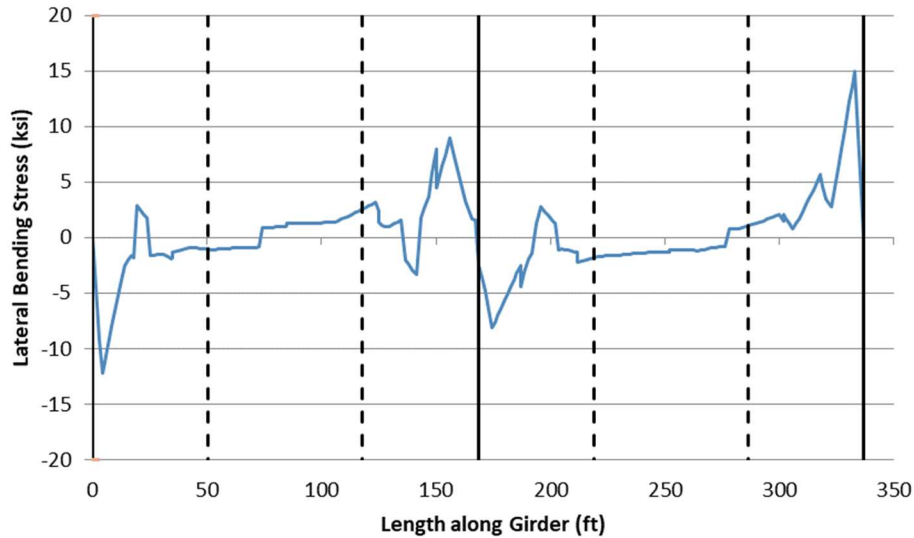
Figure 104. STR I bottom flange lateral bending stress in the central interior girder of Bridge 2C2-43.

Table 31. Maximum STR I flange lateral bending stresses (ksi) for exterior, first interior, and central interior girders near abutments and piers of continuous-span Category 2C bridges.

Bridge	$f_{\ell,maxG1}$ near Abutment (ksi)	$f_{\ell,maxG1}$ near Pier (ksi)	$f_{\ell,maxG2}$ near Abutment (ksi)	$f_{\ell,maxG2}$ near Pier (ksi)	$f_{\ell,maxG3}$ near Abutment (ksi)	$f_{\ell,maxG3}$ near Pier (ksi)
2C2-41	15.9	6.2	14.8	11.7	13.8	10.4
2C2-43	18.2	6.3	14.4	8.7	14.9	8.2
2C2-45	13.0	5.7	6.1	5.6	7.5	11.1
2C3-11	10.1	4.7	4.6	4.2	2.6	2.8
2C3-47	11.9	6.7	13.0	10.2	13.1	10.1
2C3-48	14.2	2.9	8.0	5.8	5.6	5.6
2C3-51	12.1	6.0	6.7	6.0	6.0	7.0

Table 32 lists the maximum fatigue stress range and Table 33 lists the maximum CDL flange lateral bending stress for the exterior and interior girders of Category 2C bridges. The maximum stress range of 6.4 ksi is observed for the exterior girders of Bridge 2C2-46C. The maximum CDL flange lateral bending stress is observed in the exterior girders of Bridge 2C2-43, similar to the STR I load combination.
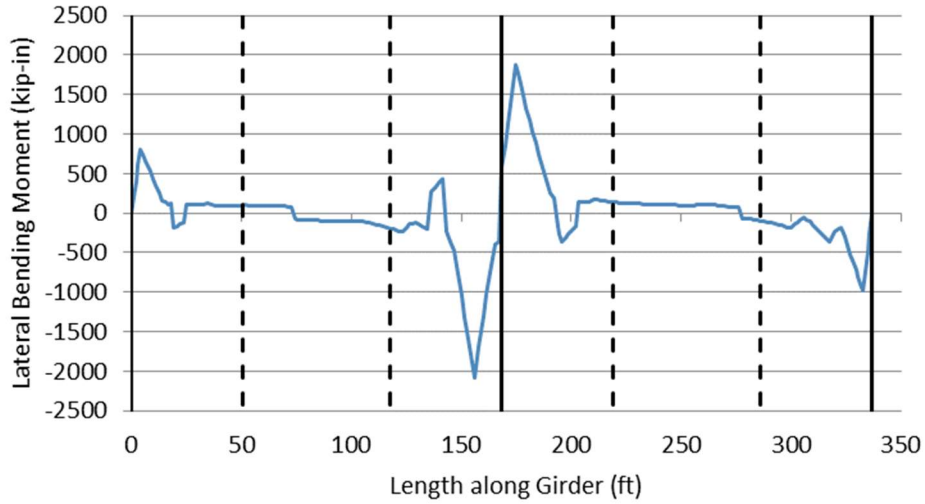
Figure 105. STR I bottom flange lateral bending moments in the central interior girder of Bridge 2C2-43.

Table 32. Maximum unfactored fatigue flange lateral bending stress range values for exterior, first interior, and central interior girders, Category 2C bridges.

Bridge	Skew Index, I_s	Skew Angle, θ (deg.)	$f_{\ell,maxG1}$ (ksi)	$f_{\ell,maxG2}$ (ksi)	$f_{\ell,maxG3}$ (ksi)	$f_{\ell,maxG4}$ (ksi)
2C1-17	0.28	42	2.8	0.4	0.6	2.8
2C1-35	0.16	44	2.8	1.0	1.0	2.7
2C1-36	0.18	44	3.6	1.4	2.5	3.6
2C1-38	0.30	50	3.0	1.5	2.1	3.0
2C1-39	0.30	37	1.6	1.5	2.1	1.6
2C2-41	0.18	50	5.5	4.1	3.7	4.5
2C2-43	0.27	50	3.0	0.4	3.6	1.5
2C2-44	0.23	40	3.7	1.1	2.0	3.7
2C2-45	0.28	50	1.9	0.6	1.3	1.3
2C2-46	0.29	44	1.8	0.6	1.4	1.3
2C2-46B	0.26	40	1.8	0.6	1.4	1.2
2C2-46C	0.21	35	6.4	4.7	5.0	6.3
2C2-46D	0.18	30	2.0	0.4	1.0	1.3
2C2-46E	0.15	30	3.0	1.0	0.6	2.9
2C3-11	0.26	38	4.9	4.6	4.6	4.9
2C3-47	0.28	50	4.8	1.5	1.3	4.8
2C3-48	0.29	50	3.6	1.2	1.3	3.6
2C3-51	0.29	47	2.8	0.4	0.6	2.8

Table 33. Maximum unfactored concrete dead load flange lateral bending stress values for exterior, first interior, and central interior girders, Category 2C bridges.

Bridge	Skew Index, I_s	Skew Angle, θ (deg.)	$f_{\ell,maxG1}$ (ksi)	$f_{\ell,maxG2}$ (ksi)	$f_{\ell,maxG3}$ (ksi)	$f_{\ell,maxG4}$ (ksi)
2C1-17	0.28	42	0.9	0.4	0.1	0.7
2C1-35	0.16	44	0.3	0.3	0.2	0.4
2C1-36	0.18	44	0.7	0.5	0.2	0.5
2C1-38	0.30	50	0.5	0.2	0.4	0.4
2C1-39	0.30	37	0.7	0.3	0.2	0.6
2C2-41	0.18	50	0.9	1.6	1.4	0.9
2C2-43	0.27	50	3.1	0.4	0.5	1.9
2C2-44	0.23	40	1.0	1.2	1.7	1.0
2C2-45	0.28	50	1.3	0.5	0.7	0.6
2C2-46	0.29	44	1.3	0.4	0.6	0.8
2C2-46B	0.26	40	1.4	0.4	0.3	0.7
2C2-46C	0.21	35	1.6	1.4	1.2	0.8
2C2-46D	0.18	30	1.4	0.3	0.3	0.7
2C2-46E	0.15	30	0.8	0.8	0.4	0.7
2C3-11	0.26	38	1.6	1.2	1.2	1.0
2C3-47	0.28	50	1.4	1.4	0.7	0.9
2C3-48	0.29	50	1.2	1.2	0.9	0.9
2C3-51	0.29	47	0.9	0.4	0.1	0.7

7.2.2.3 Category 2P Bridges

Table 34 shows the maximum STR I flange lateral bending stresses calculated by 3D FEA for the exterior and interior girders of the six Category 2P bridges studied in Project BEB13. The stresses are relatively small in the exterior girders but are large enough such that they should be considered. Conversely, the maximum flange lateral bending stresses in the interior girders are substantial in most of the bridges.

Figure 106 illustrates the variation of the STR I bottom flange lateral bending stress in the central interior Girder G3 of Bridge 2P3-49, which has the largest calculated maximum flange lateral bending stress of all the Project BEB13 bridges considered (30.2 ksi). Figure 107 shows the STR I bottom flange lateral bending stress variation in the central interior Girder G3 of Bridge 2P2-8. The central interior girder in this bridge also experiences substantial flange lateral bending, but slightly smaller than that in Bridge 2P3-49. The flange lateral bending in the central interior girders of these bridges has a local maximum near the bridge mid-span. This local maximum is due to the participation of the girder flanges in a transverse load path in the short diagonal direction between the obtuse corners of the spans. The major-axis bending moments developed by the bridge deck, the cross frames, and the girder flanges in lateral bending between the cross frames, are largest near the mid-span and mid-width of the bridges. However, depending on various attributes of the girder designs and the parallel stagger layout of the cross frames, the largest maximum flange lateral bending in the central interior girder can occur at the offset of the intermediate cross frames from the bearing lines, as shown in Figure 106 for Bridge 2P3-49, or near the mid-span and mid-width of the bridge spans, as shown in Figure 107 for Bridge 2P2-8. Smaller stagger

distances between the cross frames within parallel stagger arrangements in bridges with smaller skew angles, such as Bridge 2P2-8 which has a θ of its bearing lines of 23°, can exacerbate the magnitude of the flange lateral bending stresses in the central interior girder. However, the problem causing the large flange lateral bending near the mid-span and mid-width of the bridge is mainly one of developing nuisance transverse stiffness in the short diagonal direction between the obtuse corners of the spans. The large flange lateral bending near the ends of the central interior girders relates to transfer of load from the exterior girders to the end abutment bearings along a diagonal direction formed by the offset cross frames.

Table 34. Maximum STR I flange lateral bending stresses for exterior, first interior, and central interior girders, Category 2P bridges.

Bridge	Skew Index, I_s	Skew Angle, θ (deg.)	$f_{\ell,maxG1}$ (ksi)	$f_{\ell,maxG2}$ (ksi)	$f_{\ell,maxG3}$ (ksi)	$f_{\ell,maxG4}$ (ksi)
2P1-18	0.20	40	3.4	6.5	7.2	3.3
2P1-37	0.19	42	2.2	8.6	8.6	2.1
2P2-8	0.27	23	2.4	14.2	24.8	2.7
2P2-40	0.12	23	2.8	16.1	16.5	3.2
2P2-42	0.24	50	7.6	20.7	19.8	7.3
2P3-49	0.29	50	5.9	28.8	30.2	5.5
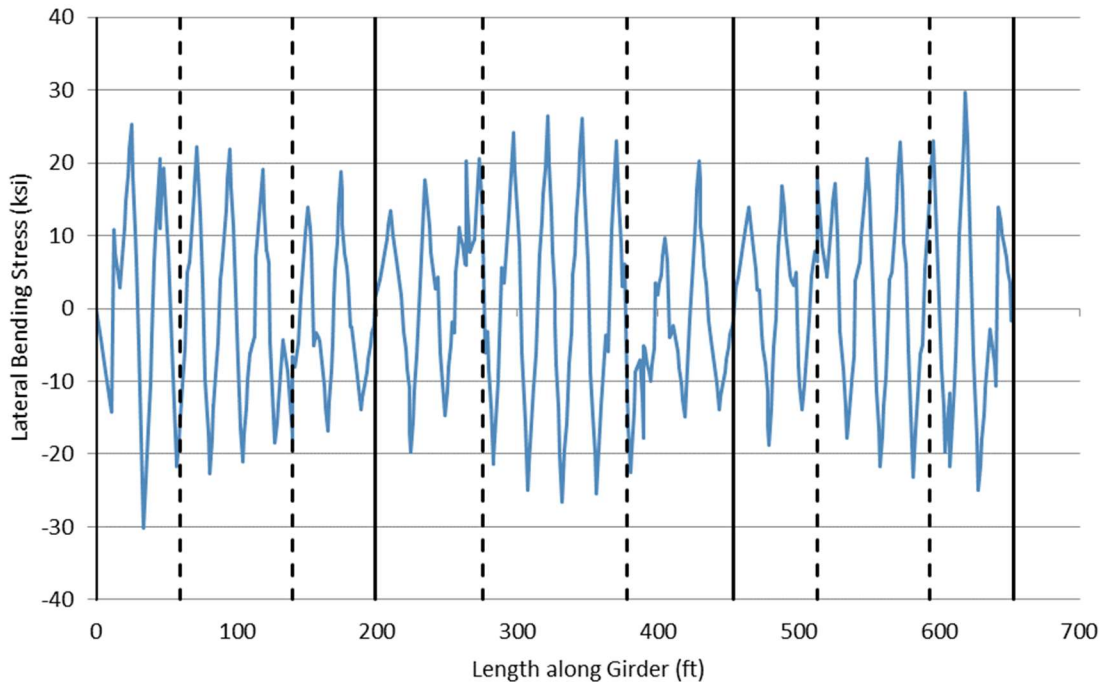
Figure 106. STR I bottom flange lateral bending stress in central interior Girder G3 of Bridge 2P3-49.
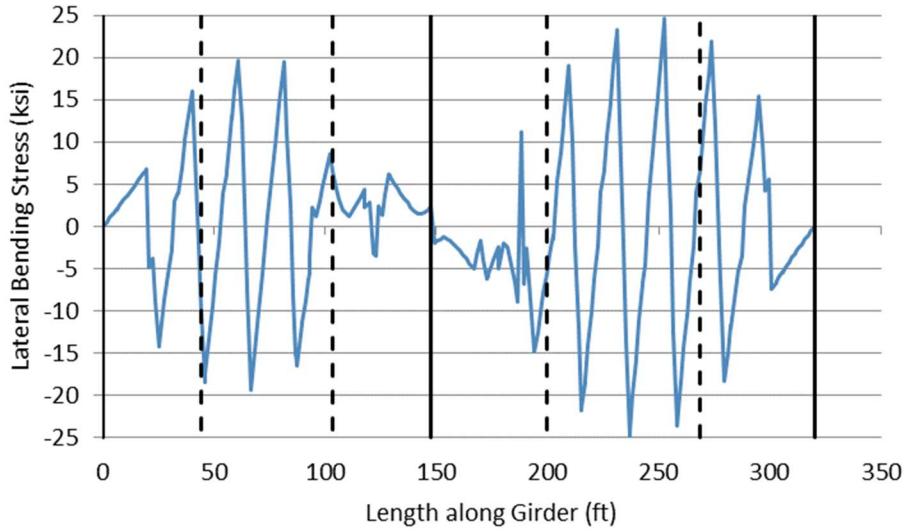
Figure 107. STR I bottom flange lateral bending stress in central interior Girder G3 of Bridge 2P2-8.

The flange lateral bending stresses in the interior girders tend to be smaller toward the middle of the spans for the girders closer to exterior girders in the bridge cross section. However, these stresses can still be relatively large near the obtuse corners of the bridge span (i.e., at the girder locations closest to the short diagonal between the obtuse corners of the bridge span). Figure 108 shows a representative plot of the flange lateral bending stresses in the first interior Girder G2 of Bridge 2P2-42. The largest spike in the flange lateral bending stresses occurs at the fourth intermediate cross frame connected to this girder, relative to the left-hand end abutment. This cross frame is in the most direct portion of the load path along the short diagonal between the obtuse corners of this bridge's left-hand span.
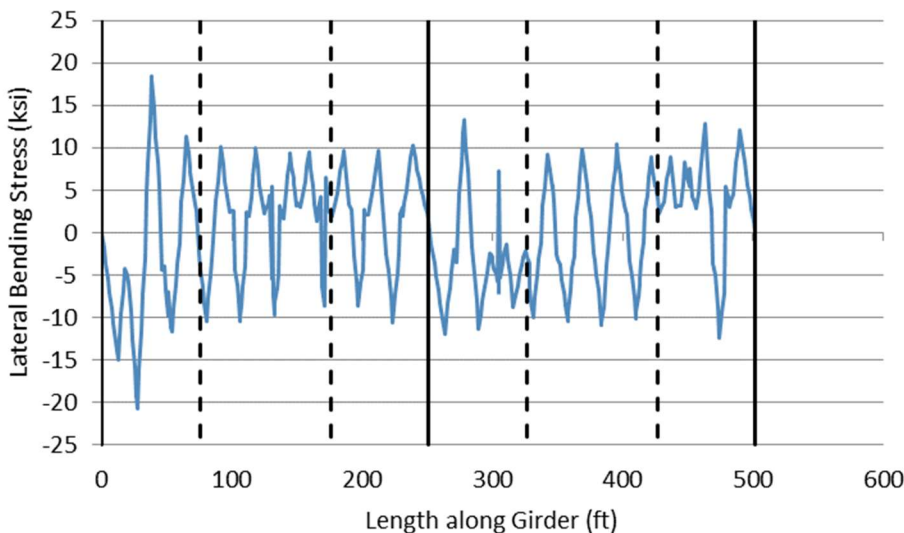
Figure 108. STR I bottom flange lateral bending stress in first interior Girder G2 of Bridge 2P2-42.

Figure 109 shows representative flange lateral bending stresses in the exterior girders of bridges having parallel stagger framing arrangements. This plot corresponds to the exterior Girder 1 of Bridge 2P2-42. As

146

can be observed from Table 34, Bridge 2P2-42 has the largest maximum flange lateral bending in its exterior girders. The maximum spike in the flange lateral bending stress occurs at the first intermediate cross frame from the obtuse corner of the left-hand span at the left-hand end abutment. Similar to the maximum stresses in a number of the previously discussed cases for the interior girders, this peak lateral bending stress is related to the development of a transverse load path in the short diagonal direction of the bridge. Smaller local spikes in the flange lateral bending stresses are generated at second intermediate cross frame from this location, and at the cross frames on each side of the interior pier bearing line for this bridge. Local variations can be observed at other locations along the exterior girder due to the eccentric lateral bending from the concrete deck load, causing twisting of the exterior girder.
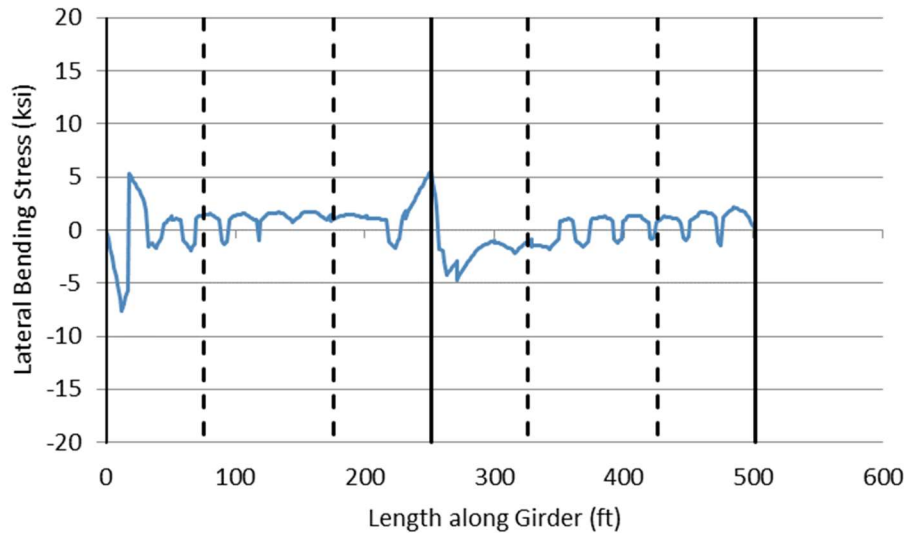
Figure 109. STR I bottom flange lateral bending stress in exterior Girder 1 of Bridge 2P2-42.

Table 35 lists the maximum fatigue stress range and Table 36 lists the maximum CDL flange lateral bending stress for the exterior and interior girders of Category 2P bridges. The maximum fatigue stress range and CDL flange lateral bending stress values are observed in the central interior girder of Bridge 2C2-49, similar to the STR I load combination.

Table 35. Maximum unfactored fatigue flange lateral bending stress range values for exterior, first interior, and central interior girders, Category 2P bridges.

Bridge	Skew Index, I_s	Skew Angle, θ (deg.)	$f_{\ell,maxG1}$ (ksi)	$f_{\ell,maxG2}$ (ksi)	$f_{\ell,maxG3}$ (ksi)	$f_{\ell,maxG4}$ (ksi)
2P1-18	0.20	40	1.0	1.7	1.9	1.0
2P1-37	0.19	42	0.6	2.7	2.7	0.6
2P2-8	0.27	23	0.5	4.8	6.0	0.5
2P2-40	0.12	23	0.9	4.8	5.2	0.7
2P2-42	0.24	50	2.1	5.2	5.9	2.1
2P3-49	0.29	50	1.5	7.6	9.0	1.5

Table 36. Maximum unfactored concrete dead load flange lateral bending stress values for exterior, first interior, and central interior girders, Category 2P bridges.

Bridge	Skew Index, I_s	Skew Angle, θ (deg.)	$f_{\ell,maxG1}$ (ksi)	$f_{\ell,maxG2}$ (ksi)	$f_{\ell,maxG3}$ (ksi)	$f_{\ell,maxG4}$ (ksi)
2P1-18	0.20	40	0.7	0.7	0.9	0.6
2P1-37	0.19	42	0.5	0.9	0.9	0.3
2P2-8	0.27	23	1.4	2.5	2.7	1.3
2P2-40	0.12	23	1.3	2.8	2.9	1.4
2P2-42	0.24	50	1.2	2.5	3.6	1.0
2P3-49	0.29	50	1.8	3.9	5.6	1.1

7.2.2.4 Recommended Estimates for Girder Unfactored Flange Lateral Bending Stresses

Comprehensive plots of the flange lateral bending stresses in all the Girders 1 through 4 of all the BEB13 study bridges are presented in Sections 8 and 9 of the project electronic data files. Table 37 provides incrementally refined recommendations for unfactored flange lateral bending stresses (f_ℓ) due to skew effects that can be employed for design, based on a synthesis of the BEB13 data, the corresponding data from the LGA amenable bridges from Project BE535, and the AASHTO (2020) Article C6.10.1 recommendations. Recommended weighted average load factors for different load combinations, which are adopted from FDOT Project BE535, have been presented previously in Table 26. Additionally, Table 37 provides estimates for unfactored fatigue flange lateral bending stress range and the unfactored CDL flange lateral bending stress.

One can observe that these recommendations closely parallel the AASHTO Article C6.10.1 recommendations, but the recommended flange lateral bending stress estimates tend to be either essentially equal to, somewhat larger than, or significantly larger than the AASHTO recommendations. The larger values in the BEB13 recommendations, relative to AASHTO, are for exterior girder locations at or near supports in skewed bridges with contiguous cross-frame framing arrangements (where the BEB13 recommendation is 12.0 ksi versus 7.5 ksi in AASTHO LRFD), and for all interior girder cross-frame locations in skewed bridges with parallel stagger cross-frame framing arrangements.

As stated in the AASHTO (2020) Article C6.10.1, the AASHTO recommendations are "based on a limited examination of refined analysis results for bridges with skews approaching 60 degrees from normal and an average D/b_f [web depth to flange width] ratio of approximately 4.0." The updated recommendations are based on the representative FDOT Category 1, 2C, and 2P bridges studied in Project BEB13, as well as the consideration of the results from Project BE535 and the results from the AASHTO Article C6.10.1.

Clearly, the precise flange lateral bending that occurs in the interior and exterior girders of skewed I-girder bridges can vary substantially and in many different ways, depending on the various attributes of the girder designs, and the cross-frame layouts, among other bridge characteristics. When larger flange lateral bending stresses are encountered in I-girder bridges designed using 3D FEA, the flanges typically would be made wider to reduce the magnitude of these stresses. The recommended stresses are believed to be based on girder designs where flange lateral bending due to skew effects likely was not considered, or was given only minor consideration such as via the coarse recommendations from AASHTO Article 6.10.1, in the design.

It should be emphasized that the regions between the solid and dashed lines (regions from 0 to 30%, and 70% to 100% of span length in each span) in Figures 103 to 109 are not indicative of a recommendation for the term "near supports." For Category 2C bridges, the maximum flange lateral bending stresses occur at points of discontinuity in the cross-frame framing arrangements at or near bearing lines. A similar spike in flange lateral bending stress is observed at cross-frame locations near the bearing lines for the exterior girders in Category 2P bridges. For the Category 2C bridges and for exterior girders in Category 2P bridges, the phrase "at or near the supports" should be interpreted as the support locations and the locations adjacent to the supports where there is a discontinuity in the cross-frame lines. For interior girders in Category 2P bridges, note that there is no distinction between "at or near the supports" and "within the span" for the interior girders. The maximum values in these girders can occur at various locations throughout the spans.

The factored f_ℓ for interior girders in Category 2P bridges from Table 37 is obtained as 28.8 ksi (1.6×18), although the maximum f_ℓ in Bridge 2P2-49 is 30.2 ksi. This is because the AASHTO Specifications limit f_ℓ to a maximum of $0.6F_y$, where F_y is the yield stress. The F_y used in all the study bridges is 50 ksi, resulting in a limit of 30 ksi for f_ℓ. Hence, the value of the recommended unfactored f_ℓ is taken as 18 ksi, such that the AASHTO Specification are not violated. The corresponding underprediction is comparable to other flange lateral bending stress underpredictions (e.g., taking f_ℓ equal to zero within the span in Category 2C bridges).

It is noted that the recommendation of an upper-bound unfactored f_ℓ of 18 ksi has as substantial impact for the design of Category 2P bridges. In a design scenario in which Bridge 2P-49 may have been designed based on a refined analysis, the engineer would typically increase the bottom flange widths to reduce the flange lateral bending stresses. An alternative approach for consideration would be to estimate the bounds for the flange lateral bending moments and use those in the design. However, given the substantial differences in magnitude of the flange lateral bending moments near the piers and near the abutments in the study bridges, determining appropriate bounds for the flange lateral bending moments may be challenging.

Table 37. Estimates of total unfactored flange lateral bending stresses due to skew effects.

Bridge Category	Cross-frame Framing Arrangement	Orientation of Intermediate Cross frames	Girder	Location	Recommended design f_ℓ (ksi)	AASHTO C6.10.1	Recommended fatigue f_ℓ range (ksi)	Recommended f_ℓ for CDL (ksi)
1	Contiguous	Parallel to skew	All	All	0	0	0	0
2C	Contiguous	Perpendicular to girders	Exterior	Near end supports	12	7.5	6.5	3.0
2C	Contiguous	Perpendicular to girders	Exterior	At or near continuous supports	4.5	7.5	6.5	3.0
2C	Contiguous	Perpendicular to girders	Exterior	Within the span	0	0	0	0
2C	Contiguous	Perpendicular to girders	Interior	Near end supports	10	10	5.0	2.0
2C	Contiguous	Perpendicular to girders	Interior	At or near continuous supports	7.5	10	5.0	2.0
2C	Contiguous	Perpendicular to girders	Interior	Within the span	0	0	0	0
2P	Parallel Stagger	Perpendicular to girders	Exterior	At or near the supports	5.0	7.5	2.5	2.0
2P	Parallel Stagger	Perpendicular to girders	Exterior	Within the span	3.0	2.0	2.0	2.0
2P	Parallel Stagger	Perpendicular to girders	Interior	All	18	10	9.0	6.0

7.3 Cross-Frame Forces

7.3.1 Prior Recommendations

Similar to the estimation of the girder flange lateral bending stresses, when LGA is employed, there is no direct way of estimating the cross-frame forces associated with the interactions between the cross frames and the girders due to the skewed geometry effects in resisting the dead load effects. AASHTO (2020) LRFD does not provide any guidance for estimating the cross-frame forces considering these actions. AASHTO (2020) Article 6.6.1.3.1 does indicate that, "In the absence of better information, the welded or bolted connection[s] should be designed to resist a 20.0-kip lateral load for straight, nonskewed bridges." Therefore, it would be appropriate to always design the connections of cross frames (supposedly at each of the chord levels) for a force that is greater than or equal to 20.0 kips. However, it can be observed that this recommendation does not address skew effects.

FDOT Project BE535 provided recommendations for estimating required design forces due to skew effects in intermediate and bearing-line cross frames of I-girder bridges having parallel skew and defined as being amenable to design by LGA. This project recommended estimates for cross-frame chord-level connection forces due to skew effects as various fractions of the maximum shear and bending moment within the bridge girders. However, Project BEB13 has determined that the bounds approximated by these estimated fractions of girder maximum shear and bending can be significantly larger than the corresponding values determined by 3D FEA in many situations, and that specified bounded values for the cross-frame member forces provide better simplicity and accuracy.

7.3.2 Synthesis of New Results

Upon further evaluation, the Project BEB13 studies have shown that the approach recommended by Project BE535, although predicting cases with smaller forces accurately-to-conservatively, often tends to give excessively conservative predictions for cases involving larger cross-frame forces. In many of the cases studied, Project BEB13 determined that simple absolute bounds on the cross-frame member forces provide a more accurate estimate of the force demands than basing the demands on a percentage of the girder maximum shear and moments. The corresponding results from the Category 1, 2C, and 2P bridge studies are discussed below. Summary recommendations for the maximum cross-frame forces are listed for each category within each of the following subsections. Detailed plots showing the specific cross-frame forces in all the members of all the cross frames for the different load cases, and for the STR I and SER II load combinations, for all the bridges are presented in Section 10 of the BEB13 electronic data files.

In the BEB13 study bridges, the intermediate cross frames were predominantly V-type and the bearing line cross frames were predominantly inverted-V-type. It is submitted that the recommended bounds can be employed sufficiently for the top chords, diagonals, and bottom chords in all cross-frame configurations.

7.3.2.1 Category 1 Bridges

Figure 110 through Figure 112 show the maximum STR I member forces in the top chords, diagonals, and bottom chords of the intermediate cross frames of the 11 Category 1 Project BEB13 bridges as determined using 3D FEA. Table 38 through Table 40 list the corresponding tension and compression axial forces. It is observed that simple absolute bounds on the forces in each of these types of cross-frame members should provide for a simple and sufficient force estimate that can be employed for design. Further, these simple estimates are less conservative than values obtained using the BE535 approach of estimating cross-frame chord-level connection forces as a percentage of girder maximum moments and shears.
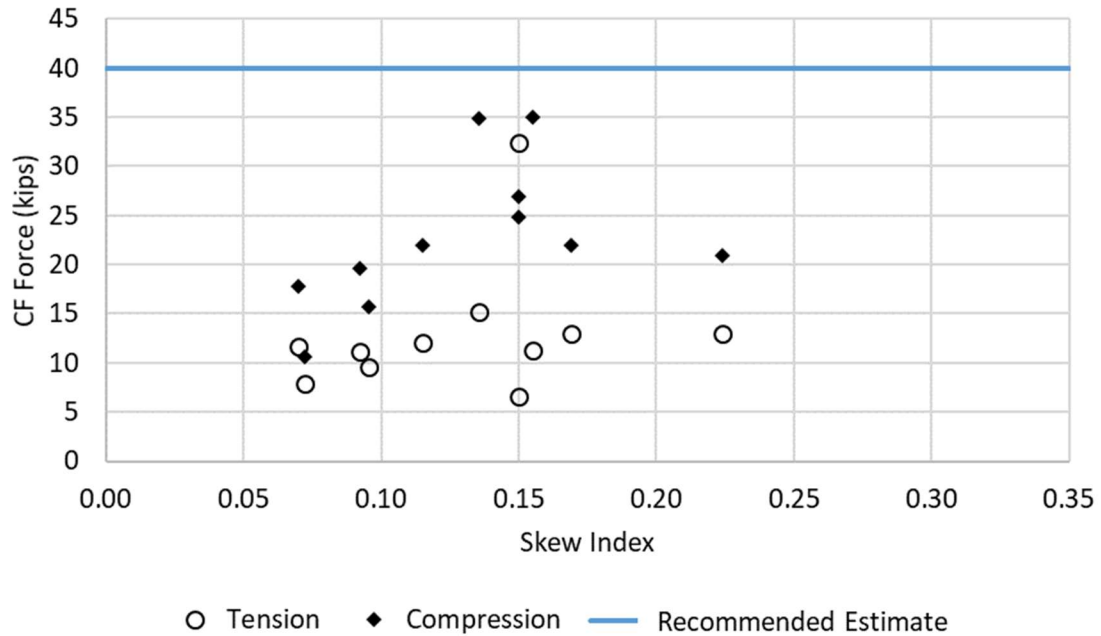
Figure 110. Maximum STR I forces in top chords of intermediate cross frames in Category 1 bridges.
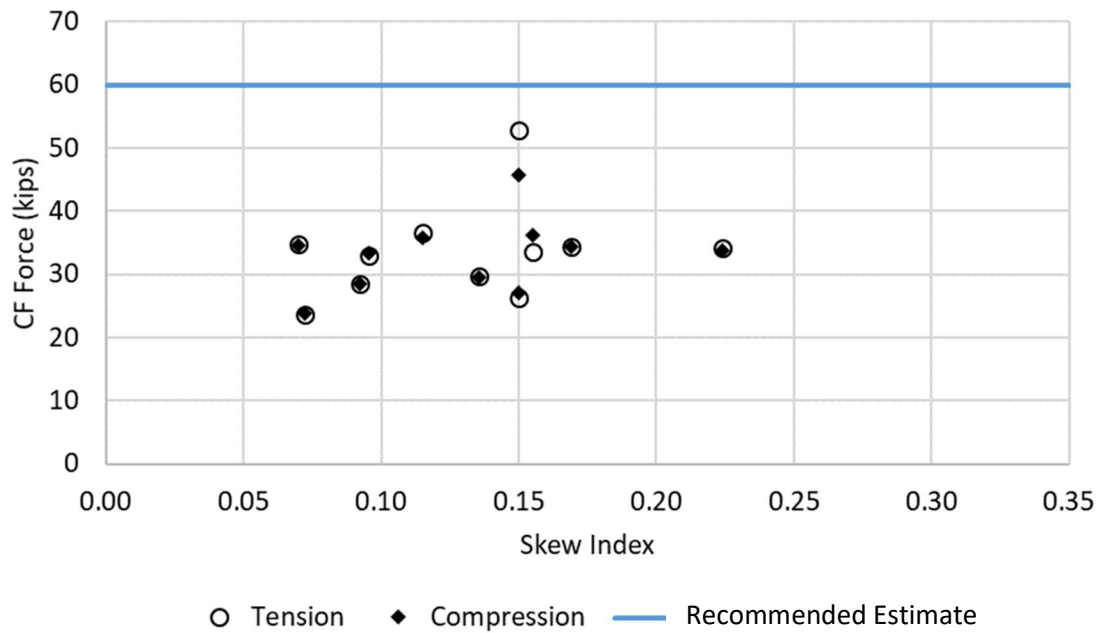
Figure 111. Maximum STR I forces in diagonals of intermediate cross frames in Category 1 bridges.
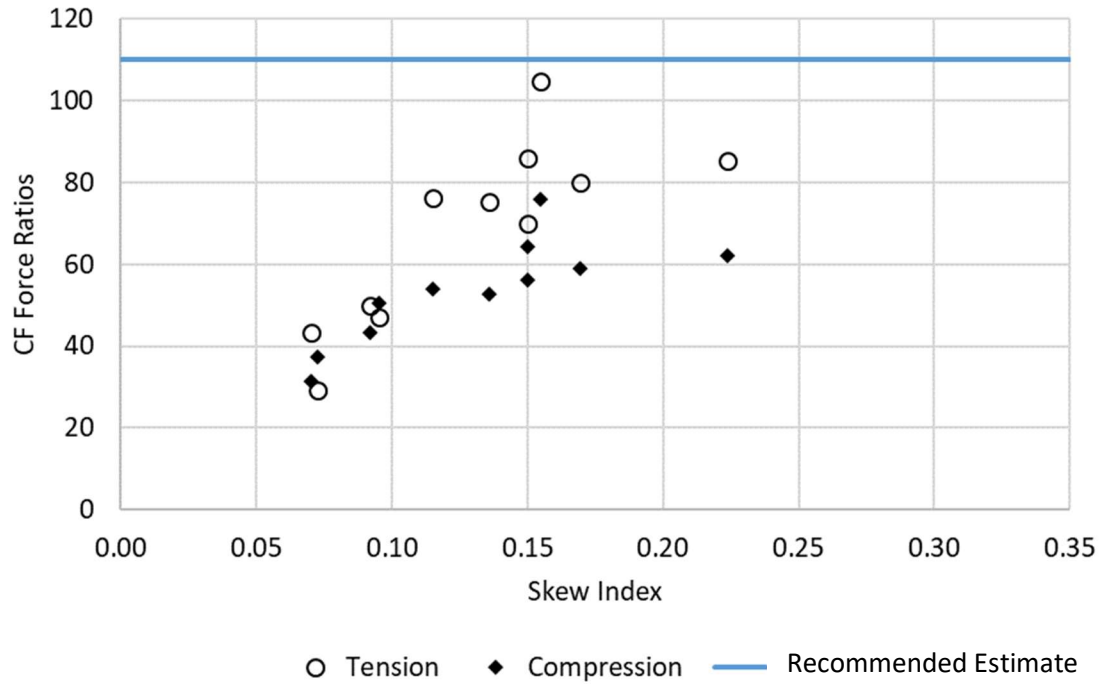
Figure 112. Maximum STR I forces in bottom chords of intermediate cross frames in Category 1 bridges.

Table 38. Maximum STR I tension and compression top chord forces for Category 1 bridges.

Bridge	Skew Index, I_s	Skew Angle, θ (deg.)	STR I Max Tension (kip)	STR I Max Compression (kip)
1C1-21	0.15	16	7	25
1C1-27	0.07	20	8	11
1C1-28	0.10	20	10	16
1C2-26	0.15	10	32	27
1C2-29	0.09	20	11	20
1C2-30	0.14	20	15	35
1C2-50	0.16	20	12	18
1C3-31	0.07	20	12	22
1C3-32	0.11	20	13	22
1C3-33	0.17	20	13	21
1C3-34	0.22	20	11	35

153

Table 39. Maximum STR I tension and compression diagonal forces for Category 1 bridges.

Bridge	Skew Index, I_s	Skew Angle, θ (deg.)	STR I Max Tension (kip)	STR I Max Compression (kip)
1C1-21	0.15	16	53	46
1C1-27	0.07	20	24	24
1C1-28	0.10	20	33	33
1C2-26	0.15	10	26	27
1C2-29	0.09	20	28	28
1C2-30	0.14	20	30	30
1C2-50	0.16	20	35	35
1C3-31	0.07	20	37	36
1C3-32	0.11	20	34	34
1C3-33	0.17	20	34	34
1C3-34	0.22	20	33	36

Table 40. Maximum STR I tension and compression bottom chord forces for Category 1 bridges.

Bridge	Skew Index, I_s	Skew Angle, θ (deg.)	STR I Max Tension (kip)	STR I Max Compression (kip)
1C1-21	0.15	16	86	64
1C1-27	0.07	20	29	37
1C1-28	0.10	20	47	51
1C2-26	0.15	10	70	56
1C2-29	0.09	20	50	43
1C2-30	0.14	20	75	53
1C2-50	0.16	20	43	31
1C3-31	0.07	20	76	54
1C3-32	0.11	20	80	59
1C3-33	0.17	20	85	62
1C3-34	0.22	20	105	76

Figure 113 through Figure 115 show the unfactored fatigue force ranges calculated in the cross-frame members using the new AASHTO (2021) 10th Edition recommendations based on NCHRP Report 962 (Reichenbach et al. 2021). It was determined that the fatigue force ranges also can be represented sufficiently by simple absolute estimates of the bounds on the forces determined from the 3D FEA solutions.

Figure 113. Maximum fatigue force ranges, AASHTO 10th edition, in top chords of intermediate cross frames in Category 1 bridges.

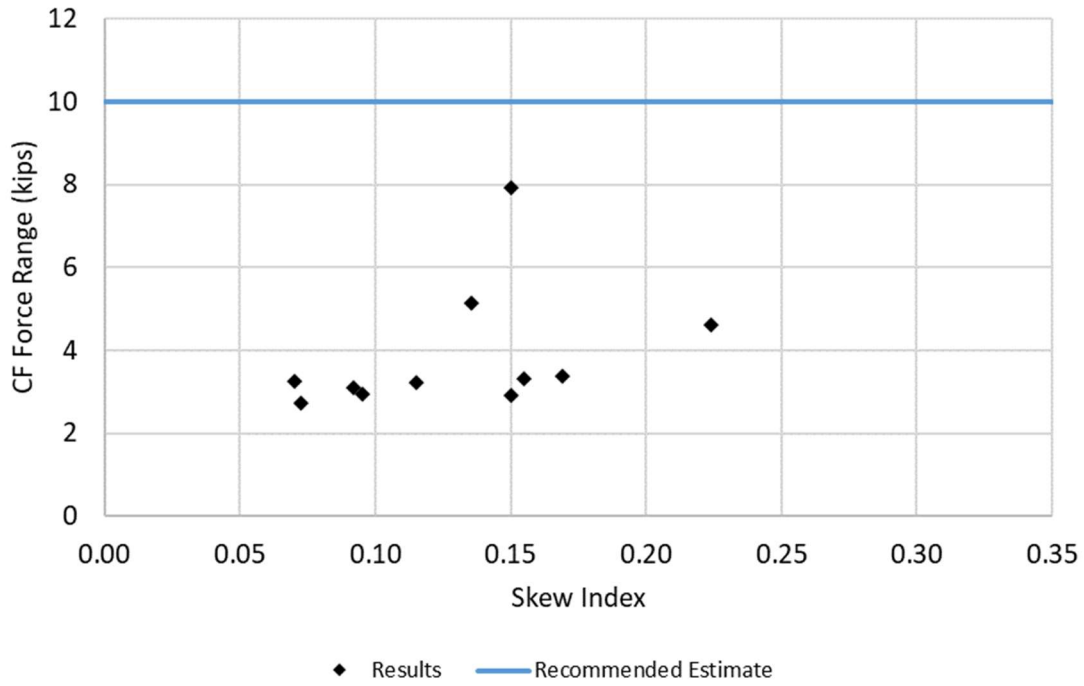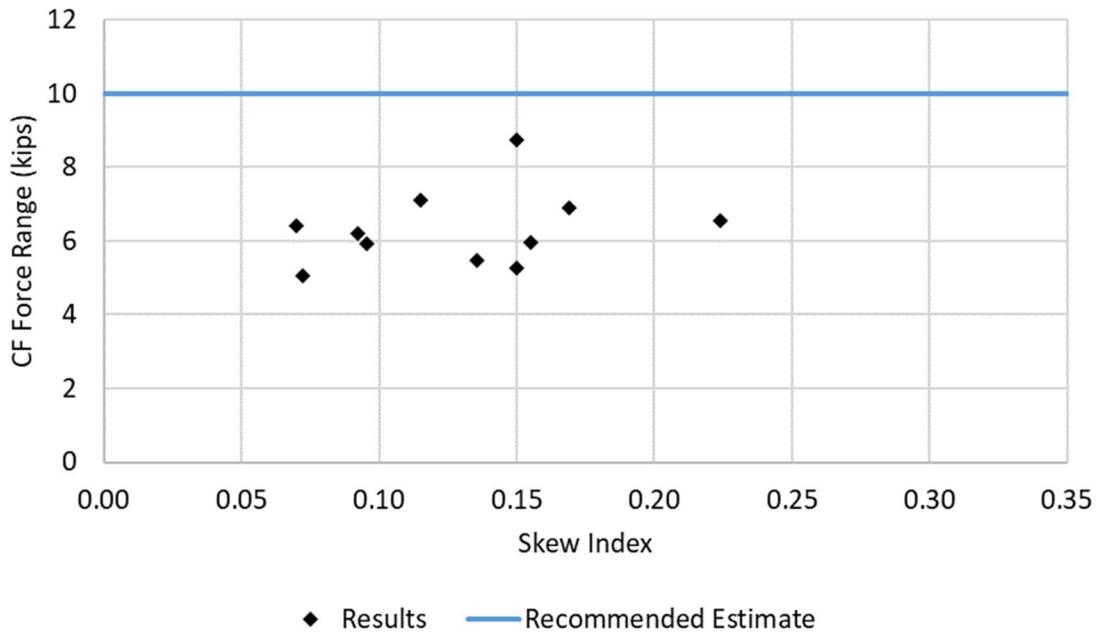**Figure 114. Maximum fatigue force ranges, AASHTO 10th edition, in diagonals of intermediate cross frames in Category 1 bridges.**
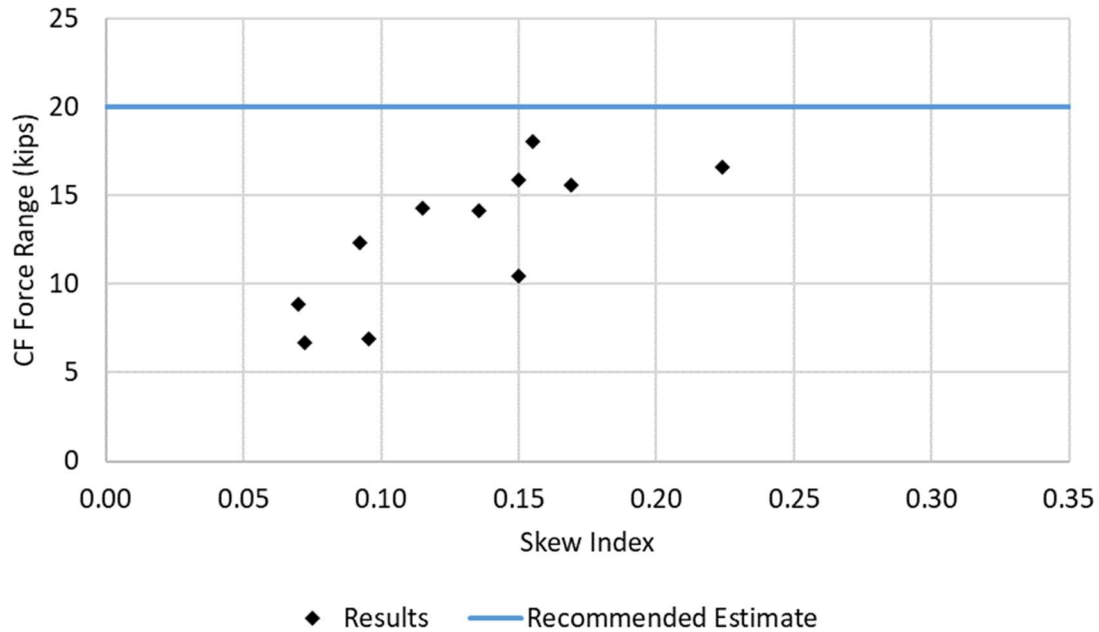
Figure 115. Maximum fatigue force ranges, AASHTO 10th edition, in bottom chords of intermediate cross frames in Category 1 bridges.

Table 41 summarizes the recommended simple upper-bound estimates for the intermediate cross-frame member forces for the various specific unfactored load cases studied, and for the STR I load combination, for Category 1 bridges. Furthermore, the table lists simple upper-bound estimates for the cross-frame member unfactored fatigue force ranges predicted using the AASHTO (2020) 9th Edition LRFD provisions prior to the adoption of the NCHRP 962 report recommendations and using the AASHTO (2021) 10th Edition LRFD provisions based on the NCHRP recommendations. Regarding the fatigue force range estimates, it can be observed that the AASHTO 10th Edition provisions result in a 33 % reduction of the bounded force ranges calculated by the 3D FEA models. It should be noted that the AASHTO (2021) provisions specify the application of an additional factor of 0.65 to the calculated cross-frame member force ranges prior to applying the Fatigue I or Fatigue II load factors. Therefore, the net resulting reduction in the cross-frame member force ranges relative to the AASHTO 9th Edition provisions is a factor of 0.43 for these bridges (i.e., a 57% ([1-0.43]x100=57%) net reduction).

Cross-frame forces in bearing-line cross frames at abutments and intermediate piers in Category 1 bridges are relatively small when compared to intermediate cross frames. It should be noted that the 3D FEA studies on which these recommendations are based, employs the assumption of negligible lateral restraint of the bridge deformations due to skew effects by the bridge bearing details. Hence, a simplified design philosophy paralleling the design philosophy adopted for flange lateral bending stresses in Section 7.2 is recommended for the estimation of forces in bearing-line cross frames in Category 1 bridges. Table 42 presents the corresponding recommended maximum bound estimates for unfactored forces due to skew effects (DC+DW+LL) and CDL load cases for the bearing-line cross frames at the abutments and at interior piers for Category 1 bridges (with the dynamic load allowance included in LL). The factored STR I force due to skew effects may be obtained by using the load factor of 1.6 from Table 26. Similarly, the estimate of unfactored forces due to skew effects may be used in other load combinations using the weighted average load factors in Table 26. Fatigue force ranges employing the procedures in AASHTO 10th Edition are significantly smaller than for the intermediate cross-frame members in all cases. Hence, fatigue force range

156

checks may be neglected in bearing-lines cross frames at abutments and intermediate piers in Category 1 bridges.

Notably, the unfactored DC2, DW and HL-93 Live Load values in Table 41 may be grouped together and a single unfactored DC+DW+LL value may be employed with the weighted-average load factors from Table 26. The DC+DW+LL value may be estimated by dividing the STR I results in the table by 1.6.

Table 41. Recommended force estimates for intermediate cross frames of Category 1 bridges.

Load Case	Top Chord (kips)	Diagonals (kips)	Bottom Chord (kips)
SDL, NLF	1	1	1
CDL	15	8	15
DC2	8	15	20
DW	1	2	3
HL-93 Live Load	25	35	65
STR I	40	60	100
Fatigue Range, AASHTO 9th Edition	15	15	30
Fatigue Range, AASHTO 10th Edition	10	10	20

Table 42. Recommended unfactored force estimates for bearing-line cross frames at abutments and intermediate piers in Category 1 bridges.

Load Case	Top Chord (kips)	Diagonals (kips)	Bottom Chord (kips)
CDL	5	5	5
DC+DW+LL	25	20	25

7.3.2.2 Category 2C Bridges

The cross-frame forces in Category 2C bridges are more sensitive to the offsets employed near obtuse corners and cross-frame member sizes employed. Stiff transverse load path effects are more prominent in Category 2C bridges. Such effects are more prominent in simple span bridges compared to continuous-span bridges. Figure 116 and Figure 117 show the maximum STR I member forces in the top chords of the intermediate cross frames of simple span and continuous-span Category 2C Project BEB13 bridges, respectively, determined using 3D FEA. Figure 118 and Figure 119 show the corresponding forces in diagonals, while Figure 120 and Figure 121 show the corresponding forces in bottom chords. Table 43 through Table 45 list the corresponding tension and compression axial forces for all bridges. The largest magnitude of the forces in the cross-frame members is observed in the bottom chords. Table 45 additionally lists the maximum span lengths for each bridge to examine the influence of span lengths on bottom chord forces. The maximum bottom chord force in simple-span bridges is 118 kips (Figure 120), which may be resisted by 6x6 angles for the girder spacing utilized in the bridges (i.e., up to 12 ft) Similarly, the maximum force in top chords is 34 kips (Figure 116), and in diagonals is 64 kips (Figure 118). Commonly used member sizes are typically sufficient to resist the forces observed in cross-frame members in the simple-

span Category 2C bridges. Hence, simple upper bound estimates are recommended, indicated by solid blue lines in the figures, for the design of cross-frame members in simple-span bridges.

The corresponding maximum forces in top chords, diagonals, and bottom chords are larger in continuous-span bridges compared to simple-span bridges. The maximum force in the top chords in intermediate cross frames of continuous-span bridges is 92 kips (Figure 117), and in diagonals is 175 kips (Figure 119). Hence, upper-bound estimates of 100 kips and 180 kips are recommended for top chords and diagonals, respectively. Significantly larger forces are observed in the bottom chords of intermediate cross frames in continuous-span bridges. Specifics related to this aspect of behavior is explained in a following section. Referring to Table 45, the maximum forces are seen in Bridges 45, 46 – 46E, 48 and 51. As stated in Section 3.5, parametric variations on Bridge 46 (i.e. 46B to 46E) were added to the study bridge matrix to closely scrutinize the behavior of continuous-span bridges resulting in large cross-frame forces. The skew indices progressively increase from Bridges 46E to 46, and forces in the bottom chords are also observed to progressively increase from Bridge 46E to 46. The recommended upper bound estimate shown in Figure 121 capture this trend and may be written as:

$$B_F = 200 + 340 \, I_s \ \ \text{for } I_s \geq 0.15 \tag{25}$$

where:

B_F = magnitude of the force in bottom chord, in kips
I_s = skew index of the bridge

Eq. 25 provides an upper bound estimate of 250 kips for bottom chords in continuous-span bridges that have skew indices, $I_s \leq 0.15$, a linear increase from 250 kips at $I_s = 0.15$ to 300 kips at $I_s = 0.29$ capping the maximum bottom chord force at 300 kips. It should be noted that the recommended estimates are strictly upper bounds and based on the study of 13 continuous-span Category 2C bridges.

Figure 116. Maximum STR I forces in top chords of intermediate cross frames of simple-span Category 2C bridges.

158

Figure 117. Maximum STR I forces in top chords of intermediate cross frames of continuous-span Category 2C bridges.
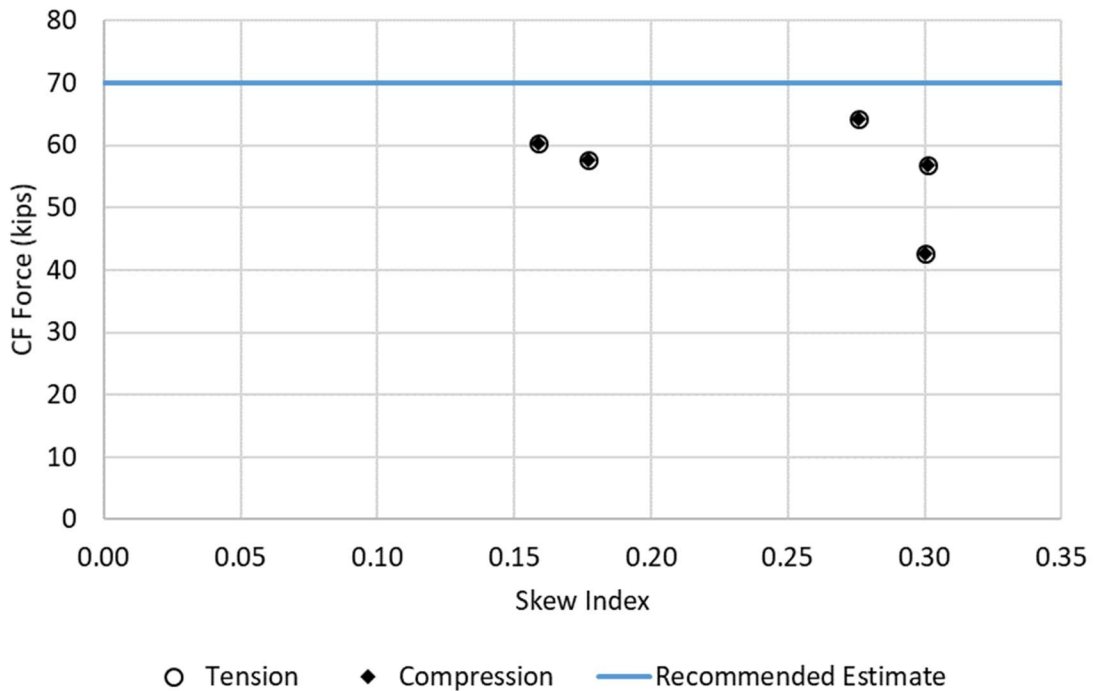
Figure 118. Maximum STR I forces in diagonals of intermediate cross frames in simple-span Category 2C bridges.
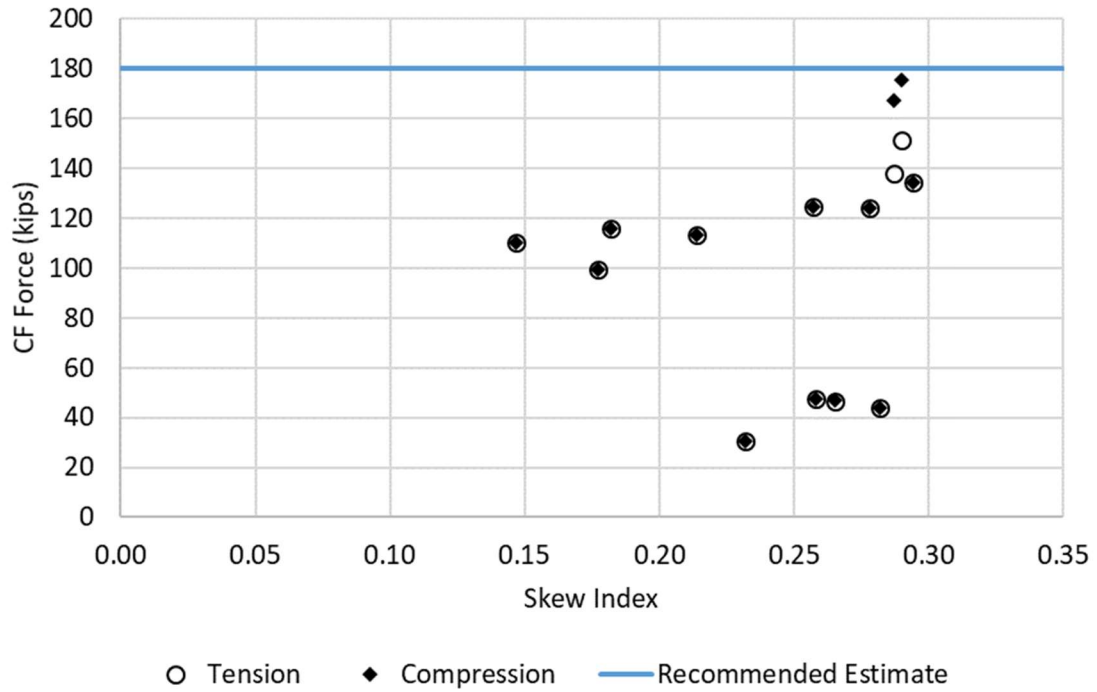
Figure 119. Maximum STR I forces in diagonals of intermediate cross frames in continuous-span Category 2C bridges.
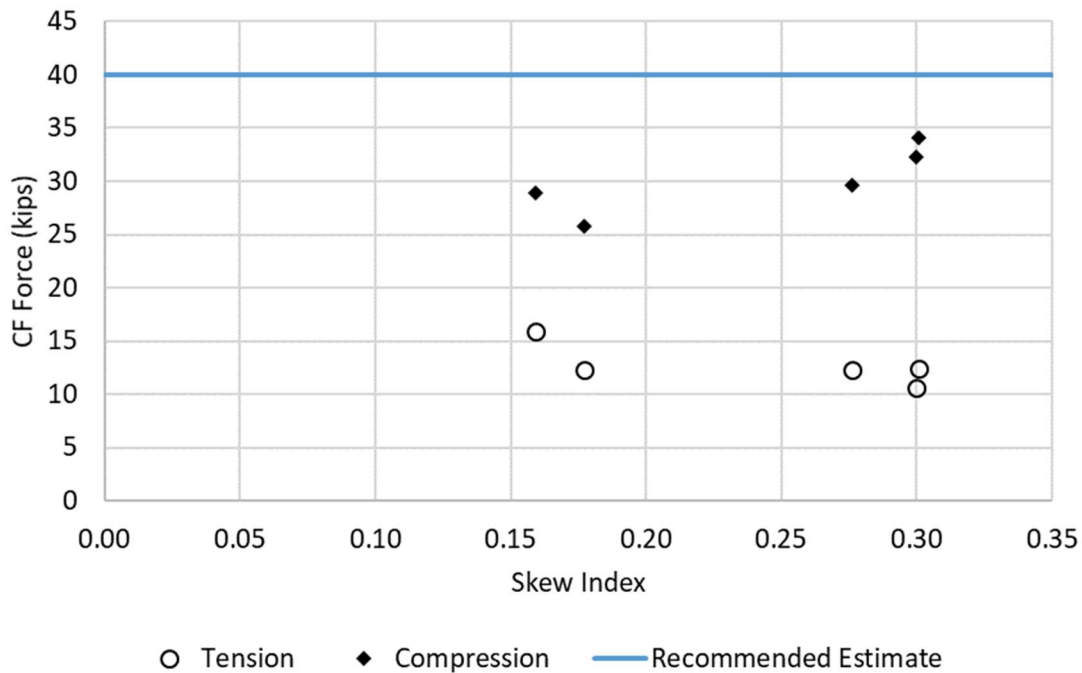

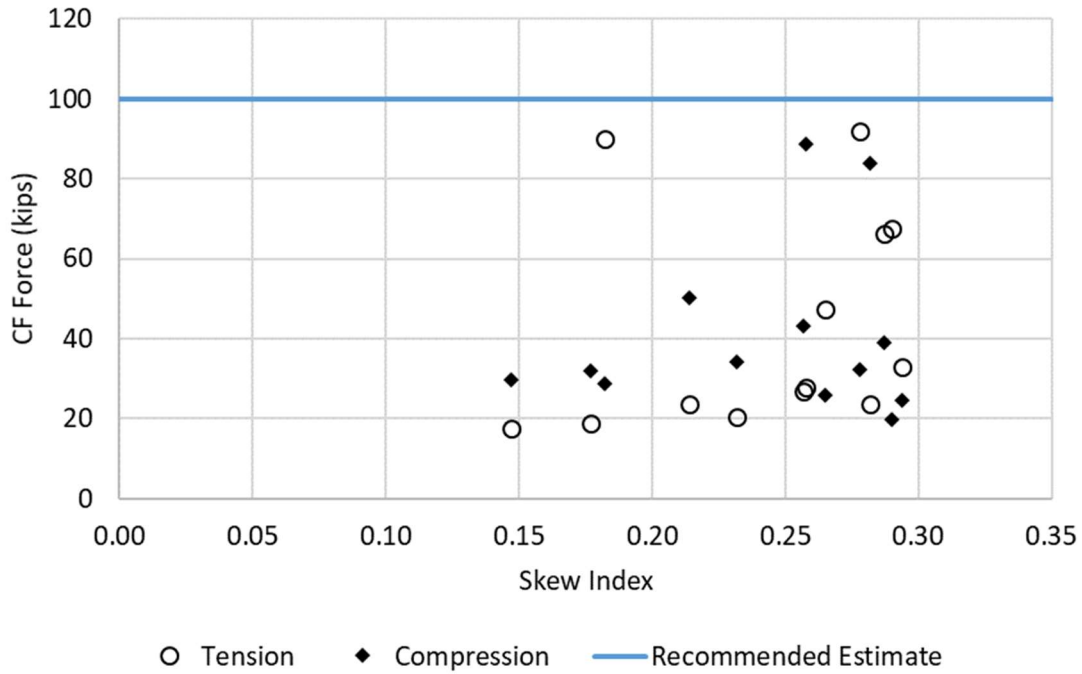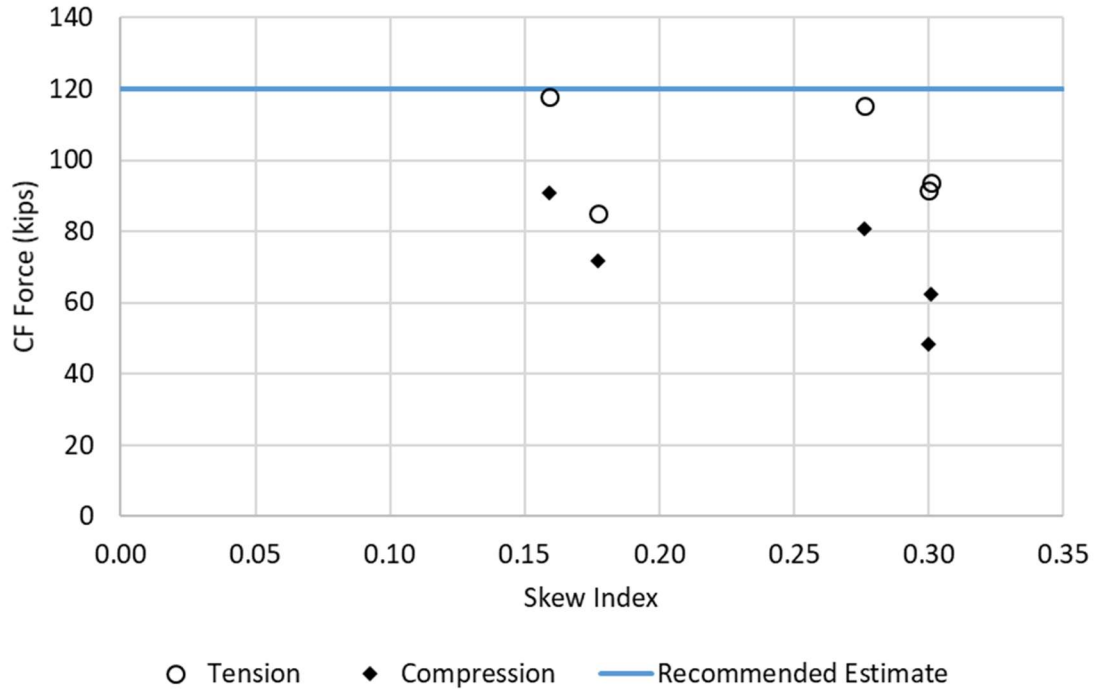**Figure 120. Maximum STR I forces in bottom chords of intermediate cross frames in simple-span Category 2C bridges.**
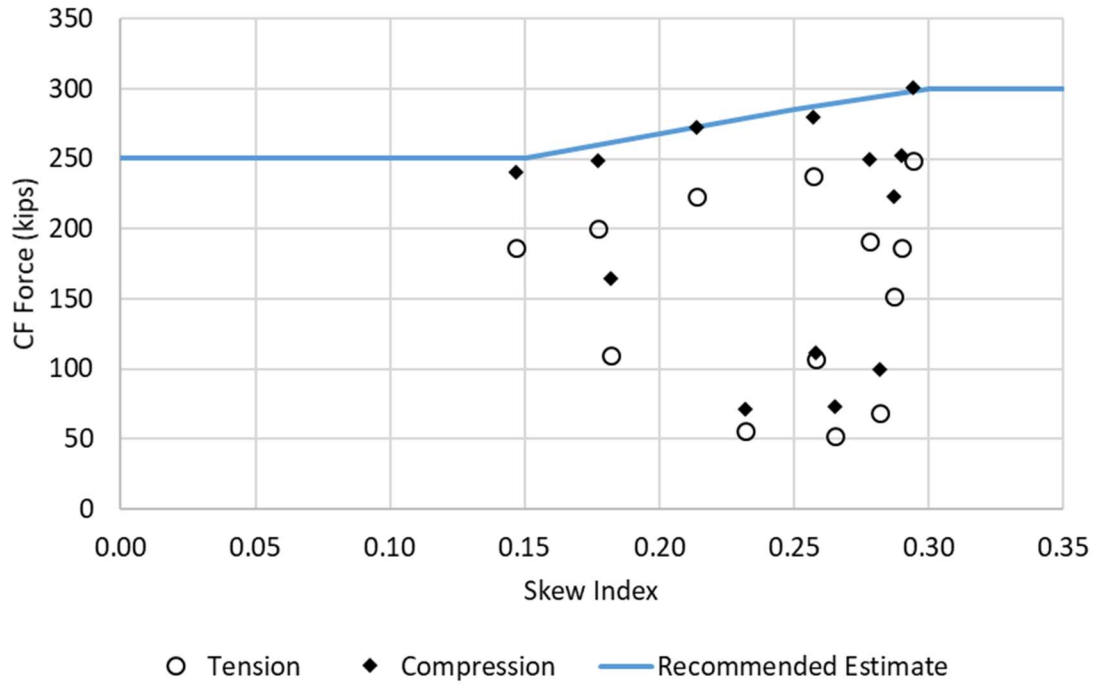
Figure 121. Maximum STR I forces in bottom chords of intermediate cross frames in continuous-span Category 2C bridges.

Table 43. Maximum STR I tension and compression top chord forces for Category 2C bridges.

Bridge	Skew Index, I_s	Skew Angle, θ (deg.)	STR I Max Tension (kip)	STR I Max Compression (kip)
2C1-17	0.28	42	12	30
2C1-35	0.16	44	16	29
2C1-36	0.18	44	12	26
2C1-38	0.30	50	12	34
2C1-39	0.30	37	11	32
2C2-41	0.18	50	90	84
2C2-43	0.27	50	47	39
2C2-44	0.23	40	21	20
2C2-45	0.28	50	92	89
2C2-46	0.29	44	33	32
2C2-46B	0.26	40	27	28
2C2-46C	0.21	35	24	26
2C2-46D	0.18	30	19	23
2C2-46E	0.15	30	18	17
2C3-11	0.26	38	28	32
2C3-47	0.28	50	24	25
2C3-48	0.29	50	66	43
2C3-51	0.29	47	68	50

Table 44. Maximum STR I tension and compression diagonal forces for Category 2C bridges.

Bridge	Skew Index, I_s	Skew Angle, θ (deg.)	STR I Max Tension (kip)	STR I Max Compression (kip)
2C1-17	0.28	42	64	64
2C1-35	0.16	44	60	60
2C1-36	0.18	44	58	58
2C1-38	0.30	50	57	57
2C1-39	0.30	37	43	43
2C2-41	0.18	50	116	116
2C2-43	0.27	50	47	47
2C2-44	0.23	40	31	31
2C2-45	0.28	50	124	124
2C2-46	0.29	44	134	134
2C2-46B	0.26	40	124	125
2C2-46C	0.21	35	113	113
2C2-46D	0.18	30	100	100
2C2-46E	0.15	30	110	110
2C3-11	0.26	38	48	48
2C3-47	0.28	50	44	44
2C3-48	0.29	50	138	168
2C3-51	0.29	47	151	175

It was stated previously that bridges exhibiting the largest bottom chord forces are continuous-span bridges and, interestingly, have spans longer than 200 ft. This is corroborated from the findings that Bridges 45, 46 – 46E, 48, and 51 are observed to have the maximum bottom chord forces. Simple-span bridges of comparable span lengths and skew indices exhibit much smaller forces. Continuous spans are typically stiffer than simple spans for comparable skew indices. In moderately wide (refer Section 3.1) continuous-span bridges that have longer span lengths (> 200 ft), large skew angles, the distance along the shorter diagonal between obtuse corners in spans traverse several contiguous cross-frame lines spanning the entire width of the bridge. As a result, the stiff transverse load path traverses through the several contiguous cross-frame lines and develops over a longer length. Conversely, in a shorter span, the stiff transverse load path develops over a shorter length and traverses fewer contiguous cross-frame lines. As a result, a longer span develops larger forces in bottom chords near obtuse corners than a shorter span with a comparable skew index. Figure 122 clearly shows that the largest forces in bottom chords of continuous-span bridges occurs in bridges that have span lengths > 200 ft. Examining Table 45, it is seen that although the skew indices of Bridges 43 and 46C are similar, the forces in the bottom chords in Bridge 46C are around 4x larger than those in Bridge 43. This indicates that the cross-frame forces in the Category 2C bridges depends on several variables such as the skew angle, span lengths, cross-frame offsets, and the skew index. The bridges that exhibit the maximum forces have many of the variables listed above at the extreme limits.

Table 45. Maximum STR tension and compression bottom chord forces for Category 2C bridges.

Bridge	Skew Index, I_s	Skew Angle, θ (deg.)	Maximum Span Length (ft)	STR I Max Tension (kip)	STR I Max Compression (kip)
2C1-17	0.28	42	202	115	81
2C1-35	0.16	44	218	118	91
2C1-36	0.18	44	243	85	72
2C1-38	0.30	50	190	94	62
2C1-39	0.30	37	150	92	48
2C2-41	0.18	50	251	110	165
2C2-43	0.27	50	168	52	73
2C2-44	0.23	40	155	56	71
2C2-45	0.28	50	250	191	250
2C2-46	0.29	44	228	248	301
2C2-46B	0.26	40	228	238	280
2C2-46C	0.21	35	228	224	273
2C2-46D	0.18	30	228	200	249
2C2-46E	0.15	30	228	186	240
2C3-11	0.26	38	188	107	112
2C3-47	0.28	50	195	68	99
2C3-48	0.29	50	255	152	223
2C3-51	0.29	47	285	187	252

Figure 123 to Figure 130 show STR I tension and compression in the bottom chords of intermediate cross frames in Bridges 45, 46, 48 and 51, respectively. Force values ≥ 200 kips are indicated in red and force values between 150 and 200 kips are marked dark blue. In the four bridges, maximum forces are observed in the first intermediate cross-frame and/or the next cross-frame line spanning across the bridge width. This indicates the importance of the offset of the first intermediate cross-frame line adjacent to the obtuse corners. The regions near the obtuse corners in Category 2C bridges where cross frames are highly stressed are referred to as the "critical regions" for cross-frame design considerations in this report. The forces reduce as one moves away from the obtuse corners.

These regions in Category 2C bridges are referred to as the "noncritical regions" for cross-frame design considerations. The results suggest that maximum bottom chord force in intermediate cross in the noncritical regions may be taken as 200 kips. However, there are several subtleties associated with aspects of transverse stiffness in Category 2C bridges that must be considered before arriving at such conclusions.
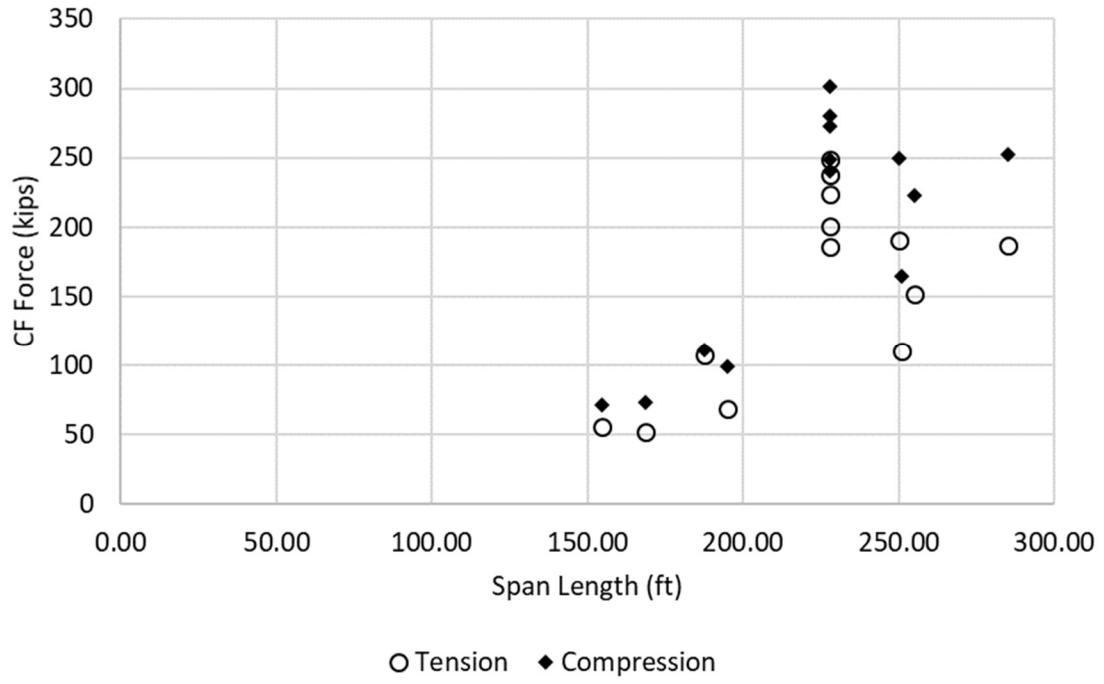
Figure 122. Maximum STR I forces vs bridge span lengths in bottom chords of continuous-span Category 2C bridges.
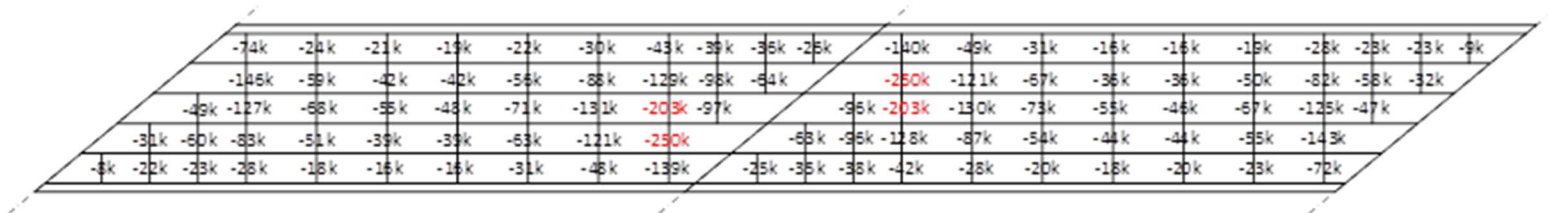
Figure 123. STR I compression forces in bottom chords of Bridge 2C2-45.
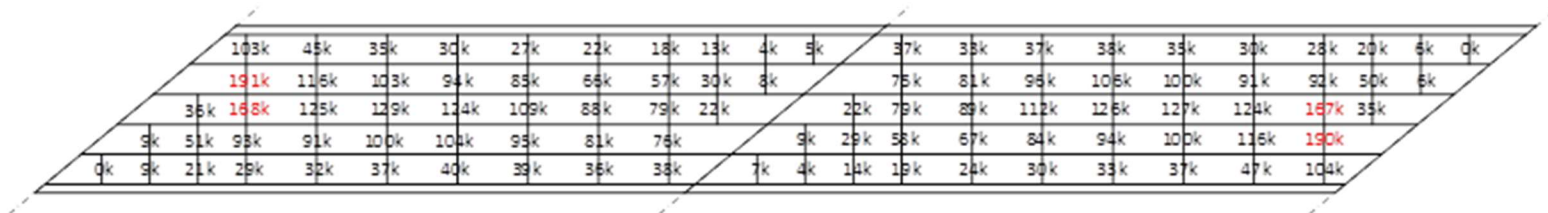
Figure 124. STR I tension forces in bottom chords of Bridge 2C2-45.

165

Figure 125. STR I compression forces in bottom chords of Bridge 2C2-46.

Figure 126. STR I tension forces in bottom chords of Bridge 2C2-46.

166

Figure 127. STR I compression forces in bottom chords of Bridge 2C3-48.

Figure 128. STR I tension forces in bottom chords of Bridge 2C3-48.

167

Figure 129. STR I compression forces in bottom chords of Bridge 2C3-51.

Figure 130. STR I tension forces in bottom chords of Bridge 2C3-51.

Limited studies indicate that the size of cross frames employed in the critical regions has a significant influence on the overall transverse stiffness of the system, and subsequently the magnitude of cross-frame forces. Consider a fictitious Category 2C continuous-span bridge where the m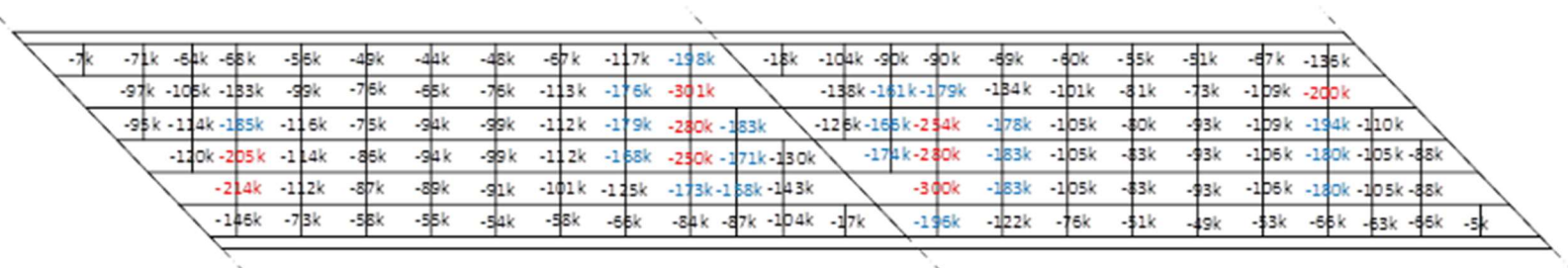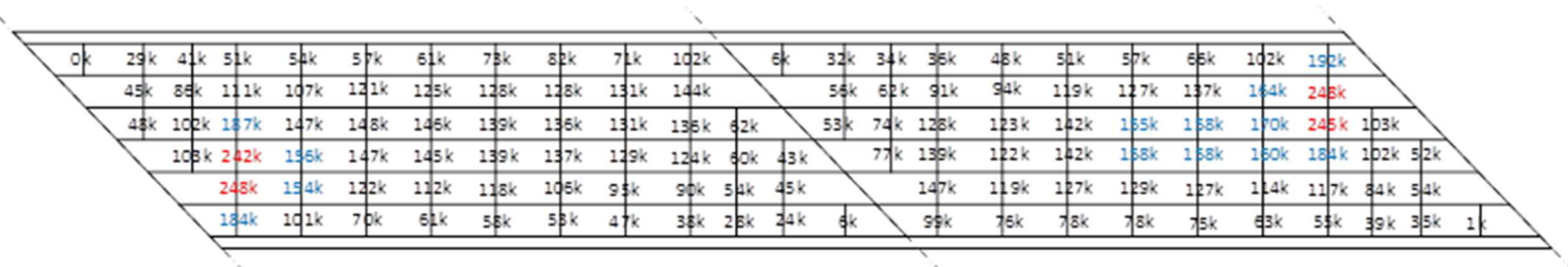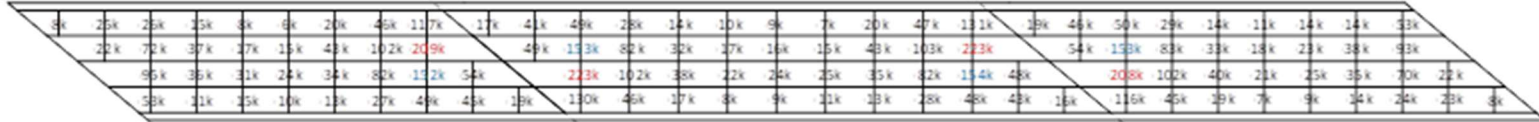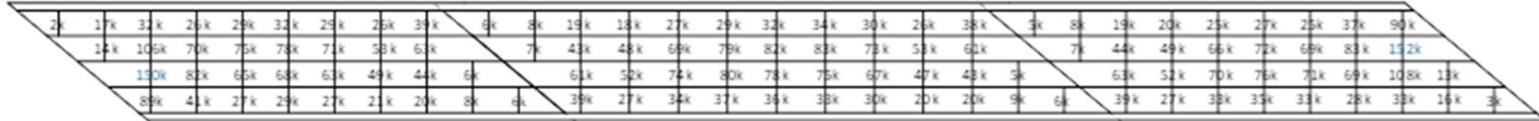aximum bottom chord force is 200 kips in the critical region. Additionally, consider the bottom chord size used in cross frames throughout the bridge in the analysis is a 6x6 angle that has a strength around 100 kips. Ideally, the next step in the analysis should be to identify the highly stressed bottom chord members and increase the member sizes to accommodate the design forces obtained from the first iteration of the analysis. This implies increasing the angle size in the critical regions to an 8x8 angle. The larger 8x8 angles are typically around 50% stiffer than 6x6 angles. The result of the next iteration in analysis would be an increase in the overall cross-frame forces. This introduces an element of iterative analysis until the member sizes utilized in the analysis have sufficient capacity for the forces obtained in the design. In this research, cross-frame member sizes used in 3D FEA models are either obtained from the structural drawings of existing bridges or newly designed for the bridges generated to fill observed gaps in the inventory. Several Category 2C bridges utilize members of insufficient capacity for the design forces in the critical regions obtained from the analyses. However, redesign and reanalysis of these bridges is outside the scope of the study, and as such, the results obtained by using cross-frame sizes from the structural drawings of bridges are used in developing recommendations.

Another aspect that has an influence, although minor, on Category 2C bridge behavior is the member sizes in cross frames in the noncritical regions. Figure 123 to Figure 130 indicate that the cross-frame forces in the noncritical regions are significantly lower than the critical regions. 3D FEA models of bridges in this research were developed by using the same cross-frame design for all intermediate cross frames throughout the bridge. In using these results, it was discovered that the members in the noncritical regions could be sized differently. Changing the size of the cross frames in the noncritical regions would ultimately influence the transverse stiffness of the bridge. Similar to the cross-frame sizes used in the critical regions, the revisions in cross-frame forces would ultimately depend on the relative change in stiffness in the member sizes used.

The discussion in the preceding paragraphs indicates that the transverse stiffness of a Category 2C bridge is sensitive to the cross-frame sizes used, especially in the critical regions. These aspects of the behavior of Category 2C bridges must be taken into consideration while sizing cross frames in Category 2C bridges. As such, the recommendations made in this research are based on a study of a limited number of bridges, with several bridges utilizing cross-frame members that do not have sufficient capacity in the critical regions. Additionally, cross-frame offsets in the critical regions influence the transverse stiffness in Category 2C bridges. Maximizing the offsets of cross frames in the critical regions should provide the most significant alleviation of transverse stiffness. Although a study of the influence of offsets was not a target of this research, it should nevertheless be a consideration in developing framing layouts for Category 2C bridges.

Figure 131 to Figure 133 show the recommended simple absolute bound estimates of the unfactored fatigue force range for the top chords, diagonals, and bottom chords of the intermediate cross frames in the Category 2C study bridges. Table 46 lists the maximum top chord, diagonal, and bottom chord fatigue force range values for the Category 2C bridges. It is proposed that these simple estimates are sufficient for designing these cross-frame members for fatigue.

Table 47 summarizes the recommended simple upper-bound estimates for the intermediate cross-frame member forces for the various specific unfactored load cases studied, and for the STR I load combination, for Category 2C bridges. Separate estimates are provided for simple-span and continuous-span bridges for the load cases of HL-93 live load and STR I. Furthermore, the table lists simple upper-bound estimates for

the cross-frame member unfactored fatigue force ranges predicted using the AASHTO (2020) 9th Edition LRFD provisions, prior to the adoption of the NCHRP 962 report recommendations, and using the AASHTO (2021) 10th Edition LRFD provisions based on the NCHRP recommendations. Regarding the fatigue force range estimates, it can be observed that the AASHTO 10th Edition provisions result in a 29 to 33 % reduction of the bounded force ranges calculated by the 3D FEA models. It should be noted that the AASHTO (2021) provisions specify the application of an additional factor of 0.65 to the calculated cross-frame member force ranges prior to applying the Fatigue I or Fatigue II load factors. Therefore, the net resulting reduction in the cross-frame member force ranges relative to the AASHTO 9th Edition provisions is a factor of 0.43 to 0.46 for these bridges.

Similar to the design philosophy for bearing-line cross frames of Category 1 bridges, Tables 48 and 49 present the corresponding recommended maximum bound estimates for unfactored forces due to skew effects (DC+DW+LL) and CDL load cases for the bearing-line cross frames at the abutments and at interior piers, respectively, for Category 2C bridges. The factored STR I force due to skew effects may be obtained by using a load factor of 1.6 from Table 26. Similarly, the estimate of unfactored forces due to skew effects may be used in other load combinations using the weighted average load factors in Table 26. Fatigue force ranges employing the procedures in AASHTO 10th Edition are smaller than 15 kips in all cases. Hence, fatigue force range checks may be neglected in bearing-lines cross frames at abutments and intermediate piers in Category 2C bridges.

Notably, the unfactored DC2, DW and HL-93 Live Load values in Table 47 may be grouped together and a single unfactored DC+DW+LL value may be employed with the weighted-average load factors from Table 26. The DC+DW+LL value may be estimated by dividing the STR I results in the table by 1.6.

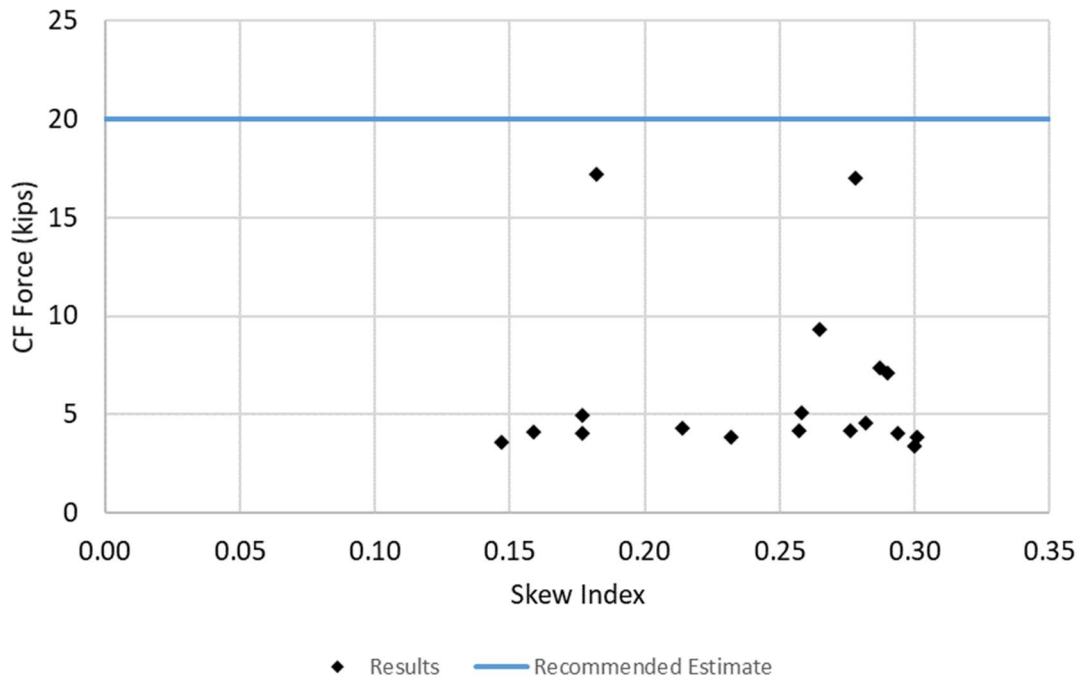Figure 131. Maximum fatigue force ranges, AASHTO 10th edition, in top chords of intermediate cross frames in Category 2C bridges.
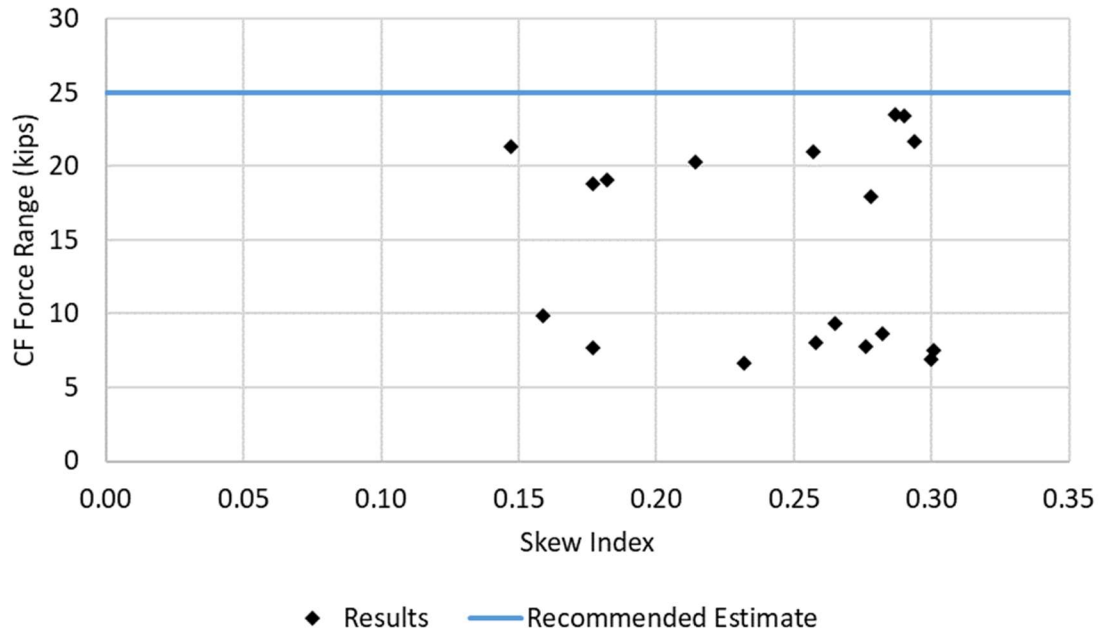
Figure 132. Maximum fatigue force ranges, AASHTO 10th edition, in diagonals of intermediate cross frames in Category 2C bridges.
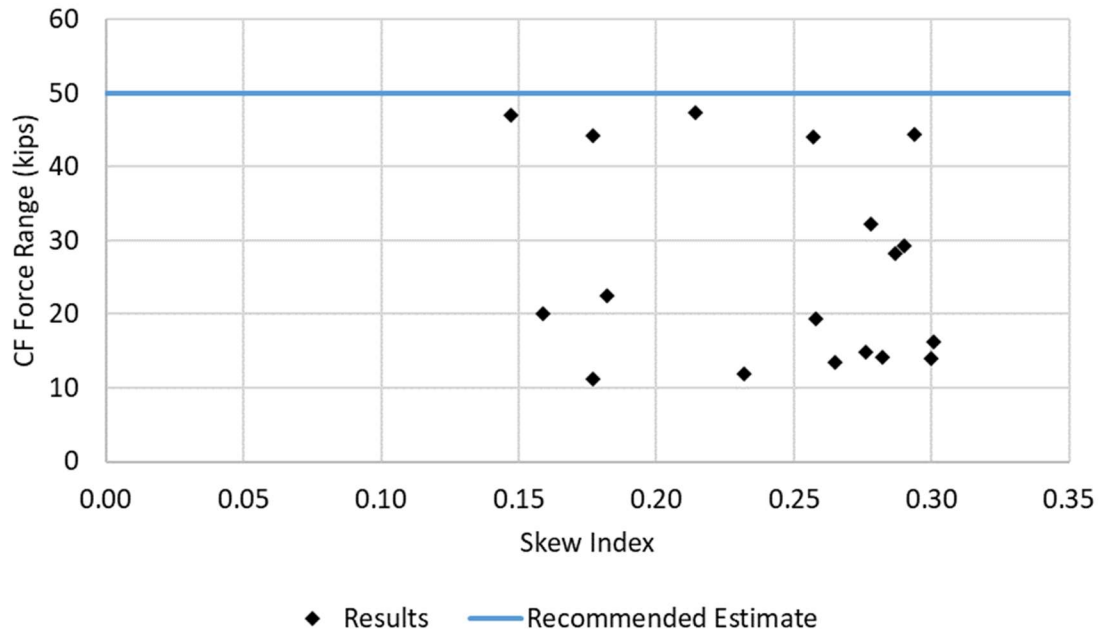
Figure 133. Maximum fatigue force ranges, AASHTO 10th edition, in bottom chords of intermediate cross frames in Category 2C bridges.

Table 46. Maximum fatigue top chord, diagonal and bottom chord force range for Category 2C bridges.

Bridge	Skew Index, I_s	Skew Angle, θ (deg.)	Top Chord Force Range (kip)	Diagonal Force Range (kip)	Bottom Chord Force Range (kip)
2C1-17	0.28	42	4	8	15
2C1-35	0.16	44	4	10	20
2C1-36	0.18	44	4	8	11
2C1-38	0.30	50	4	7	16
2C1-39	0.30	37	3	7	14
2C2-41	0.18	50	17	19	23
2C2-43	0.27	50	9	9	14
2C2-44	0.23	40	4	7	12
2C2-45	0.28	50	17	18	32
2C2-46	0.29	44	4	22	44
2C2-46B	0.26	40	4	21	44
2C2-46C	0.21	35	4	20	47
2C2-46D	0.18	30	5	19	44
2C2-46E	0.15	30	4	21	47
2C3-11	0.26	38	5	8	19
2C3-47	0.28	50	5	9	14
2C3-48	0.29	50	7	24	28
2C3-51	0.29	47	7	23	29

Table 47. Recommended force estimates for intermediate cross frames in Category 2C bridges.

Load Case	Top Chord (kips)	Diagonals (kips)	Bottom Chord (kips)
SDL, NLF	20	10	20
CDL	45	20	40
DC2	15	15	30
DW	3	3	5
HL-93 Live Load, Simple Span Bridges	20	40	70
HL-93 Live Load, Continuous-Span Bridges	60	80	140
STR I, Simple Span Bridges	40	70	120
STR I, Continuous-Span Bridges	100	180	$200 + 340\, I_s \leq 300$ for $I_s \geq 0.15$
Fatigue Range, AASHTO 9th Edition	30	40	70
Fatigue Range, AASHTO 10th Edition	20	25	50

Table 48. Recommended force estimates for bearing line cross frames at abutments in Category 2C bridges.

Load Case	Top Chord (kips)	Diagonals (kips)	Bottom Chord (kips)
CDL	5	4	5
DC+DW+LL	40	20	25

Table 49. Recommended force estimates for bearing line cross frames at intermediate piers in Category 2C bridges.

Load Case	Top Chord (kips)	Diagonals (kips)	Bottom Chord (kips)
CDL	10	10	7
DC+DW+LL	60	60	45

7.3.2.3 Category 2P Bridges

Figure 134 to Figure 136 show the maximum STR I member forces in the top chords, diagonals, and bottom chords of the intermediate cross frames of the six Category 2P Project BEB13 bridges as determined using 3D FEA. Table 50 to Table 52 list the maximum STR I tension and compression axial forces determined in the top chord, diagonal, and bottom chord cross-frame members from 3D FEA considering all the intermediate cross-frames of the six Category 2P bridges studied.

Similar to the Category 1 bridges, it is observed that simple absolute bounds on the forces in each of these types of cross-frame members should provide a sufficient force estimate that can be employed for design. Further, these simple estimates are less conservative than values obtained using the BE535 approach of estimating cross-frame chord-level connection forces as a percentage of girder maximum moments and shears. However, the estimates for the Category 2P bridges are generally larger than those determined for the Category 1 bridges.

In addition, Figure 137 to Figure 139 show the unfactored force ranges calculated in the cross-frame members using the new AASHTO (2021) 10th Edition recommendations based on NCHRP Report 962 (Reichenbach et al. 2021). It was determined that these force ranges also could be represented by simple absolute estimates of the bounds on the forces determined from the 3D FEA solutions.

Table 53 summarizes the recommended simple upper-bound estimates for the intermediate cross-frame member forces for the various specific unfactored load cases studied, and for the STR I load combination, for Category 2P bridges. Furthermore, the table lists simple upper-bound estimates for the cross-frame member unfactored fatigue force ranges predicted using the AASHTO (2020) 9th Edition LRFD provisions, prior to the adoption of the NCHRP 962 report recommendations, and using the AASHTO (2021) 10th Edition LRFD provisions based on the NCHRP recommendations. Regarding the fatigue force range estimates, it can be observed that the AASHTO 10th Edition provisions result in a 25 to 40 % reduction of the bounded force ranges calculated by the 3D FEA models. It should be noted that the AASHTO (2021) provisions specify the application of an additional factor of 0.65 to the calculated cross-frame member force ranges prior to applying the Fatigue I or Fatigue II load factors. Therefore, the net resulting reduction in the cross-frame member force ranges relative to the AASHTO 9th Edition provisions is a factor of 0.39 to 0.49 for these bridges.

173

Table 54 and Table 55 present the corresponding recommended maximum bound estimates for unfactored forces due to skew effects (DC+DW+LL) and CDL load cases for the bearing-line cross frames at the abutments and at interior piers respectively in Category 2P bridges The factored STR I force due to skew effects may be obtained by using a load factor of 1.6 from Table 26. Similarly, the estimate of unfactored forces due to skew effects may be used in other load combinations using the weighted average load factors in Table 26. Fatigue force ranges employing the procedures in AASHTO 10th Edition are smaller than 15 kips in all cases. Hence, fatigue force range checks may be neglected in bearing-lines cross frames at abutments and intermediate piers in Category 2P bridges.

Notably, the unfactored DC2, DW and HL-93 Live Load values in Table 53 may be grouped together and a single unfactored DC+DW+LL value may be employed with the weighted-average load factors from Table 26. The DC+DW+LL value may be estimated by dividing the STR I results in the table by 1.6.

Figure 134. Maximum STR I forces in top chords of intermediate cross frames in Category 2P bridges.
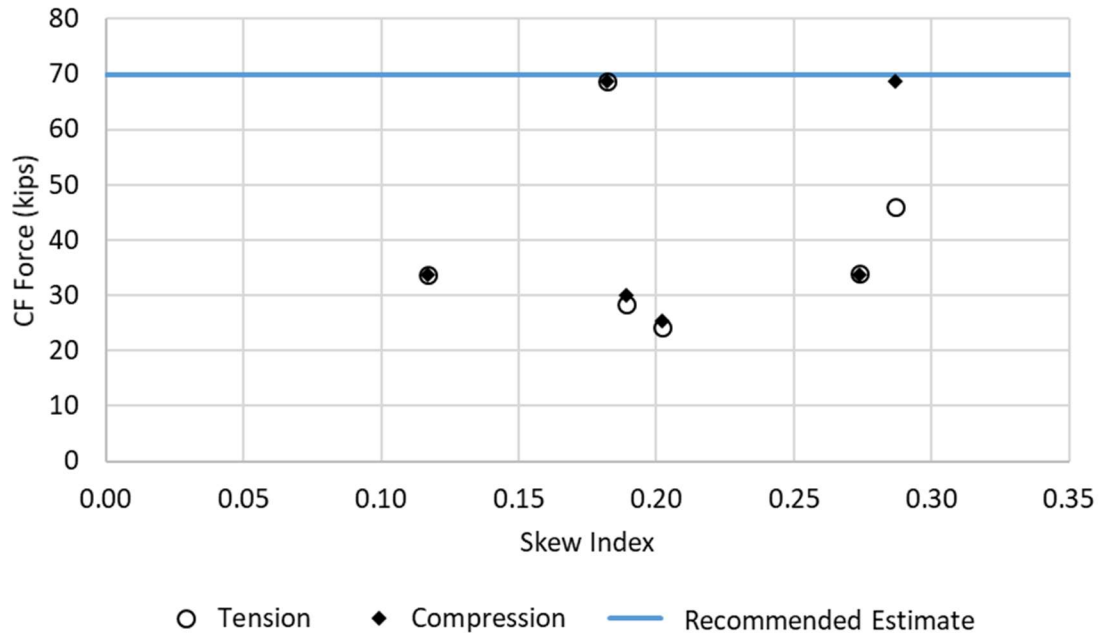
Figure 135. Maximum STR I forces in diagonals of intermediate cross frames in Category 2P bridges.

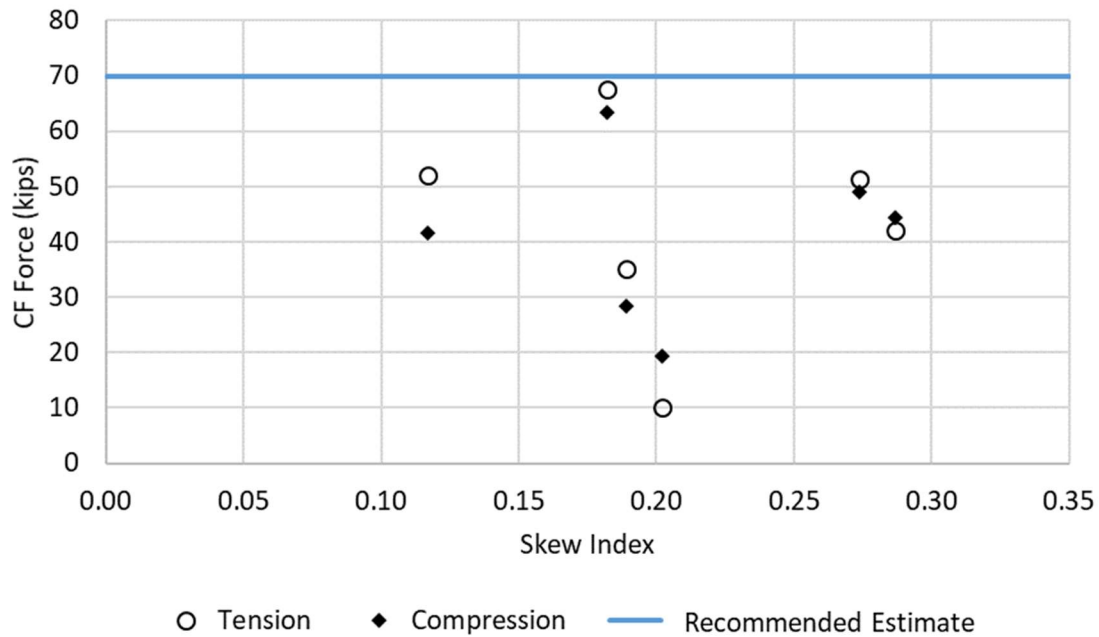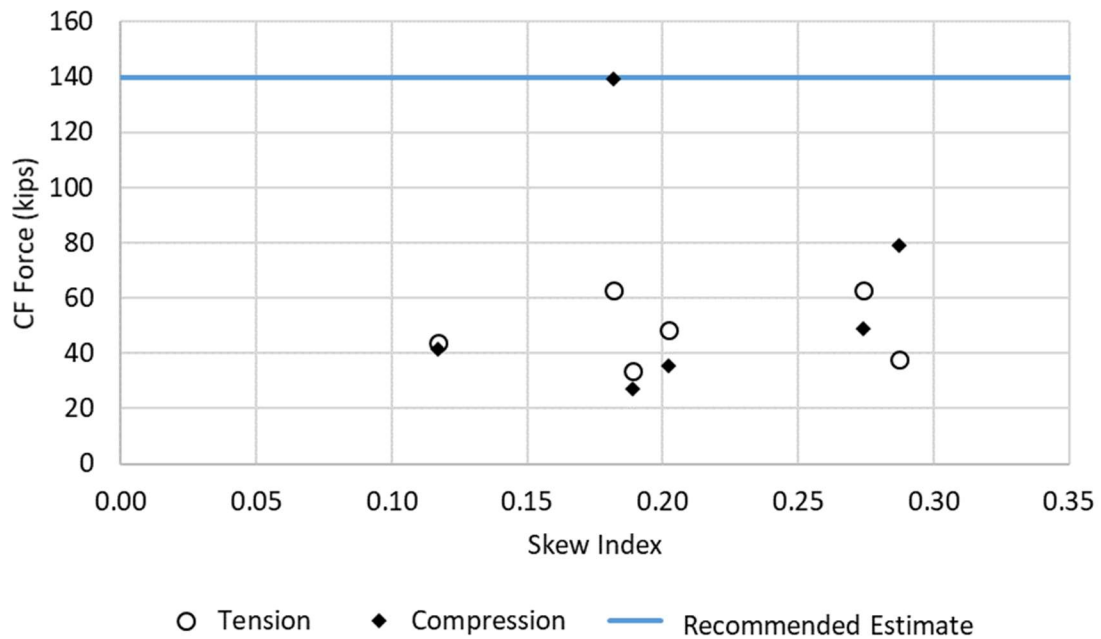**Figure 136. Maximum STR I forces in bottom chords of intermediate cross frames in Category 2P bridges.**
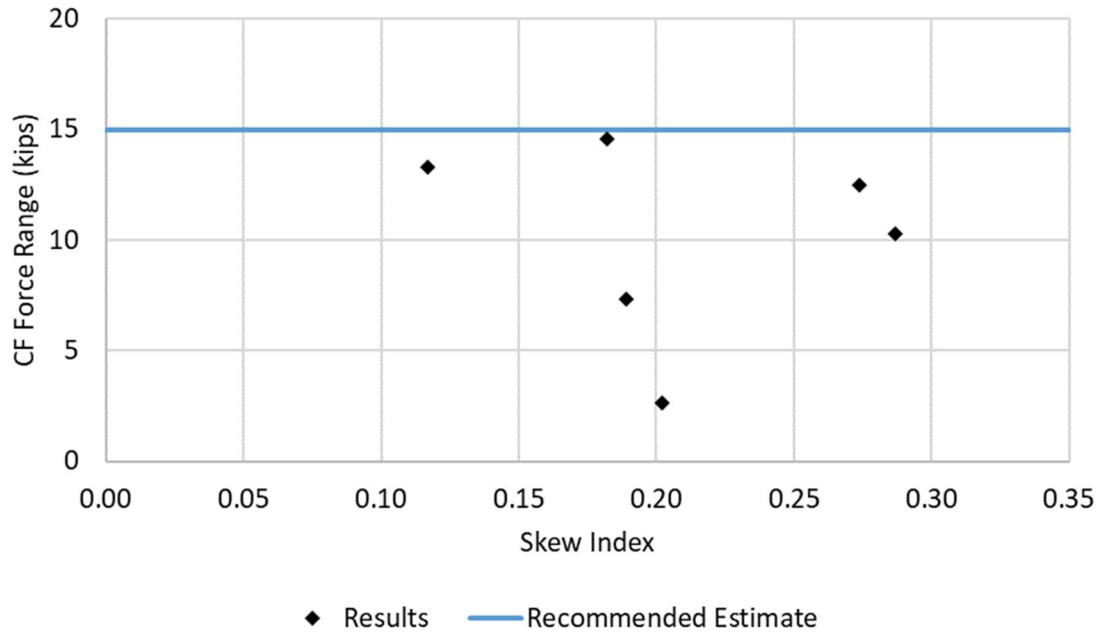
Figure 137. Maximum fatigue force ranges, AASHTO 10th edition, in top chords of intermediate cross frames in Category 2P bridges.
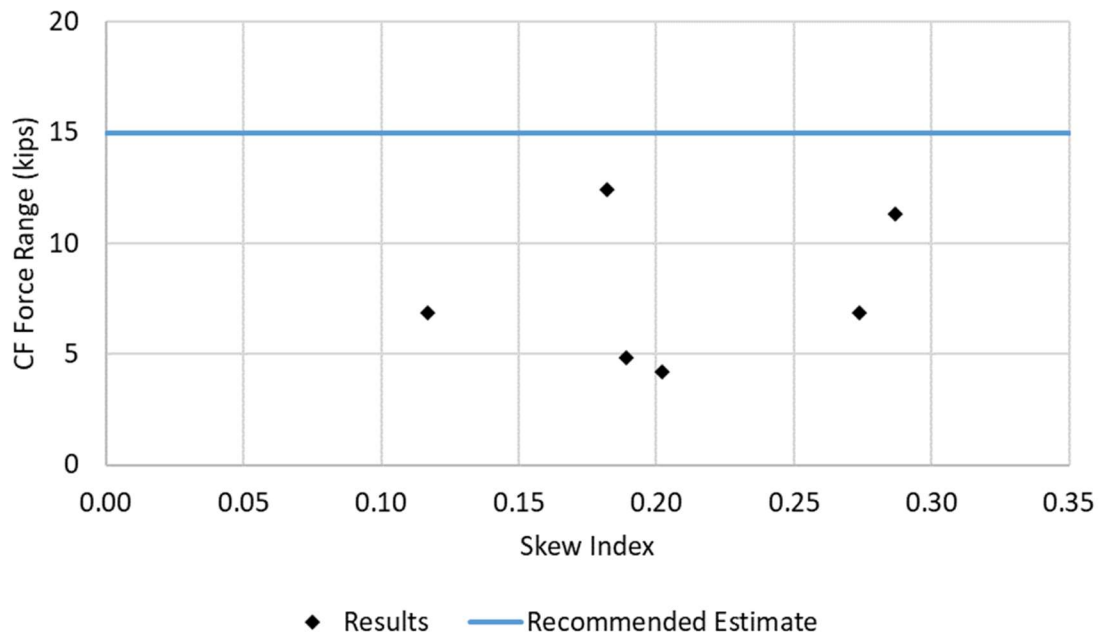
Figure 138. Maximum fatigue force ranges, AASHTO 10th edition, in diagonals of intermediate cross frames in Category 2P bridges.
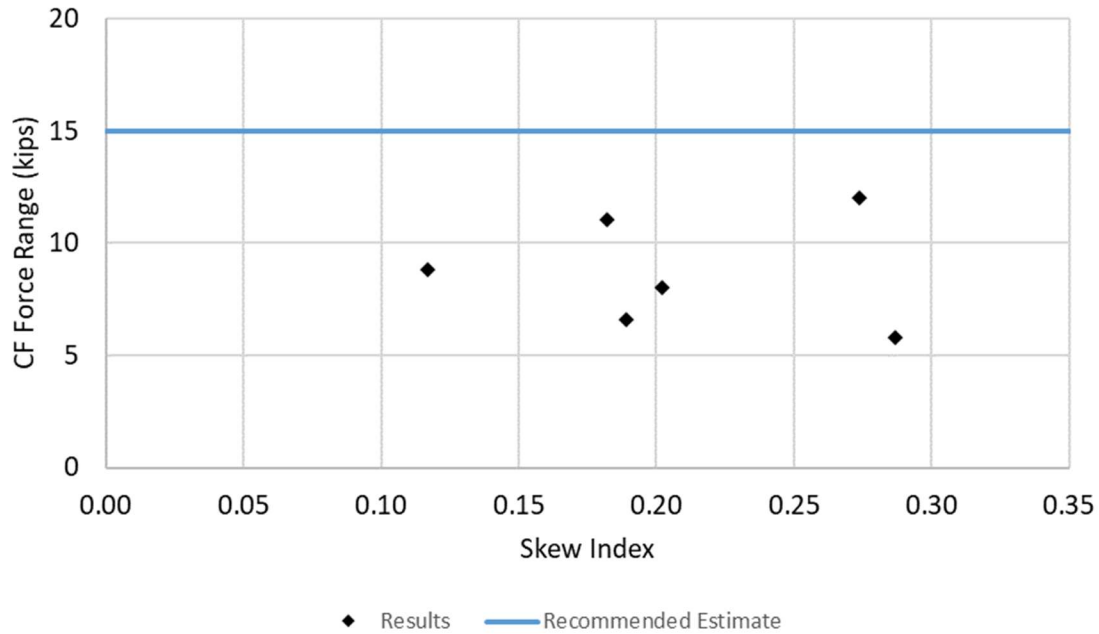
Figure 139. Maximum fatigue force ranges, AASHTO 10th edition, in bottom chords of intermediate cross frames in Category 2P bridges.

Table 50. Maximum STR I tension and compression top chord forces for Category 2P bridges.

Bridge	Skew Index, I_s	Skew Angle, θ (deg.)	STR I Max Tension (kip)	STR I Max Compression (kip)
2P1-18	0.28	42	10	19
2P1-37	0.16	44	35	28
2P2-8	0.18	44	51	49
2P2-40	0.30	50	52	42
2P2-42	0.30	37	68	63
2P3-49	0.18	50	42	45

Table 51. Maximum STR I tension and compression diagonal forces for Category 2P bridges.

Bridge	Skew Index, I_s	Skew Angle, θ (deg.)	STR I Max Tension (kip)	STR I Max Compression (kip)
2P1-18	0.28	42	24	25
2P1-37	0.16	44	28	30
2P2-8	0.18	44	34	34
2P2-40	0.30	50	34	34
2P2-42	0.30	37	69	69
2P3-49	0.18	50	46	69

Table 52. Maximum STR I tension and compression bottom chord forces for Category 2P bridges.

Bridge	Skew Index, I_s	Skew Angle, θ (deg.)	STR I Max Tension (kip)	STR I Max Compression (kip)
2P1-18	0.28	42	49	35
2P1-37	0.16	44	34	27
2P2-8	0.18	44	63	49
2P2-40	0.30	50	44	41
2P2-42	0.30	37	63	140
2P3-49	0.18	50	38	79

Table 53. Recommended force estimates for intermediate cross frames in Category 2P bridges.

Load Case	Top Chord (kips)	Diagonals (kips)	Bottom Chord (kips)
SDL, NLF	10	5	7
CDL	20	15	20
DC2	15	10	15
DW	2	2	3
HL-93 Live Load	40	35	60
STR I	70	70	140
Fatigue Range, AASHTO 9th Edition	25	20	25
Fatigue Range, AASHTO 10th Edition	15	15	15

Table 54. Recommended force estimates for bearing line cross frames at abutments in Category 2P bridges.

Load Case	Top Chord (kips)	Diagonals (kips)	Bottom Chord (kips)
CDL	4	3	3
DC+DW+LL	20	15	7

Table 55. Recommended force estimates for bearing line cross frames at intermediate piers in Category 2P bridges.

Load Case	Top Chord (kips)	Diagonals (kips)	Bottom Chord (kips)
CDL	7	5	4
DC+DW+LL	40	40	35

8. CONCLUSIONS

8.1   Satisfaction of Research Objectives

The objectives of this research are to (1) confirm the recommended LGA-based design guidance developed in Project BE535 holds true for a larger sample size of bridges and (2) recommend any needed refinements to the procedures based on the larger sample size of bridges.

To achieve these objectives, a parametric study was conducted for 35 bridges canvasing a wide range of characteristics of skewed steel I-girder bridges designed in Florida. Emphasis was given to bridges with geometric characteristics that fit within the boundaries of the Categories 1 and 2 identified by Project BE535 as being amenable to design by LGA. In particular, the studies focused predominantly on four-, five-, and six-girder bridges and contiguous and parallel stagger cross-frame framing arrangements. The selected parametric study bridges were divided into three groups:

- Category 1, corresponding to the Category 1 recommendations in Project BE535: bridges with parallel bearing lines and skew angle $\theta \leq 20°$, having contiguous cross-frame lines that are turned parallel to the skew;
- Category 2C, corresponding to the Category 2 recommendations in Project BE535: bridges with parallel bearing lines, $\theta \leq 50°$, and with a skew index $I_s \leq 0.3$, but specifically having contiguous cross-frame lines that are oriented perpendicular to the girders; and
- Category 2P, also corresponding to the Category 2 recommendations in Project BE535: bridges with $\theta \leq 50°$ and with a skew index $I_s \leq 0.3$, but specifically having a parallel stagger cross-frame framing arrangement (i.e., discontinuous lines of cross frames oriented with a selected work point on each of the cross frames positioned along a line parallel to the bearing lines).

The results from the research are presented in two chapters. The applicability of LGA is assessed through comparison of its responses with 3D FEA responses in Chapter 6, while the development of estimates for 3D responses are addressed in Chapter 7.

Some of the essential qualitative aspects pertaining to the behavior of straight skewed bridges and application of LGA-based procedures are as follows:

1. The variations in LLDFs obtained by the application of AASHTO Article 4.6.2.2 by extending the range of applicability by 25% on $L_{s,max}$ and 75% on K_g are similar in nature to the LLDFs obtained for bridges that fall within the range of applicability. In other words, the conservatism or unconservatism associated with the LLDF estimates is similar regardless of satisfaction or violation of the range of applicability of the AASHTO Article 4.6.2.2 procedures within the above-stated limits.
2. The STR I positive and negative bending moments predicted by LGA are within the suggested maximum limit of 5% of 3D FEA solutions. STR I shear forces are within 7% of the 3D FEA solutions in all cases. The SER II solutions have similar trends. Hence, it can be concluded that the LGA-based procedures produce acceptable solutions for girder bending moment and vertical shear forces.
3. 3D FEA TDL (SDLF) girder vertical displacements tend to be larger than corresponding LGA displacements in most of the bridge girders evaluated in this study. This is due to the subtleties associated with the application on dead load in LGA and 3D FEA. However, the magnitude of the difference between the 3D FEA and LGA displacements is small in each case. As such, the LGA solutions for vertical displacements are also acceptable for the bridges studied.

4. Three-dimensional skew effects tend to increase the load transferred to obtuse corners in straight skewed bridge spans. LGA solutions are fundamentally unable to capture this effect short of the application of skew correction factors; however, the present skew correction factors appear to be inadequate, particularly in Category 2C bridges. This is reflected in the unconservative LGA solution of HL-93 live load vertical shear forces at obtuse corners of spans. This unconservatism is in spite of the application of the AASHTO Article 4.6.2.2.3c skew correction factors for shear. The maximum differences are observed in Category 2C bridges. However, the unconservatism associated with the HL-93 live load does not significantly impact the STR I and SER II vertical shear force estimates. This is because the assumption of equal distribution of dead load to all girders in LGA provides sufficient compensation to produce acceptable STR I and SER II solutions for the bridges studied in this research.

5. Fatigue live load shear force range estimates were found to be highly unconservative for Category 2C bridges. LGA solutions for Category 2C bridges do not produce acceptable estimates for fatigue shear force ranges.

6. The AASHTO Article 4.6.2.2 provisions for LLDFs were evaluated in detail considering empirical equations, the lever rule, and RCA separately. It was found that the empirical equations are not formulated to handle skew considerations, including the skew correction factor for Category 2C bridges. RCA calculations are observed to govern for bridges that have relatively large span-to-width ratios. However, the improvements obtained from RCA calculations for the bridges studied in this research were marginal at best.

7. Optional girder live load deflection calculations perform better relative to 3D FEA solutions by applying the AASHTO Article 4.6.2.2 moment LLDFs.

8. This research provides additional evidence to support the finding from Project BE535 that the cross-frame framing arrangement significantly influences the behavior of straight skewed I-girder bridges. Transverse load path effects were found to be more prominent in Category 2C bridges. Category 2P bridges mitigate the transverse load path effects to an extent, however, at the expense of larger girder flange lateral bending stresses. The transverse stiffness in Category 2C bridges is sensitive to the cross-frame sizes and offsets selected near the obtuse corners of the spans.

8.2   Recommendations for Implementation

Given the findings from this research and Project BE535, it is evident that LGA can be utilized as a sufficient tool for design of straight skewed I-girder bridges belonging to Categories 1, 2C, and 2P. This research has further refined guidelines for estimation of cross-frame forces and flange lateral bending stresses for bridges belonging to Categories 1, 2C, and 2P. Therefore, it is recommended that the FDOT (2022a) Structures Design Guidelines may be modified to extend the allowable use of LGA within these limits.

8.3   Recommendations for Future Research

Projects BEB13, BED03 and BE535 have provided ample insight into the behavior of straight skewed I-girder bridges. However, there are a number of related research thrusts that may benefit from additional focused research studies. A few of them are listed below:

- The accuracy of LGA-based procedures with respect to 3D FEA solutions depend on the assumptions of dead load distribution within girders in the skewed bridge. Equal dead load distribution to the girders is a poor approximation when it comes to line-type concentrated loads along the bridge length (e.g., barrier rails, walls, sidewalks, etc.). A targeted research study should make it feasible to develop a reasonable simplified approximate analysis model for the distribution of these types of loads. Such a

model can potentially extend the limits of LGA to a more complete range of situations, as long as the magnitudes of these loads are not large enough to require significantly different sizes and stiffnesses for the girders within the vicinity of these loads.

- The current research findings show that the AASHTO 4.6.2.2 provisions for calculation of LLDFs results in inadequate estimates in many cases. Additionally, a disconnect exists in the philosophy of calculation of LLDFs for exterior and interior girders. Improvements in empirical equations for estimation of single-lane distribution factors and skew correction factors are especially required. Furthermore, it is likely necessary to consider the cross-frame framing arrangement while formulating improvements or refinements to the distribution factor equations.

- It is clear that the cross-frame framing arrangement heavily influences the behavior of straight skewed I-girder bridges. Specifically, additional studies should be conducted considering the cross-frame framing arrangement as a parameter. There is tremendous value in investigating variations of contiguous, staggered, and lean-on framing arrangements and the suitability of each in the context of straight skewed I-girder bridges. It is envisioned that certain framing arrangements will be more suitable for certain bridge geometries. A research study that specifically focuses on the framing arrangement as a parameter has the potential to formulate insights into the behavior of each framing arrangement and further elevate the framing arrangement as a design variable.

- The bottom flange lateral bending stresses were shown to be particularly large in the evaluation of the six Category 2P bridges in this research. In continuous-span bridges, the flange lateral bending stresses were found to be comparable near abutments and intermediate piers. However, the flange lateral bending moments were observed to be significantly larger near intermediate piers (as much as 10 times larger in one case) compared to those near abutments. This was because the size of the bottom flange near abutments is much smaller than at the intermediate piers. This indicates a potential sensitivity of flange lateral bending stress estimates to the size of the flanges utilized. The influence of variation of flange sizes on the flange lateral bending moments and subsequently flange lateral bending stresses needs to be studied. The findings from this study can potentially refine LGA-based design guidance established in this research for Category 2P bridges.

- The extension of Category 1 type designs to skew angles larger than 20° should be considered, both with and without the use of continuous cross-frame framing arrangements. One of the considerations that may be a limiting factor on the skew angles with some traditional connection details to the girders is the fact that the fatigue performance of these details may degrade with increases in the skew angle. This consideration relates to the fatigue performance of transversely-welded versus longitudinally-welded attachments, such as in Sections 4.1 and 6.1 of Table 6.6.1.2.3-1 of AASHTO (2020). The use of split-pipe stiffeners for the connection of skewed cross-frames, as investigated by Quadrato (2010), may be a very beneficial solution that avoids these issues. It is important to avoid bent-plate type details for intermediate cross-frames that may soften the cross-frame stiffnesses such that geometry control of the bridge is lost during construction.

- In all the 3D FEA studies conducted in this research, the bearings were assumed to be designed and detailed such that bearing horizontal forces are negligible under gravity loads. Particularly as skewed geometries become more severe, the design of bearing details to allow for minor lateral displacements under gravity loads (via tolerances, etc.) while providing for sufficient lateral restraint under extreme loads becomes more difficult. These aspects of the bearing design details, such as captured within AASHTO/NSBA (2004) need to be better understood.

REFERENCES

AASHTO/NSBA (2004). *Steel Bridge Bearing Design and Detailing Guidelines*, G9.1, AASHTO/NSBA Steel Bridge Collaboration, American Association of State Highway and Transportation Officials, Washington, D.C. and National Steel Bridge Alliance, Chicago, IL.

AASHTO (2021). *AASHTO LRFD Bridge Design Specifications*, 10th Edition approved ballot items, American Association of State Highway and Transportation Officials, Washington, DC.

AASHTO (2020). *AASHTO LRFD Bridge Design Specifications*, 9th Edition, American Association of State Highway and Transportation Officials, Washington, DC.

AASHTO (2014). *AASHTO LRFD Bridge Design Specifications*, 7th Edition, American Association of State Highway and Transportation Officials, Washington, DC.

AASHTO (2002). *Standard Specifications for Highway Bridges*, 17th Edition, American Association of State Highway and Transportation Officials, Washington, DC.

AISC (2022). *Specification for Structural Steel Buildings*, ANSI/AISC 360-22, American Institute of Steel Construction, Chicago, IL.

AISC (2016). *Specification for Structural Steel Buildings*, ANSI/AISC 360-16, American Institute of Steel Construction, Chicago, IL.

AISC (2010). *Specification for Structural Steel Buildings*, ANSI/AISC 360-10, American Institute of Steel Construction, Chicago, IL.

AWS (2020). *AWS D1.5 Bridge Welding Code*, American Welding Society, Miami, FL.

CSi (2022). CSiBridge Advanced w/Rating, Version 24.0.0, Computers and Structures, Inc., Berkeley, CA.

FDOT (2022a). "Structures Design Guidelines," *Structures Manual*, Volume 1, Florida Department of Transportation, Tallahassee, FL.

FDOT (2022b). *Standard Specifications for Road and Bridge Construction*, Florida Department of Transportation, Tallahassee, FL.

FDOT (2021). "Applicability of Approximate Methods of Analysis for Skewed Straight Steel I-Girder Bridges," DOT-RFP-21-9028-SD, Request for Proposal, Florida Department of Transportation, Tallahassee, FL.

FDOT (2018). "Simplified Method to Determine Girder Layover at Simply Supported Girder Ends," private communication from the project steering group, Florida Department of Transportation, Tallahassee, FL.

Grubb, M.A., Hall, D.H., Yadlosky, J.M., Wilson, K.E. and Volle, L.E. (2010). *Analysis and Design of Skewed and Curved Steel Bridges with LRFD – Reference Manual*, NHI Course No. 130081, 130081A, and 130081B, Publication No. FHWA-NHI-15-047, National Highway Institute, Federal Highway Administration.

HDR (1993). "AASHTO Springs for New Live Load Distribution, Old Wheel Fractions Hang in the Balance," *HDR Bridgeline*, Vol. 3, No. 2, January.

Modjeski and Masters (2015). *Bridges for Service Life Beyond 100 Years: Service Limit State Design*, SHRP 2 Report S2-R19B-RW-1, Transportation Research Board, National Research Council, Washington, DC.

NSBA (2015). *Continuous Span Standards V1.1*, National Steel Bridge Alliance, Chicago, IL.

NSBA (2021). LRFD Simon, Version 10.4.0.0 (AASHTO 9th Edition), National Steel Bridge Alliance, Chicago, IL.

Quadrato, C.E. (2010). *Stability of Skewed I-Shaped Girder Bridges Using Bent Plate Connections*, Ph.D. dissertation, University of Texas at Austin, Austin, TX.

Reichenbach, M., White, J., Park, S. Zecchin, E., More, M. Liu, Y. Liang, C., Kövesdi, B. Helwig, T., Engelhardt, M., Connor, R. and Grubb, M. (2021). *Proposed Modification to AASHTO Cross-Frame Analysis and Design*, NCHRP Report 962, Transportation Research Board, National Research Council, Washington, D.C.

Su, D., Brown, J., Suksawang, N., (2022). *Evaluate Effects from Shored Construction on Steel Composite Bridges.*, Project BE929 Report, Florida Department of Transportation, Tallahassee, FL.

White, D., Kamath, A., Heath, J.A., Adams, B.K., Anand, A. (2020). *Straight Steel I-Girder Bridges with Skew Index Approaching 0.3.*, Project BE535 Report, Florida Department of Transportation, Tallahassee, FL.

White, D.W., Nguyen, T.V., Coletti, D.A., Chavel, B.W., Grubb, M.A., and Boring, C.G. (2015). *Guidelines for Reliable Fit-Up of Steel I-Girder Bridges*, NCHRP 20-07/Task 355, Transportation Research Board, National Research Council, Washington, D.C.

White, D.W., Coletti, D., Chavel, B.W., Sanchez, A., Ozgur, C., Jimenez Chong, J.M., Leon, R.T., Medlock, R.D., Cisneros, R.A., Galambos, T.V., Yadlosky, J.M., Gatti, W.J., and Kowatch, G.T. (2012). *Guidelines for Analytical Methods and Construction Engineering of Curved and Skewed Steel Girder Bridges*, NCHRP Report 725, Transportation Research Board, National Research Council, Washington, D.C.

Yura, J.A. (2001). "Fundamentals of Beam Bracing," *Engineering Journal*, AISC, 38(1), 11-26.

Zokaie, T., Osterkamp, T.A., Imbsen, R.A., (1991). *Distribution of Wheel Loads on Highway Bridges*, NCHRP Report 12-26, Transportation Research Board, National Research Council, Washington, D.C.

APPENDIX A.   ALTERNATIVE LIVE LOAD DISTRIBUTION FACTOR CALCULATIONS EMPLOYED BY LRFD SIMON FOR BRIDGES VIOLATING THE AASHTO ARTICLE 4.6.2.2 LIMITS

Section 6.8 explains that a number of the parametric study bridges considered in this research violate one or both of the following AASHTO limits:

- Maximum span length, $L_{s,max}$, less than or equal to 240 ft
- Girder longitudinal stiffness parameter, K_g, less than or equal to 7 x 10^6 in.[4]

An alternative LLDF procedure is implemented by Simon when the range of applicability of the AASHTO provisions is exceeded. This Appendix summarizes the alternative SIMON LLDF calculations.

Multiple-Lane Exterior-Girder Moment LLDFs

For the multiple-lane exterior-girder moment LLDFs, Simon employs what it refers to as the lever rule. However, Simon implements the lever rule in a different and more generalized way than the basic lever rule applied to the exterior girders in the AASHTO provisions. The resulting procedure is referred to in this appendix as the *Simon lever rule*. For the Simon lever rule, Simon takes the LLDF for the exterior girders as the larger of:

1) The two-lane *Simon lever rule* LLDF from the interior girders, multiplied by *e*, and
2) The single-lane lever rule (as defined in AASHTO Article C4.6.2.2.1) on the exterior girder.

The single- and two-lane lever rule calculations employed by Simon are discussed below. It should be emphasized that the first calculation in the above list is a specific implementation defined only by Simon.

In addition, it should be noted that Simon does not apply any RCA in bridges where the applicability of the AASHTO provisions is exceeded.

Multiple-Lane Interior-Girder Moment LLDFs

For the multiple-lane interior-girder moment LLDFs, Simon employs the *Simon lever rule*. In this case, Simon takes the LLDF for the interior girders as the value obtained from the two-lane *Simon lever rule* (discussed below) applied to the interior girders.

Single-Lane Exterior-Girder Fatigue Moment LLDFs

For the single-lane exterior-girder fatigue moment LLDFs, Simon performs the calculation simply as the single-lane lever rule (as defined in AASTHO Article C4.6.2.2.1) on the exterior girder.

As noted above, Simon does not apply any RCA in cases where the applicability of the AASHTO provisions is exceeded.

Single-Lane Interior-Girder Moment LLDFs

For the single-lane interior girder fatigue moment LLDFs, Simon calculates the single-lane LLDF simply as the single-lane *Simon lever rule* calculation on the interior girders (discussed below).

As noted in Section 6.8.1 AASHTO Article 4.6.2.2.2e defines a reduction factor that can be applied to its calculated moment LLDFs to account for the effects of skew. This factor is not applied in the Simon programmed LLDF procedures.

<u>Shear LLDFs, Multiple- and Single-Lane on Exterior and Interior girders</u>

For the shear LLDFs, the LRFD Simon rules for bridges that violate the limits of the AASHTO provisions follow the above outline for the moment LLDFs.

In bridges where the range of applicability of the AASHTO provisions is exceeded, Simon does not apply any skew correction to the results of any of its calculations.

<u>Multiple Presence</u>

Whenever any LLDF calculations are applied and "a sketch is required to determine the load distribution" as stated in AASHTO (2020) Article 3.6.1.1.2, a multiple presence factor is applied to the results of the calculations (i.e., 1.2 for a single lane, 1.0 for two lanes, 0.85 for three lanes, and 0.65 for four or more lanes). Since the *Simon lever rule* involves a sketch of the form indicated above, Simon applies multiple presence factors to its results.

<u>Lever Rule Calculations Employed by Simon (i.e, the *Simon level rule*)</u>

The single-lane lever rule calculation specified by the AASHTO Article 4.6.2.2 for the exterior girders is relatively well known but is stated here for completeness. Figure A-1 shows the statical model for the single-lane lever rule for the exterior girders. The deck is supported by the exterior girder and the first interior girder. A frictionless hinge is assumed in the deck over the first interior girder. Summing moments about the first interior girder, one obtains

$$Rs = 0.5P(s + d_e - 2') + 0.5P(s + d_e - 8')$$

Solving for R, one obtains

$$R = P(1 + d_e/s - 5'/s)$$

where P is the truck axle load, $0.5P$ are the truck wheel loads, d_e is the distance from the curb or rail to the centerline of the exterior girder in ft, and s is the girder spacing in ft. The expression within the parentheses is the corresponding exterior girder LLDF. This illustration assumes that $d_e + s$ is greater than $2' + 6' = 8'$.
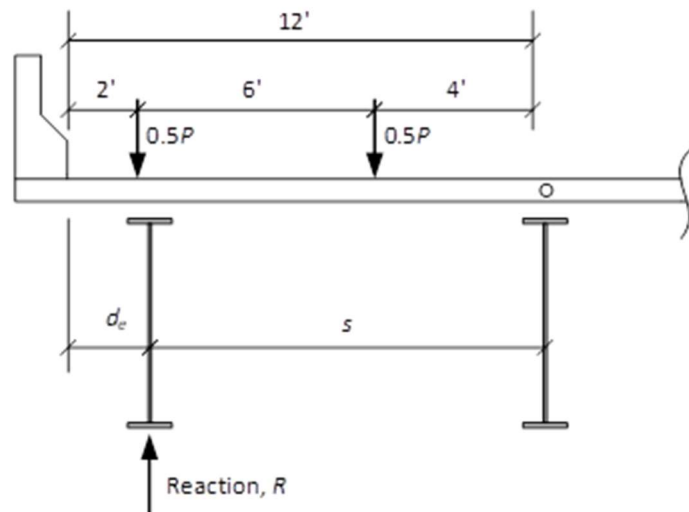

Figure 140. Statical model for the single-lane lever rule calculation per AASHTO Article C4.6.2.2.1 on the exterior girders.

185

The single-lane *Simon lever rule* calculation for the interior girders is similar, employing the statical model shown in Figure A-2. A frictionless hinge is assumed over the top of each girder within the deck. Summing the moment about the right-hand girder in the sketch, one obtains

$$Rs = 0.5Ps + 0.5P(s-6')$$

which gives

$$R = P(1 - 3'/s)$$

The expression within the parentheses is the corresponding LLDF. It should be noted that the same LLDF expression applies if the truck is placed anywhere between the position shown and the position with the right-hand wheel located over the top of the girder for which the reaction is being obtained. It is assumed that the girder spacing s is greater than 6 ft in this illustration.
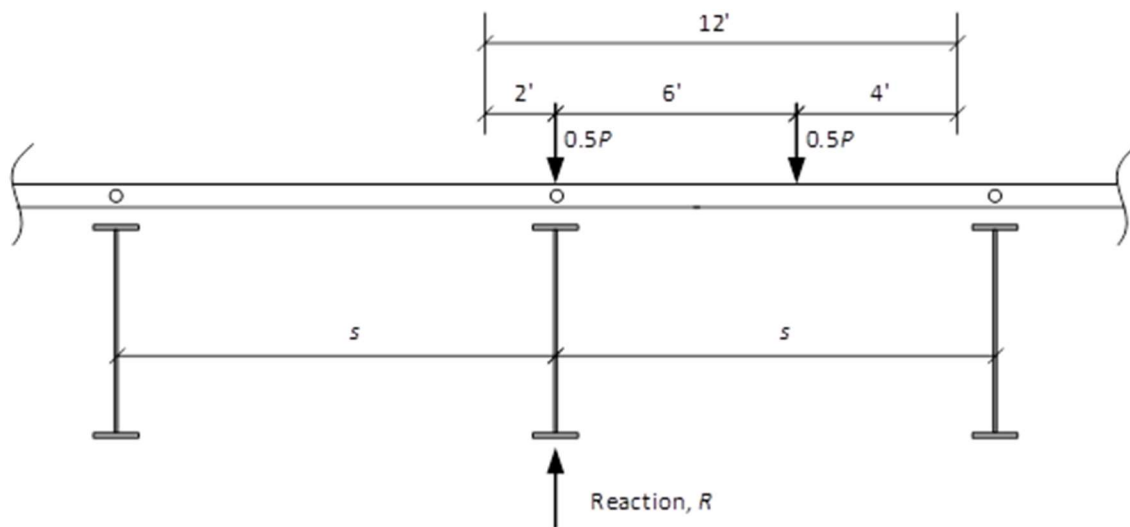

Figure 141. Statical model for the single-lane *Simon lever rule* calculation on the interior girders.

The two-lane lever rule utilized by Simon, i.e., the *Simon lever rule*, for the calculation of multiple-lane LLDFs on the interior girders is generated using the statical model shown in Figure A-3. The moment equation for the bay on the right-hand side of the girder under consideration is

$$Rs = 0.5P(s-8') + 0.5P(s-2')$$

which gives

$$R = P(1 - 5'/s)$$

as an intermediate result. The moment equation for the bay on the left-hand side of the girder gives the same result. Summing the two contributions to the reaction at the girder under consideration, we obtain

$$R = P(2 - 10'/s)$$

The expression within the parentheses is the corresponding LLDF employed for the two-lane *Simon lever rule*. It is assumed that the girder spacing s is greater than 8' in this calculation. The two trucks can be shifted to the left or right by up to 2' and the same equation applies, assuming $s < 10'$.

As explained previously, Simon calculates a "two-lane lever rule" LLDF for moment and shear by applying the *e* parameter from AASHTO Article 4.6.2.2.2d to the two-lane lever rule result for the interior girders.
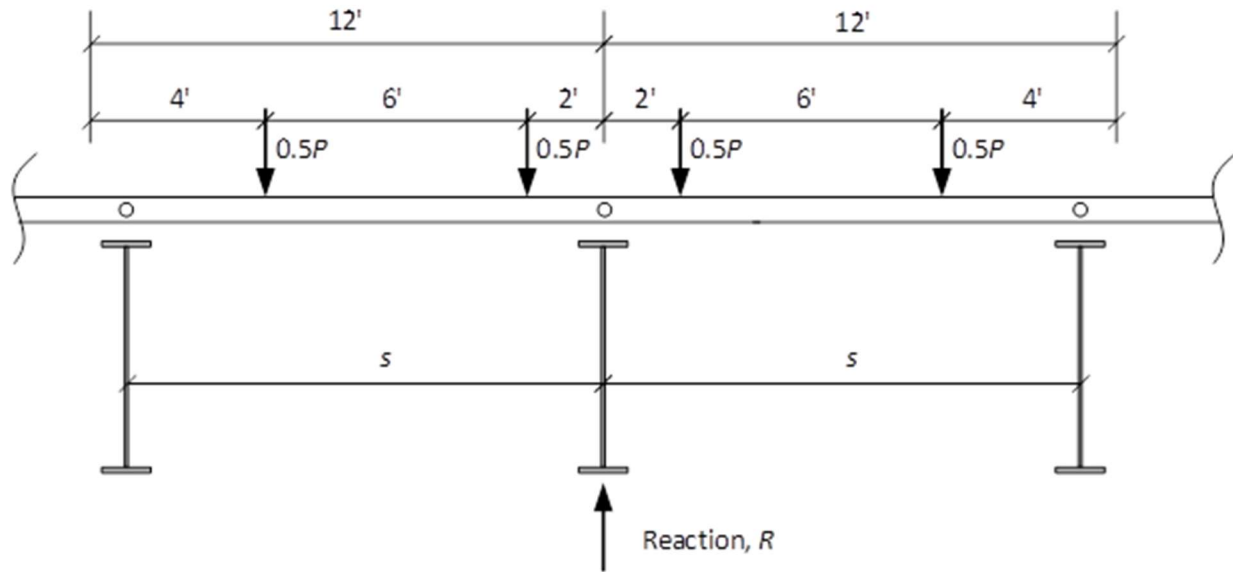

Figure 142. Statical model for the two-lane *Simon lever rule* calculation on the interior girders.

Other definitions of the "lever rule" for interior girders are specified in the literature that would include more than just two trucks in the calculation, such as (Bentley, 2022). However, the described process is the definition employed by Simon. As indicated previously, the multiple-lane *Simon lever rule* LLDF for the exterior girders is calculated by multiplying the above interior girder LLDF by *e*, borrowing from the way that AASHTO determines its exterior girder empirical multiple-lane LLDF from the interior girder empirical value.

Simon's alternative LLDF procedure produces significantly larger moment LLDFs for the interior and exterior girders than the application of the AASHTO Article 4.6.2.2 provisions outside of their stated range of applicability, and the results are typically very conservative relative to corresponding rigorous 3D FEA LLDFs. However, for the shear LLDFs, Simon's alternative procedure tends to underpredict the rigorous 3D FEA values in many situations due to the lack of consideration of the shear skew correction factor.